Georg Angenendt

Operation, Optimization and Additional Market Participation of Households with PV Battery Storage System and Power-to-Heat Application

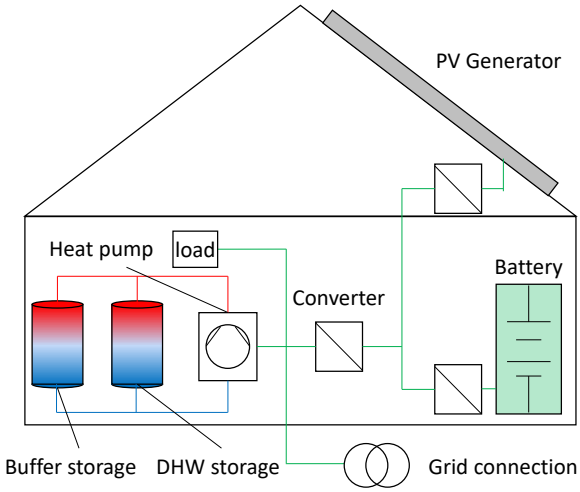

Aachener Beiträge des ISEA Band 139

Operation, Optimization and Additional Market Participation of Households with PV Battery Storage System and Power-to-Heat Application

Von der Fakultät für Elektrotechnik und Informationstechnik
der Rheinisch-Westfälischen Technischen Hochschule Aachen
zur Erlangung des akademischen Grades eines Doktors der
Ingenieurwissenschaften genehmigte Dissertation

vorgelegt von

Georg Angenendt, M. Sc.
aus Kleve

Berichter:
Univ.-Prof. Dr. rer. nat. Dirk Uwe Sauer
Univ.-Prof. Dr.-Ing. Bernd Engel

Tag der mündlichen Prüfung: 7. November 2019

AACHENER BEITRÄGE DES ISEA
Vol. 139

Editor:
Univ.-Prof. Dr. ir. h. c. Rik W. De Doncker
Director of the Institute for Power Electronics and Electrical Drives (ISEA)
RWTH Aachen University

ISSN 1437-675X

Institute for Power Electronics and Electrical Drives (ISEA), RWTH Aachen University
Jaegerstr. 17/19 • 52066 Aachen • Germany
Tel: +49 (0)241 80-96920
Fax: +49 (0)241 80-92203
post@isea.rwth-aachen.de

Georg Angenendt

Operation, Optimization and Additional Market Participation of Households with PV Battery Storage System and Power-to-Heat Application

Danksagung

In meiner Zeit am Institut habe ich fachlich viel gelernt, aber auch das ISEA als einen Arbeitsplatz mit großem Gemeinschaftsgefühl und Spaß und Freude am Arbeiten schätzen gelernt. Ich möchte die Gelegenheit nutzen, mich für die Zeit am Institut und die Unterstützung bei der Erstellung der Dissertation zu bedanken.

Zuallererst gilt mein Dank Dirk Uwe Sauer. Er hat mir die Gelegenheit zur Promotion gegeben und mich dabei immer mit viel Rat unterstützt und mir sehr viel Vertrauen entgegengebracht. Weiterhin bedanke ich mich sehr herzlich bei Prof. Engel für die Übernahme des Korreferats und den fachlichen Austausch im Vorfeld.

Auch möchte ich mich bei meinen unzähligen Kolleginnen und Kollegen bedanken. Besonders natürlich bei Sebastian: Vielen Dank für die gemeinsame Zeit im Studium und Büro, der Unterstützung bei den Veröffentlichungen und die gegenseitige Motivation.
Ein weiterer besonderer Dank gilt meinen Kollegen KP, Michael, Jan, Ilka, Chris, Fabian, die meine Arbeit Korrektur gelesen und mich bei meinen Veröffentlichungen unterstützt haben. Aber auch alle anderen Kollegen von NIS möchte ich herzlich für die Unterstützung beim Probevortrag und dem fachlichen Austausch bedanken.

Gerade in der Anfangszeit hatte ich eine Menge an praktischem Know-how zu erlernen. Hier standen mir insbesondere Patrick, Frank und Yusuf mit Rat und Tat zur Seite.

Zudem möchte ich mich bei der Verwaltung, der IT und dem Sekretariat für die Unterstützung bedanken. Insbesondere bei Nadine für die Organisation dieses Tages und bei Ute für die Unterstützung bei den Veröffentlichungen.

Auf dem Weg zur Promotion haben mich eine Vielzahl von Studenten, im Rahmen ihrer Abschlussarbeiten oder als Hiwis, unterstützt. Bei denen möchte ich mich auch herzlich bedanken: Danke an Markus, Roman, Felix, Christan, Bahram, Roia, Chaoyi, Gregor, Stefan, Lars und Ramin.

Mein letzter und wichtigster Dank gilt meinen Eltern und meinem Bruder, die mir das Studium ermöglicht haben und mich die lange Zeit vom Studium bis zu diesem Tag unterstützt haben.

Executive Summary

Sector coupling allows the use of electricity from renewable sources in different sectors to reduce their greenhouse gas emissions. Among others, renewable electricity from domestic photovoltaic systems can be used in the heating sector through power-to-heat coupling. The power generated by the photovoltaic system is then used for space heating as well as hot water preparation. In this dissertation, a detailed simulation model of an integrated home consisting of a photovoltaic system, a battery storage and power-to-heat coupling is developed to investigate cost reduction potentials. Cost reduction can be achieved by advanced operation strategies, optimization of the component sizes and market participation.

Operation strategies

This thesis presents advanced operation strategies for the electrical and thermal system and examines the gain in efficiency by combined operation strategies. Forecast-based operation strategies that reduce battery aging and costs are developed and compared to state-of-the-art operation strategies. The results of the thesis indicate that advanced operation strategies can reduce the annual costs of photovoltaic battery energy storage systems up to 12 %.

Optimization of component sizes

The most important aspect to improve the economics of integrated homes is system sizing. Dimensioning of the different system components heavily influences the economics of photovoltaic battery storage systems with power-to-heat coupling. The thermal and electrical load profile as well as the solar radiation profile must be considered to find optimal component dimensions. An optimization tool is presented that finds the most economic sizing for each system component. The results indicate that integrated homes with optimized component sizes and advanced operation strategies are economically competitive to households with fossil heating concepts.

Additional market participation

During winter, storage systems in integrated homes are not used to their full capacity due to the low solar irradiation. These unused capacities can be used to improve the economics of integrated homes by implementing a second-use scheme. Second-use describes the value stacking of home storage operation and participation on energy markets, e.g. the control reserve market. Besides enhanced economics, a participation in the control reserve market can improve grid stability and hence support further integration of renewable energies. A major advantage of integrated homes with power-to-heat coupling in comparison to standalone battery storage is the additional flexibility to absorb the negative control reserve power, provided by the heating sector. This allows an extension of the operating limits of a power-to-heat coupled battery.

This thesis presents a dual-use operation of an integrated home participating in the primary and secondary control reserve markets. Results show that a dual-use operation can increase the profitability of residential storage systems. The economics of the market participation are highly sensitive to numerous factors. Participating on the negative secondary control reserve market can lead to reduced annual cost up to 14.5 % in the investigated scenario. These savings are mainly driven by “free-of-charge” energy. If a system participates on the primary control reserve market, savings are mainly driven by additional revenues from market remuneration. Annual net cost reductions of up to 12.5 % are possible.

Table of Content

1. Energy supply in residential households

Still increasing emissions of greenhouse gases cause climate change and therefore the global warming. In the last 55 years, the carbon dioxide emissions globally quadrupled [1]. This is why the United Nations arranged the Paris agreement. The Paris agreement aims to reduce the greenhouse gas emissions in order to reduce the risks and impacts of climate change [2]. Reduction of greenhouse gas emissions should start in the year 2020. The goal of the Paris agreement is to limit the increase of the global mean temperature to a maximum of two degrees Celsius above pre-industrial levels. To reach this goal, the expansion of renewable energy production is one major prerequisite.
Modern renewable energies grow more than twice as fast as the demand in the last 10 years. Leading to an estimated renewable share of 19.3 % of the total global energy consumption in 2015 [3]. Nevertheless, to fulfill the goals of the Paris agreement the share of renewable energies hast to be doubled in the next 5 to 7 years [4].
The German government aims to reduce the CO_2 emissions by 61-62 % in the electricity sector and by 66-67 % in the building sector until 2030 in comparison to 1990 [5]. 53.4 % of the total energy consumption in Germany is used for heating [6] and one quarter of the German energy production is consumed in the residential sector [7]. Therefore, residential households can play a major role in the decarbonisation process. Over two third of the energy demand in residual households occurs for heating, especially for space and water heating [7]. The majority of the energy consumed for residential heating is generated by fossil energies. In 2016, 83 % of the energy for heating was produced by fossil energy e.g. gas, coal or oil in Germany [8]. This is why 60 % of the CO_2-emissions in German households are generated by space heating. 12 % of the emissions are produced for the provision of domestic hot water (DHW) [6].
To reach the targets of the German government, a change in the residential heating sector is required [9]. A typical two-person household in Germany has an electricity consumption from 1,500 kWh to 3,000 kWh and a heating demand from 8,000 kWh to 18,000 kWh [10]. In the heating sector the share of renewable energy is 13.9 % and in the electricity sector 37.8 % in 2018. Figure 1 illustrates this correlation. In Germany, a growing share of renewable energies is seen. From 2010 to 2018 the share of renewable energy in the electricity sector doubled, but the share in the heating sector rose only by 12 % [11]. With power-to-heat coupling in residential households the renewable energy from the electricity sector can be used in the heating sector and contribute to the CO_2 reduction goals.

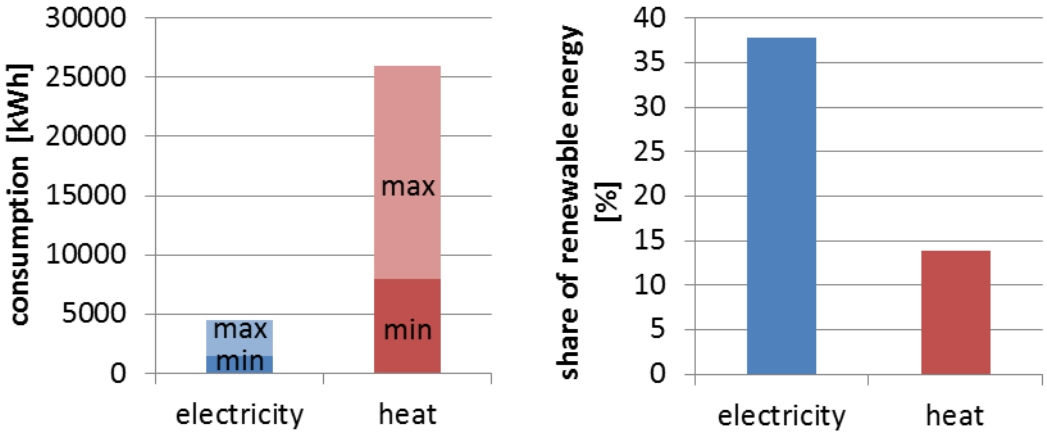

Figure 1: Left: electricity consumption of a typical two-person household in Germany [10]. Right: share of renewable energy in the electricity sector and heating sector in Germany in 2018 [11].

2. Introduction: The integrated home

One option for the decarbonisation of the residential heating sector is the coupling of the heating sector with the electric power generation from PV systems in residential households. The power generated by the photovoltaic (PV) system can be used for space heating and domestic hot water to contribute to the energy transition in residential households. Sector coupling of heat and power can be achieved, among others, by using heat pump systems.
Nevertheless, PV generated energy is supply-dependent and only available when the sun is shining. Energy demand on the other hand, is independent of the solar radiation. Storage systems are able to increase the share of locally used PV energy in residential households. Photovoltaic battery energy storage systems can increase the self-consumption from residential PV systems and therefore contribute to a decentralized renewable electricity system. Section 2.1 provides an overview of PV battery storage systems in Germany.
Integrated homes incorporate power-to-heat coupling into photovoltaic battery energy storage systems. The combined system is capable of providing renewable energy to the household demand for heat and electricity. Furthermore, the flexibility of the battery storage is combined with the flexibility of the heating system given by the thermal storage capacity of the building itself and the thermal storage unit of the heating system. Section 2.2 provides details of the power-to-heat coupling in integrated homes.
Integrated homes can contribute to the decarbonisation process and support the integration of renewable energies by using them in the heating sector. To enhance the share of integrated homes, their economics need to be improved. This can be achieved through advanced operation strategies and optimization of the component sizes. Both topics are addressed in this dissertation. Operation strategies are investigated in section 4 and the optimization of the component sizes are presented in section 0.
Additionally, the economics of integrated homes could be enhanced by the gain of additional revenues. These additional revenues could be generated on the control reserve markets. Beside the enhanced economics, the contribution on the control reserve market, can enhance the system stability and therefore pave the way for further integration of renewable energies. The provision of control reserve with integrated homes is investigated in this dissertation and introduced in section 2.3. Section 2.4 presents the structure of the thesis.

2.1 Residential photovoltaic battery energy storage systems

The growing number of PV systems leads to a rising generation of renewable energy in the residential sector [12]. With the continuously increasing penetration of residential photovoltaic systems, the number of PV battery energy storage systems (PV BESS) is steadily increasing [13]. Regarding to [14], energy storage deployments in emerging markets worldwide are expected to grow over 40 percent annually in the coming decade. In Germany, the costs for electricity are rising [15] and the subsidies for PV systems in form of feed-in tariffs are decreasing [16]. This forms an incentive to use PV BESS in order to increase self-consumption of energy from photovoltaic systems. At the end of 2018 around 125,000 PV battery energy storage systems (BESS) with a total capacity of 900 MWh were installed [17].

By 2030, a total capacity of 2 GWh of stationary batteries could be installed in German households according to [18]. This trend can also be observed in other countries. In the UK, for example, benefits in terms of lower energy costs, increased security of supply, increased decarbonization and reduced network investment are expected [19]. In California, most new homes built after January 1, 2020 will be required to include solar systems by law. This is expected to also promote wider use of energy storage systems [20]. A growing interest in PV BESS can also be seen in other countries, as PV BESS are investigated in many countries:

- Photovoltaic self-sufficiency of Belgian households using lithium-ion batteries and its impact on the grid are investigated in [21]
- In [22], a performance investigation of grid-connected residential PV battery systems focusing on enhancing self-consumption and peak shaving in Kyushu, Japan is presented. The results show that PV systems influence the grid and can act grid-friendly.
- A comparison of PV-based self-consumption and self-sufficiency in Germany and Ireland is presented in [23]. The results show that self-sufficiency rates of up to 75 % in Germany and 65 % in Ireland can be achieved.

Prices for battery storage and the overall cost of electricity for self-consumption from PV are widely discussed. Bruch et al. calculate the cost-effectiveness of a PV battery system and examine different battery technologies [24]. Bruch et al. conclude that PV Systems without storages systems are more economical. A lithium-ion battery cost analysis in PV-household application is done in [25]. The authors predict that, for the German market system profitability is expected to be reached in the very near future. Weniger et al. investigate the sizing of residential PV battery systems [26]. The results show that in a long-term scenario, the conjunction of PV systems with batteries will be the most economical solution.

2.2 Heat power coupling in residential households

Coupling of power generation form PV systems with the heating sector is one option for the decarbonisation of the residential heating sector in prosumer households. In this case, the PV system generates electricity, which can be used by a heat pump system to heat up water. Other opportunities are solar thermal collectors. Solar thermal collectors generate hot water directly from solar energy without electricity production.

In the thesis, integrated homes with PV system and heat pumps systems are investigated. Solar thermal collectors are not investigated in this thesis as explained in section 3.1.2. Integrated homes combine PV BESS with heat pumps to use the PV power in the heating sector. Figure 2 depicts an illustration of an integrated home.

One of the major technologies for the sector coupling in households are heat pumps [27]. In Germany the number of heat pumps in the residential sector [28] has been grown sharply: In 2017 around 800,000 heat pumps were installed in Germany [29]. Hence, the growth rate of heat pumps is not sufficient to meet the future heat pump demand of six million in 2030 according to [9].

Heat pumps can increase the self-consumption rate of residential PV generators and therefore reduce the grid feed-in of PV systems which leads to grid-relieving effects [30, 31]. Furthermore, distributed battery systems can be applied in combination with a heat pump in residential buildings [32] and office buildings [33].

An overview of the different kinds of heat pumps is provided in [34]. In this dissertation, an air-water heat pump is investigated, because the installation is location-independent. Heat pumps that are able to incorporate into smart grids are labeled as *SG ready* heat pumps (smart grid ready). Modern inverter-based heat pumps are able to adapt their output power in dependency of a set input power by frequency adjustment. Therefore, they are able to operate modularly. The flexibility, as a result of modular operation, can be used to compensate variations of solar radiation

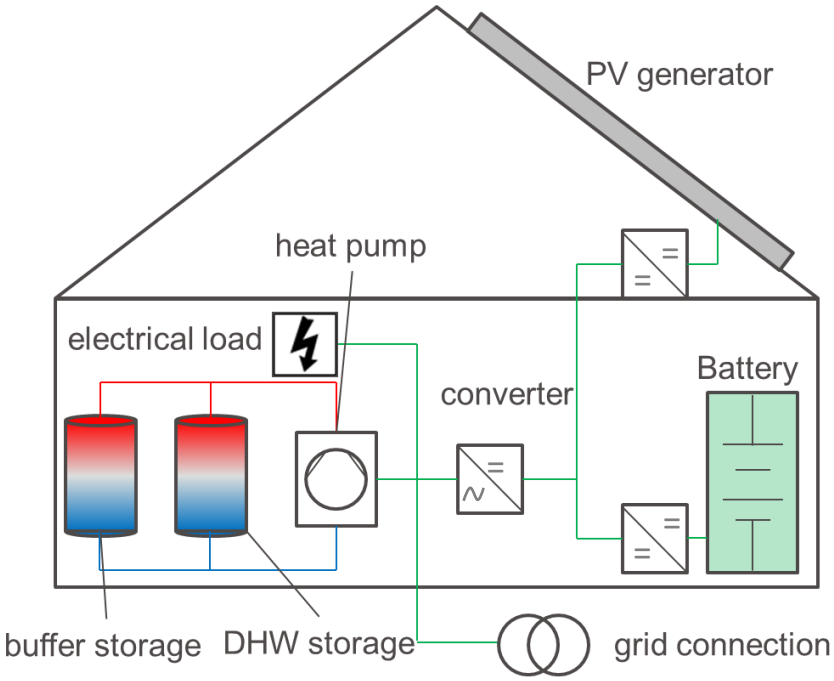

Figure 2: Schematic of an integrated home with a DC-coupled PV BESS and a heat pump for power-to-heat coupling.

2.3 Providing control reserve with battery energy storage systems

The growing share of renewable energies [3] leads to a growing fluctuation of the feed-in and therefore growing needs for flexibility options. Additionally, the decarbonisation process leads to a reduced number of conventional power plants, which are today providing auxiliary services. This is why, the request for provision of grid services is expected to increase with a large share of renewable generation [35]. Hence, costs for grid balancing are expected to increase [36]. Nevertheless, the German need for control reserve remained constant in the recent years [37]. BESS can provide these flexibility options in the power grid [38]. Not only grid scale battery systems but also distributed PV battery energy storage systems can provide these flexibilities. Distributed battery systems can provide control reserve, if connected to a virtual power plant [39]. These energy storage systems are often located in residential households in combination with PV power plants and are used to increase the self-consumption of the PV power plant [40] as pointed out in section 2.1.
During winter, storage systems in an integrated home and in particular the battery are not used to their full capacity due to low solar radiation [41]. This potential can be used to enhance

the economics of integrated homes by applying a second use scheme. Second use describes the value stacking of home storage operation and participation on the reserve market, for example. Besides enhanced economics, a participation in the control reserve market can support grid stabilization and therefore enable potential for further integration of renewable energies.

In Germany, the primary and secondary control reserve markets are promising markets for integrated homes because of the favorable requirements regarding the energy-to-power ratio of participating storage units. A major advantage of integrated homes with power-to-heat coupling in comparison to standalone battery storage is the additional flexibility to absorb negative control reserve power by means of the heating sector. This allows an extension of the operating limits of a power-heat coupled battery. Figure 3 depicts the advantage of an integrated home in comparison to a standalone battery system on the example of the primary control reserve market.

A contribution in the control reserve market could support the pathway for further integration of renewable energies and generate additional revenues [42]. Additional revenues can support the market penetration of integrated homes. Besides enhanced economics, a participation in the control reserve market could support the grid stabilization and therefore enable potential for further integration of renewable energies.

Some countries decided a nuclear power phase-out. In Germany, all nuclear power plants are scheduled to shut down until 2022. After 2020, these power plants are not available for auxiliary services. With a decreasing share of conventional power plants and an increasing share of renewables in the grid, there was a need to adapt the balancing power market rules to the new conditions. This was one reason, the Germany primary and secondary control reserve market was updated to remove burdens for participation of renewable energies and storage units on the market. The update of the primary control reserve market became effective in July 2019. The product time slot was shortened from a whole week to one day. Additionally the 30-minute criterion was replaced by a 15-minute criterion in May 2019.

In July 2018, the latest revision of the German secondary control reserve market became effective. The regulatory update of the market leads to an increased auction frequency and shortened tendered time slot.

The German secondary control reserve market is dived in a positive and negative control reserve. In the negative control reserve market, the energy has to be obtained from the grid if necessary. In this case energy can be gained, which has lower costs compared to grid consumption. Therefore, households with PV battery energy storage systems can gain additional energy from market participation and benefit from energy at very low cost or revenues from market participation.

Additional revenues on the secondary control reserve market can be generated especially in winter months, when the BESS is only used few days a month for home storage operation. The additional revenues from market participation increase the economics of integrated homes and can support the market penetration. Primary control reserve is also known as the frequency containment reserve (FCR) and secondary control reserve is also known as automated frequency restoration reserve (aFRR). In this thesis the terms primary and secondary control reserve are used.

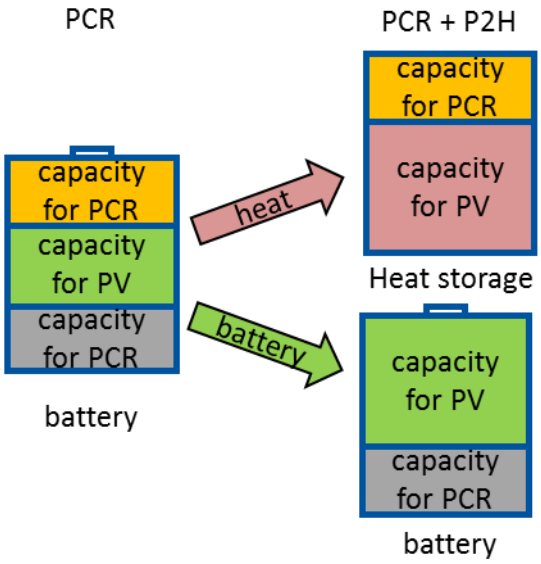

Figure 3: Operation of an integrated home participating in the primary control reserve market in comparison to a standalone battery system. Left: operation of a standalone PV BESS participating on the primary control reserve market. Capacity on the top and on the bottom of the battery has to be reserved in order to meet the 30-minute criterion. Right: operation of an integrated home participating on the primary control reserve market. Negative control reserve can be transferred in the heating sector, leading to higher useable capacity for home storage operation.

2.4 Structure of the thesis

This thesis is structured in the following way. In **section 3** the model of the integrated home, considering a DC-coupled PV BESS with a power-to-heat coupling, is presented. In the beginning of the section a literature review is given. The presented model is the base for the analysis in the following sections. The model is based on real data measurement. Extensive battery cell tests are preformed to parametrize the battery model. Additionally, the approach for the economic evaluation is presented in this section as well. To evaluate the economics, a separate analysis of levelized costs of energy (LCOEnergy), levelized costs of electricity (LCOEle) and levelized costs of heat (LCOH) is made. The separate analysis enables the potential of an inter-sectorial comparison.

To enhance the economics of the integrated home intelligent operation strategies are investigated in **section 4**. In this section, new forecast-based operation strategies for increased battery lifetime and reduced curtailment of PV power feed-in to enhance system economics are presented. In addition, these strategies are compared to other commonly used operation strategies in terms of economics and self-sufficiency of the system. Increased battery lifetime is achieved by reducing the average state of charge of the battery by limiting the stored energy according to the predicted energy demand during night. Forecast-based operation strategies are used in combination with variable power feed-in limits of the PV battery storage system to relieve the grid. Two different forecast strategies are discussed: The perfect forecast, which is used as the best case, and the persistence forecast, representing the worst case in terms of forecast accuracy. Additionally, an economic evaluation of combined operation strategies for the heat and power sector is presented. Finally, different approaches for the operation of heat

systems and combinations with the aforementioned forecast-based operation strategies for PV BESS are compared.

Section 0 presents an economic optimization of the component sizes of the integrated home. The section starts with a literature review. The dimensioning of the different system components heavily influences the economics of photovoltaic battery storage systems with power and heat coupling. Capital-intensive components such as photovoltaic generators, battery storages systems, heat pumps, and thermal storage units play a major role in increasing profitability. Moreover, the thermal and electrical load profile of the residential household as well as the solar radiation profile must be considered to define efficient or optimal component dimensions. This is why an optimization of component sizing is necessary in order to enhance the economics of the system. The presented optimization results are based on an evolutionary algorithm.

Section 6 and **7** present the participation on the control reserve market to gain additional revenues. In the beginning of the sections a literature review is given. Section 6 provides an overview of the operating reserve market in Germany. **Section 7** addresses the topic of integrated homes participating in the control reserve market. The first part of the section presents an extension of the single-use operation of the integrated home to a dual-use operation with participation in the primary control reserve market. This section investigates the influence on the home storage operation as well as the influence on the battery aging. An overall cost analysis of the household is performed. Therefore, revenues from the market participation are taken into account, as well as additional savings due to the uses of the degrees of freedom. Degrees of freedom, when providing primary control reserve can lead to additional savings. Costs for market participation and reserved battery capacity are taken into account. Advantages of integrated homes, due to the flexibility from the heating sector, in comparison to standalone battery systems are evaluated. Seasonal variation of feed-in from photovoltaics is considered by an advanced strategy for variable provision of primary control reserve power. The second part of section 7 investigates the participation of the integrated home on the secondary control reserve market. The negative control reserve provides energy for the integrated home for lower costs compared to the grid. The participation influences the operation, as well as the battery aging. Possible revenues from the secondary control reserve market are calculated. Based on the revenues and the additional costs for battery aging, the marginal costs and savings for the market participation are calculated.

The thesis closes with a conclusion and outlook presented in **section 8**. This thesis incorporate different Publications An overview of the publications related to the thesis at hand is presented in **section 0**.

3. Power-to-heat coupling model for household

To evaluate the costs of a household with power-heat coupling a distinguished model of an integrated home is used. The integrated home combines a DC-coupled PV BESS with a head pump for heat-power coupling. An overview of the model is given in section 3.1. Different system topologies for the PV BESS are presented in section 3.1.1. Solar thermal collectors are not investigated in this thesis as explained in section 3.1.2.

3.1 Model overview

In the thesis, an integrated home with heat-power application is investigated. The used model of the integrated home has separate electric and heating parts, which are inter-connected via the heat pump and the energy management system (EMS). This integrated home consists of a PV BESS and a heat-system to provide heat energy and domestic hot water (DHW). A heat pump couples the electric DC-coupled PV BESS with the heat system. Different system topologies for PV BESS are presented in section 3.1.1. Figure 4 provides an overview of the model components.
A description of the electrical part is given in section 3.2. A detailed overview of the heating part is presented in section 3.3. Section 3.4 presents the sizes of the analyzed integrated home. The economic evaluation and the parameters are presented in section 3.5.

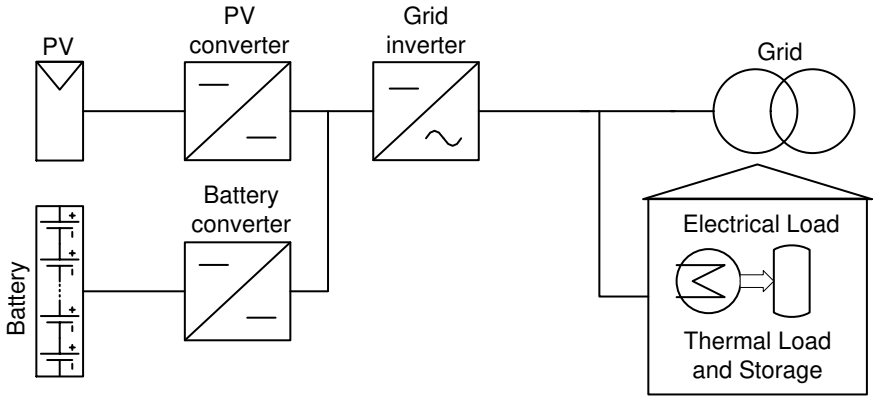

Figure 4: Schematic model of the grid connected DC-coupled PV BESS (section 3.2) with heat power coupling (section 3.3).

3.1.1 System topologies of PV BESS

Battery energy storage systems can be connected in the household in different ways. Three different topologies can be distinguished regarding the electrical connection of the battery storage device. Battery storage systems can be coupled on the DC side or on the AC side. A further option is to connect the battery directly to the PV generator DC output.

An AC-coupled BESS is connected to the 230 V AC link via its own inverter. An AC-coupled BESS is depicted in Figure 5. In a DC-Topology, they share the grid inverter. In this case, the PV

System and the BESS are connected with a DC-DC converter to an intermediate circuit. The intermediate circuit is connected via a DC-AC inverter to the AC link. A DC-coupled PC BESS is depicted in Figure 4.

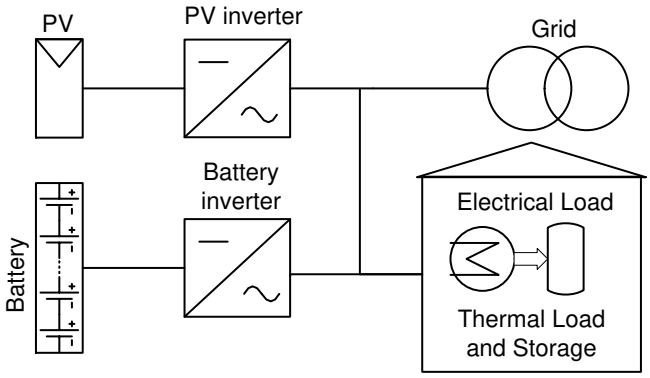

Figure 5: Schematic model of the grid connected AC-coupled PV BESS.

A special version of the DC connected PV BESS is the DC generator connected PV BESS. The topology is presented in Figure 6. The BESS is connected directly to the PV generators DC output. The advantage of this topology is that is possible to retrofit an exciting PV system. The same advantage applies for the AC connected BESS.

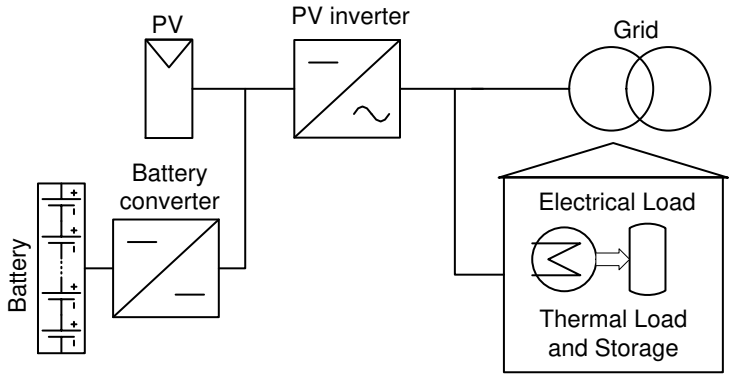

Figure 6: Schematic model of the grid connected DC-generator-coupled PV BESS.

The DC and AC topologies have advantages and disadvantages, which depend, among other things, on the remuneration model. Currently the self-consumption is remunerated if the losses occurred after the feed-in meter. In the DC topology, the losses occur before the feed-in meter and were thus at the expense of the BESS operator. This situation will become irrelevant with abolition of the feed-in tariff. In an AC system, stored energy has to pass one conversion stage more compared to a DC system. On the other hand, the independent scaling of the grid inverters can help the AC system to operate the battery inverter in better efficiency range. Nevertheless, no big difference in overall system behavior is expected. A further difference of BESS in privet households is the connection. A BESS can be connected to a single phase or be connected to 3-phases. A comparison of AC and DC systems for the case of Tesla's powerwall is presented in [43].

3.1.2 Comparison of photovoltaic heat pump systems and solar thermal collectors

Two common alternatives to use solar radiation for the heating demand in residential households exist: PV systems in combination with heat pumps and solar thermal collectors. PV systems are distinguished between Thin-film solar panels, Monocrystalline or polycrystalline solar panels. Solar thermal collectors are distinguished between flat plate collectors and evacuated tube collectors.
PV system generates electricity, which can be used by a heat pump system to generate heat. Solar thermal collectors generate heat directly from solar energy without electricity production. This is why the efficiency rates of solar thermal collectors are higher compared to PV systems. The average efficiency rate of a modern PV system is 17 %. Efficiency rated over 20 % are possible [12]. According to [44] the efficiency of a solar thermal systems is up to 44 %. In [45] it is reported that the overall thermal efficiency of a solar collector is around 40 %. Data from a field trial of solar water heating systems is analyses in [46]. An annual average efficiency rate of 52 % is presented. The efficiency rate depends on the specifications of the application. Even though the efficiency of a PV system is lower compared to a solar thermal collector, more heat can be produced with a PV system because of the seasonal performance factor (SPF) of the heat pump. The seasonal performance factor of a modern air-water heat pump is close to four [47]. This is why from one kWh of PV generated electricity four kWh heat can be produced. However, a general statement that PV heat pump systems are better cannot be made, since the investment costs and seasonality have to be minded. The seasonality and therefore the simultaneity of heating demand and PV radiation plays an important role, especially because of the high heating demand and low solar radiation in winter.
An economic comparison is presented in the thesis from S. Poppi [48]. In the thesis, Poppi investigate the techno-economics of solar systems, thermal and photovoltaic, in combination with heat pump systems. He concludes a faster payback time of a solar photovoltaic heat pump system for space heating (SH) and domestic hot water (DHW) preparation in comparison to a solar thermal heat pump system.
Different systems for the use of solar energy to generate domestic hot water (DHW) and electricity are compared in [49]. The cash return in dependency of the size of the PV power plant is analyzed and lead to the result, that a PV heat pump system have a higher cash return after 20 years in comparison to solar thermal systems.
In the publication the following reasons are given: lower investment and maintenance costs, the possibility to use the generated electricity in different sectors and enhanced self-consumption rate of the PV systems due to the use for DHW. These are reasons why in a study from *Agora Energiewende* the number of solar thermal collectors are assumed to maintain at the same level in most future scenarios [50]. Only if the prices for solar thermal collectors are decreasing significantly, solar thermal collectors will play a more important role compared to PV and heat pump systems.
[51] presents an economic analysis of solar thermal and PV in combination with a heat pump. The paper reveals that the trends indicate advantage of PV over solar thermal systems. The advantages of heat pumps systems with solar thermal collectors are shown in [52]. The combination of solar thermal systems with heat pumps is investigated in [53] as well. The

publication concludes that a combined solar thermal heat pump system the system performance compared to a conventional heat pump system can be increased. In publication [54] solar thermal systems with heat pumps are combined with different storage technologies. A further opportunity is to combine solar thermal power plants with PV systems. The combination with the goal of autarky is investigated in [55]. The enhanced investment costs for both systems can reduced the economics as discussed in [56].
The thesis at hand focus on PV heat pump system, since according to [48] and [49] these systems lead to reduced costs in comparison to solar thermal systems with heat pumps. Additionally combination of solar thermal systems with heat pumps is already widely discussed in literature. The combination of PV and solar thermal systems is not investigated. The combination could be addressed in further research.

3.2 Electrical model of integrated home components

The electrical model of the integrated home represents a DC-coupled BESS with a PV power plant as depicted in Figure 4. It consists of the PV panel model [57], a PV and a battery converter model, one grid inverter model, the BESS model, the household load model and the grid connection. A load profile to represent the household is included as well as a grid connection to feed-in PV generated energy or for grid supply. The BESS is separated into an electrical, a thermal and an aging model of the battery.

3.2.1 Load profile

The standard profile (H0 profile) for a residential household in Germany with a 15 min resolution does not suffice for the simulation of an integrated home, because load peaks are smoothed. These load peaks highly influence the performance of the integrated home, because the gap between solar radiation and load peaks are neglected or reduced if the resolution of the PV radiation data and load profile data is too low. This topic is discussed in literature. In [58] the dynamic mismatches between the battery power and the residual power are analyzed. The paper concludes that a slow-reacting battery system diminishes the economic benefit for the owner of the PV-battery system. Publication [59] concludes that recommendation on dimensioning of BESS, when the self-sufficiency rate is calculated, can only be given if data is available in high temporal resolution.
The load profile used for this model offers the consumption data of a German household in a 60-second temporal resolution. Instantaneous values are given. The consumption data is based on synthetic load profiles by the “Institut für ökologische Wirtschaftsforschung” (IöW) [60]. Therefore, the average power consumption of 32 different devices was determined from measurement and market data. The profile provides the electricity consumption of a 4-person household in Germany without holiday. Standard weeks with different usage profiles for summer, winter and transition periods were modelled in order to consider seasonal effects. A detailed description of the data is presented in [60]. The resulting annual electricity demand for the 4-person household is 4,674 kWh_{el}/a. The electricity consumption for a day in April is depicted in Figure 7. This is the day with the highest load peak of 11,538 W. The total electrical energy consumption on this day is 15.2 kWh.

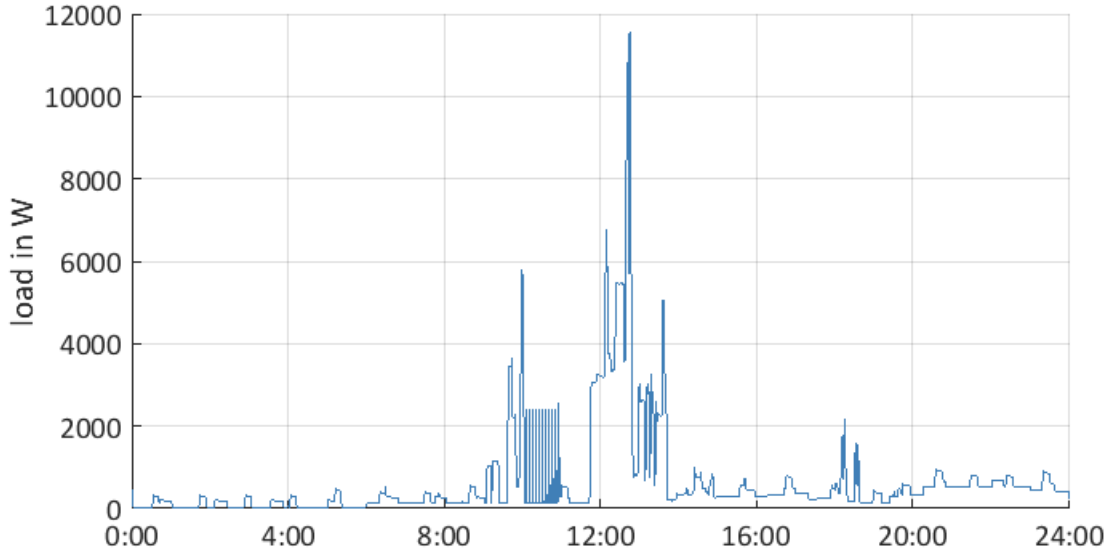

Figure 7: Exemplary electricity consumption of a 4-Person household in Germany based on a synthetic load profile with a 60-second resolution.

3.2.2 Grid connection

The grid connection of the integrated home is modeled without constrains. Therefore, infinite grid consumption as well as infinite grid feed-in is possible. The feed-in power is limited to 70 % of the installed PV generator power (§9 EEG 2014 Abs. 2 Nr. 2b). The influence of PV feed-in limitations is analyzed in section 4.5.3.

3.2.3 PV Generator

The PV generator model is based on publication [57] and simulates the electric behavior of a STP 210-18Ud by Suntech Power PV generator. The STP 210-18Ud Suntech Power PV generator is a polycrystalline silicon-based solar cell. One module has a power of 210 W. Further information can be found in the datasheet [61]. The PV model calculates the power and DC voltage output of the maximum power point tracker (MPPT). Therefore, irradiation data in form of global, diffuse and beam irradiation, and the temperature profile of the solar modules are used. The thermal behavior of the PV system is modeled as well. The model is used to calculate location-dependent PV power generation based on a local measurement profile. For this thesis, the measured radiation data for Lindenberg (Tauche), close to Berlin, provided by BSRN from the year 2006 [62] is used. The data is provided in a 60-second temporary resolution. The annual PV energy production in dependency of the azimuth angle and the tilt angle is illustrated in Figure 8. For the integrated home, the optimal orientation of the PV system is used. The maximum energy is generated with a tilt angle of 30° and an azimuth angle of -5°. This result is based on the optimization preformed in [63], resulting in an annual PV generation of 1140 kWh/kWp. A detailed explanation of the PV generator model as well as a validation of the model is provided in [63].

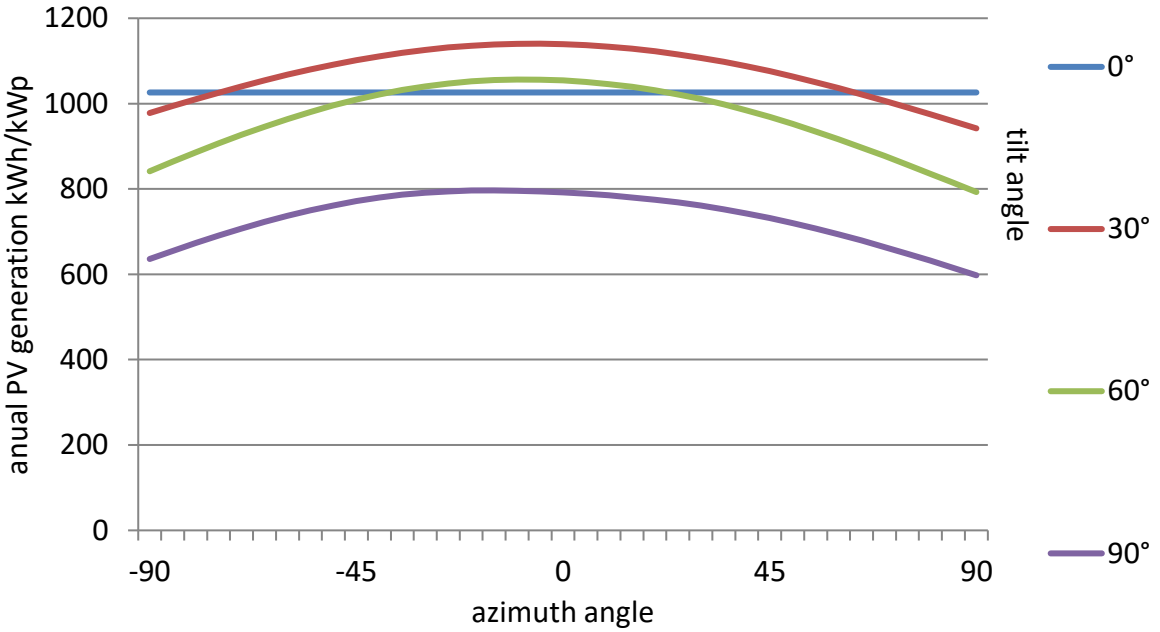

Figure 8: Annual PV energy production in dependency of the azimuth angle and the tilt angle of a PV power plant located in Lindenberg (Tauche) close to Berlin.

3.2.4 Converter

The electric model of the integrated home represents a DC-coupled PV battery system and therefore uses three converters. The converter systems are defined by the efficiency characteristic of their input and output power and a voltage-dependent efficiency and are based on [57] and [64]. The intermediate circuit voltage is set to 650 V based on [63]. The battery voltage is variable, as well as the PV output voltage. This is why the voltage dependency has to be considered for the PV converter and the battery converter, because the input voltages of these converters are variable. To depict the different voltage levels, multiple sets of parameters of efficiency curves for different voltage level are used as inputs. The resulting efficiency curves are linearly interpolated from the input efficiency curves. The influence of the input voltage on converter efficiencies are presented in [63] and illustrated in Figure 9 for the battery converter. The efficiency of the battery converter is analyzed in [65]. The battery voltage differs between 220 V and 336 V, depending on the state of charge (SoC). The transmission ratio of the grid inverter is fixed, since the grid voltage as well as the intermediate circuit voltage is fixed.
The efficiency is defined as the ratio between the input and the output power. The output power is equal to the input power minus the converter losses.

$$\eta = \frac{P_{out}}{P_{in}} = \frac{P_{in} - P_{loss}}{P_{in}} \quad (1)$$

The losses are calculated with a polynomic description presented in [63, 66]. Therefore, the different kinds of losses are taken into account:

- no-load losses $P_{no-load}$
- voltage based losses, with a linear relation to the output current U_{loss}
- ohmic losses, with a quadratic relation to the output current R_{loss}

Equation (2) depicts the evaluation of the converter losses [67].

$$P_{loss} = P_{no-load\ losses} + U_{loss} \cdot I_{out} + R_{loss} \cdot I_{out}^2 \quad (2)$$

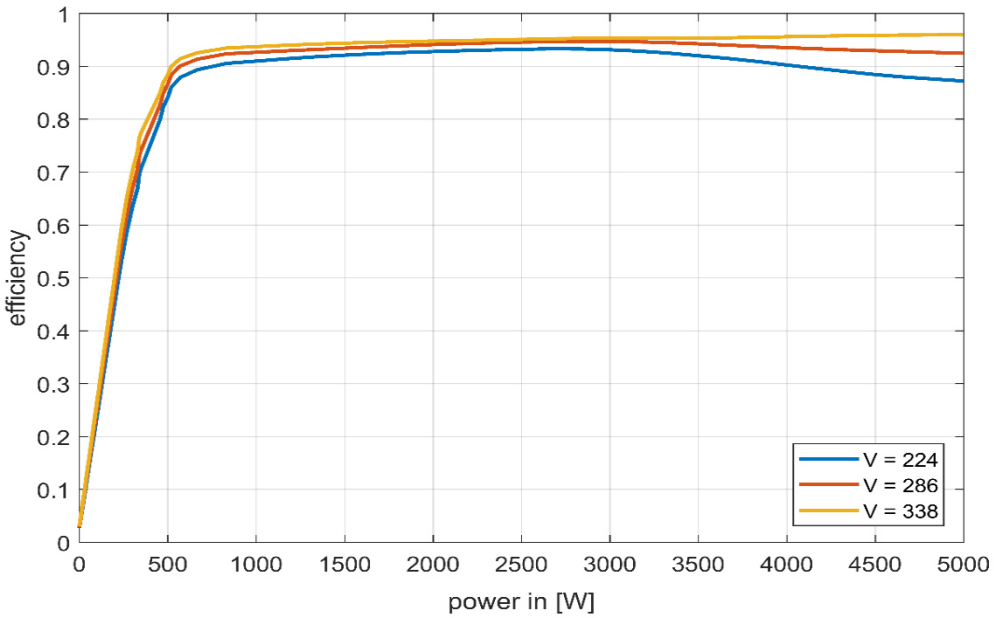

Figure 9: Efficiency curve of the battery converter in dependency of the input voltage of a 5 kW converter.

3.2.5 Battery system

A detailed battery model is used in this thesis. The battery model is based on the model presented in [68] and consists of a electrical model, thermal model and aging model. In [63] the model is parameterized with a 45 Ah battery cell from Saft. The aging model consists of a separated calendric and cyclic aging model. In section 3.2.5.1 the electrical model and in section 3.2.5.2 the thermal battery model is presented. The model to calculate the battery aging is presented in section 3.2.5.3. The calendric aging is specified in section 3.2.5.4 and the cyclic aging is specified in section 3.2.5.5. In this thesis extensive battery cell tests are performed to parametrize the battery model. The battery model is parametrized with the test results of a cylindrical lithium-nickel-manganese-cobalt-oxide (NMC) 18650 lithium-ion battery cell from LG-Chem (LG ICR18650MF1) with 2.15 Ah. The cell testing results are presented in [69]. Additionally the battery aging model is enhanced as pointed out in section 3.2.5.3. To model the battery energy storage system (BESS), 80 battery cells are connected in serial and 16 battery cells are connected in parallel (80s16p). A first approach to investigate the influence of parallel and serial connection on the battery aging and efficiency is made in [65] by the author and therefore not investigated in this thesis.

<u>Battery Management System (BMS):</u>

Besides the battery system, a Battery management system (BMS) is applied in the model. The BMS monitors the battery and ensures that the battery is operated in the given operation range. Therefore, the BMS prevents overcharging or deep discharging. Furthermore, it monitors the temperature of the battery. A temperature derating is applied for the charging

case. The BMS limits the c-rate of the battery, which determines the maximum charging and discharging power of the battery. In the charging case, the c-rate is limited to one, therefore the battery can be fully charged in one hour. In the discharging case, the c-rate is limited to two. The battery can be fully discharged within half an hour.

Energy Management System (EMS):
The Energy management system used in the model depends on the application. Section 4 presents the overall EMS and describes the different examined operation strategies. Operation strategies for the electric system are presented in section 4.1. Operation strategies for the heating system are presented in 4.2. Adjustments of the EMS for the participation on the primary control reserve are presented in section 7.3. The adjustments for secondary control reserve market participation are presented in section 7.6.

3.2.5.1 Electrical model of the battery behavior

To model the electric behaviour of batteries different approaches are known. Physical-chemical approaches model the battery behaviour at molecular level considering physical and chemical laws. These models are rather complex and require high computational efforts. An overview of different physical-chemical models can be found in [70]. To simulate the whole lifetime of the battery the dynamic electric behaviour of the battery is important. For this thesis, an impedance based battery model is used, because such a model requires less computable effort and simultaneously offers a sufficient accuracy. To determine the electric parameters of the battery the electrochemical impedance spectroscopy (EIS) is used. The impedance spectroscopy is widely known and discussed in numerous publications. Publication [71] analyses the impedance spectroscopy for industrial batteries. Impedance based simulation models for automotive are analyzed in [72].
For impedance spectroscopy, AC signals with different frequencies are induced into the batteries. The response of the battery is measured and the impedance can be calculated. The impedance is measured for different SoC and different temperatures of the battery. The resulting impedance spectrum is used to parametrize the electrical model. The impedance of the battery is modelled with a serial connection of an inductance, a resistance and two ZARC-elements and Warburg impedance. A ZARC element consists of a parallel connection of a resistance and a Constant Phase Element (CPE) [73]. The measured impedance spectrum for the LG ICR18650MF1 battery cell and the corresponding elements of the impedance model is depicted in Figure 10.

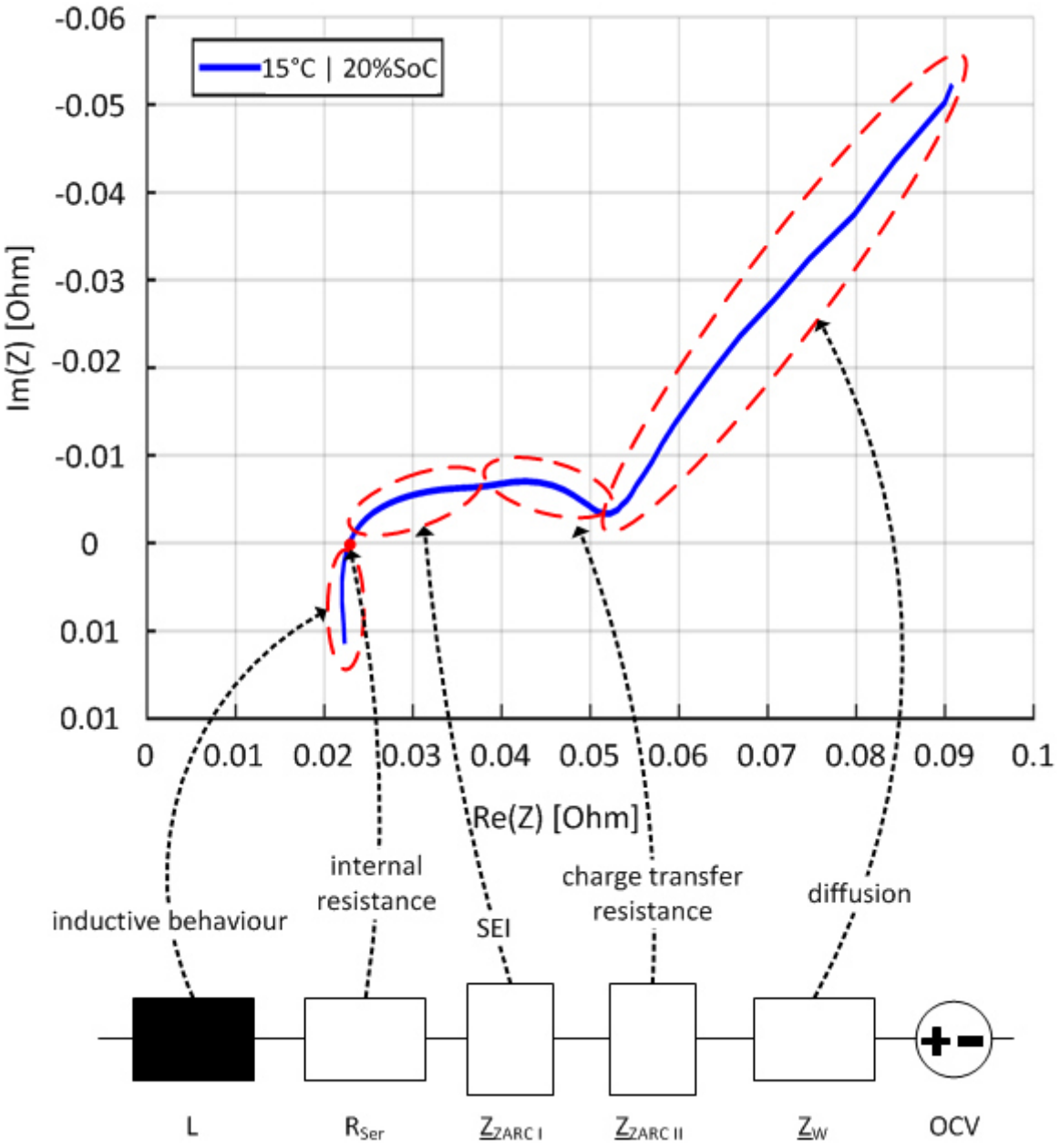

Figure 10: Impedance spectrum of the LG ICR18650MF1 battery cell and the corresponding elements of the impedance model.

The battery in this application is used for a home storage system. For this purpose, the high frequency parts are less important, because the input data uses a 60-second resolution as presented in section 3.2.1 and section 3.2.3. The resolution of the input parameters does not provide data to analyze the high frequency parts. Therefore the high frequency parts can be neglected [63]. The impedance model can be simplified to the model presented in Figure 11. The simplified model consists of a resistance and a serial connected Warburg impedance. The Warburg impedance $\underline{Z}_W$ represents the diffusion of the battery cell.
The Warburg impedance is described with equation (3). The parameters R_D presenting the diffusion resistance and τ_D representing the diffusion time constant. A derivation of equation (3) is given in [63].

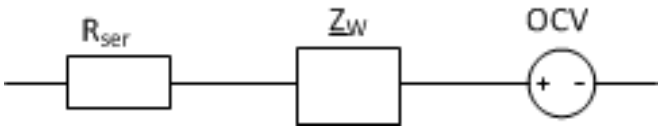

Figure 11: Simplified impedance model of a battery used for a PV battery energy storage system.

$$\underline{Z}_W = R_D \cdot \frac{\tanh\left(\sqrt{j\omega\tau_D}\right)}{\sqrt{j\omega\tau_D}} \tag{3}$$

For the parametrization, the measurements of the EIS impedance are not sufficient since the measurement for low frequencies does not fulfil the requirement of a quasi-stationary measurement. The requirements are not fulfilled, because the energy charging and discharging the battery cannot be neglected. Therefore, the battery cell is induced with the current profiles depicted in the first picture in Figure 12 and the voltage response depicted in the second picture in Figure 12 is measured. The resulting fitting parameters of R_{ser}, R_D and τ_D are shown in Figure 13. The Open circuit voltage (OCV) curve is depicted in Figure 14.

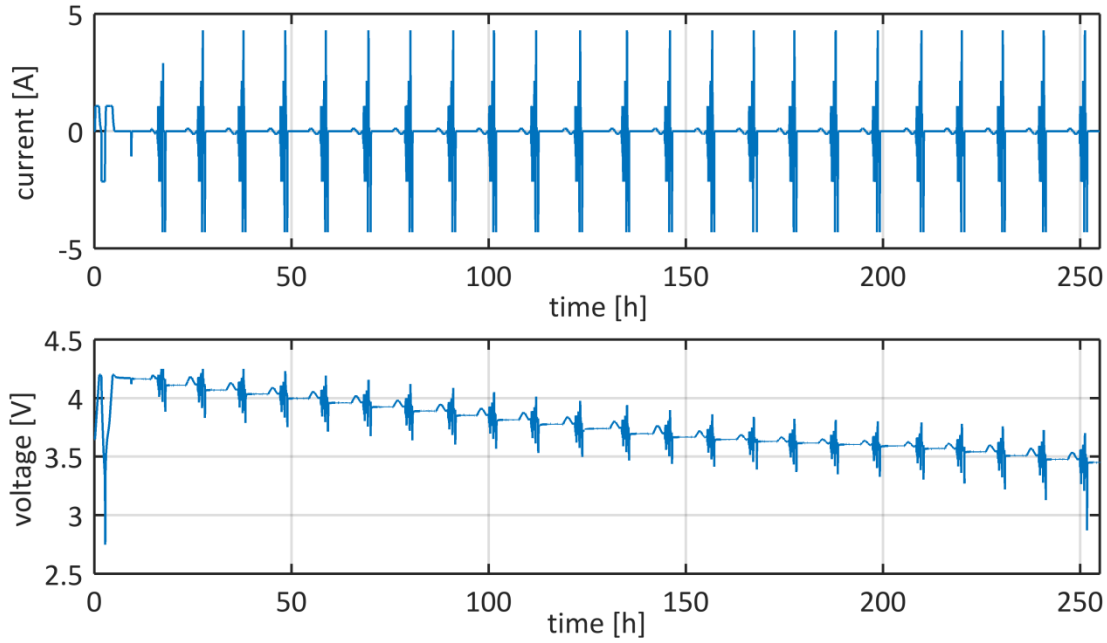

Figure 12: First picture depicts the current profile induced into a LG ICR18650MF1 battery cell at 25°C. The second picture depicts the resulting voltage profile of the LG ICR18650MF1 battery cell.

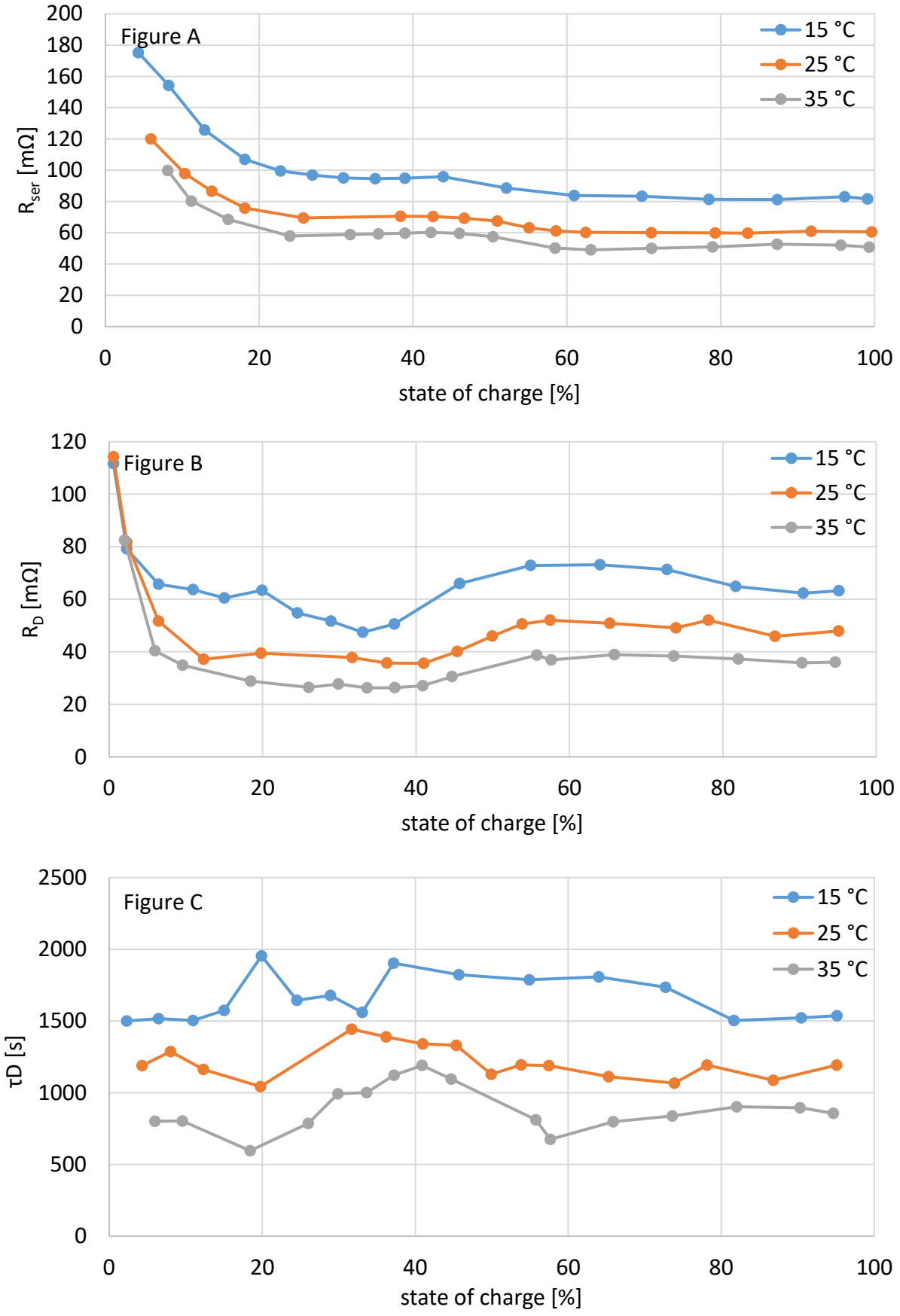

Figure 13: Fitting of the impedance parameters for different temperatures and SoC of the LG ICR18650MF1 battery cell. Figure A R_{ser} , figure B R_D and figure C τ_D.

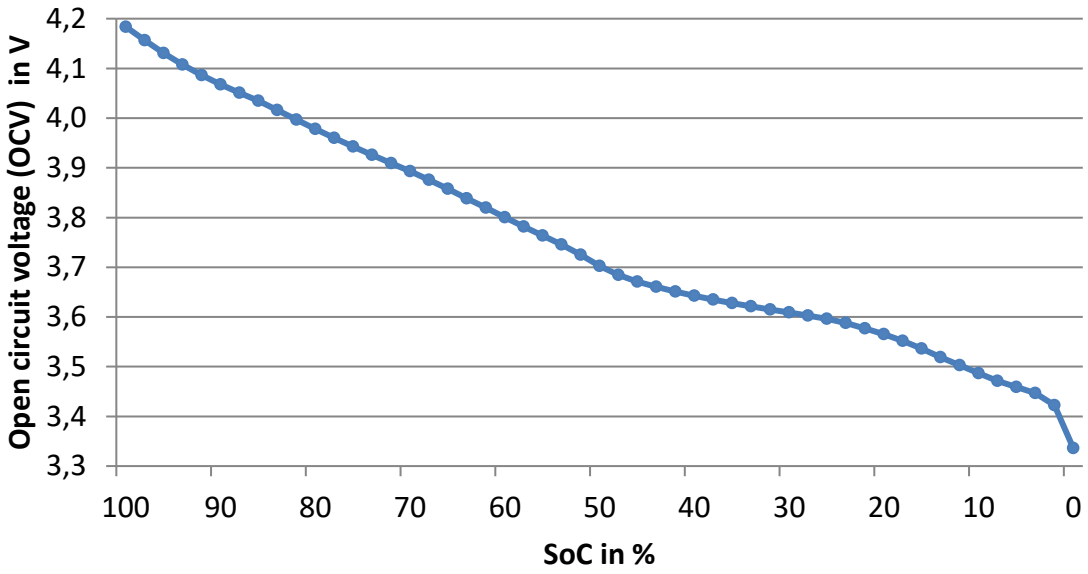

Figure 14: Open circuit voltage (OCV) curve of the LG ICR18650MF1 battery cell at 25 °C with 1 C and a relaxation time of 3 hours.

Validation of the impedance model

The validation is made with a measurement for the OCV curve. After the battery is fully charged with 1 C the battery is discharged in 5 % steps with a current of 1 C. After each discharge step, a relaxation time of 3 hours is minded. Figure 15 depicts the comparison of the simulation and the measurement. The results show a similar behavior of the measurement and the simulation. Only for low SoC a significant deviation is visible. The reason for the deviation at low SoC is the inaccuracy of the OCV measurement at low SoC. For the 0 % SoC value an end of discharge voltage is defined. This voltage can be reached before the Ah based definition of the 0 % SoC is reached. Since the battery is used for a home storage application, the accuracy is sufficient. Additionally, the model uses acceptable computational effort. Figure 16 depicts the comparison of a discharge from 50 % SoC to 55 % SoC.

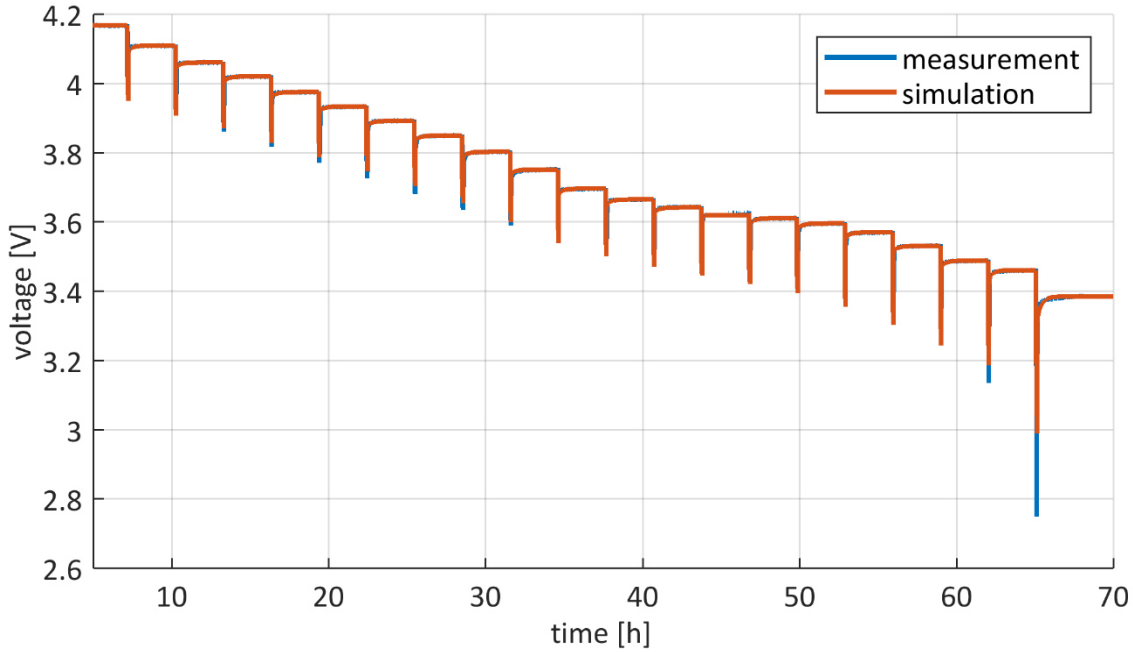

Figure 15: Voltage of the discharging process of the LG ICR18650MF1 battery cell at 25 °C. A discharge from 100 % to 0 % is performed in 5 % steps with 1 C and a relaxation time of 3 hours between every step.

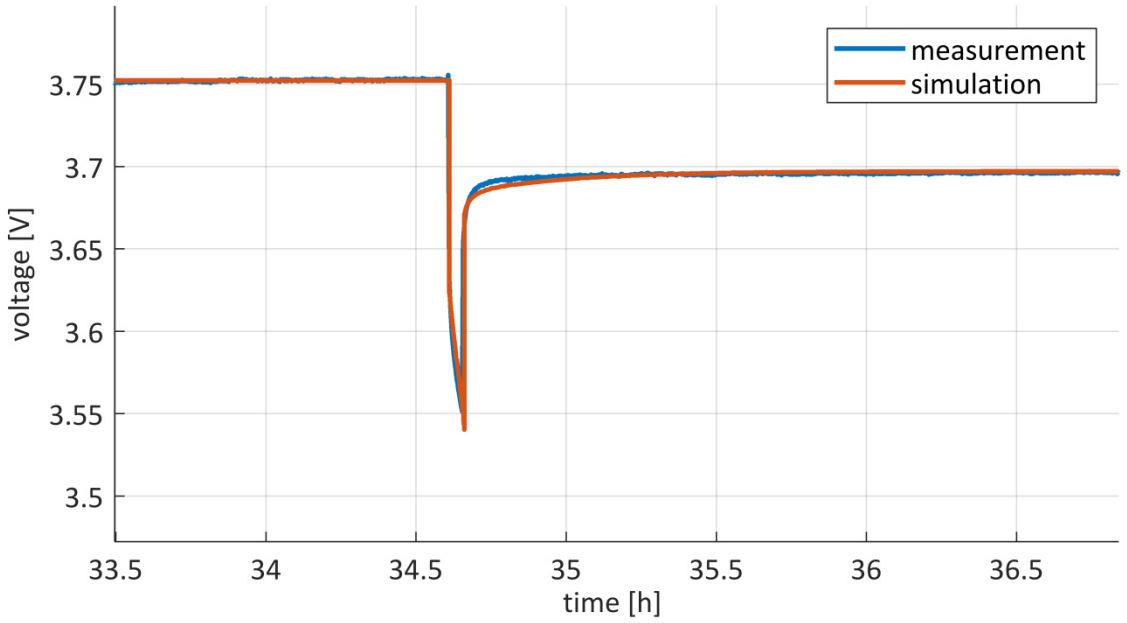

Figure 16: Voltage of the Discharging of the LG ICR18650MF1 battery cell at 25 °C from 55 % to 50 % with 1 C and a relaxation time of 3 hours.

3.2.5.2 Temperature Model

The temperature model influences the electric behavior of the battery cell as well as the aging. Therefore, a thermal model of the battery is applied. The thermal model from [63] is used and parametrized with the measurements of the LG ICR18650MF1 battery cell. The battery cell is modelled as a dot-shaped heat source as shown in Figure 17. The thermal losses of the battery

cell are the ohmic losses of the battery. Minding a heat transfer coefficient, the battery cell transfers heat to the ambient. Therefore, the ambient temperature and the losses of the battery influence the temperature model. The heating capacity of a NMC 18650 battery cell is between 700 to 880 $\frac{\mathrm{J}}{\mathrm{kg} \cdot \mathrm{K}}$ based on [74] and [75]. This is why a heating capacity of 800 $\frac{\mathrm{J}}{\mathrm{kg} \cdot \mathrm{K}}$ is assumed. The heat transfer coefficient is adjusted so that measurement and simulation fit best. The thermal model is depicted in Figure 17.

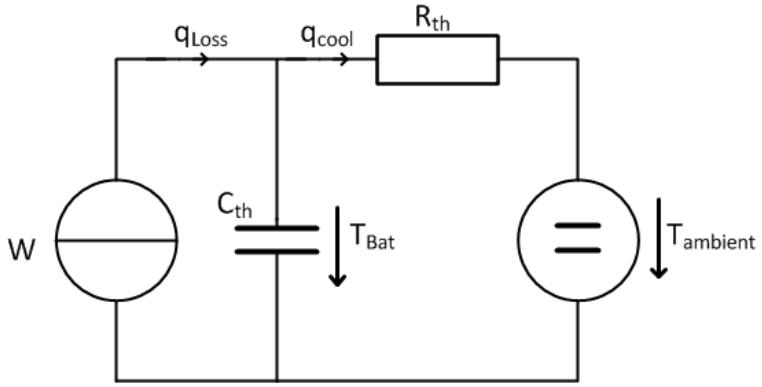

Figure 17: Temperature model of the battery cell: battery is considered as a point-shaped heat source W feed from the ohmic thermal losses q_{Loss}. The thermal capacity C_{th} determines the battery temperature T_{bat}. The battery temperature is higher compared to the ambient temperature $T_{ambient}$. Cooling of the battery by the surrounding is approximated with the heat transfer resistance R_{th} and the cooling energy q_{cool}.

Validation of the temperature model of the battery cell

Figure 18 depicts the surface temperature of a battery cell when discharging with a constant current of 1 C. This temperature is compared to the temperature of the simulation model. The deviation of the measured temperature and the simulated temperature is less than one Kelvin. The simulation model calculates the temperature for a dot-shaped heat source, whereas the measured temperature is surface temperature of the battery cell. The measured surface temperature deviated from the inner temperature of the battery cell. The inner temperature influences the aging of the battery cell. The simulated temperature could be closer to the inner temperature in comparison to the surface temperature.

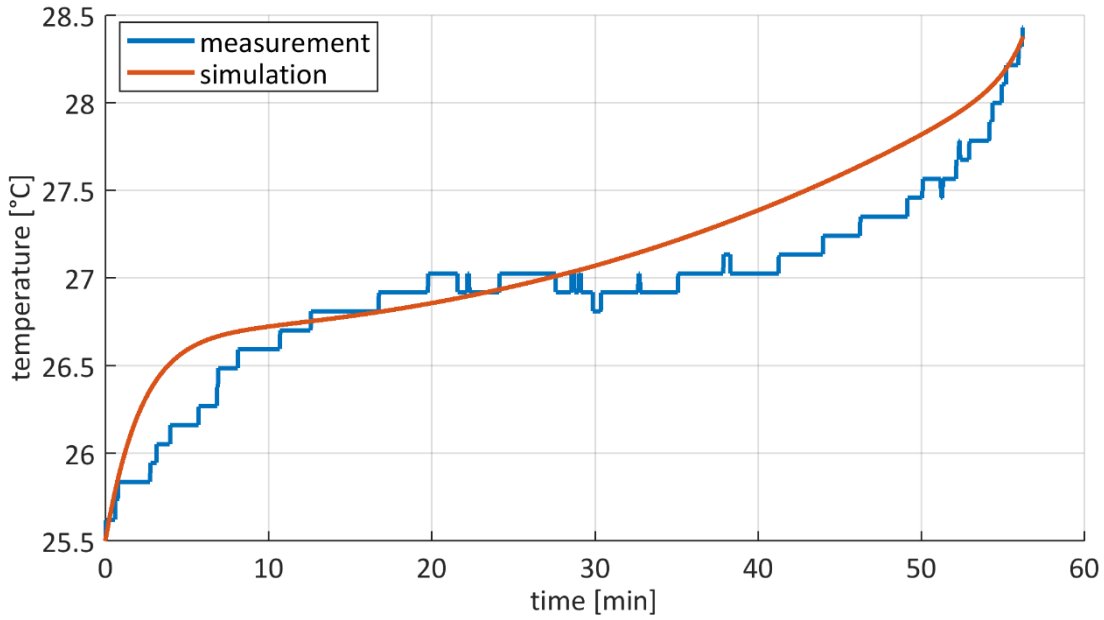

Figure 18: Temperature of the LG ICR18650MF1 battery cell, while discharging with a constant current of 1 C. Stepwise temperature increase in the measurement is due to the resolution of the temperature sensor.

3.2.5.3 Battery aging

The applied battery model is based on the model presented in [68] and described in great detail in [63]. In this thesis extensive battery aging tests are performed, to parametrize the battery model with the investigated LG-Chem (LG ICR18650MF1) battery cell. The test procedure for the calendar and cycle aging tests and the test results are described in great detail in [69]. For the simulation a battery system is used, which consists of 80 serial and 16 parallel-connected cells. The battery management system (BMS) limits the c-rate of the battery to one in the charging case and to two in the discharging case. The influence of number of serial and parallel connected battery cells on the efficiency and lifetime is analyzed in [65]. The capacity of a battery is reduced and the internal resistance is increased due to calendric and cyclic aging. When the remaining capacity reaches 70 % of the initial capacity, the battery reaches its end of life. The end of life is reached as well, if the internal resistance is doubled. In this case the state of heath (SoH) of the battery is zero and the battery system will be replaced with a new one. The state of the battery aging is represented by the parameter c_{sum}. This aging parameter c_{sum} is the inverse element of the SoH. Therefore, c_{sum} is defined as the factor of aging. $c_{sum} = 1$ describes the end of life of the battery. At begin of life of the battery $c_{sum} = 0$. The end of life is defined as 70 % of the initial capacity or a double internal resistance. With the common definition of the SoH, the aging factor c_{sum} is defined as:

$$c_{sum} = 1 - SoH \tag{4}$$

The loss of capacity and the increase of the impedance are results of the aging of lithium-ion batteries. Both aging results can be divided into reactions depending on time (calendric aging) and usage (cyclic aging). A common approach is to assume an additive superposition of both effects. Therefore, the applied aging model uses a separate calendric and cyclic aging model based on [63, 76]. The total aging c_{sum} is the sum of both aging models.

$$c_{sum} = c_{cal} + c_{cyc} \quad (5)$$

The calendric aging is presented in section 3.2.5.4 and the cyclic aging is presented in section 3.2.5.5. The charging and discharging losses of the battery cell are assumed as constant over the battery lifetime. In this thesis, only the reduced capacity is used as the end of life criteria. The aging results of the investigated battery cell presented in [69] show that the end of life criteria considering the capacity loss is reached before the end of life criteria considering the internal resistance. This finding is supported by publication [77]. Publication [77] investigated the degradation of lithium-ion battery cells used for frequency regulation. The publication points out, that the capacity loss of the battery limits the lifetime and not the power capability.

3.2.5.4 Calendric aging of the battery

The main calendric aging effect is the formation of the Solid Electrolyte Interface (SEI) on top of the graphite anode [78]. The electrolyte reacts with the graphite and forms a layer, which is still permeable for lithium-ions. Yet active lithium and parts of the electrolyte are bound during the process and lead to a performance loss of the battery [79]. The loss of active lithium is often referred as the loss of lithium inventory (LLI).

The calendric aging is determined by storage tests under float conditions. To get valid results three battery cells are stored under identical conditions. Float conditions means that battery cells are stored under constant voltage conditions. Doing this, the self-discharge is counteracted. Additionally, the battery cells are stored at different temperatures (25 °C, 35 °C, 45 °C and 55 °C) and different SoC. The capacity change is measured every 2 to 4 weeks depending on the temperature. The test matrix and the check-up test procedure are presented in [69]. Exemplary results of the calendric aging tests are shown in Figure 19 for a storage temperature of 25 °C and in Figure 20 for a storage temperature of 45 °C. The depicted results represent the average value of the battery cells. A detailed analysis is presented in [69]. The simulation results are depicted as well.

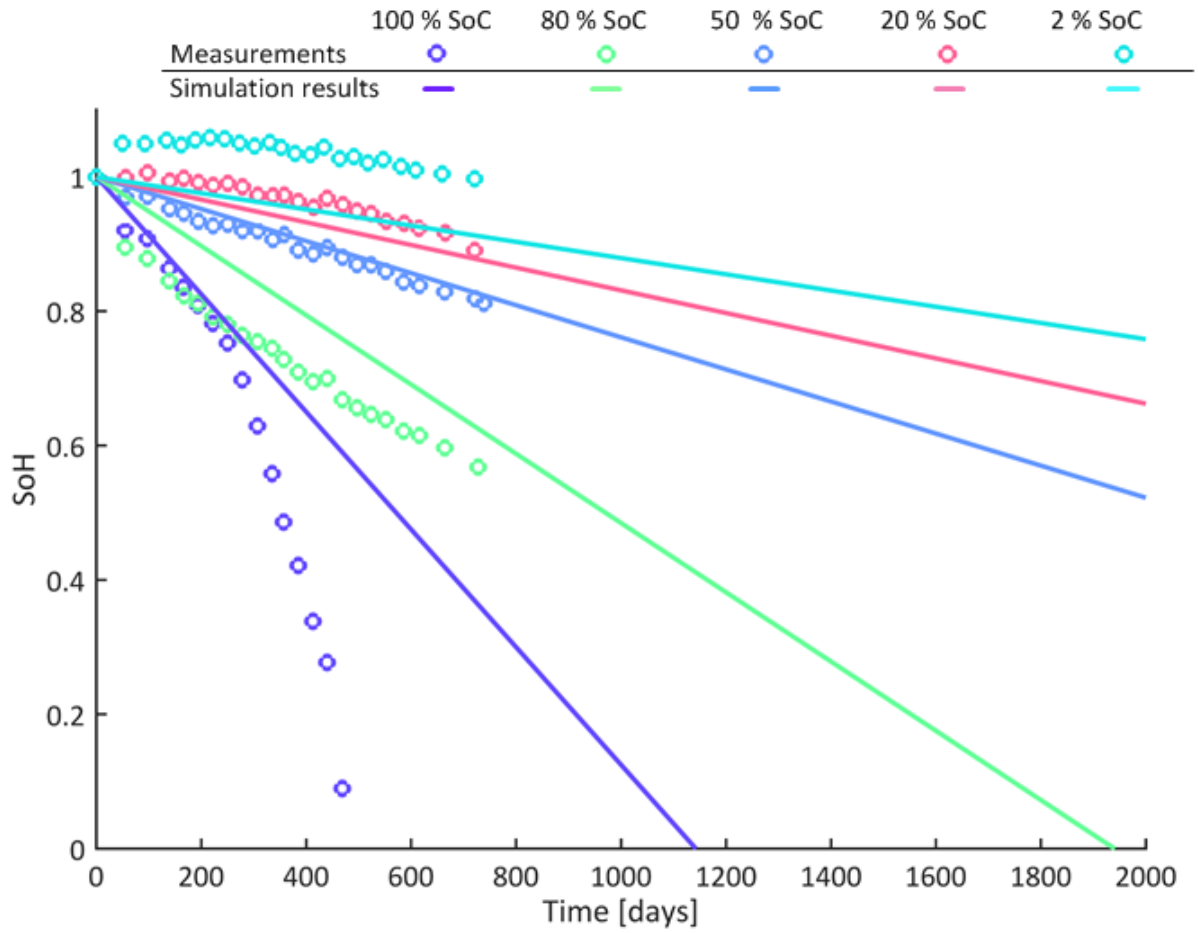

Figure 19: Calendric aging test results: relative capacity change of the LG ICR18650MF1 lithium-ion battery cell stored at 25 °C. When the SoH_C is 0 % the battery has 70 % of the initial capacity left. Simulation and measurement results are depicted.

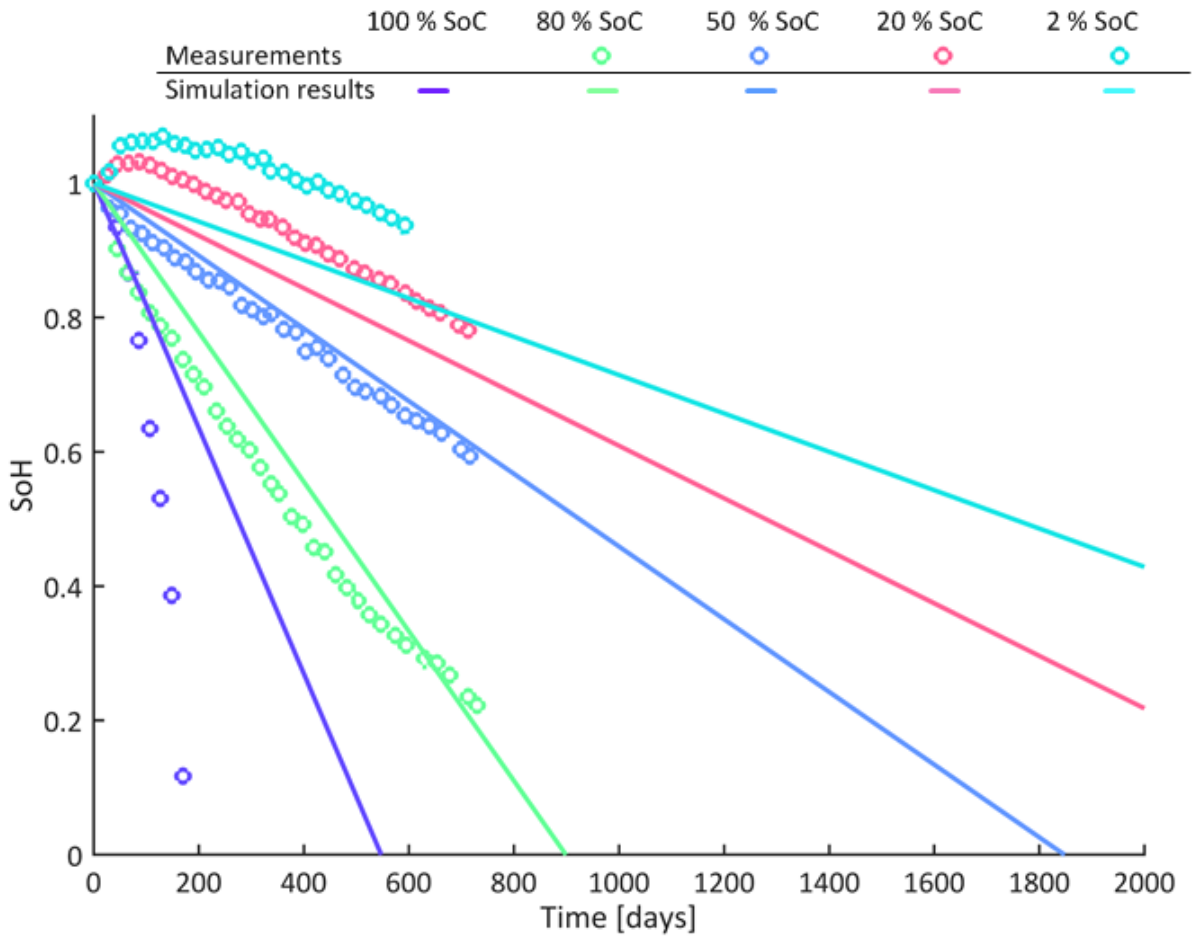

Figure 20: Calendric aging test results: relative capacity change of the LG ICR18650MF1 lithium-ion battery cell stored at 45 °C. Simulation and measurement results are depicted.

Modelling the calendric aging

In literature, different approaches to model the calendar aging e.g. linear, square or exponential functions are presented. In [80] an overview of different approaches to model the calendric aging of commercial lithium-ion cells is presented. The irreversible aging mechanism in this work is modelled with a linear function. Additionally, the extrapolated aging is extracted minding the passive electrode effect. This effect describes a reversible capacity increase or decrease due to a change of the SoC as investigated in [81, 82]. For the given case, the initial SoC of the calendric tested cells was around 44 %. This is why the initial and reversible capacity rise for the 2 % and the 20 % SoC tests and the initial capacity loss for 50 %, 80 % and 100 % SoC test is neglected for the irreversible aging modelling.

The applied aging model is presented in [63] and parameterized in [83]. The linear aging model is based on the Arrhenius equation and the Tafel equation. The Arrhenius equation describes the dependency of the aging on the temperature, which is shown in equation (6). The Tafel equation is given in (7) and presents the dependency of the aging on the state of charge and therefore on the voltage of the battery. The calendric aging is calculated with equation (8). This equation incorporates the Arrhenius and the Tafel equation. The average temperature and the average voltage are used as input parameters.

Arrhenius equation:

$$k_T = \exp\left(-\frac{E_a}{R_{ug}} \cdot \left(\frac{1}{T_{avg}} - \frac{1}{T_0}\right)\right), \text{parameter } E_a \quad (6)$$

Tafel equation:

$$k_V = \exp\left(\frac{\alpha \cdot F}{R_{ug}} \cdot \left(\frac{U_{avg}}{T_{avg}} - \frac{U_0}{T_0}\right)\right), \text{parameter } \alpha \quad (7)$$

With the use of equation (6) and (7), the calendric aging can be calculated with equation (8).

$$c_{cal} = a_{cal} \cdot k_T \cdot k_V \cdot t \quad (8)$$

Table 1 shows the input parameters for the applied calendric aging model. All values are based on cell tests.

Parameter	Value	description
E_a	57573	Arrhenius parameter
R_{ug}	8.3144621 $\frac{J}{mol \cdot K}$	universal gas constant
T_0	25 °C	nominal temperature
U_0	3.6970 V	nominal voltage
α	0.0709	Tafel parameter
a_{cal}	2.388e-4	calendric aging parameter
F	96485.3365 As/mol	Faraday constant

Table 1: Input parameters for the aging model based on the calendric aging tests of the LG ICR18650MF1 lithium-ion battery cell.

Validation of the calendric aging

The simulation of the calendric aging has a slight deviation of the measurements as shown in Figure 19 and Figure 20. For high SoC the deviation is higher and especially for 100 % SoC the calendric aging follows an exponential function. Ecker et al. [84] have performed calendric aging tests for NMC cells in 5 % steps. The results show a linear aging trend for all cells until 95 % SoC and an exponential aging for 100 % SoC. They assume that “the disproportionally faster aging compared to other SoC, (is) probably due to electrochemical instability of the electrolyte in this potential window” (Ecker et al. S. 844 [84]). Käbitz et al. set up the theory, that the anode can be subdivided into good and bad connected parts [85]. The bad connected parts can be only charged until 85 % SoC and therefore the good connected parts are slightly overloaded, which leads to increased stress and aging for the anode at very high SoC.

A further influencing factor on the extractable capacity is the homogeneity of the lithium distribution (HLD) in the cell as described in [86, 87]. “A considerably low homogeneity might lead to less extractable capacity due to reaching the cut-off voltage earlier, or even lithium plating during charging” (Lewerenz et al. S. 4 [86]). In accordance a high HLD leads to more extractable capacity and slower aging. The constant storage conditions of the calendric aging tests (very little cycling with low c-rate and storage under floating conditions with constant temperature) increase the HLD. This leads to a smaller slope of capacity fade over time in a late stage of aging [88]. This positive influence is detected here and could also be observed in other publications [81, 82, 89]. This effect should be noted for applications, which have long resting periods without cycling. However, the battery home storage system is cycled almost daily, so this effect is not considered in the model.

3.2.5.5 Cycle aging of the battery

To determine the cycle aging of the battery system accelerated cycle aging tests were performed. The cycle aging tests are performed on macro cells. A macro cell is a parallel connection of nine single cells. This is why the presented results of the aging test are the average aging of nine battery cells. A detailed description of the macro cells is presented in [69]. To identify the cyclic aging without the calendric superposition, the calendric aging is subtracted from the cycle aging as depicted in equation (9). The cyclic aging c_{cyc} depicts the aging mechanism of the battery during operation.

$$c_{cyc} = c_{sum} - c_{cal} \quad (9)$$

Lithium Plating is a major factor and describes the formation of metallic lithium in the battery and is caused by low temperature, high c-rates and inhomogeneities inside the battery due to bad cell design and pressure differences [79]. As described in [87] for NMC cells and in [82] for LFP cells, new and unaged batteries already show inhomogeneities in the laser microscope analysis: little parts of the battery are bad connected or even isolated. This is why some lithium-ions are not settled in the graphite after the discharge process and might form metallic lithium and decrease the capacity of the battery. During the following charging process most of the metal ionizes. But parts of the metallic lithium is electrically disconnected and decreases the performance of the battery permanent, in addition this metallic lithium clogs the graphite anode and accelerates the SEI formation [79].

The loss of active material (LAM) describes the destruction of both electrodes while usage. On the cathode the mechanical stress of lithium intercalation leads to a dissolution of metallic particles, which clog the anode and increase the SEI just as the plated lithium [79, 90]. Considering the anode, the intercalated lithium leads to an volume expansion for up to 10 % [91, 92] or 13 % [93]. It is reported that this effect causes contact loss of the graphite anode, additional mechanical stress and faster aging [87, 94, 95]. Generally speaking the main aging process takes place at the graphite anode, while the NMC cathode shows good stability [81, 82, 87, 96].

Modelling the cyclic aging: DOD dependency and cycle counting

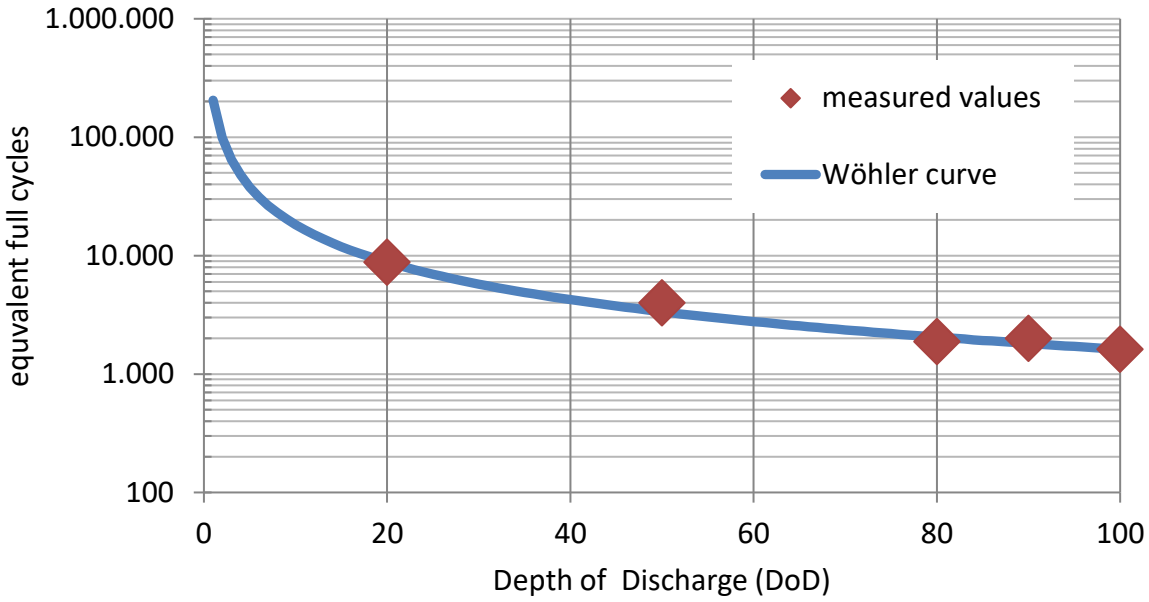

Figure 21: Wöhler curve of the LG ICR18650MF1 lithium-ion battery cell at 25°C. The equivalent full cycles until the EOL criteria for measurement points of 20 % DoD and 50 % DoD, are linear extrapolated based on the available data.

The cyclic aging is described by the Wöhler curve, which is depicted in Figure 21. This is the aging in dependency of the full cycles subtracted by the calendar aging. This is why, the given number of full cycles are a cannot be reached, because the influence of the calendar aging is not minded. The equivalent full cycles until the EOL criteria for measurement points of 20 % DoD and 50 % DoD, are linear extrapolated based on the available data. The cycle aging follows the nth root characteristic in dependency of the Depth of Discharge. The energy throughput is described by the number of equivalent full cycles $N(\Delta SoC)$. The equivalent full cycles are calculated by the sum of the energy throughput divided by the nominal capacity. The number of full cycles represents the cycle lifetime without the calendar aging. The cycle aging c_{cyc} can be calculated with equation (10).

$$c_{cyc} = a_{cyc} \cdot N(\Delta SoC)^{b_{cyc}}, 0 \leq b_{cyc} \leq 1 \quad (10)$$

The number of the equivalent full cycles can be determined with the Wöhler function. The Wöhler curve can be described with the exponential function presented in equation (11) [97] and depicts the correlation between Depth of Discharge (DoD) and the equivalent full cycles.

$$N(\Delta SoC) = a_w \cdot \Delta SoC^{b_w}, \text{ free parameters } a_w \text{ and } b_w \quad (11)$$

The performed aging tests used constant cycle depths, however in reality the cycle depths are not constant and micro and macro cycles occur. Therefore, a cycle counting algorithm is necessary. To determine the number of cycles, with respect to micro- and macro-cycles, the rainflow algorithm is used. The implemented rainflow algorithm is based on [98] and advanced in [99].

Modelling the cyclic aging: SoC dependency

Beside the dependency on the Depth of discharge, the cycle aging depends on the average SoC as well. The cycle lifetime is accelerated for low and high SoC, therefore an acceleration function is defined.

$$\mathrm{N}\left(\Delta\mathrm{SoC}, \mathrm{SoC}_{\mathrm{avg}}\right) = \mathrm{k}_{\mathrm{SoC}_{\mathrm{avg}}} \cdot \mathrm{a}_{\mathrm{w}} \cdot \Delta\mathrm{SoC}^{\mathrm{b_w}} \quad (12)$$

The acceleration function influences the number of cycles as depicted in equation (12). The acceleration function is one for $\mathrm{SoC}_{\mathrm{avg}} = 50\ \%$ and shows an exponential development as shown in equation ((13).

$$k_{\mathrm{SoC}_{\mathrm{avg}}} = \begin{cases} \dfrac{1}{\exp\left(\left(50\ \% - \left(100\ \% - \dfrac{\Delta\mathrm{SoC}}{2}\right)\right) \cdot f_{\mathrm{SoC}_{\mathrm{avg}}}\right)} & SoC_{\mathrm{avg}} + \dfrac{\Delta\mathrm{SoC}}{2} > 100\ \% \\ \dfrac{1}{\exp\left(\left(50\ \% - SoC_{avg}\right) \cdot f_{\mathrm{SoC}_{\mathrm{avg}}}\right)} & other \\ \dfrac{1}{\exp\left(\left(50\ \% - \left(0 + \dfrac{\Delta\mathrm{SoC}}{2}\right)\right) \cdot f_{\mathrm{SoC}_{\mathrm{avg}}}\right)} & SoC_{\mathrm{avg}} - \dfrac{\Delta\mathrm{SoC}}{2} < 0\ \% \end{cases} \quad ((13)$$

With $\mathrm{f}_{\mathrm{SoC}_{\mathrm{avg}}}$ free curve parameter.

With the known number of cycles, the cycle aging can be calculated with equation (14).

$$\mathrm{c}_{\mathrm{cyc}} = \mathrm{a}_{\mathrm{cyc}} \cdot \left(\mathrm{k}_{\mathrm{SoC}_{\mathrm{avg}}} \cdot \mathrm{a}_{\mathrm{w}} \cdot \Delta\mathrm{SoC}^{\mathrm{b_w}}\right)^{\mathrm{b_{cyc}}} \ \text{mit}\ 0 \leq \mathrm{b}_{\mathrm{cyc}} \leq 1 \quad (14)$$

The parameter $\mathrm{a}_{\mathrm{cyc}}$ depends on the average SoC and the DoD and is described in equation (15). The derivation of the presented cycle aging calculation is shown in [63].

$$\mathrm{a}_{\mathrm{cyc}}\left(\Delta\mathrm{SoC}, \mathrm{SoC}_{\mathrm{avg}}\right) = \frac{1}{\left(\mathrm{N}\left(\Delta\mathrm{SoC}, \mathrm{SoC}_{\mathrm{avg}}\right)\right)^{\mathrm{b_{cyc}}}} \quad (15)$$

The resulting parameters from the cell tests are shown in Table 2.

Parameter	Value	Description
b_{w}	-43.4934	Wöhler parameter
a_{w}	14254.37	Wöhler parameter
$\mathrm{b}_{\mathrm{cyc}}$	1	cycle aging parameter
$f_{\mathrm{SoC}_{\mathrm{avg}}}$	-0.014	acceleration factor cycle aging

Table 2: Input parameters for the Wöhler curve based on the cycling aging tests of the LG ICR18650MF1 lithium-ion battery cell.

Modelling the cyclic aging: phase transitions

Besides the influence of the SoC on the cycle aging, the measurement results presented in [69] show a dependency of cycle aging on phase transitions of the lithium during intercalation and deintercalation in the electrode host structure.

To identify the phase transition accelerated aging tests are performed with a constant DoD of 20 % and a variation of the SoC. The test results are depicted in Figure 22. The highest aging occurs, when the average SoC is 50 %. The reason for the accelerated aging at 50 % SoC could be the phase transition of graphite (stage 2) [68] and [100].

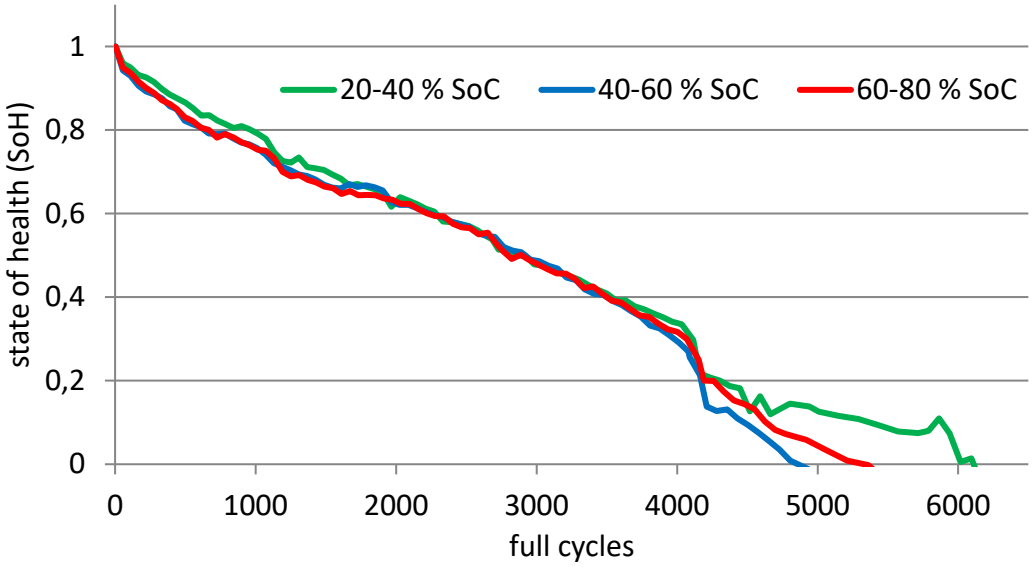

Figure 22: Results of the accelerated cycling aging tests with a constant depth of discharge (DoD) of 20 % and a variation of the average state of charge (SoC).

According to recent models the lithium intercalation into the graphite structure can be described by different stages [79, 90, 101, 102]. [103] explained it in the following way: "The stage (n) […] is determined by the number of graphene layers between two intercalant layers" (Xu et al. S.3 [103]). The first stage for lithium-ions is stage-4 and is composed of four graphene sheets in-between each lithium-ion layer. Loading the cell fills up the layers and Stage-1 is the last stage describing a fully loaded cell with one graphene layer in-between each two li-ion layers. The additional aging results from mechanical stress on the graphite anode due to transitions from the different stages [84, 104].

To detect phase transitions the differential voltage analysis ($\frac{\mathrm{dU}}{\mathrm{dSoC}}$ curve) is used. The $\frac{\mathrm{dU}}{\mathrm{dSoC}}$ curve represents the voltage gradients of the SoC regarding the SoC. The local maximums of the $\frac{\mathrm{dU}}{\mathrm{dSoC}}$ curve suggest phase transitions. The $\frac{\mathrm{dU}}{\mathrm{dSoC}}$ curve is depicted in Figure 23 and leads to the assumption that a phase transition occurs at an SoC of 50 %, 10 % and 80 %. According to [100] the peak at 50 % SoC is associated with stage transition of graphite (stage 2). The first peak around 10 to 15 % SoC is associated with other stages from graphite (stage 3 and 4). The peak at 80 % SoC could be caused by the cathode (NMC) [105]. The two other transitions at 10 % and 80 % SoC are less distinct and therefore more difficult to identify with accelerated aging tests.

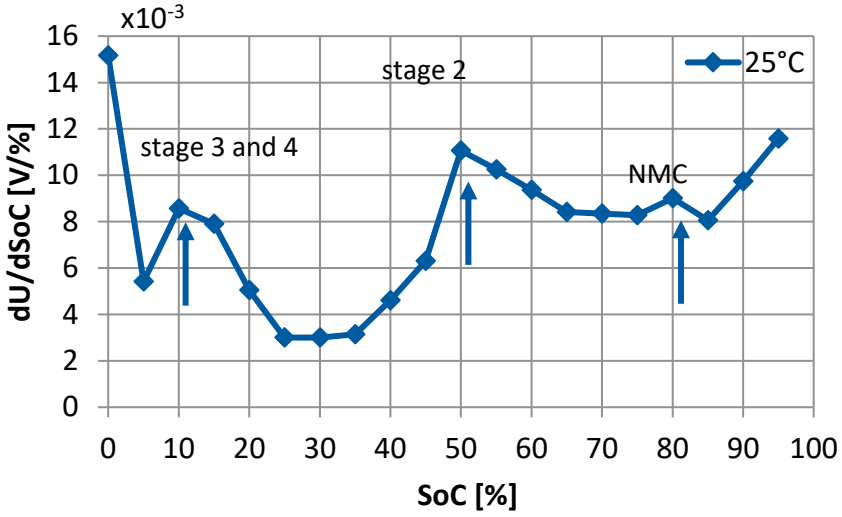

Figure 23: Voltage gradient of the SoC with respect to the state of charge ($\frac{dU}{dSoC}$ curve). The maximum at 50 % SoC implies a phase transition at 50 % SoC. This peak is associated with stage 2 of graphite [100].

To verify the effect of the phase transition the differential voltage analysis ($\frac{dU}{dSoC}$ curve) is applied during the cycle aging. The stage 2 peak changes as depicted in Figure 24. This leads to the assumption, that stage 2 transition leads to an additional aging. A reason for the additional aging might be the additional pressure in the cell. More details on the effects are given in [105] for NMC battery cells and in [106] for NCA battery cell.

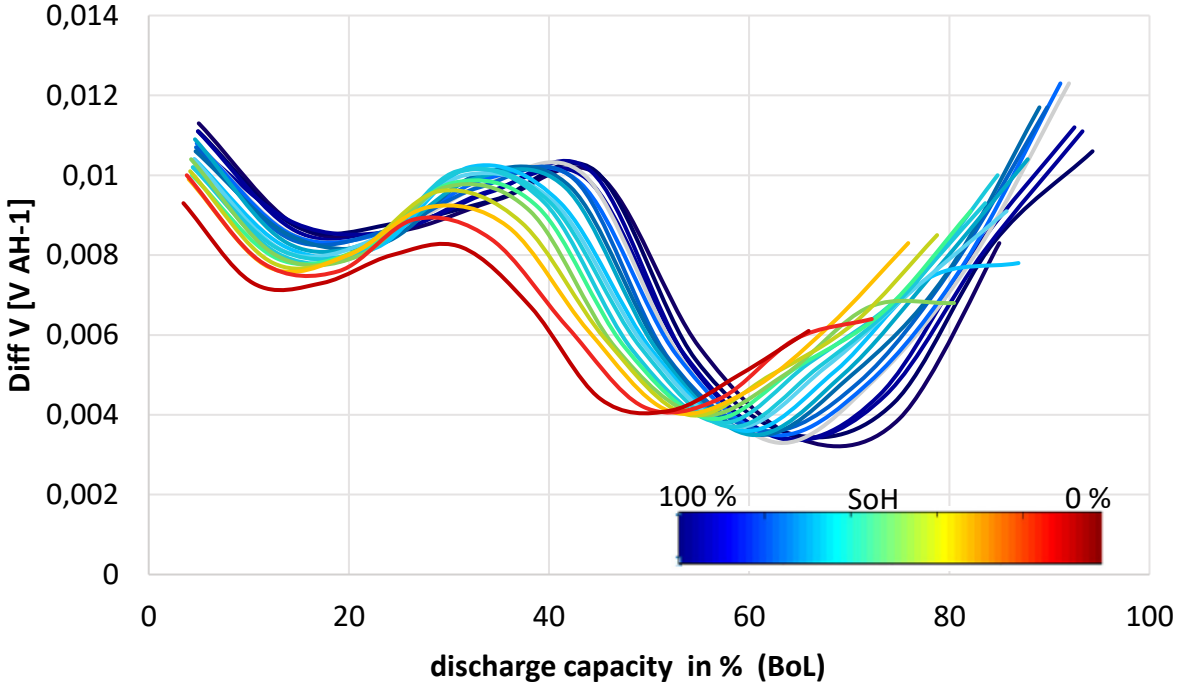

Figure 24: Differential voltage analysis ($\frac{dU}{dSoC}$ curve) of the LG ICR18650MF1 battery cell over the battery lifetime.

To model the influence of the phase transition on the cycle aging an penalty function from [63] is adopted. The penalty function increases the battery aging, if the critical SoC is passed. The critical SoC is passed, when the battery is charged from below to above 50 % SoC or discharged from above to below 50 % SoC. The penalty function is modelled as a triangular function. Additional aging is added, when the SoC passes the critical SoC of 50 %. The penalty function of the phase transition is illustrated in Figure 25.

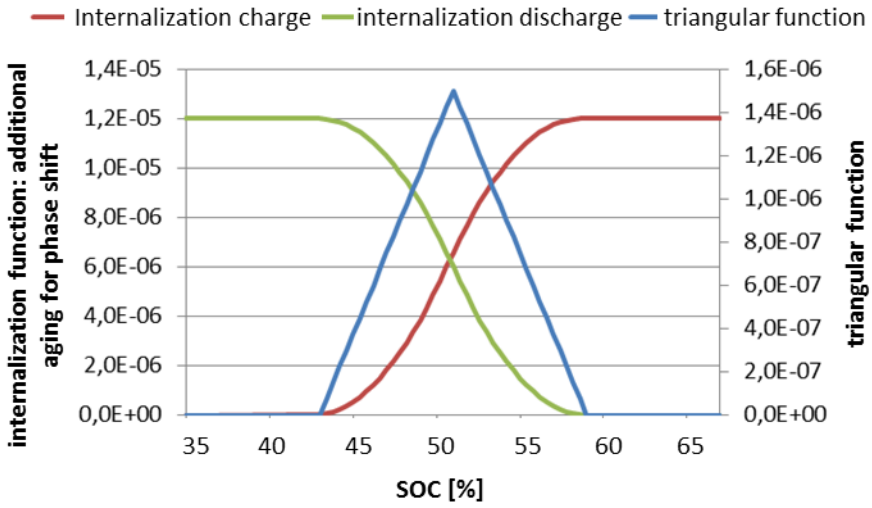

Figure 25: Triangular penalty function for to mind additional aging of phase transition regarding [69].

Validation of the cyclic aging

The measurement results and the simulation results of exemplary cyclic aging tests are shown in Figure 26 for variation of the SoC and in Figure 27 for variation of the DoD. The simulation results are close to the measurement results.

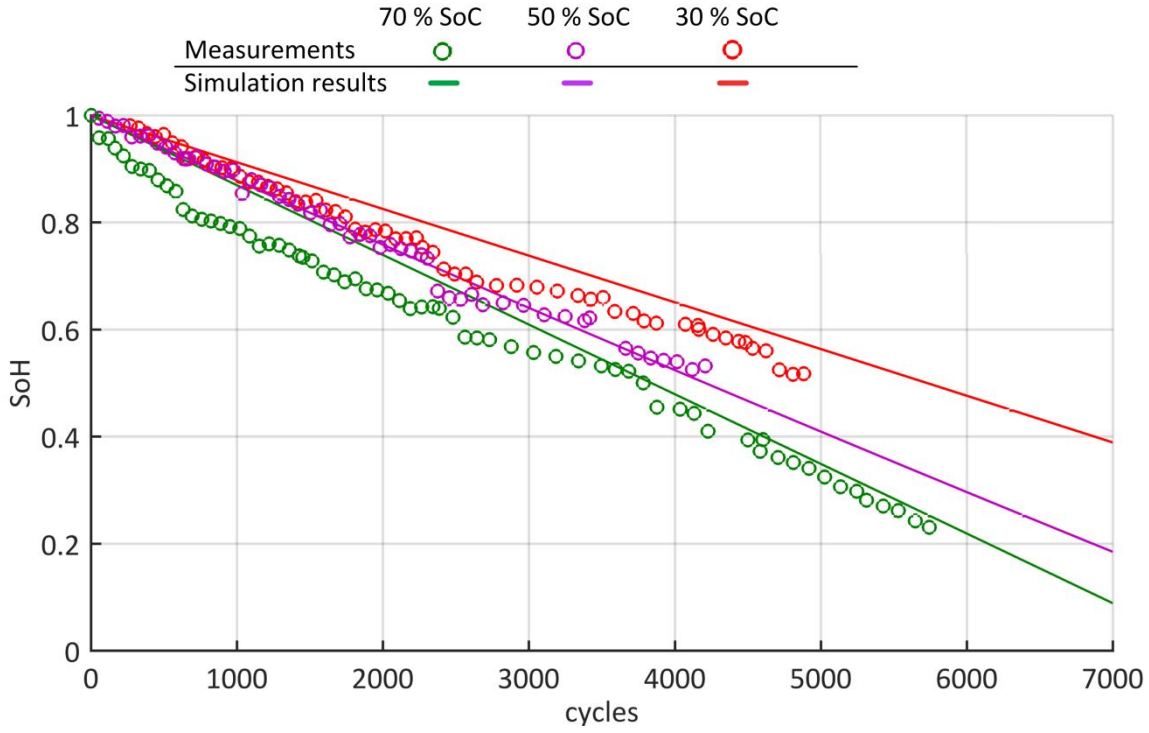

Figure 26: Cyclic aging test results and simulation: relative capacity change of the LG ICR18650MF1 lithium-ion battery cell stored at 25 °C. When the SoH is 0 % the battery has 70 % of the initial capacity left. Simulation and measurement results are depicted.

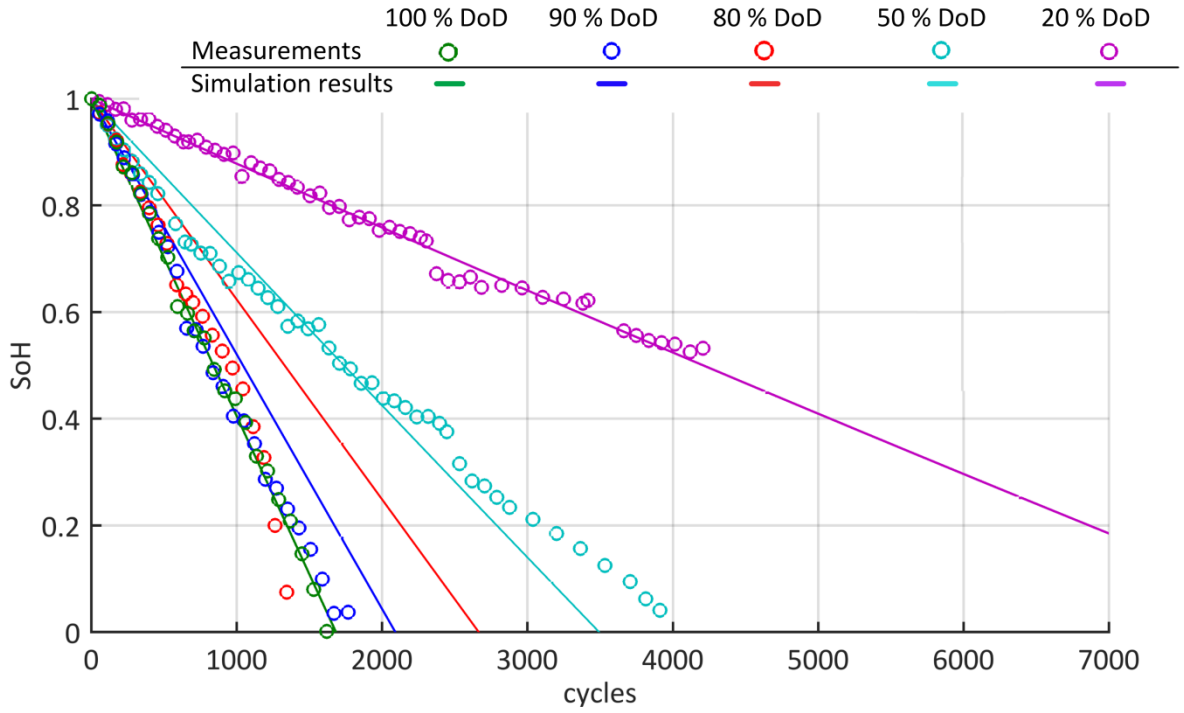

Figure 27: Cyclic aging test results and simulation: relative capacity change of the LG ICR18650MF1 lithium-ion battery cell stored at 45 °C. Simulation and measurement results are depicted.

3.2.5.6 Sudden cell-death and limits of the used model

As described, the main aging mechanism during calendric aging tests is the formation of a consistent layer on the graphite anode (SEI). The constant aging conditions lead to an improvement of the homogeneity of the lithium distribution (HLD) and a decrease of the aging slope. This positive effect in a late stage of aging should be noted for applications, which have long resting periods without cycling and does not match to a battery home storage system.
Considering the cyclic aging mechanism, usage of the battery decreases the HLD. In particular, the initial formation of plated lithium and metallic deposits from the cathode lead to pressure differences, which in turn lead to even more plating and SEI on the graphite anode [79, 87, 107]. Furthermore, the locally concentrated mix of SEI, metallic particles and plated lithium is not permeable for li-ions [82, 86, 87, 108]. This effect “rapidly alters the balancing of the electrodes, generating a self-amplifying circle of active material and lithium loss” (Bach et al. S.1 [87]). The turning point is, when these individual particles form a dense covering layer and thus deactivate great parts of the graphite anode electrically [88]. The li-ions behind this layer are inactive and decrease the capacity significantly. Research on this effect is published and a guideline for avoidance is given in [82, 88, 96]: high charging c-rates, high DoD and low temperature speed up the formation of the dense covering layer.
For many publications this sudden degradation of the capacity could be observed in the range between 80 % and 70 % remaining initial capacity [84, 85, 96]. For the model presented here an End of life (EoL) criteria at 70 % is chosen, because the battery storage system is cycled with low c-rate and kept at room temperature. Furthermore, the cyclic aging tests show that the batteries can be safely operated in this range with good simulation consistency [69].

3.3 Thermal model

The heat pump couples the thermal model and the electrical model. This heat pump supplies a heat storage system with buffer storage and domestic hot water (DHW) storage. The buffer storage is in flow line of the heating system and the DHW storage is parallel to the buffer storage based on [109]. Figure 28 shows the topology of the heating system. The model of the heat pump is presented in section 3.3.1. Different operation modes of the heat pumps are shown in Section 3.3.6. Section 3.3.2 and 3.3.3 describe the modeling of the buffer storage and the DHW storage. The building model (3.3.4) and the models of the pumps (3.3.5) are presented in the following sections.

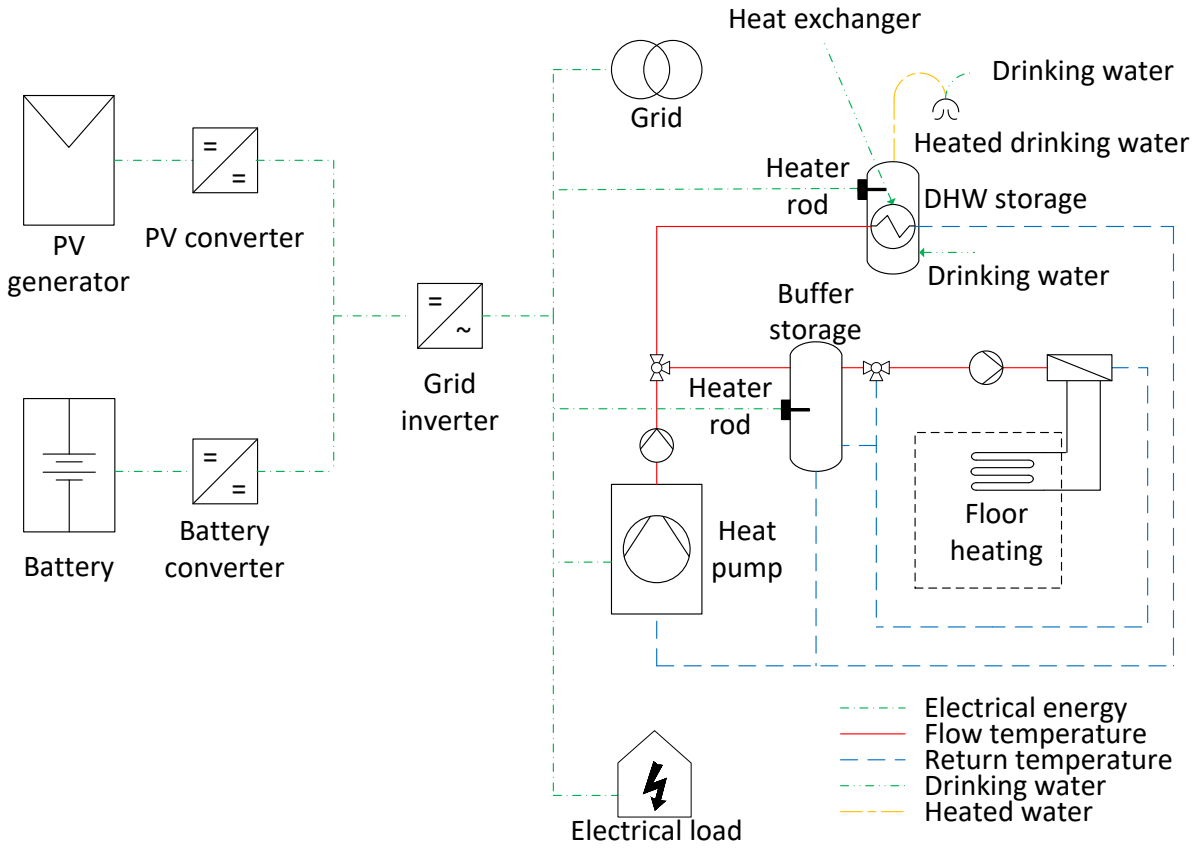

Figure 28: Model of the heating system with a heat pump, DHW storage and buffer storage. This heating system is part of the integrated home and is connected to grid and PV-BESS.

3.3.1 Heat Pump

The used heat pump model is presented in [109] and implemented in [110]. This model is parametrized based on a Vitocal 200-S split heat pump from Viessmann [111]. The model is verified in [112]. This heat pump is an air-water heat pump. The nominal thermal power of the heat pump is 10 kW and under nominal conditions (A 7 °C / W 35 °C) (air-temperature/water-temperature) the heat pump has a COP (Coefficient of Performance) of 5.1. The COP is defined as

$$\varepsilon = \frac{P_H}{P_A} \tag{16}$$

P_H represents the emitted heat power and P_A the consumed electric power. For modeling the emitted heat power and the consumed electrical power, the respective ambient temperature has to be known. These values were measured and linearized in the simulation model. Figure 29 show the measured values as well as the linearized values for the model. Figure 29 illustrates the heating power in dependency of the ambient temperature and the flow temperature. Figure 30 depicts the consumed electric power in dependency of ambient temperature and the flow temperature. The COP is proportional to the heating energy and inversely proportional to the temperature difference between the ambient temperature T_U and the room temperature T_H as depicted in equation (17) [113].

$$P_{room} \propto COP \propto \frac{1}{T_{room} - T_{ambient}} \text{ for } T_{room} > T_{ambient} \quad (17)$$

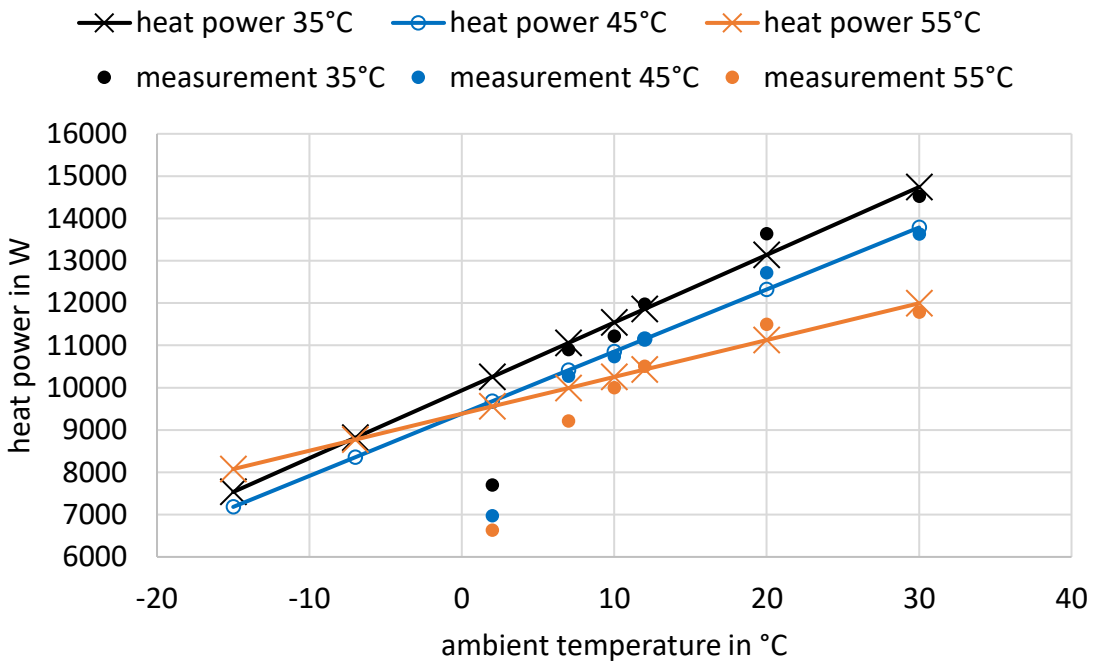

Figure 29: Heating power of the heat pump in dependency of ambient temperature and the flow temperature according to [112]. The related electrical power is depicted in Figure 30.

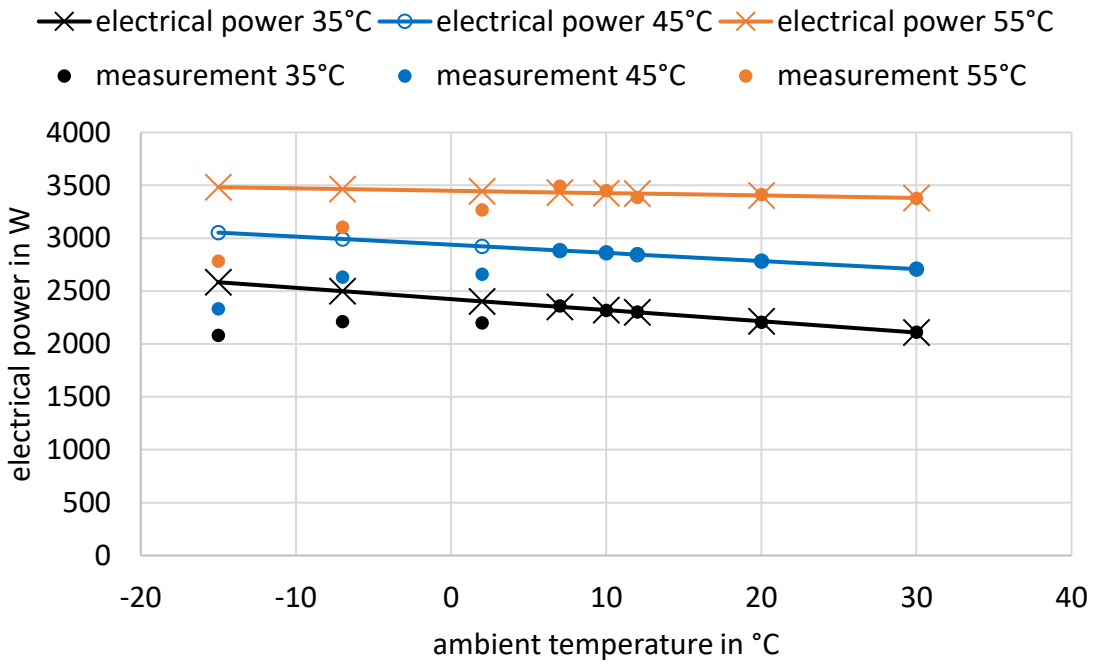

Figure 30: Consumed electric power of the heat pump in dependency of ambient temperature and flow temperature according to [112]. The related heat power is depicted in Figure 29.

With the known electrical and heating power the COP of the heat pump can be calculated. The COP depends on the ambient temperature as well as on the flow temperature as shown before. This is illustrated in Figure 31.

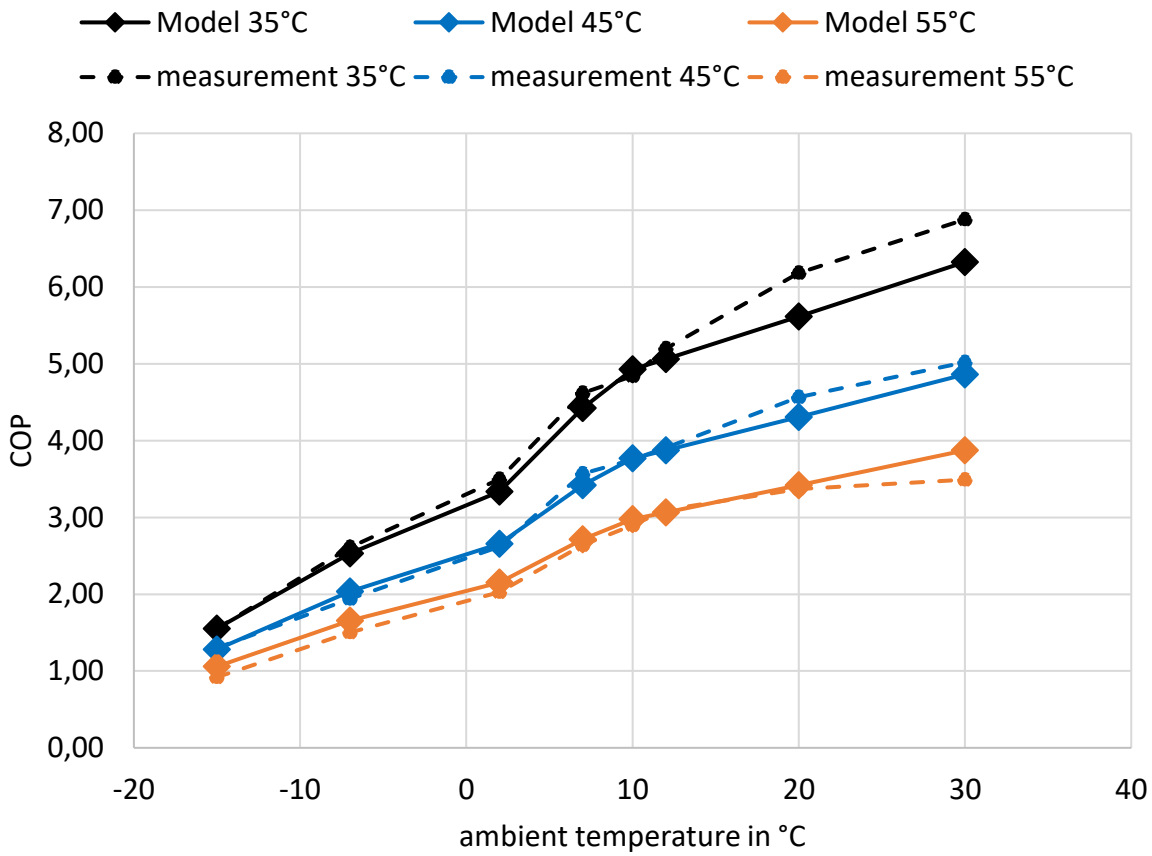

Figure 31: COP in dependency of the ambient temperature and the flow temperature according to [112].

With increasing ambient temperature, the deviation between values in the model and measured values is increased. This effect is neglected since the ambient temperature is rarely around 30 °C. The values from Figure 29 and Figure 30 are used in look-up tables in the simulation model. These values are interpolated. Furthermore, the air defroster as well as the fan, which sucks the air into the vaporizer, is modelled. The modelling is presented in [110].

3.3.2 Buffer storage

The heat storage is implemented as a stratified system with multiple layers. The volume of storage is divided in five layers of horizontal slices. Each layer has a defined temperature range within it is operated. Interactions with adjacent layers are considered. The lower and upper temperature of each layer and the respective volume – as a fraction of the total volume of the storage – define its thermal capacity. The heat losses of the storage are calculated separately for each layer, depending on the respective temperature in every time step. Therefore, for

each layer the energy balance equation according to [114] is solved. A heat loss coefficient of 1 W/(m²K) is assumed. The initial temperatures range from 32 °C to 40 °C in 2 K steps.

To determine the size of the buffer storage, the mass flow m_F of the water in the buffer storage has to be determined. Therefore, the following rule of thumb is used:

$$m_F = \frac{P_H \cdot t_{min}}{c_F \cdot \Delta T} \tag{18}$$

P_H describes the heat power (10 kW) of the heat pump and ΔT describes the temperature spread between water output and water input. ΔT is approximately 10 K [115]. c_F describes the heat capacity of the water and t_{min} the minimum runtime of the heat pump. The minimum runtime is 20 minutes. Therefore, the minimum volume of the heat buffer storage is presented in equation (19). Equation (19) is based on equation (56) in section 5. Section 5 presents the equations for the minimum volume in the optimization algorithm.

$$m_F = \frac{10\ \text{kW} \cdot 20\ \text{min}}{1.163\ \frac{\text{Wh}}{\text{kg} \cdot \text{K}} \cdot 10\ \text{K}} = 287\ \text{kg} \tag{19}$$

This is why the parameterization of the buffer storage is based on a real storage from Schindler und Hoffmann which contains 300 l [116].

3.3.3 Domestic hot water storage

The DHW storage is similar to the buffer storage, but additionally the DHW storage contains an electric heater and a heat exchanger. The heat exchanger separates the heating water from the drinking water. The input energy is calculated with the integral over the heating power.

$$Q_{Input} = \int \dot{m}_F \cdot c_F \cdot (T_{flow,Input} - T_{return,Input})\, dt \tag{20}$$

$T_{flow,Input}$ is the flow temperature of the heating water and $T_{return,Input}$ is the return temperature of the heating water. Accordantly the output energy Q_{Output} is calculated under consideration of the drinking water temperature T_{Output}. The spreads between input and output energy are the thermal losses of the DHW storage. The thermal losses of the DHW storage are calculated based on the publications [117]. A further insight of the thermal loses is given in [118]. Further information of the model of the DHW storage can also be found in these publications.

$$Q_{Output} = \int \dot{m}_F \cdot c_F \cdot (T_{flow,Output} - T_{return,Output})\, dt \tag{21}$$

For a four person household a 300 l DHW storage is recommended [115]. Therefore DHW storage from Schindler und Hofmann is used for parameterization [119].

3.3.4 Model of the building

The building model consists of different sinks (walls, windows etc.) and a floor heating as a source block. The building model is based on the “Conventional And Renewable eNergy

systems Optimization Toolbox“ (CARNOT) for Matlab/Simulink [120]. The modeled house is a bungalow with 110 m^2 building area, which is built according to EnEV 2013 [121]. The mass of the building is able to store heat energy and has the storage capacity of concrete. The total storage capacity of the building is 16 kWh/K. The calculation of the total storage capacity of the building is presented in the annex in Annex Table 1. Heat transfer from the windows, ceiling and walls are considered. The dynamic convective heat transfer coefficients are modeled according to [122]. A constant air ventilation rate of $0.5\frac{1}{\mathrm{h}}$ [123] is assumed. The house is equipped with a floor heating system. The floor heating systems are applied to reduce the flow temperature of the heat pump. The hot water consumption is based on a static time series generated with „Domestic Hot Water (DHW) calc“ [124] tool. A hot water consumption of 200 l/day for the four-person household is chosen, based on [125].

3.3.5 Pumps

For the transport of the heating water, pumps are modeled. These pumps transport the heating water from the heat pump to the heat sinks of the house (buffer and DHW storage, floor-heating systems). The pumps are controlled, so that the mass flow can be adjusted. Furthermore, the pumps ensure a satisfying mass flow for the heat pumps. The pumps require electrical energy, which is considered in the electrical energy consumption of the heating system.

3.3.6 Modular Heat Pump

As mentioned in section 3.3.1, the heat pump model is based on a Vitocal 200-S heat pump from Viessmann. To optimize the size of the heat pump, a modular heat pump-model is necessary. The COP of the heat pump is reduced when the thermal power of the heat pump is reduced [111]. Figure 32 shows this COP in relation to the thermal power with respect to different operating points. Therefore, the COP of the heat pump is scaled to illustrate this effect. The modified parameters in comparison to the parameters of the heat pumps, based on the datasheets, are shown in Figure 32.

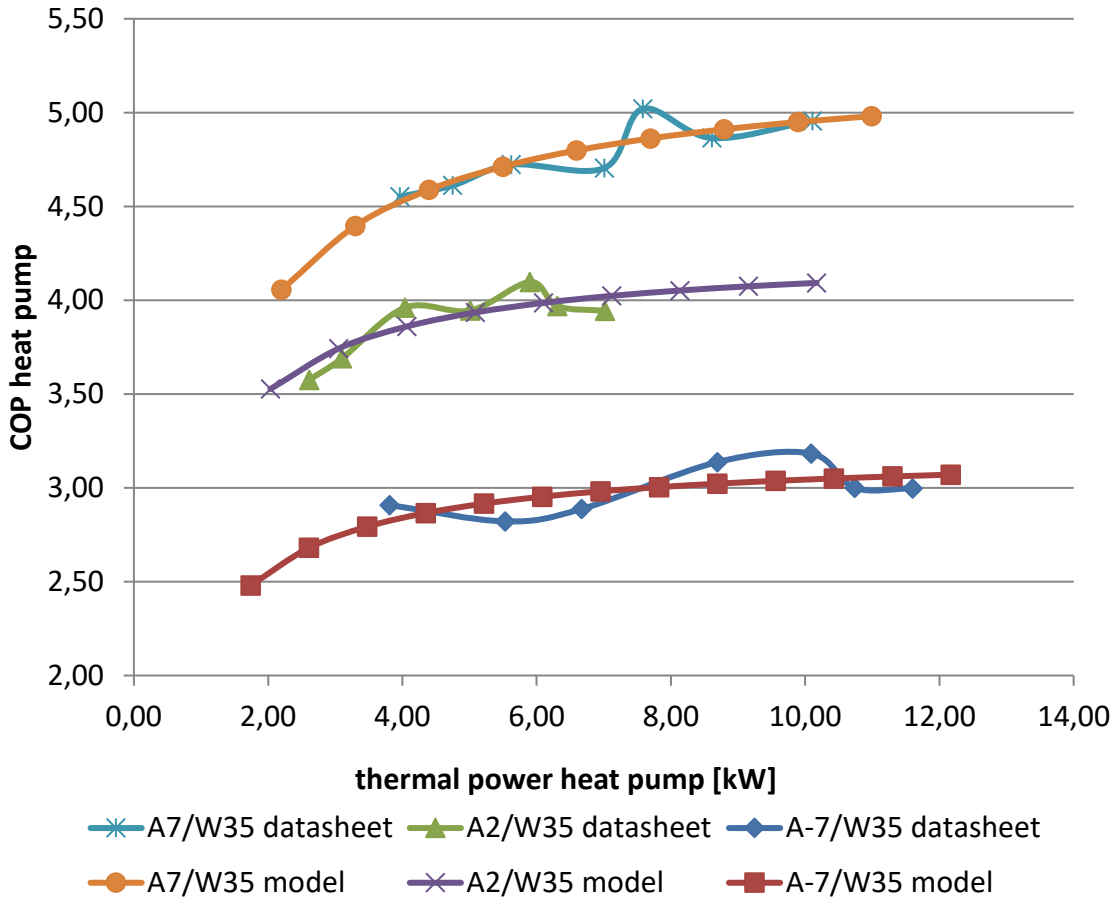

Figure 32: Comparison of simulation results and manufacturers data [111] for the COP subject to the thermal power of the heat pump. Different operation points of the heat pumps are analyzed. The operation points are defined as the ratio between air- or ambient temperature and water- or flow temperature (A/W).

Modern inverter-based heat pumps are able to adapt their output power in dependency of a set input power by frequency adjustment. Therefore, they are able to operate modularly. The flexibility, as a result of modular operation, can be used to compensate variations of solar radiation. The power as a share of the maximum power A_{HP} is calculated with equation (22):

$$A_{HP} = \frac{(P_{PV} - P_{load})}{P_{maxHP}} \quad (22)$$

The heat pump is only operated modularly if residual energy from the PV generator is available. If heat power is necessary for room heating or hot water, the heat pump is operated with maximum power. Figure 33 shows the heat consumption of the heat pump, if the heat pump is operated in either modular or static mode.

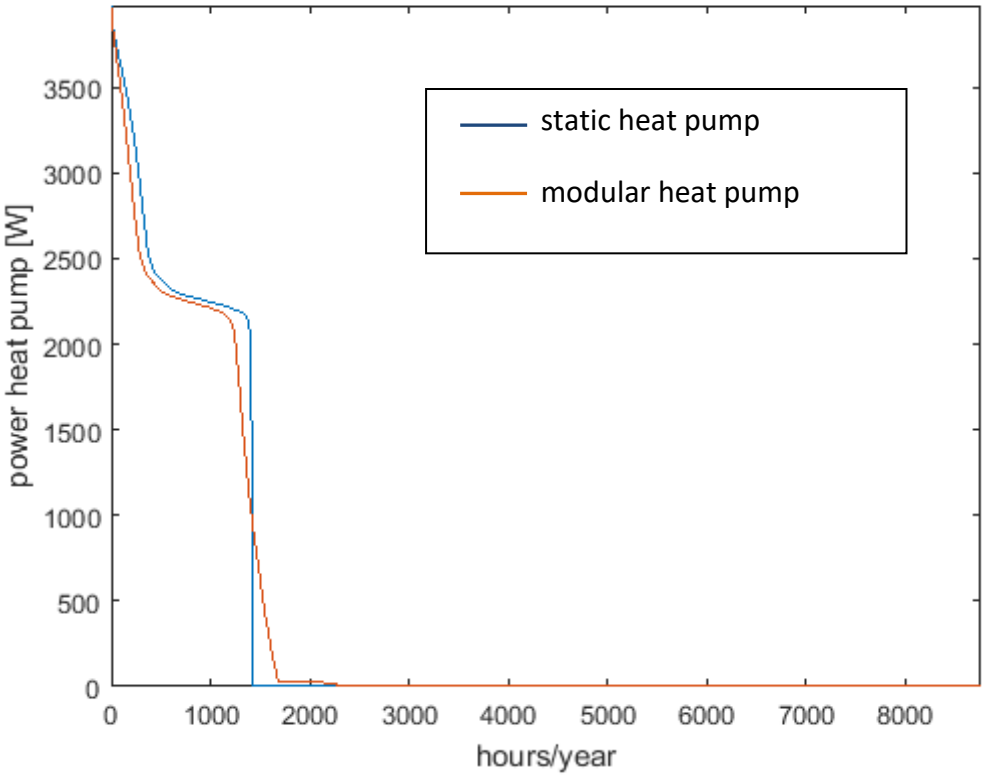

Figure 33: Comparison modular heat pump and static heat pump (pareto chart). If the heat pump is operated in modular mode, the operating duration can be prolonged.

3.4 Component sizes non-optimized integrated home

The sizes of the integrated home are based on typical sizes for commercially available components and the component sizes used for parametrization. Both storage systems have a volume of 300 l as recommended for a four person household [115]. The simulated BESS has a storage capacity of 10 kWh, according to typical sizes of commercially available systems with the highest market penetration [13]. This model is parametrized with measurement data of a Vitocal 200-S split heat pump from Viessmann [111] with a thermal heating power of 10 kW_{th}. Table 3 depicts the component sizes of the non-optimized integrated home, which is used to calculate the influence of different operation strategies and the participation on the control reserve market. The presented sizes are typical component sizes for residential households. Except of the inverter size, which is oversized to offer control reserve (section 7).

Electric system	size	Heating system	size
PV power plant	10 kW	Heat pump	10 kW_{th}
converter sizes	10 kW	DHW storage	300 liter
inverter	10 kW	Buffer storage	300 liter
Li-ion battery	10 kWh		

Table 3: Component sizes of the non-optimized integrated home.

3.5 Economic Evaluation

The economic evaluation of the integrated home is based on the annuity. The annuity incorporates all costs over the system's lifetime. Since each component has a different lifetime, investment costs, operation costs, maintenance costs, the annuity has to be calculated for every component individually. The annuity is the sum of the investment costs A_I, the variable costs A_V and the fix costs A_F. The calculation of the annuity is presented in section 3.5.1. Based on the annuity the levelized costs can be calculated as presented in section 3.5.2. The input data for the calculation are presented in section 3.5.3.

3.5.1 Calculation of the annuity

The annuity is calculated with equation (23). The product of the annuity factor F_A and the net present value (NPV) of the component is resulting in the annuity of the investment cost.

$$A_I = F_A \cdot NPV_I \tag{23}$$

The annuity factor can be calculated with equation (24) considering the interest rate i.

$$F_A = i + \frac{i}{(1+i)^{t_{calc}} - 1} \tag{24}$$

The NPV approach in finance uses the difference between the present value of cash flows and the present value of cash flows over a period under investigation. The net present value incorporates the adjustments for inflation and discount rates over time and enables an assessment at present time values. The interest rate i represents an alternative reference investment and incorporates inflation. The discount rate d represents savings by cost regression or additional cost due to a price increase. The net present value is time-dependent, since the time of the cash flow determines the influence of interest and discount rate. Therefore, the net present value calculation is calculated for the time t_{calc} with equation (25), minding the costs C_j in every time step. L represents the lifetime of the component and d represents the costs degression.

$$NPV_I = \sum_{j=0}^{t_{calc}-1} \left(\frac{1+d}{1+i}\right)^j \cdot C_j(d, L) \tag{25}$$

The NPV has to be calculated for every component individually. Therefore, the NPV for the battery as well as the NPV for the three converters and the PV system has to be calculated. Cost for reinvest as well as savings, because of residual values at the end of the simulation, are taken into account accordingly. Due to economics of scale the costs for BESS are expected to decrease [126]. The cost degression in case of a reinvest is taking into account. The NPV depends on the lifetime of the component, since the lifetime determines the point in time of the reinvestment. The costs are the product of the specific costs and the size of the component. In equation (26) the costs for the batteries are calculated. The costs for the three converters, the PV generator, the buffer and DHW storage, the heat pump and the pumps are calculated accordingly.

$$C_{bat} = c_{bat} \cdot cap_{battery} \tag{26}$$

The variable costs consist of the cost for the grid exchange, concerning the net present value of the electricity costs and earnings due to the PV feed-in tariff.

$$A_V = F_A \cdot NPV_V \tag{27}$$

The NPV of the variable costs are calculated similar to equation (25), but do not have to incorporate a lifetime.

$$NPV_V = \sum_{j=0}^{t_{calc}-1} \left(\frac{1+d}{1+i}\right)^j \cdot C_j(d) \tag{28}$$

The revenues for the feed-in depend on the energy fed into the grid. Since the feed-in tariff is guaranteed over 20 years, this value remains constant.

$$C_{j,feed-in} = c_{feed-in} \cdot E_{feed-in} \tag{29}$$

The changes of the electricity prices are evaluated by using an electricity price-increasing factor. The annual costs for electricity can be calculated with equation (30).

$$C_{j,grid\ consumption} = c_{electricity}(1 - d_{electricity}) \cdot E_{grid\ consumption} \tag{30}$$

The annuity of the fix cost term depicts the maintenance cost for each component. Therefore, the investment costs of the components and the factor $f_{maintenance}$ are taken into account.

$$A_F = C_j \cdot f_{maintenance} \tag{31}$$

3.5.2 Calculation of the levelized costs

Based on the annuity, the levelized costs (LCO) can be calculated for an inter-sectorial comparison. For the calculation of the levelized costs of energy (LCOEnergy), the weighted sum of the levelized costs of heat (LCOH) and the levelized costs of electricity (LCOEle) are used. With this separate consideration of the LCOH and the LCOEle, an inter-sectorial evaluation is possible. The following formula depicts the calculation of the LCOEnergy.

$$LCOEnergy = LCOH \cdot \frac{Q_{heat}}{E_{total}} + LCOEle \cdot \frac{E_{elect}}{E_{total}} \tag{32}$$

$$E_{total} = E_{elect} + Q_{heat} \tag{33}$$

The LCOEle are the net present value of the unit-cost of energy for the lifetime of a generating asset [127]. Therefore, the annuity of the electric system is divided by the electricity consumption. The following equation (34) depicts the formula to calculate the LCOEle.

$$\mathrm{LCOEle} = \frac{\mathrm{A_I} + \mathrm{A_v} + \mathrm{A_F}}{\sum_{t=1}^{n} \mathrm{E_t}} = \frac{\mathrm{Asum_{total}}}{\sum_{t=1}^{n} \mathrm{E_t}} \quad (34)$$

The LCOH is the present value of the unit cost of heat over the lifetime of a generating asset and therefore calculated with the same method as the LCOEle. The load of the heating sector can be covered either by the PV panel or by the grid. This might lead to additional battery costs or savings if the lifetime of the BESS is influenced by the heat system.
To consider this, the calculation of the LCOH is made in two steps. At first, the annuity value of the overall balance of costs and revenues ($\mathrm{Asum_{total}}$) is calculated with the operation of the heat system. In this case, the investment costs include the cost for the electric system as well as the cost for the heat system. Furthermore, the variable costs include the consumption of electricity of the heat system and the electric system. In a second step, the annuity value of the overall balance of costs and revenues of the electricity system ($\mathrm{Asum_{ele}}$) without the heat system is calculated. The annuity value of the overall balance of costs and revenues of the heat system ($\mathrm{Asum_{heat}}$) is the difference between these two costs and it is calculated with the following formula.

$$\mathrm{Asum_{heat}} = \mathrm{Asum_{total}} - \mathrm{Asum_{ele}} \quad (35)$$

The resulting LCOH are the calculated annuity costs divided by the total heat consumption.

$$\mathrm{LCOH} = \frac{\mathrm{Asum_{heat}}}{\sum_{t=1}^{n} \mathrm{H_t(i,d)}} \quad (36)$$

$\mathrm{H_t}$: Heat consumption in t

3.5.3 Input data for economic evaluation

The target of the optimization presented in section 0 is to increase the economics of integrated homes. Therefore, the target function is to minimize the annuity of the integrated homes.
Table 4 and Table 5 provide an overview of the input data of the model. The investigated integrated house is located in Lindenberg (Tauche, Berlin). The load is based on [128] resulting in an electrical demand of 4,674 $\mathrm{kWh_{el}}$/a. The thermal demand depends on the operation of the heating system, because the COP of the heat pump depends on flow temperature. The economic parameters for the calculation of the LCOEle are depicted in Table 4. Table 5 illustrates the input parameters for the LCOH calculation.

Parameter	Value	Unit	Description
t_{calc}	15	a	calculation period for invest assessment
i_{calc}	1.3	%/a	interest rate [63]
$c_{bat,NMC}$	250	€/kWh	specific battery cost
$c_{bat,NCA}$	550	€/kWh	specific battery cost [63]
i_{bat}	7	%/a	annual battery cost degression [63]
$d_{bat,KfW}$	13	%	subsidy rate on battery investment cost from KfW funding Q3 and Q4 2017 [129]
c_{conv}	equ. (37)	€/kW	specific converter cost of one converter, the model contains three converters
L_{conv}	20	a	converter lifetime [63]
c_{PVgen}	1170	€/kWp	specific PV generator cost [63]
L_{PVgen}	20	a	converter lifetime [63]
$c_{feed-in}$	0.122	€/kWh	feed-in tariff (Sep. 2017) [130]
$c_{electricity}$	0.292	€/kWh	electricity costs (Sep. 2017) [131]
$i_{electricity}$	1.85	%/a	annual electricity price increase [63]
$i_{maintenance}$	1.5	%/a	annual maintenance cost relative to investment cost [63]
c_{EPEX}	0.0367	€/kWh	average price EPEX 2017 [132]

Table 4: Input data for LCOEle calculation [133].

Heat system

Parameter	Value	Unit	Description
$c_{heat\ pump}$	equ. (38)	€	specific costs heat pump
c_{buffer}	equ. (39)	€	specific costs buffer storage
c_{DHW}	equ. (40)	€	specific costs DHW storage
$c_{pump\ DHW}$	150	€	costs DHW pump [134]
$c_{pump\ heat}$	150	€	costs heat system supplying pump [134]
$c_{heater\ rod,buffer}$	275	€	costs heater rod buffer storage [135]
$c_{3\ way\ valve}$	300	€	costs 3 way valve [136]
$c_{elec.\ installation}$	500	€	costs elec. installation [137]
$i_{maintenance,HP}$	150	€/a	annual maintenance costs of the heat system [137]
$L_{heat\ pump}$	20	a	heat pump lifetime [138]
$L_{heater\ rod}$	25	a	heater rod lifetime [139]
$L_{storage}$	25	a	storage lifetime [138]
$L_{3\ way\ valve}$	20	a	3 way valve lifetime
$L_{elec.\ installation}$	20	a	elec. installation lifetime [139]
L_{pump}	10	a	pump lifetime [138]

Table 5: Input data for LCOH calculation [140].

The specific converter costs of one converter are calculated with equation (37) and they are based on a market research done in [141]. The electric model contains three converters; a DC-topology is used.

$$c_{conv} = \min\left(1000, \frac{970.3 \cdot (\frac{p_{conv}}{kW})^{-1.957} + 304.5}{2}\right)\frac{€}{kW} \quad (37)$$

c_{conv}	=	specific converter cost of one converter	[€/kW]
p_{conv}	=	maximum power of one converter	[kW]

Similar to the calculation of the converter costs, the calculation of the specific costs of the heat pump and the thermal storages is based on formulas (38), (39) and (40). The equations are based on market research. Therefore, the prices for different sizes of the heat pump [111] and storages (buffer storage [116] and DHW storage [119]) have been analyzed. The costs are calculated using linear interpolation.

$$C_{heat\ pump} = 1{,}119.25\ € + 801.11\ \frac{€}{kW} \cdot p_{heat\ pump} \quad (38)$$

$C_{heat\ pump}$	=	costs heat pump	[€]
$p_{heat\ pump}$	=	thermal power heat pump	[kW]

$$C_{buffer} = 480.33\ € + 656.53\ \frac{€}{m^3} \cdot V_{buffer} \quad (39)$$

C_{buffer}	=	costs buffer storage	[€]
V_{buffer}	=	volume buffer storage	[m³]

$$C_{DHW} = 62.90\ € + 3{,}337.10\ \frac{€}{m^3} \cdot V_{DHW} \quad (40)$$

C_{DHW}	=	costs DHW storage	[€]
V_{DHW}	=	volume DHW storage	[m³]

To enable the possibility for a comparison of different heating concepts, the costs of radiators are not taken into account. The costs of material and installation of floor heating depend on the size and geometry of the building. Therefore, a statement on precise total costs is difficult to make.

The specific battery costs represent the cost for a battery module and incorporate the cost for the battery cells and assembling, but exclude cost for the converter. With regard to recent market research, the NMC battery cells by LG Chem can be purchased for 163 €/kWh and probably cheaper in larger quantities [142]. With respect to the cost for assembling, a module price of 250 €/kWh is estimated. The NMC battery cell represents a low-cost and low-performance consumer variant that is currently not representative for batteries used in PV BESS. The NCA battery cell on the other hand is a high-performance cell already used for this type of application. The main difference is the lifetime expectancy provided by the manufacturers. The price for the NCA battery cell is based on [63].

The economic evaluation is used to compare the different operation strategies and used as the target function for the optimization. The optimization requires linearized values for the evaluation. Therefore, the economic values and the model are described with the presented

functions. Additionally, the economic evaluation is used to compare an operation of the investigated home with and without participation on the control reserve markets. In this thesis, it is evaluated if the additional incomes from market participation exceed the additional costs for market participation.

4. Behind the Meter: Operation

This section investigates different operation strategies for integrated homes. The goal is to reduce the costs of the integrated home behind the meter. Therefore, the integrated home aims to reduce the energy purchase from the grid, while enhancing the grid feed-in. The integrated home has an electrical and a heating part. In section 4.1, operation strategies for the electrical part are investigated. In the beginning of the section a literature review is given. Operation strategies for the heating sector are presented in section 4.2. This section provides a literature review as well. Three different ways to combine the operation strategies of the electrical part and the heating part are presented in section 4.3. Some of the presented operation strategies use forecasts. Section 4.4 presents two different forecast methods: the perfect and the persistence forecast. The perfect forecast is used as a best-case scenario and the persistence forecast is used as the worst-case scenario. The presented operation strategies for the electricity part are investigated in section 4.5. Additionally, the influence of different system topologies is investigated in section 4.6. Section 4.7 investigates the operation of integrated homes. In this section, the operation strategies of the heating system as well as the combination of electrical and heating operation strategies are examined. The conclusions for the operation of integrated homes are presented in section 4.8.

4.1 Operation strategies for battery energy storage systems

Section 4.1 presents a new forecast-based operation strategy to enhance the battery lifetime and therefore the economics of PV battery energy storage systems (4.1.6). To increase the lifetime of PV BESS, forecast-based operation strategies are used to limit the average state of charge (SoC) of the battery by storing only the amount of energy predicted to be needed during the following night. The lifetime of the lithium-ion battery systems can be increased, because higher SoC conditions lead to faster aging, as shown by the evaluation of the aging tests in section 3.2.5 and in various publications e.g. [68, 143]. With these strategies, the lifetime of PV battery energy storage systems can be enhanced without drastic reduction of the self-consumption rate. This is an advantage in comparison to the fixed state of charge (SoC) limit investigated in [63].
These newly developed operation strategies are compared to commonly known operation strategies. Therefore, an overview of different operation strategies is provided in this section. This enables an understanding of the importance of intelligent operation strategies for BESS and of the advantages and disadvantages of certain operation strategies. All strategies are explained in detail and the mathematics behind these strategies are presented.
To evaluate the influence of forecast inaccuracies, two different methods of forecast algorithms are introduced. The perfect forecast represents the best case and the persistence forecast represents the worst case (4.4). These operation strategies are applied to the DC-coupled model of a PV BESS presented in section 3.2. To evaluate the performance of the different strategies, the levelized costs of electricity (LCOEle) are used (3.5).

Due to the use of persistence forecasts, the presented operation strategy can be implemented without an additional communication interface. More advanced forecast concepts can further enhance the efficiency of the operation strategy.
The forecast-based operation strategies to enhance battery lifetime are combined with strategies to reduce cut-off energy, as suggested in [144]. Two different strategies to store cut-off energy are investigated: the fixed feed-in limitation and the variable feed-in limitation. Additionally, two different forecast methods are investigated: perfect forecast and persistence forecast, similar to [145]. The effectiveness of the presented operation strategies is investigated with simulations using a model of a DC-coupled PV BESS. The influence on battery lifetime is investigated on parameter sets for two different battery cell types implemented in the model. These are based on the results of extensive lithium-ion cell tests that are also presented in detail.
Different combinations of the strategies are discussed as well as the influence of the KfW funding (see section 4.1.1), which results in lower investment costs but decrease possible feed-in revenues. Furthermore, the influence of the battery size is discussed in this section. Sensitivity analyses regarding feed-in limitations, different profiles for load and solar radiation are investigated to validate the positive influence on the economics of the home storage system provided by the developed operation strategy. The optimal system configuration in dependency of the operation strategy is presented in section 5.3.1.

4.1.1 Literature review operation strategies BESS

Different operation strategies for residential PV battery storage systems are investigated in numerous publications. The most common operation strategy is the maximization of self-consumption. This operation strategy is addressed in different publications. In [40], Luthander et al. investigate the PV self-consumption in buildings. Their findings show that the potential for increased self-consumption is higher with battery storage than by demand side management. Braun et al. investigate battery storage systems to enhance PV self-consumption and conclude that PV battery systems increase the local consumption of PV energy at the point of common coupling [66]. The enhancement of the self-consumption rate in households with an electric vehicle with home charging is investigated in [146]. The increased rate of utilization of residential photovoltaic generation by electric vehicle charge-discharge control is examined in [147].
Furthermore, the operation of PV battery storage systems under consideration of different feed-in tariffs is investigated. Schreiber et al. examine capacity-dependent tariffs and residential energy management for photovoltaic storage systems [148]. Ratnam et al. investigate battery storage with solar PV operation strategies under consideration of feed-in tariffs and conclude that the majority of customers exhibited annual savings in the context of feed-in tariffs [149]. Hassan et al. investigate the optimal battery storage operation for PV systems with tariff incentives [150].
Further publications focus on operation strategies to enhance the battery lifetime. Li and Danzer investigate optimal charge control strategies for PV BESS and conclude that the battery lifetime is prolonged by minimizing the dwell time at high states of charge [143]. To minimize the dwell time at high states of charge, a fixed maximum state of charge limit is used in [63]. Additional operation strategies, e.g. limiting the charging power [151] or delayed charging [152] are discussed as well.

Another important topic is the influence of PV systems on the distribution grid and the role of battery storage systems. In [153], PV BESS with limited feed-in power and their impact on the distribution grid are examined. Similar results are shown in [154], with focus on curtailment in distribution grids with high PV penetration. The limitation of PV feed-in power in combination with battery energy storage systems is discussed in this thesis as well.
An incentive to use PV BESS in Germany is the funding scheme introduced in 2014 by the KfW Group, a German banking group focused on economic development [129]. To receive the funding, the KfW Group demands additional grid relief of a funded PV BESS in the form of a reduction of PV power feed-in to a maximum of 50 % of the rated PV power [13]. This reduction of the feed-in power leads to loss of energy that cannot be fed into the grid. This energy is called cut-off energy. Forecast-based operation strategies can reduce the cut-off energy, as shown in a study by HTW-Berlin [144]. Two different strategies to store the cut-off energy are investigated: the fixed feed-in limitation and the variable feed-in limitation [155]. The influence of forecast-based operation strategies on the grid are investigated in [145]. This thesis compares a persistence forecast and a perfect forecast algorithm as forecasting methods. A comparison of different operation strategies under consideration of feed-in limits is conducted in [156]. The reduced impact on the energy system when using a forecast-based operation is investigated in [157]. The authors conclude that forecast-based strategies for grid-friendly operation are less profitable. Other publications focus on operation strategies for PV BESS in micro grids [158].

4.1.2 Operation strategies

A huge variety of different operation strategies for PV BESS exists. The most common ones are direct self-consumption and a fixed SoC limit to reduce the battery aging. These strategies are compared with forecast-based operation strategies that pursue the goal of reduced battery aging as well. Furthermore, operation strategies to gain grid relief are introduced. Some of these strategies use forecasts to reduce the power feed-in to the grid. This might be necessary e.g. to obtain the KfW funding for PV BESS in Germany [129]. Table 6 shows the discussed operation strategies and the sections in which they are discussed. Furthermore, the abbreviations, to identify the strategies, are shown. The two different kinds of strategies are limiting the SoC to reduce battery aging and limiting the feed-in power of the PV systems to gain grid relief. Table 6 gives an overview of the discussed strategies divided into these two categories. Furthermore, a classification is given on how the feed-in limitation is realized.

		limiting SoC		
		no limit	fixed limit	variable limit
limiting power	no limit	max SC (4.1.4)	fix SoC (4.1.5)	FOS (4.1.6)
	fixed limit	fix P (4.1.7)	fix SoC, fix P(4.1.8)	FOS fix (4.1.9)
	variable limit	X	X	FOS variable (4.1.10)

Table 6: Overview of PV BESS operation strategies and their abbreviations and inter-dependencies (section numbers in parentheses).

4.1.3 PV power plant without BESS

In a household with a PV power plant, without battery storage system, the aim is to cover as much of the occurring load of the household directly with the energy from solar generation as possible. Therefore, the goal of this strategy is to maximize the direct consumption of the PV-generated energy. If the residual power at the grid connection $P_{Residual}(t)$ is positive, the remaining power is fed into the grid. The negative residual power is covered by the grid. Figure 34 shows the solar power production of a PV power plant and the covered load. The green curve shows the PV-generated power. This energy is used to cover the load. Load covered by PV generation is marked in dark blue. The excess energy is fed into the grid, marked by the light green area. Load that cannot be covered by PV generation has to be taken from the grid, marked in light blue. As seen in the picture, the PV generation reaches its peak at lunchtime, which leads to a high grid feed-in during this time [159]. The residual power $P_{Residual}(t)$ is calculated as

$$P_{Residual}(t) = P_{PV,AC}(t) - P_{Load,AC}(t) \quad (41)$$

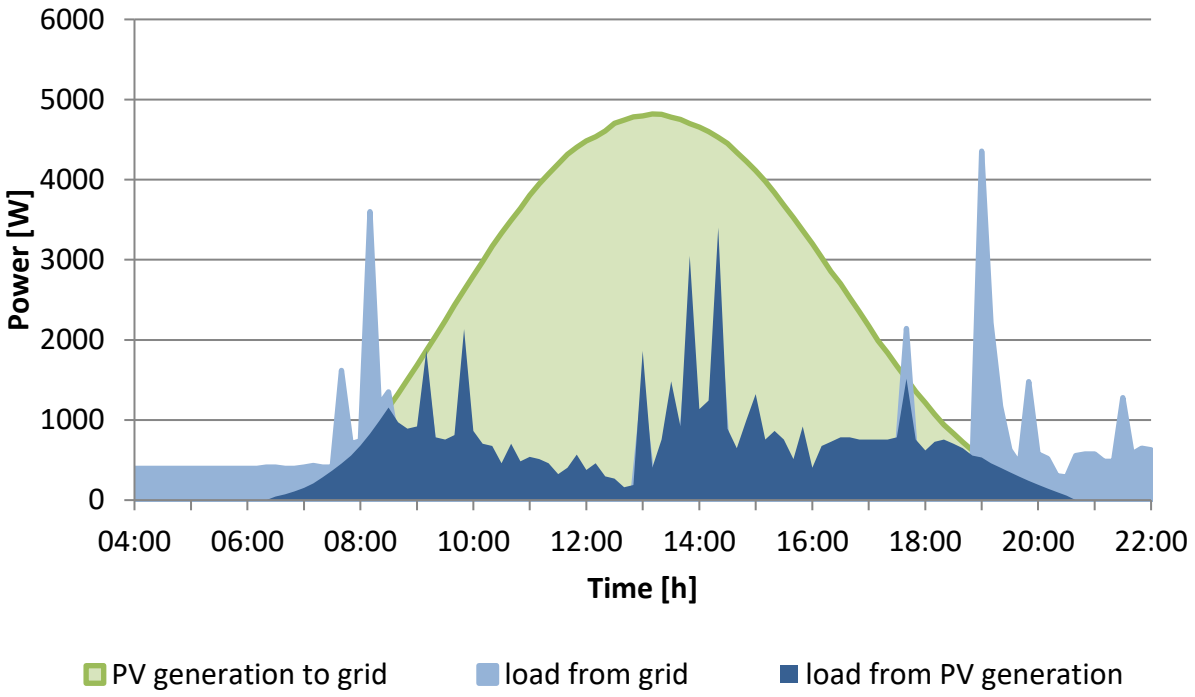

Figure 34: PV generation (6 kWp PV system) and load of a residential household with a PV power plant without BESS. Load from the household is partly covered by PV generation.

4.1.4 Maximizing PV self-consumption

Maximizing self-consumption (max SC) is a simple operation strategy for BESS aiming to use as much solar power for self-consumption as possible. The battery will store energy as soon as positive residual power is available. This energy covers the demand of the household at times of negative residual power. If the residual power is positive and the BESS is not fully

charged, the PV BESS stores the residual energy. When the SoC of the battery reaches 100 %, the positive residual power is fed into the grid. When the residual power is negative and the battery is not fully discharged, the load is covered by discharging the battery. If the required power of the household is higher than the maximum discharge power of the battery, the missing energy is covered by the grid. As shown in Figure 35, the solar energy is shifted by this strategy to cover load at times when there is not enough solar radiation available. So if there is enough PV-generated energy and storage capacity, this strategy makes it possible to cover the whole load. Figure 35 illustrates this scenario. The load is covered completely by the PV generation and therefore marked in dark blue. This is due to energy stored during the day, indicated by the dark green area. The load that occurs after the battery is fully charged is fed into the grid, which is highlighted by the light green area. This operation strategy mainly aims to reduce energy consumed from the grid [155]. On sunny days, the battery may reach the target SoC already in the morning, subsequently the PV system feeds the surplus energy into the grid. Thus, this strategy is not suitable to reduce feed-in peaks [160]. However, it can partly contribute to the grid relief. Nevertheless, this operation strategy represents an economical way for the use of a battery [155]. If the battery is oversized, the stored energy cannot be fully discharged during the night and thus the full potential of the PV BESS cannot be used.

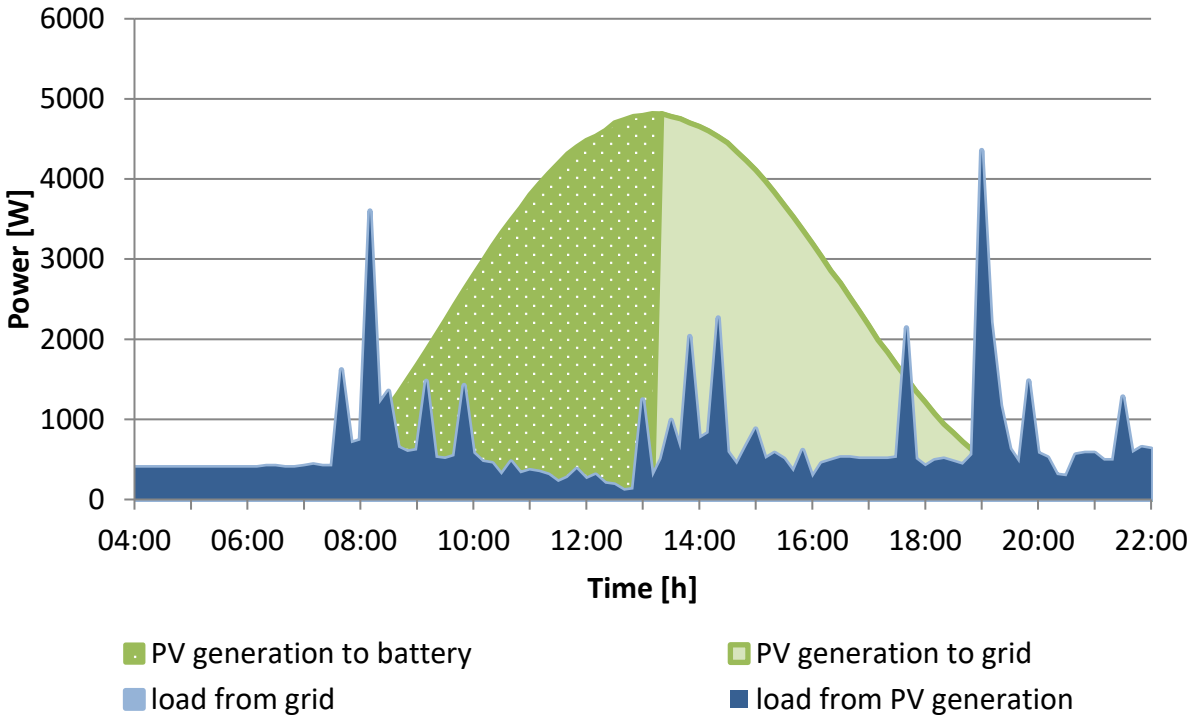

Figure 35: PV generation (6 kWp PV system) and load of a residential household with a PV BESS. Energy produced by the PV power plant is used to cover the load. Surplus energy is stored in the BESS until the BESS is fully charged. The load is covered from the direct self-consumption of the PV generated energy and the energy stored in the BESS (blue area). This operation strategy maximizes the self-consumption of the PV power plant.

4.1.5 Fixed SoC limit

The calendric lifetime as well as the cyclic lifetime of a lithium-ion battery, depends on the average state of charge (SoC). An increase of the lifetime of a lithium-ion based battery system can be achieved by reducing the average SoC [68]. Therefore, PV BESS often use fixed SoC limits to reduce battery aging. The operation strategy remains more or less the same as for the maximized self-consumption, except that the battery is not fully charged because of the upper SoC limit. Depending on the solar energy production and the load demand of the household, the limit could lead to a non-optimal use of the battery, for example if the SoC limit is reached before the battery has stored enough energy to satisfy the energy demand of the following night. This case is illustrated in Figure 36. The load that occurs in the morning has to be covered from the grid as shown by the light blue area. The load in the afternoon and night can by covered by the energy stored in the battery during day. This is highlighted by the dark blue area.
A limit for the minimum SoC could also be applied. This limit is used to prevent deep discharging of the battery. Deep discharging of the battery leads to severe aging of lithium-ion batteries as shown in section 3.2.5.5 and [161]. Depending on the application, self-discharge can lead to deep discharging if the battery is not stored correctly [162].

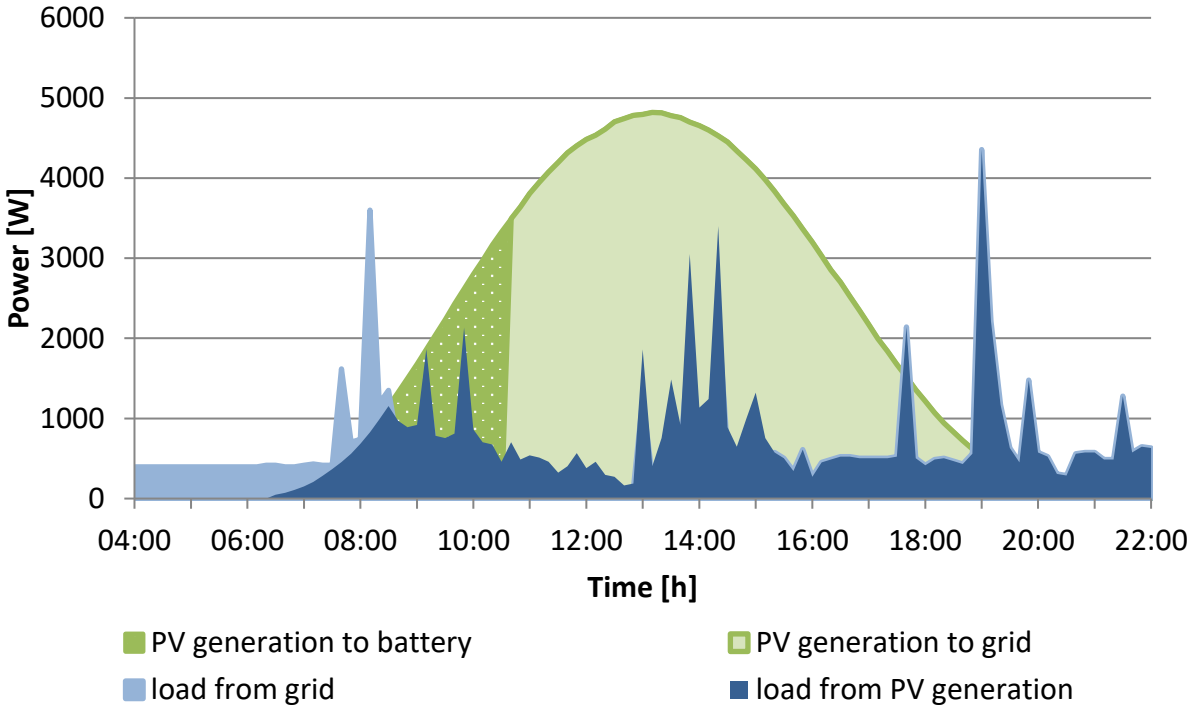

Figure 36: PV generation (6 kWp PV system) and load of a residential household with a PV BESS. Energy produced by the PV power plant is used to cover the load. Surplus energy is stored in the BESS until the BESS reaches a fixed SoC limit. The load is partly covered from the direct self-consumption of the PV generated energy and the energy stored in the BESS (dark blue area). Partly the load is covered from the grid (light blue area). The SoC limit is set to enhance the lifetime of the BESS.

4.1.6 Forecast-based operation strategies

As mentioned in the introduction, a high average SoC leads to quicker aging of lithium-ion batteries [68]. Operation strategies that maximize the self-consumption tend to store positive residual power from PV when the energy is not needed. As a result, the battery might be charged during day, but not completely discharged during night. This leads to the effect that the average SoC is unnecessarily high and decreases the battery lifetime. Therefore, an operation strategy is developed which stores only the amount of energy that is predicted to be needed during the following night [163]. With this information the target SoC is calculated, which stores exactly the amount of energy that is needed during night. The operation strategy only stores energy until the target SoC is reached. It will not exceed the target SoC even if there is more positive residual load available during daytime. This strategy is illustrated in Figure 37. The dark blue load is covered from the PV-generated energy. Only the load that occurs when PV generation is available but not sufficient to satisfy the complete power demand, needs to be covered from the grid. This load is highlighted by the light blue area. However, most of the load is covered by PV generation and thus indicated as the dark blue area. Besides the forecast horizon of one night, longer forecast horizons are possible. In this thesis a one-, two- and three-day forecast horizon is discussed.

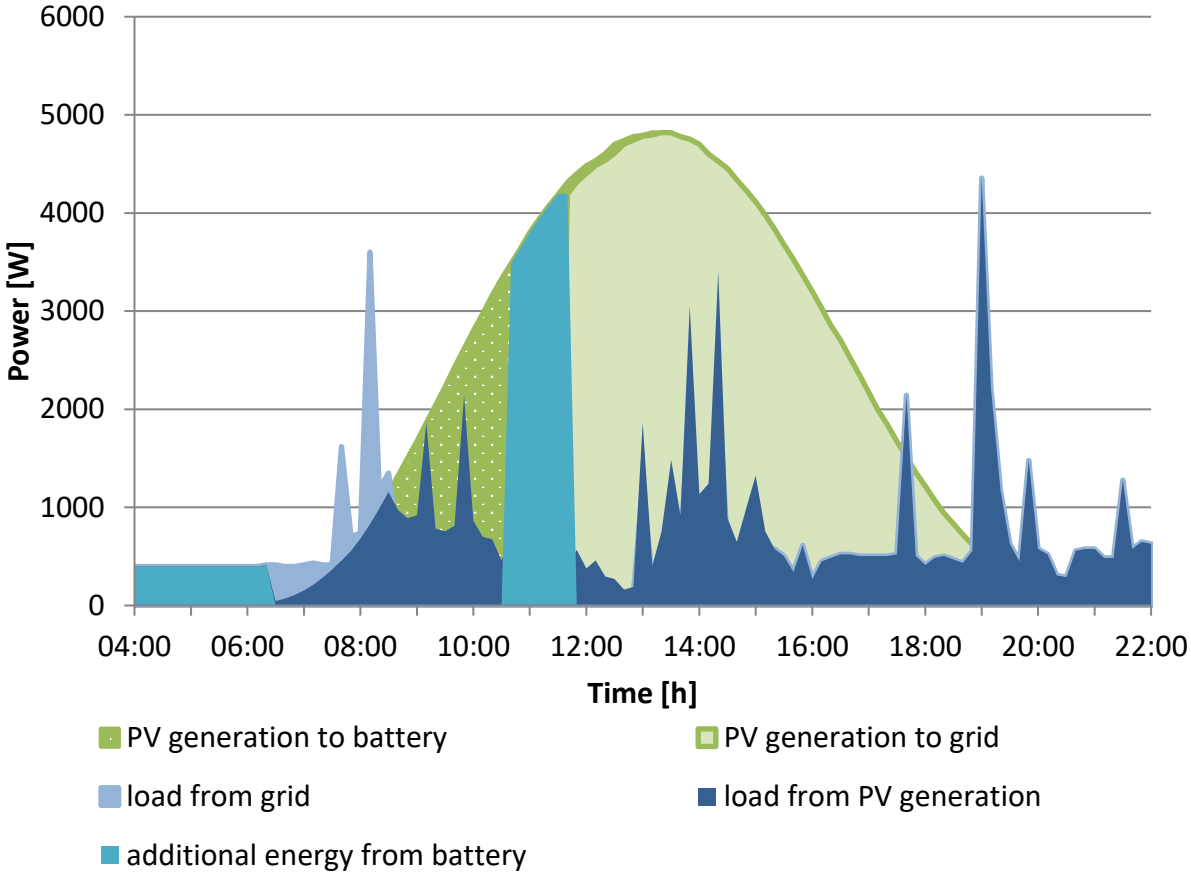

Figure 37: PV generation (6 kWp PV system) of a residential household with PV BESS using the forecast-based operation strategy to enhance battery lifetime. Due to a flexible SoC limit of the BESS the self-consumption can be enhanced in comparison to a fixed SoC limit shown in Figure 36. Additional energy from battery is the additionally stored energy due to the use of the forecast-based operation strategy.

The prediction of the energy that is needed during night is essential to determine the target state of charge. Therefore, the determination of day and night time is crucial. The applied approach defines the beginning of the night as the point where the residual power becomes negative for the first time, and accordingly the end of the night is defined as the point when the residual power becomes positive again. As a boundary condition, the time between these two points should be a least seven hours. The seven-hour boundary condition is chosen because an analysis of PV generation data from Lindenberg (Tauche), close to Berlin in Germany, has shown that the shortest night of the year has 7.24 hours without sunlight [62]. If the time between negative and positive residual power is less than 7 hours, the negative residual power is considered as a drop in generation during the day and not as the beginning of nighttime. The energy demand during night ($E_{consumption\_night}$) is the integral of the residual power demand during night ($P_{residual}$):

$$E_{consumption\_night} = \int_{begin\ night\ time}^{end\ night\ time} P_{residual}(t)dt \quad (42)$$

To determine $P_{residual}(t)$, load forecasts are necessary. Two different forecast algorithms that represent the best and the worst case are used. These algorithms are presented in section 4.4. The target SoC (SoC_{target}) for a one-day forecast is determined as:

$$SoC = \frac{E_{consumption\_night}}{cap_{battery}} \tag{43}$$

$cap_{battery}$ is the capacity of the battery. If the target SoC for a longer forecast horizon shall be calculated, a PV production forecast is necessary. If the surplus PV production on the second day ($E_{PV,2nd\_day}$) is able to cover the energy demand ($E_{consumption\_2nd\_night}$) of the second night, the target SoC is the same as the target SoC of the one-day forecast. If the PV production during the second day is not able to cover the energy demand of the second night, the determination of the missing energy ($\Delta E_{pv-load,2nd\_night}$) is necessary. $E_{pv-direct,2nd\_night}$ describes the direct self-consumption of the second night.

$$\Delta E_{pv-load,2nd\_night} = E_{PV,2nd\_day} - E_{consumption\_2nd\_night} - E_{pv-direct,2nd\_night} \tag{44}$$

This leads to a new target SoC for the first night ($SoC_{target,2\ day\ prog}$). This SoC will be calculated with equation (45).

$$SoC_{target,2\ day\ prog} = \frac{E_{consumption\_night} + \Delta E_{pv-load,2nd\_night}}{cap_{battery}} \tag{45}$$

The three-day forecast strategy needs to calculate the energy demand of the following three nights. If the energy production of the two following days can cover the corresponding energy demand, the target SoC is calculated in the same way as the one-day forecast. If not, the target SoC is calculated as

$$SoC_{target,3\ day\ prog} = \frac{E_{consumption\_night} + \Delta E_{pv-load,2nd\ night} + \Delta E_{pv-load,3th\ night}}{cap_{battery}} \tag{46}$$

$\Delta E_{pv-load,2nd\ night}$ and $E_{pv-load,3th\ night}$ are calculated as described in equation (44). The target SoC determination for the two- and three-day forecast is done on a daily basis to minimize the influence of forecast errors. For these forecast horizons the additional aging due to the increasing SoC needs to be evaluated. This is presented in section 4.5.1. A penalty function to internalize the additional battery aging is not minded by the operation strategy. Therefore, the operation strategy does not take the costs due to increased battery aging into account. This function could be used to optimize the operation strategy. Instead, this analysis uses static forecast horizons.

4.1.7 Fixed cut-off limit

To reduce the influence of PV BESS on the grid [160] the new funding scheme for PV BESS by the KfW Group in Germany requires additional grid relief. To gain this grid relief, a reduction of PV feed-in power to a maximum of 50 % of the rated PV power [13] is required. The feed-in power limit leads to energy that cannot be fed into the grid. The most direct operation strategy to gain this grid relief is to cut off the feed-in power. The energy that has been cut-

off cannot be fed into the grid and causes losses of PV production. This energy is called cut-off energy. The corresponding limit value is called cut-off limit.
This strategy charges the battery as quickly as possible, similar to maximizing self-consumption. If the battery is already fully charged, the PV facility feeds the residual power below the cut-off limit P_{cutoff} into the low-voltage grid, while the surplus energy is discarded by power derating of the converter. Figure 38 illustrates the strategy. The green curve shows the PV production. The part that is used to charge the battery is represented by the dark green area, and the part that is fed into the grid is represented by the light green area. The cut-off energy is the cyan space below the green curve. Disadvantages of this operation strategy are the losses of PV energy due to the limitation. Nevertheless, this strategy can contribute to the grid relief and can help to avoid feed-in peaks [155].

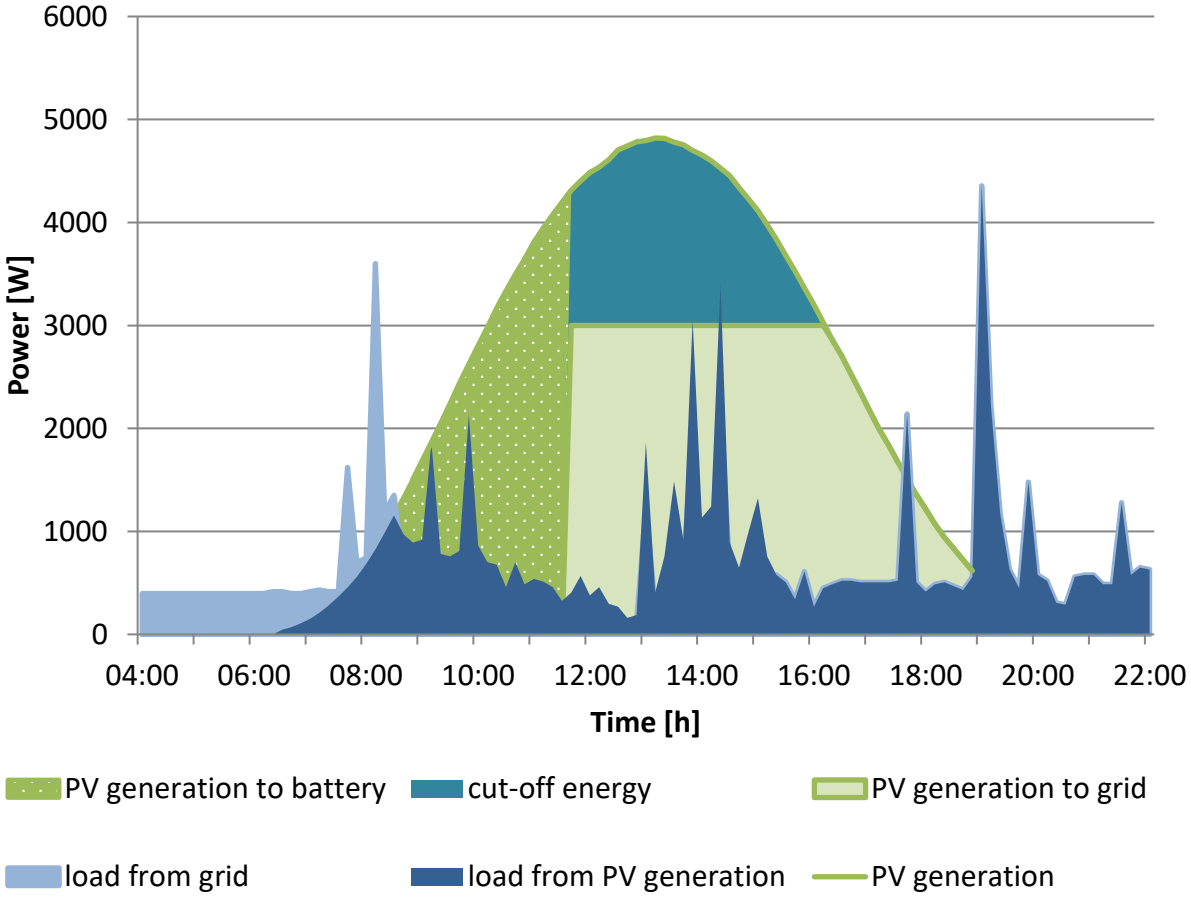

Figure 38: PV generation of a residential household with a 6 kWp PV power plant and a BESS under consideration of a feed-in limit of 50 % of the rated PV power. Residual PV-generated energy is stored in the battery until the battery is fully charged. PV-generated power, which exceeds the feed-in limitation and cannot be stored in the battery, has to be cut-off.

4.1.8 Fixed SoC limit with fixed cut-off limit

The fixed SoC limit with fixed cut-off limit combines the strategies limiting SoC (4.1.5) and applying a fixed cut-off limit (4.1.7). The power feed-in to the grid is limited to a fixed value to gain grid relief, and the target state of charge is limited to a fixed value to reduce battery aging.

4.1.9 Fixed cut-off limit with forecast-based operation strategy

Both forecast-based operation strategies with cut-off limits, the fixed limit as well as the variable limit pursue two goals. The first goal is to enhance the battery lifetime without reducing energy throughput of the battery dramatically. To fulfil the goal of enhancement of battery lifetime, the algorithm as described in section 4.1.6 is applied. Only the amount of energy predicted to be needed during night is stored to reduce the average SoC.

The second goal is to store the cut-off energy if a cut-off limit is set. To reduce the cut-off energy, the PV BESS stores energy as soon as the residual power is higher than 50 % of the maximum normalized power of the solar panels [164].
This energy is stored in the BESS, even though it exceeds the energy demand of the following night. In this case excess energy for the following day is produced. The calculation of the energy limit of the following day considers this surplus energy.
The forecast-based operation strategies estimate the energy that is stored in the PV BESS due to the PV rated power limit. If this cut-off energy is not able to cover the energy demand during the following night, the missing energy will be stored in the battery using the residual power below the limit in the morning. After charging in the morning, the battery will only be charged with the residual power above the PV rated power limit, shown by the dark green area in Figure 39. Energy that is not directly used or stored in the battery is fed into the grid, represented by the light green area in Figure 39.
If the residual energy that is needed to be stored due to the feed-in limitation exceeds the battery storage capacity, energy is cut-off.

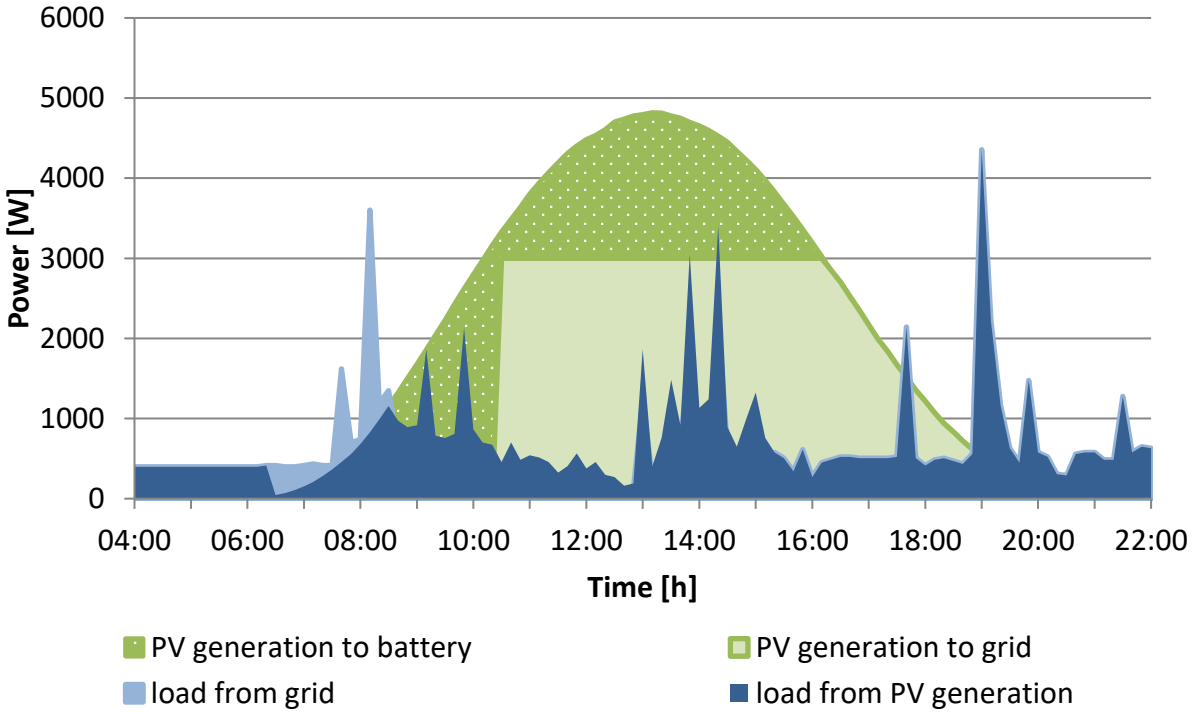

Figure 39: PV generation of a residential household with a 6 kWp PV power plant and a BESS under consideration of a feed-in limit of 50 % of the rated PV power. The BESS is operated with a forecast-based operation strategy. The BESS stores the PV-generated power over the feed-in limitation to avoid cut-off energy. Additional energy is stored in the morning to cover the energy demand of the following night.

To calculate the cut-off energy E_{cutoff} of the current day for a household with PV system and battery storage, the predicted daily course of the residual power $P_{residual}(t)$ is used. The different prediction strategies are described in section 4.4. The residual load values $P_{residual,order}(t)$ are arranged in a so-called Pareto chart according to their value in descending order [145]. With the ordered residual power values, the cut-off energy E_{cutoff} can be calculated with equation (47).

$$E_{cutoff} = \int \max\{P_{residual,order}(t) - P_{cutoff,fix}(t), 0\}\, dt \quad (47)$$

$P_{cutoff,fix}$ is the fixed cut-off limit. If the KfW funding requirements shall be fulfilled, this limit is set to 50 % of the PV nominal peak power. The SoC limit to which the battery needs to be charged in the first phase can be calculated with equation (48). Therefore, the battery is charged with the cut-off energy. If the cut-off energy is not enough to fulfil the energy demand of the following night, some additional energy needs to be charged into the battery. The SoC until the battery needs to be charged in this first phase is called first phase SoC limit ($SoC_{target,first\ phase}$). In the case this limit is reached, the battery will store enough energy to cover the load in the following night.

$$SoC = \max\{SoC_{target,first\ phase} - \frac{E_{cutoff}}{cap_{battery}}, 0\} \quad (48)$$

4.1.10 Variable cut-off limit with forecast-based operation strategy

The variable cut-off limit with forecast-based operation strategy is similar to the strategy described in 4.1.9. Both strategies pursue the same goals: enhancing the battery lifetime without reducing the energy throughput dramatically and storing the cut-off energy. The advantage of the variable feed-in limitation is a higher grid relief compared to the fixed feed-in limitation as shown in [31]. The variable cut-off strategy calculates a power feed-in limit for every day depending on the predicted energy demand at the following night. Only the energy above the power limit will be stored at the battery system. In Figure 40 this energy is highlighted by the dark green area. All the energy below this limit would be fed into the grid as well. If the calculated cut-off limit is higher than 50 % of the PV rated power, the limit is set to 50 % of the PV rated power [164]. The principle of this strategy can be seen in Figure 40.
Similar to the aforementioned strategy this strategy in section 4.1.9 stores the entire residual load above the feed-in limit, even though this energy exceeds the energy demand of the following night. In this case the surplus energy is taken into account for the calculation of the feed-in limit of the following day.

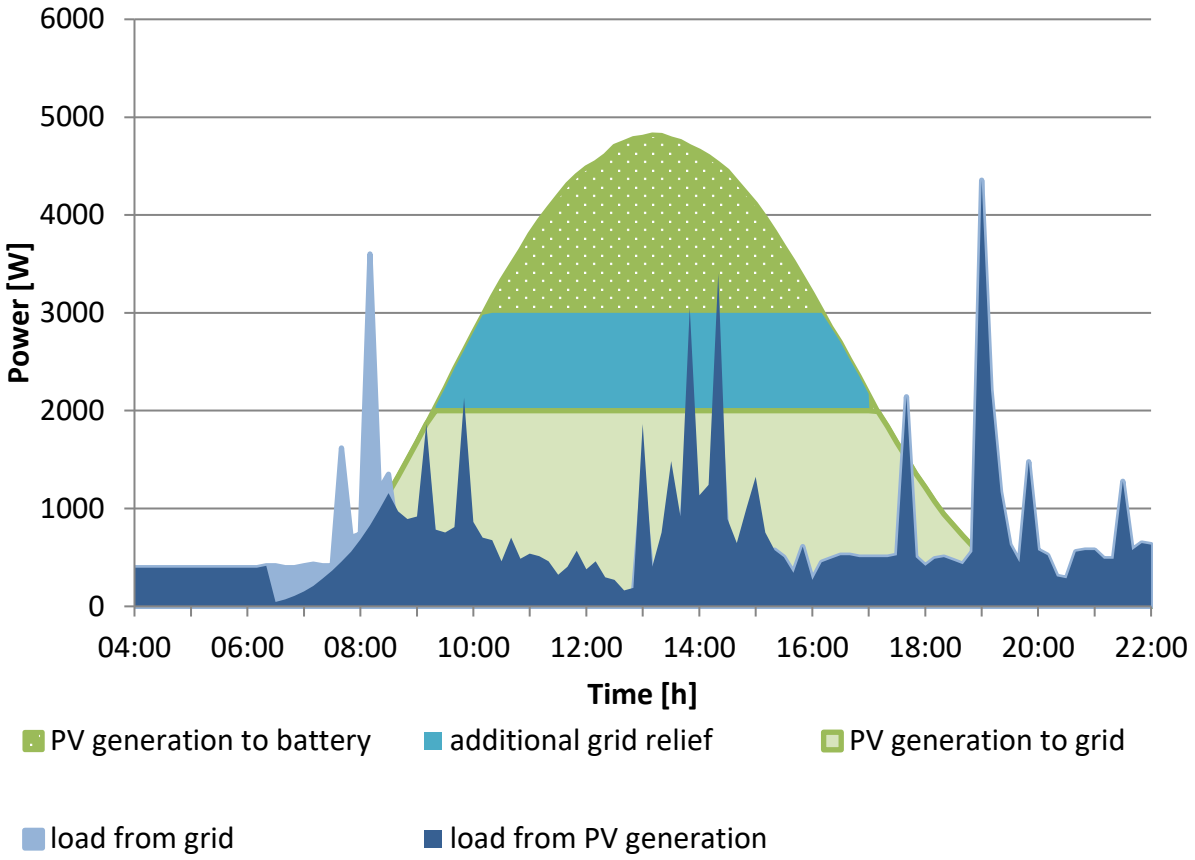

Figure 40: PV generation of a residential household with a 6 kWp PV power plant and a BESS under consideration of a feed-in limit of 50 % of the rated PV power. The BESS is operated with a forecast-based operation strategy and a variable cut-off limit. The BESS stores the PV-generated power over the feed-in limitation to avoid cut-off energy. Additional energy is stored to cover the energy demand of the following night. To gain further grid relief the additionally stored energy reduces the PV feed-in limit over the 50 % feed-in limit. The PV feed-in is less than 50 % of the rated PV power even though more is produced.

The feed-in limit is set for every day. Considering the forecast, the limit is daily adjusted to cover the demand during the night. The battery is charged only with the energy above this limit, which is presented in Figure 40. To calculate the feed-in limit, an iterative algorithm searches for the cut-off limit $P_{cutoff,var}$ until equation (49) is satisfied. The algorithm makes sure that the variable cut-off limit is always below the fixed cut-off limit $P_{cutoff,fix}$. If not, the fixed cut-off limit is applied.

$$\int \eta_{charge} \cdot \max\{P_{residual,ordered}(t) - \max\{P_{cutoff,var}(t), P_{cutoff,fix(t)}\}, 0\}dt = E_{residual,neg} \quad (49)$$

The energy demand $E_{residual,neg}$ is calculated based on equation (50). This equation is similar to equation (42).

$$E_{residual,neg} = \frac{\int_{begin\ night\ time}^{end\ night\ time} P_{residual}(t)dt}{\eta_{discharge}} \quad (50)$$

4.2 Operation strategies heat system

4.2.1 Literature review

The literature review is focused on literature concerning operation strategies for integrated homes. Numerous publications deal with topics related to operation and sizing of BESS. A review of energy storage technologies is given in [165] and a review addressing the BESS size is given in [166]. Furthermore, a wide range of publications addresses the topic of PV systems with power-to-heat coupling in residential households. [167] investigates the operation of PV heating systems without storage systems. Other publications address PV BESS heat coupling systems. Publication [168] for example, focusses on the influence on the self-consumption. Klingler et al. investigate the influence of heat pump and electric vehicles (EV) on the self-consumption rate and the market potentials of PV systems [169]. Operation strategies for heat systems are analyzed in further publications. In [170], the heat storage system is charged preferred to the battery system. The approach in [171] investigates a preference charge of the battery storage system. Further publications focus on the demand side management (DSM) potential of these systems and the different roles they play in the market [172]. [173] presents a work on cost-optimal and rule-based control for buildings with PV, heat pumps and storages to increase the value of PV for the prosumer. The rule-based control aims at maximizing PV self-consumption. The demand side management through heat pumps, thermal storage and battery storage to increase local self-consumption and grid compatibility of PV systems is investigated in [174]. The influence of residential power-to-heat systems on the gird is investigated in further publications. The reduction of heat pump induced peak electricity use through thermal energy storage and demand response is investigated in [175]. [176] presents a scheduled operation of heat pump systems for voltage control. Fixed feed-in limits are addressed in [177], where the PV curtailment reduction with smart homes and heat pumps by appropriate control of the heat pumps is discussed. In [178] the authors examined different topologies and sizing of PV-heat systems.

4.2.2 Heat sector operation strategies

A heat management system (HMS) ensures a reliable operation of the heat system. The heat management system is required to ensure that the demands of domestic hot water (DHW) and heating are covered at all time. To accomplish that, the HMS requests electric energy to operate the heat pump. Two boundary conditions have to be considered. In accordance to DIN EN 15450, the heat pump has a minimum runtime of 20 minutes and thus maximum three

switching operations are allowed each hour in order to ensure sufficient lifetime. Furthermore, the coverage of the DHW demand has priority over the coverage of the heat demand. If the demand of heat could not be covered by the storages, the heat pump is operated with full power ($A_{HP} = 1$) to ensure that the demand is always covered. In the case that the heat pump is not able to cover the demand, the electric heaters in the storages are used to deliver the additional heating energy.

Room Heating:
The most important control variable for room heating is the room temperature. Regarding DIN EN 12831, the minimum temperature for the living area is 20 °C. Furthermore, the maximum heat flux density of 100 W/m^2 considering DIN EN 1264-1 is considered as well as the maximum surface temperature of floor heating, which is 35 °C. A heating period from October 1st to April 30th is applied. Apart from this heating period, the heat system is shut down [179].

DHW:
The DHW should have a temperature of 40 °C [172]. To provide this temperature and considering the maximum output temperature of the heat pump of 55 °C, the minimum temperature of the heat storage is set to 45 °C. If a higher temperature is requested, the electric heaters have to support the system.

The HMS reacts to the charge order from the EMS. The three storages, buffer storage, DHW storage and the room temperature, can provide flexibility. These storages operate in a certain temperature range. If one of them reaches the lower boundary temperature, the heat pump starts and charges the storages until one storage reaches the upper boundary temperature. If the HMS should charge the storages in order to enhance the self-consumption, the charge boundaries are considered. The charge boundaries are the normal boundaries plus the spread temperatures. The spread temperatures are determined by the optimization. In this case, the temperatures are higher in order to store energy for shortages. The storage units are kept at a higher temperature in the charging case in comparison to the non-charging case. Therefore, the minimum boundary temperature is higher in the charging case.
A layered storage model is used. Therefore, the temperature of the top layer is considered. If the room or the DHW storage falls short of a certain temperature limit, the “necessary” mode is activated. In this case, the electric heater provides additional heating power. During the summer months, the buffer storage is not charged because the buffer storage supplies the room heating.

	CHARGE==true		CHARGE==false		Necessary
	T_{min} [°C]	T_{max} [°C]	T_{min} [°C]	T_{max} [°C]	
Buffer storage	$T_{Buffer,min}$ =32 °C+ $T_{Buffer,spread}$	$T_{Buffer,max}$ =$T_{Buffer,upper}$+ $T_{Buffer,spread}$	$T_{Buffer,min}$ =32 °C	$T_{Buffer,max}$ =$T_{Buffer,upper}$	
DHW storage	$T_{DHW,min}$ =45 °C + $T_{DHW,spread}$	$T_{DHW,max}$= $T_{DHW,upper}$+ $T_{DHW,spread}$	$T_{DHW,min}$= 45 °C	$T_{DHW,max}$= $T_{DHW,upper}$	T_{DHWTop} <44.5 °C
Room temperature	T_{room}= 20 °C	T_{room}= 22 °C	T_{room}= 20 °C	T_{room}= 21 °C	T_{room} <19.5 °C

Table 7: Storage temperatures in dependency of the operation mode.

The data of maximum temperature of the DHW storage and buffer storage as well as the data of spread temperature of the buffer storage are used as optimization variables. For the non-optimization setting, the values given in Table 8 are used. These values are illustrated in Figure 41.

	[°C]	[kWh]
$T_{Buffer, max}$	40	6.1
$T_{Buffer, spread}$	5	1.75
$T_{DHW, max}$	55	10.5
$T_{DHW, spread}$	5	1.75

Table 8: Temperatures applied to the non-optimized scenario. The maximum storage capacity is calculated based on a 300 l storage volume (300 l DHW, 300 l buffer) and a minimum temperature of 20 °C for the lowest layer.

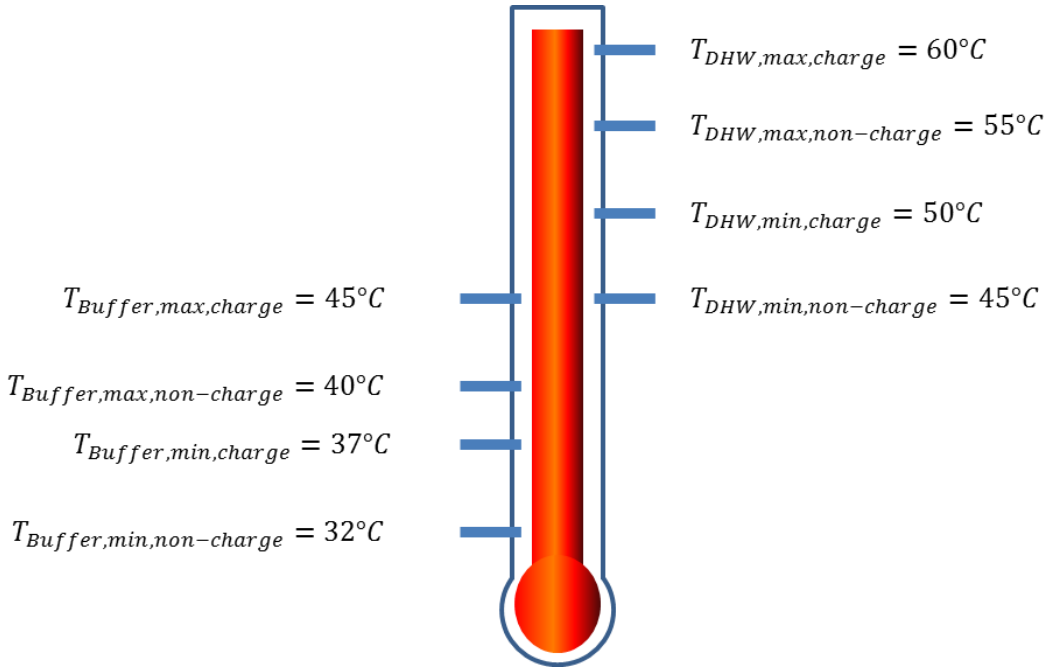

Figure 41: Boundary temperatures of the DHW and buffer storage in the non-optimization scenario. The temperatures of the water storage units in the charging case and non-charging case are depicted.

4.3 Combined operation strategies

This section combines the operation strategies for the electrical part presented in section 4.1 and for the electrical part presented in section 4.2. The operation of the heat-power coupling system is based on a Master-Slave-Architecture. The Energy management system (EMS) receives information from the heat management system (HMS) and the battery management system (BMS). Hence, the EMS operates as the master. The EMS priority is to satisfy the demand of electric power and heating power of the household. To satisfy the heat demand, the HMS requests an electric demand for the heat pump and the auxiliary heating. Based on this information, the EMS calculates the residual load. The operation of the heat storage and the battery storage depends on the residual load. The calculation of the residual load is based on the following equation:

$$P_{RL} = P_{LH} - P_{PV} \quad (51)$$

P_{RL} = residual load[W]
P_{LH} = load of household with heat pump [W]
P_{PV} = PV feed − in [W]

If the residual load is negative, which means that more PV energy is available than needed for the actual demand, the EMS charges the storages. Therefore, the EMS sends a charging order to the different storage facilities in dependency of the applied operation strategy. An overview of the investigated operation strategies is presented in Figure 42. The operation of heating is independent of the operation of the electrical system. Both sectors are coupled with an intelligent energy management system that controls the operation of the storages.

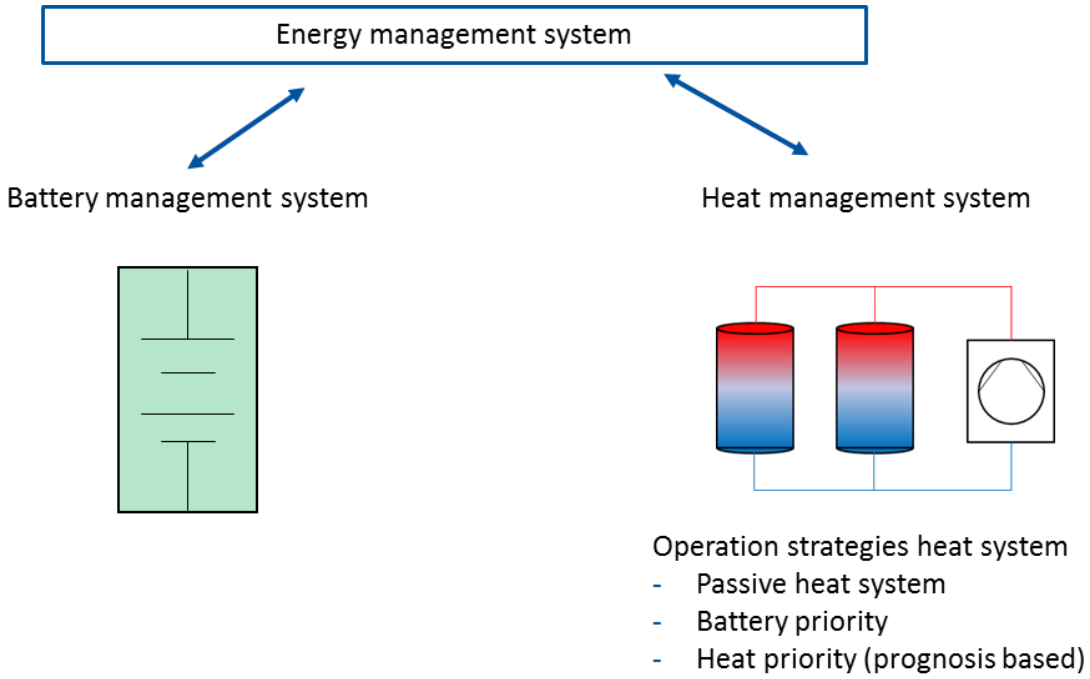

Figure 42: Investigated operation strategies and their interdependencies.

The operation strategy of the heat system is not influenced by the operation strategies applied to the battery system. In dependency of the applied operation strategies of the heat system, the EMS charges the battery or the heat storages. The examined operation strategies are explained in the following sections.

4.3.1 Heat storage as a passive element

The simplest strategy is to let the heat system work only as a passive element. In this case, the heat system is used as an additional load. The storage units are only used to reduce the number of cycles of the heat pump and to make sure that the heat pump is only operated in an efficient mode. The heat storage units are not used to increase the self-consumption of the PV system by storing surplus energy.

4.3.2 Priority battery charging

The operation strategy “priority battery charging”, charges the battery storage system first, because electric energy is a “higher” form of energy than heat. Only if the battery storage is fully charged in case of the maximized self-consumption strategy, or the BESS is charged until the max SoC limit in case of the forecast based operations strategy (FOS), and there is still negative residual load available, the thermal storages are charged. The battery is employed if the EMS sends a charging order to the BMS. Before the EMS sends a charge command to the HMS, the EMS checks whether the available negative residual power is enough to run the heat pump. Otherwise, the residual power is fed into the grid. The modeled heat pump is only

switched on or off in the static operation mode, therefore there has to be enough surplus power to run the heat pump. The algorithm does not check if the surplus will be high enough to run the heat pump for the minimum runtime.

4.3.3 Priority heat storage charging

This operation strategy for heat systems charges the heat storage with highest priority. Therefore, the EMS sends a charging order to the HMS whenever residual power is available. This operation strategy aims to avoid conversion losses of the BESS. If energy is stored in the battery during daytime and is used for heating after sunset, conversion losses due to charging and discharging of the battery occur, as well as additional battery aging. Therefore, the heat storages are charged preferentially in order to avoid these conversion losses. To prevent that too much energy is stored in the heat system, a persistence prognosis is applied. The assumption is made, that the heat demand will be the same as the heat demand of the previous day. Therefore, the residual energy is only charged to the heat storage as long as the actually stored thermal energy is less or equal to the total thermal energy of the previous day.

4.4 Forecasting methods

The aforementioned forecast-based operation strategies use generation and consumption forecasts. To investigate the influence of forecast errors, two different scenarios are presented, which represent the variety of prediction methods. A perfect forecast is used, which constitutes the best case and a persistence forecast is used to constitutes the worst case [145]. The perfect forecast cannot be reached in reality, because this strategy uses the assumption that we can predict the future without forecast errors. The persistence forecast is a widely known method of meteorology. The assumption is that the weather changes very slowly. It is assumed that today's weather is similar to yesterday's weather and therefore the PV generation will be the same as the day before.

$$\mathrm{P_{PV,forecast}(t) = P_{PV,measured}(t - 1d)} \tag{52}$$

The advantage of this strategy is that it is easy to integrate into other models. The implemented strategy assumes the load demand for the actual weekday as well. The assumption is made that the load will be identical to the load last week on the same day [145], which is presented in equation (53).

$$\mathrm{P_{load,forecast}(t) = P_{load,measured}\,(t - 7d)} \tag{53}$$

The comparison between perfect forecast and persistence forecast is used to present a worst-case scenario (persistence forecast) and a best-case scenario (perfect forecast or ideal forecast-based operation strategy). The implementation of advanced forecasting methods, for instance artificial neural networks or the incorporation of weather forecasts would enhance the forecast accuracy in comparison to the worst-case scenario presented in this work. The disadvantage of advanced forecasting methods is additional computational effort, which leads to higher losses of the BESS and data availability. If weather forecasts are used, additional costs for forecasting fees and a connection to the internet might add to the other cost. The

influence of further, advanced forecast-based operation strategies on the economics of home storage systems is not investigated in this thesis.
The forecast-based operation strategies are only applied in the summer months, to use the full potential of the storage system during winter, because only in the summer months a violation of feed-in limitations appears.

4.5 Comparison of operation strategies for photovoltaic battery storage systems

The strategies presented in section 4.1 are applied on the presented PV BESS model. In this section, the power-to-heat coupling is not presented. The analyses in section 4.5.1 to section 4.5.4 are performed on the PV BESS model with the aging characteristic of the 18650 LG Chem cell. Finally, the influence of the operation strategies is evaluated on the PV BESS model parametrized with the 45 Ah NCA Saft cell, leading to the results presented in section 4.5.5. The forecast-based operation strategies (FOS) are combined with the two forecast strategies and are analyzed for different forecast horizons. Table 9 contains the abbreviations for the analyzed strategies. These abbreviations are used to identify the strategies precisely.

Name of the strategy	Section	Abbreviation
PV power plant without a PV BESS	4.1.3	without PV BESS
maximize PV self-consumption	4.1.4	max SC
limiting SoC	4.1.5	fix SoC limit
ideal one-day FOS	4.1.6	ideal one-day FOS
ideal two-day FOS	4.1.6	ideal two-day FOS
ideal three-day FOS	4.1.6	ideal three-day FOS
persistence one-day FOS	4.1.6	persistence one-day FOS
persistence two-day FOS	4.1.6	persistence two-day FOS
persistence three-day FOS	4.1.6	persistence three-day FOS
fixed cut-off limit	4.1.7	fix P limit
fixed SoC limit with fixed cut-off limit	4.1.8	fix SoC fix P limit
fixed cut-off limit with ideal FOS	4.1.9	ideal one-day FOS fix
fixed cut-off limit with persistence FOS	4.1.9	persistence one-day FOS fix
variable cut-off limit with ideal FOS	4.1.10	ideal one-day FOS variable
variable cut-off limit with persistence FOS	4.1.10	persistence one-day FOS variable

Table 9: Abbreviations of the analyzed PV BESS operation strategies.

4.5.1 Analysis of battery lifetime enhancement due to forecast-based operation strategies

Forecast-based operation strategies (FOS) are used to enhance the battery lifetime. Therefore, the influence of FOS on the battery lifetime is analyzed. This analysis is based on [163].
The state of charge (SoC) characteristic during a week in July is illustrated in Figure 43. The blue curve shows the SoC behaviour when the maximize PV self-consumption operation strategy (max SC) is used. The red curve shows the SoC behaviour when the ideal one-day FOS is applied. The battery reaches exactly a SoC of 0 % at the end of the nightly discharge. Using the max SC strategy, the average SoC from July 1st to July 6th is 68 %, while the use of the ideal one-day FOS strategy reduces the average SoC to 29 %. With this strategy the average SoC for the selected week in July can be halved. The annual average SoC can be reduced as well. The SoC of the max SC strategy is 30 %, whereas the annual average SoC using the ideal one-day FOS is 17 %. Due to the reduction of the average SoC, the lifetime of the battery is enhanced by around 4.3 years as shown in Figure 45.

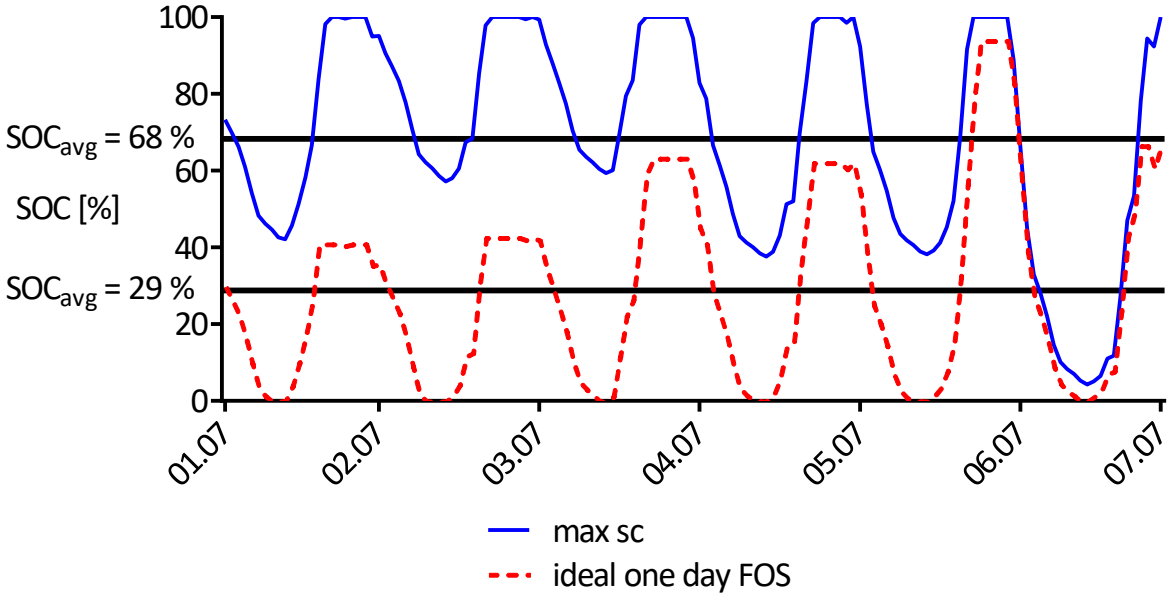

Figure 43: State of charge of the PV BESS with and without a forecast-based operation strategy from July 1st to July 6th.

To analyze the influence of the forecast horizon the FOS are used with different forecast horizons on the same household. Longer forecast horizons aim to use an excess of PV energy on the first day to overcome shortages of PV generation on the next days. For this analysis, a one-day forecast horizon is compared to a two- and a three-day forecast horizon. The result is depicted in Figure 44.

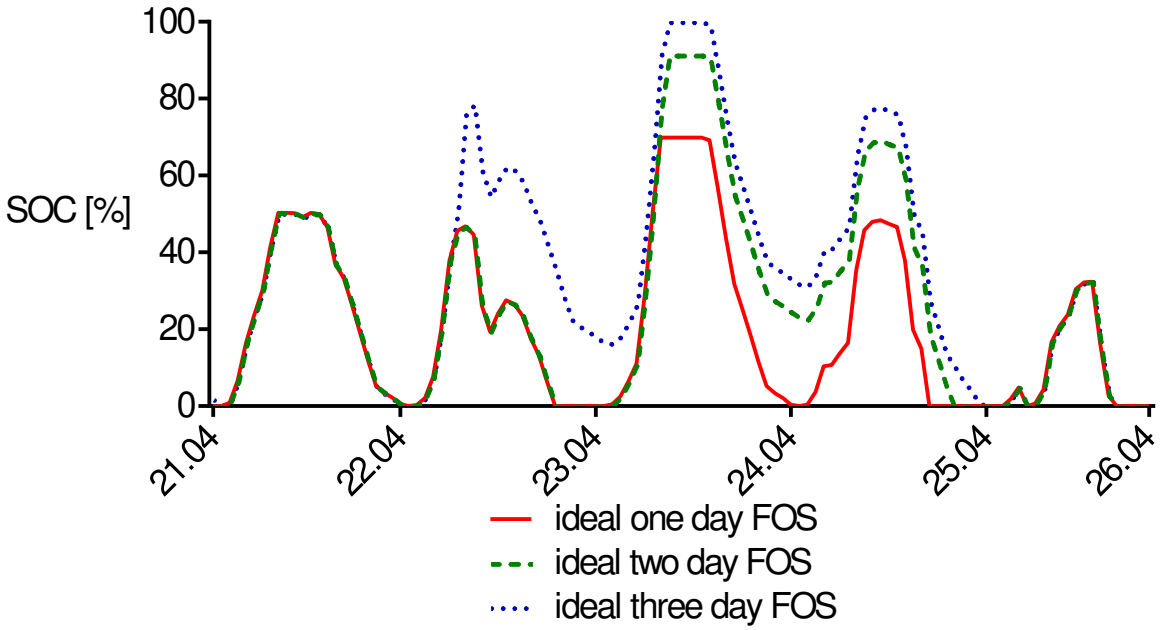

Figure 44: State of charge of the PV BESS operated with forecast-based operation strategies from April 21st to April 26th. Comparison of different forecast horizons for one-, two- and three-day forecast.

The red line in Figure 44 represents the ideal one-day FOS which uses a load forecast for the following night. The green line depicts a forecast horizon of two days, and the blue line represents the SoC when a three-day forecast is applied on the FOS. The selected example shows changes of the SoC curve at multiple points if different forecast horizons are applied. At these points, energy is stored over two or three days to satisfy the energy needs of the following nights. The analysis shown in Figure 44 is based on an ideal forecast.
The SoC is strongly related to the battery lifetime, according to [68]. Figure 45 illustrates the lifetime of the battery for different operation strategies. The correlation between SoC and lifetime can be observed. Due to the use of FOS, the SoC can be reduced as shown in Figure 43. This leads to an enhanced battery lifetime as shown in Figure 45. The increased SoC of a two- or three-day forecast as shown in Figure 44 leads to a reduced lifetime according to Figure 45. The simulations show that due to forecast errors the average SoC of the persistence forecast is lower compared to the multi-day forecasts, which leads to a longer battery lifetime.

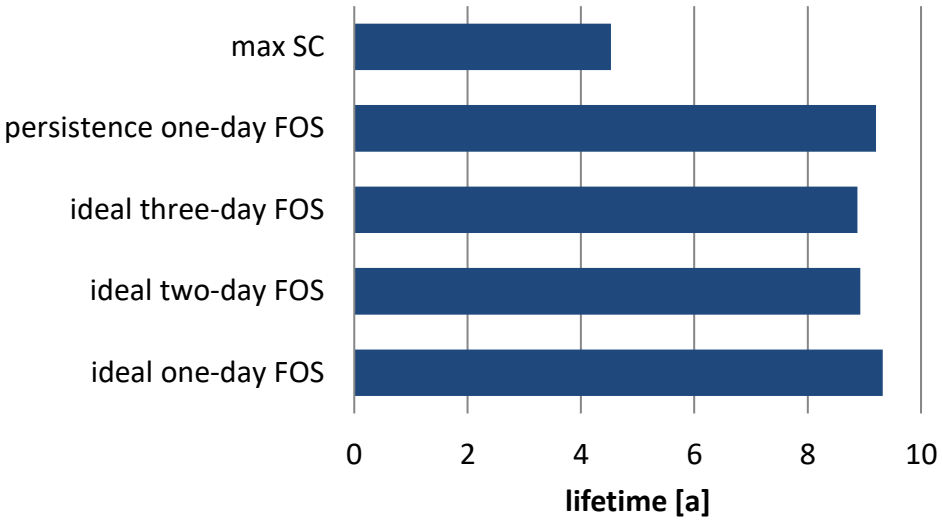

Figure 45: Influence of different forecast strategies and different forecast horizons on the battery lifetime of a PV BESS with a 10 kWp PV power plant and a 10 kWh BESS.

4.5.2 Influence of forecast-based operation strategies on the LCOEle of PV BESS

This section focuses on the influence of FOS on the LCOEle of households with PV BESS. To assess the economy of the operation strategies, the LCOEle described in section 3.5 is used. Besides the lifetime of a battery, the energy throughput of a BESS plays an important role for the LCOE. Analogous to Figure 45, the annual energy throughput of the different operation strategies is illustrated in Figure 46. The comparison of these results shows a strong correlation between battery lifetime and annual energy throughput. The annual throughput increases while the lifetime decreases. The highest annual energy throughput is reached when the max SC strategy is used. This is obvious because in this case energy is stored as soon as positive residual power occurs and the battery is not fully charged. If the ideal three-day FOS is used, the annual energy throughput is closer to the max SC strategy. Accordingly, the ideal one- and two-day FOS strategies have a lower annual energy throughput.
When the persistence forecast is used, the predicted target SoC differs from the one when the ideal forecast is used. If the target SoC is overestimated by the persistence forecast, the PV BESS cannot store enough energy to gain the calculated target SoC at times. This is the case when there is not enough residual energy available. If the target SoC is underestimated, the chance that enough residual energy is available to achieve the target SoC is higher. This is why the forecast inaccuracies lead to lower annual energy throughput when the persistence forecast is used. If the persistence forecast is used, the battery lifetime is higher because the battery has a lower average SoC compared to the ideal forecast.

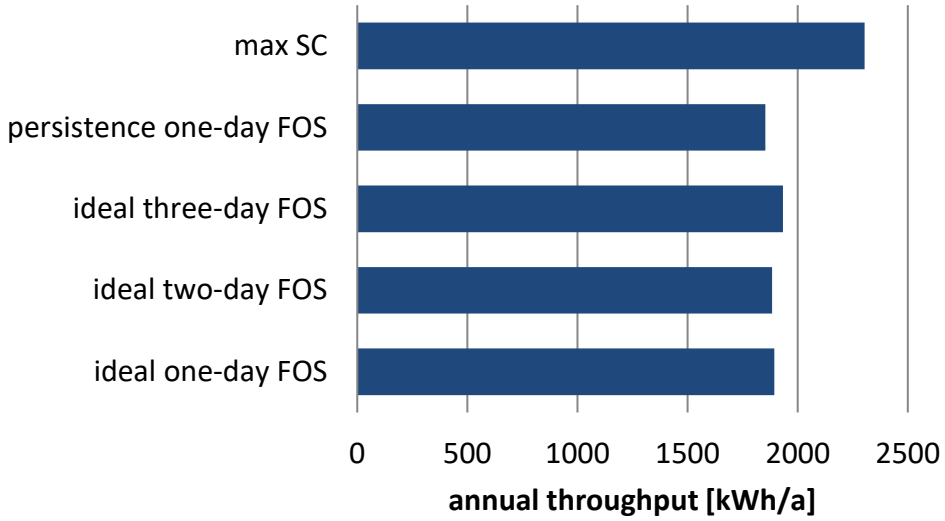

Figure 46: Influence of different forecast strategies and different forecast horizons on the annual energy throughput of a PV BESS with a 10 kWp PV power plant and a 10 kWh BESS.

To compare the efficiency of the different operation strategies, the total energy throughput over the battery lifetime has to be taken into consideration. This value shows how efficient the same asset is used. If the BESS has a higher energy throughput over its lifetime, the BESS is being used in a more efficient way. Therefore, the energy throughput over the battery lifetime E_{life} can be used as an indicator to determine how efficiently a PV BESS is used.

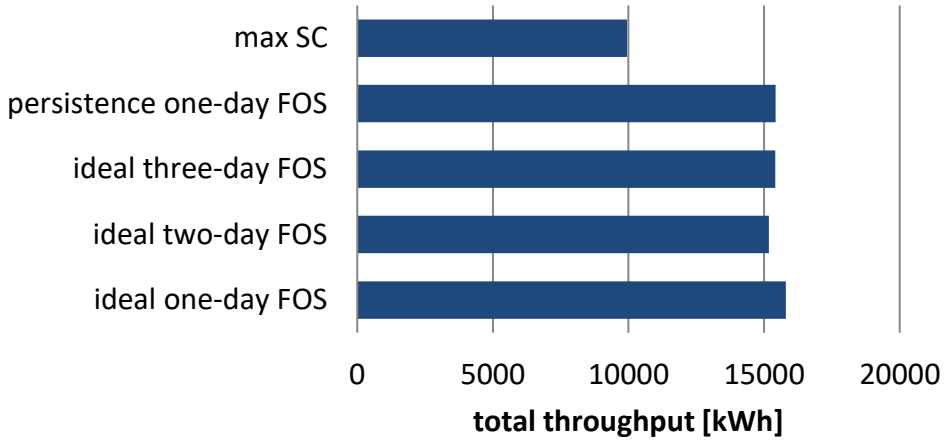

Figure 47: Influence of different forecast strategies and different forecast horizons on the total energy throughput over the battery lifetime of a PV BESS with a 10 kWp PV power plant and a 10 kWh BESS.

The resulting total energy throughput for the different operation strategies is shown in Figure 47 and calculated by a simulation over the whole lifetime of the BESS. The reduction of battery lifetime when the max SC strategy is used leads to the lowest overall energy throughput. The highest energy throughput over the battery lifetime is reached with the ideal one-day FOS. As described in section 4.1.6 a penalty function to internalize the additional battery aging is not implemented in the operation strategy. This is why multi-day forecast horizons lead to an over proportional battery aging. Nevertheless, all FOS have significantly higher energy throughputs

compared to the case of the max SC strategy. The persistence one-day FOS shows a slightly reduced energy throughput over the battery lifetime compared to the ideal one-day FOS.
The annual energy throughput has a higher influence on the revenue than the battery lifetime due to scale and annuity effects. Scale effects lead to lower costs for future PV BESS, often favoring the implementation of cheaper and less long-lasting PV BESS. Annuities lead to the effect that payments in the future are less valuable than payments in the present due to interest rates. BESS with a long battery lifetime generate more revenues in the future, which are less valuable than revenues in the present. This is why the levelized cost of electricity (LCOE) is used to evaluate the economy of PV BESS.

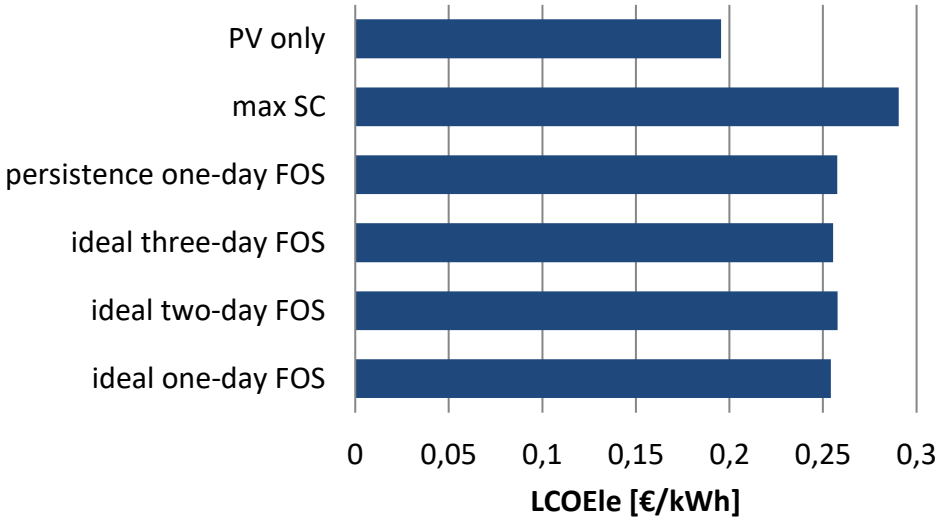

Figure 48: Levelized cost of electricity (LCOEle) of different operation strategies of a PV BESS with a 10 kWp PV power plant and a 10 kWh BESS.

The illustrated results in Figure 48 confirm the results of Figure 47. A higher energy throughput over the battery lifetime leads to lower LCOEle and therefore to a higher profitability. The ideal one-day FOS is the most profitable strategy and reduces the LCOEle in comparison to the max SC strategy. Even the utilization of the persistence one-day FOS leads to a reduction of the LCOEle compared to the max SC strategy. When the persistence forecast is used, the one-day forecast horizon leads to lower LCOEle as well as shown in Figure 49. Certainly, the three-day forecast leads to lower LCOEle than the two-day forecast, because the forecast inaccuracies compensate for each other. A system with sole use of photovoltaics leads to the lowest LCOEle.

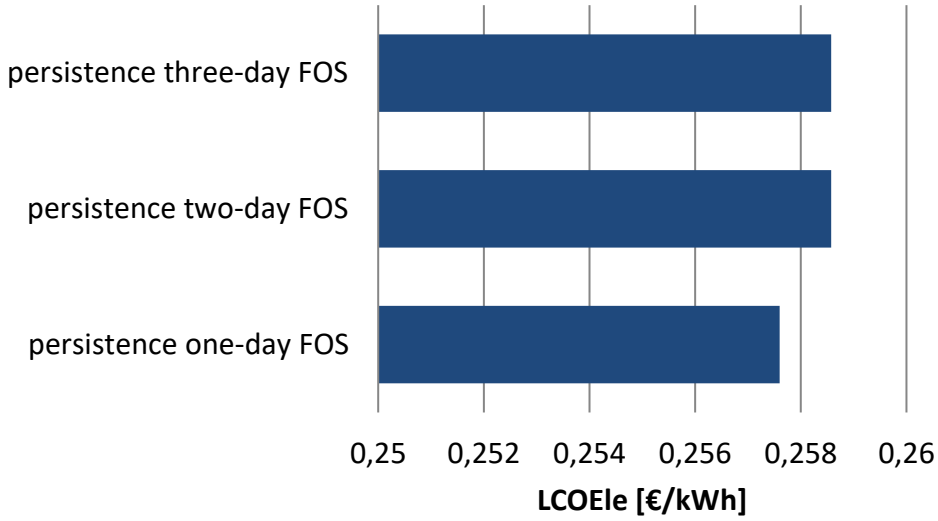

Figure 49: Effect of different forecast horizons on the LCOEle using persistence forecast. Results are for a residential 4-person household with a PV BESS with a 10 kWp PV power plant and a 10 kWh BESS.

4.5.3 Usage of forecast-based operation strategies with feed-in limitations

As described in section 4.1.6, the consideration of feed-in limits for PV BESS can be useful. Section 4.1.8 and section 4.1.10 pointed out that FOS for PV BESS could be used to reduce the cut-off energy of PV systems. The cut-off energy could be stored in the battery in order to reduce cut-off losses. In this section, the introduced strategies FOS fix and FOS variable are compared with a fix P limit strategy and a PV system without a BESS. Furthermore, the influence of different forecast strategies is investigated as well.

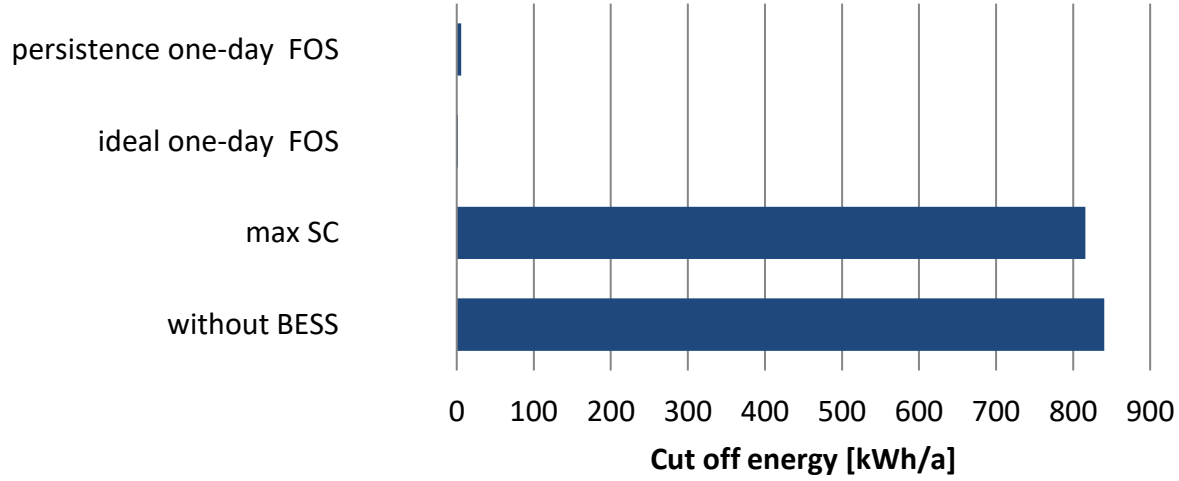

Figure 50: Cut-off energy using forecast-based strategies.

If the PV feed-in is limited to 50 % of the initial PV rated power, as claimed by the KfW to obtain the funding, about 840 kWh/a have to be cut off from a 10 kWp PV system if no BESS is installed. Figure 50 shows the comparison of the cut-off energy for different operation strategies. If a 10 kWh PV BESS is used, which focuses on increasing the self-consumption, the cut-off energy can be reduced to about 816 kWh/a, if the PV BESS considers the feed-in limit (fix P limit strategy). This result is comparable to the results in [144] and [31]. When the ideal one-day FOS or the persistence one-day FOS is used, the cut-off energy can be stored almost completely because the used battery size is big enough to store the complete energy of the midday peak. It is evident that cut-off energy can be reduced by using forecast-based operation strategies as shown in Figure 50 and presented in [144].
The funding of a PV BESS by the KfW Group requires a feed-in limit for the PV system. The KfW Group grants a subsidy to the installation cost of the BESS. The amount of the subsidy depends on the installation year of the BESS [129]. In this thesis, an installation of the BESS in 2017 and therefore a subsidy of 13 % is assumed as shown in Table 4.
The subsidy leads to reduced LCOE. The feed-in limit leads to rising LCOEle because the cut-off energy needs to be compensated. This specifically applies to the maximized self-consumption strategy. The LCOEle of the forecast strategies are increased because more energy is stored on days with high-energy supply than needed in the following night. The BESS stores more electricity to minimize the cut-off losses than needed due to forecast inaccuracies.

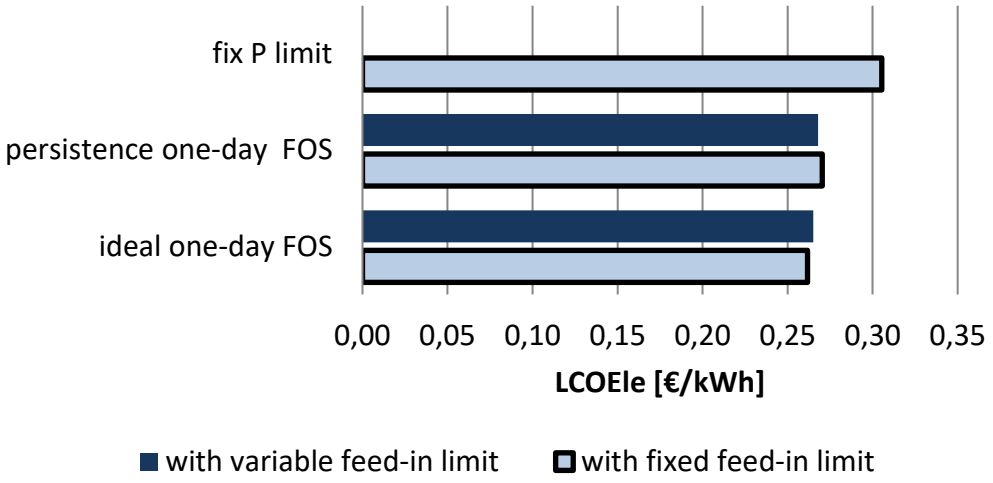

Figure 51: LCOEle of a residential 4-person household with a PV BESS (10 kWp PV power plant; 10 kWh BESS) under consideration of cut-off limitation of the PV-system to 50 % of the peak power. Two different cut-off methods are analyzed: variable feed-in limitation and fixed feed-in limitation.

Figure 51 shows the resulting LCOEle under consideration of the PV cut-off limit and the KfW funding. The reduced installation cost due to the funding overcompensates the cost of curtailment. The small difference between the variable and the fixed feed-in limitation using the ideal FOS can be explained by the efficiency of the battery converter. When the fixed feed-in limit is used the converter operates in a slightly more efficient range, due to higher charging power in the morning. The higher forecast inaccuracies using the persistence forecast lead to increased LCOE.
The limitation of the target SoC is a strategy often used to enhance battery lifetime and is described in section 4.1.5. Concerning [63], an SoC limit of 70 % of the maximum capacity is used when the fix SoC limit strategy is applied. This limit is also applied on the one-day ideal

FOS. Figure 52 shows the comparison of the LCOEle under consideration of the fixed SoC limit. The fixed limit reduces the LCOE. The positive influence of the FOS on the LCOEle remains, especially under consideration of a PV feed-in limitation. The results presented in Figure 52 indicate that a fixed SoC limit leads to lower LCOE. A reason might be that the BESS is oversized. The oversized BESS was chosen because the market analysis based on [180], which was mentioned in section 3.4, shows that 10 kWh is a very common size for the PV BESS available today.

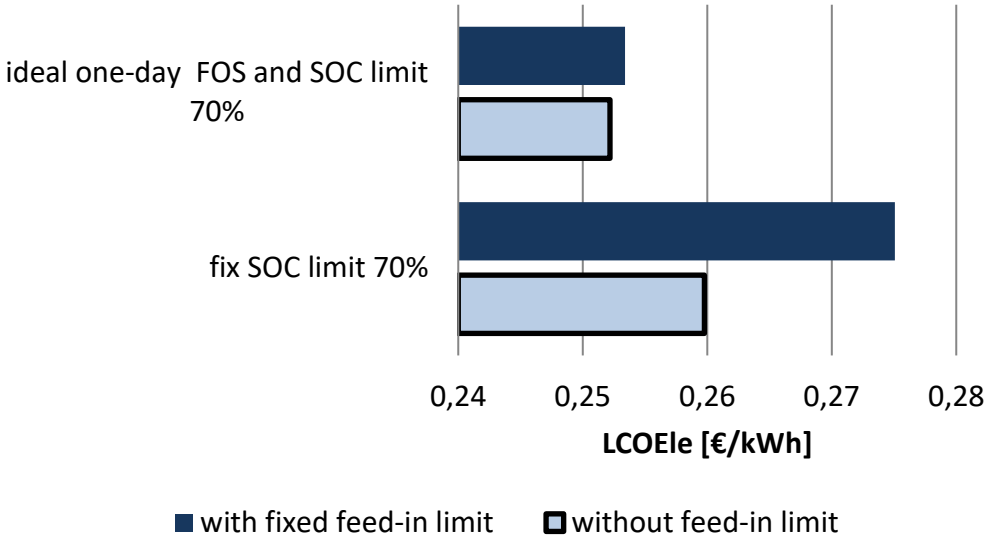

Figure 52: LCOEle of a residential 4-person household with a PV BESS (10 kWp PV power plant; 10 kWh BESS) under consideration of cut-off limitation of the PV-system to 50 % of the peak power. The max SoC limit is considered to reduce the battery aging.

4.5.4 Influence of the battery size on the LCOEle of forecast-based operation strategies

An alternative to limiting the maximal SoC is a reduction of the battery size. A reduced battery size leads to a higher burden on the battery, but also to lower investment cost. A battery size of 5 kWh is chosen for this analysis. In this case, the cut-off energy, under consideration of the max SC operation strategies, is increased to 831 kWh/a compared to 816 kWh/a if a 10 kWh BESS is installed. The resulting LCOEle is depicted in Figure 53. Even though the battery size is smaller, the one-day ideal FOS still has a positive influence on the LCOEle compared to the max SC operation strategy, due to a longer lifetime of the BESS.

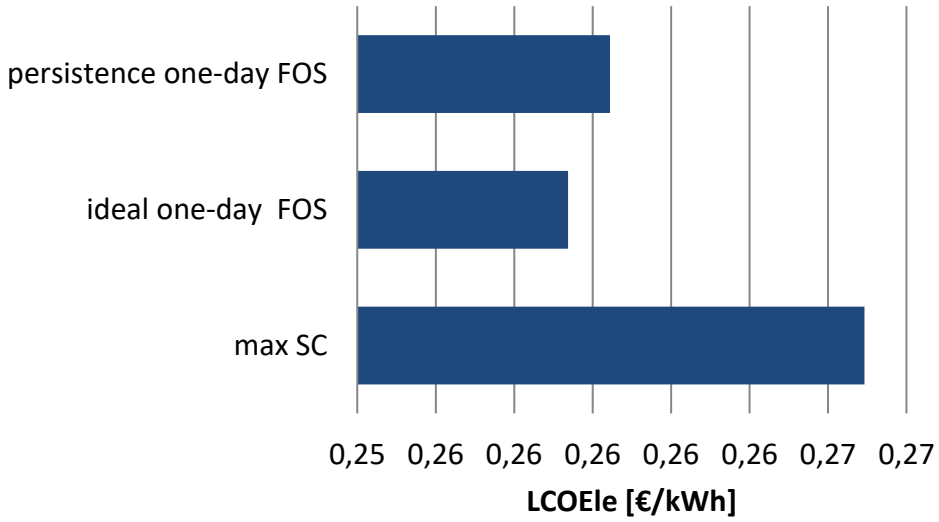

Figure 53: LCOEle of a residential 4-person household with a PV BESS (10 kWp PV power plant; 5 kWh BESS).

Figure 54 depicts a sensitivity analysis of different battery sizes regarding the self-sufficency SS_{rate} rate and the LCOEle. The calculation of the self-sufficency rate is presented in equation (54).

$$SS_{rate} = \frac{E_{PV_{used}}}{E_{total\ load}} \tag{54}$$

The self-sufficiency rate is enhanced with increasing battery size. The self-sufficiency rate when the ideal-one-day FOS is applied leads to saturation because of the forecast horizon of one day. This is why the self-sufficiency rate is higher when the max SC operation strategy is applied at BESS with higher capacities. The LCOEle, under consideration of the max SC operation strategy and the ideal-one-day FOS, is presented. The utilization of the ideal-one-day FOS has a positive influence on the LCOEle and increases the economics of the BESS accordingly, especially under consideration of BESS capacities greater than 5 kWh. The reason for the lower LCOEle when the ideal-one-day FOS is used is the longer lifetime of the BESS. The analyses point out that lower capacity of BESS leads to lower LCOE, which is consistent to [63]. The optimal system configuration in dependency of the operation strategy is presented in section 5.3.1.

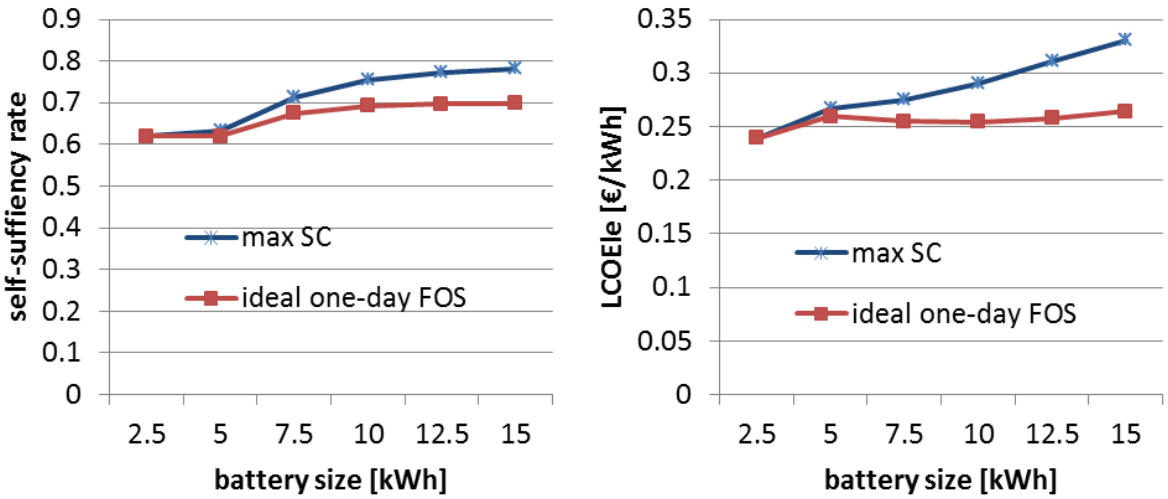

Figure 54: Self-sufficiency rate (left) and LCOEle (right) of a residential 4-person household with a PV BESS (10 kWp PV power plant). Different battery sizes are compared.

4.5.5 Influence of the rated PV power on the LCOEle of forecast-based operation strategies

To test performance of the presented FOS with a different size of the PV system the following analysis is presented. For this analysis, a 5 kWp PV power plant is chosen instead of the 10 kWp PV power plant. Analog to the analysis in section 4.5.4, the feed-in limitation to 50 % of the PV peak power and no feed-in limitation is examined. A reduced rated PV power of 5 kWp leads to reduced cut-off energy of 353 kWh/a compared to 840 kWh/a with a 10 kWp PV system. An additional 10 kWh BESS, operated with a max SC strategy, reduces the cut-off energy to 252 kWh. Figure 55 shows the results of the analysis for the LCOE. The decreased rated PV power increases the LCOE, because generation costs for PV energy are lower than the feed-in tariff for PV energy. The application of the one-day ideal FOS reduces the LCOEle compared to the max SC operation strategy. In this case, a PV system without a BESS leads to the lowest LCOE.

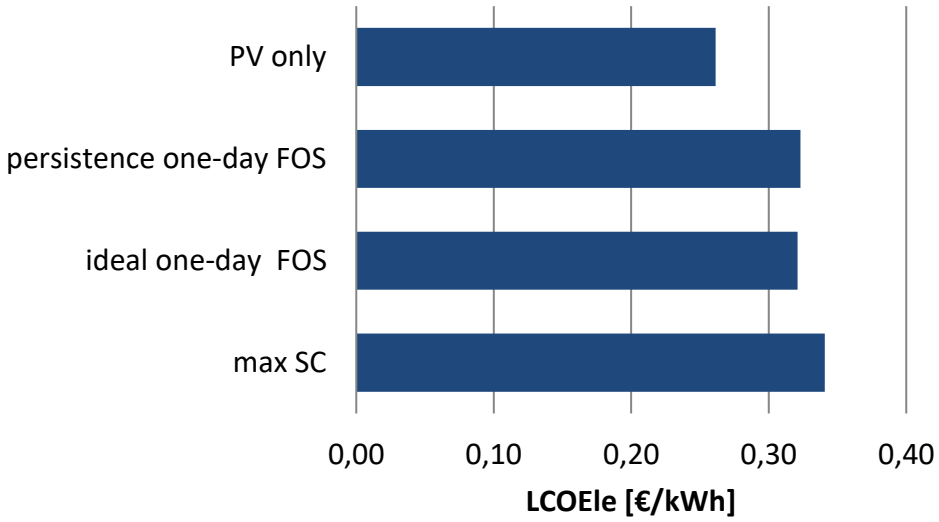

Figure 55: LCOEle of a residential 4-person household with a PV BESS (5 kWp PV power plant; 10 kWh BESS) under consideration of different operation strategies.

4.5.6 Influence of the load profile on the LCOEle of forecast-based operation strategies

To determine the influence of different load profiles, the used load profile is scaled by a factor of 1.2. This is due to the fact that the applied profile amounts to an annual energy consumption in accordance to the standard load profile of a 4-person household. Findings from the WMEP monitoring program [13] suggest that the type of analyzed households has a 20 % higher energy consumption in comparison. Figure 56 presents the resulting LCOEle for the variation of the load profile. The increased load leads to slightly higher LCOE. Due to the higher load, a higher amount of energy needs to be stored during the day. This leads to a increased battery aging, which increases the LCOEle slightly. Nevertheless, the one-day ideal FOS still has a positive influence on the LCOE. If the load is increased by the factor 1.2, the cut-off energy under consideration of a max SC operation strategy is reduced to 808 kWh/a compared to 816 kWh/a.

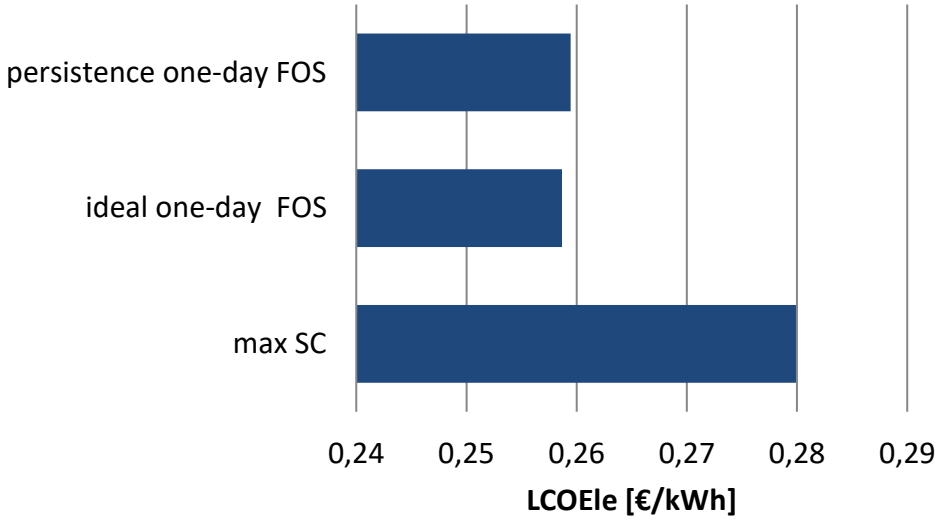

Figure 56: LCOEle of a residential 4-person household with a PV BESS (10 kWp PV power plant; 10 kWh BESS) under consideration of cut-off limitation of the PV-system to 50 % of the peak power. The load of the household is increased by the factor 1.2 compared to the aforementioned scenarios.

4.5.7 Evaluation of the influence of the operation strategies on the 45Ah NCA Saft cell

The influence of the forecast-based operation strategies is verified on the 45 Ah NCA battery cell from Saft. This battery cell is used for the analysis published by [163] and [164] as well. The specifications of the cell are given in [181]. This battery has a higher quality and therefore a higher lifetime and a higher price compared to the LG Chem 18650 battery cell. The price for high quantities is assumed to be 550 €/kWh based on [63] and is applied for the LCOEle calculation. All other input data and costs for the LCOEle calculations are the same as in Table 4. Figure 57 compares the lifetime of ideal one day FOS and persistence one day FOS compared to the max SC strategy.

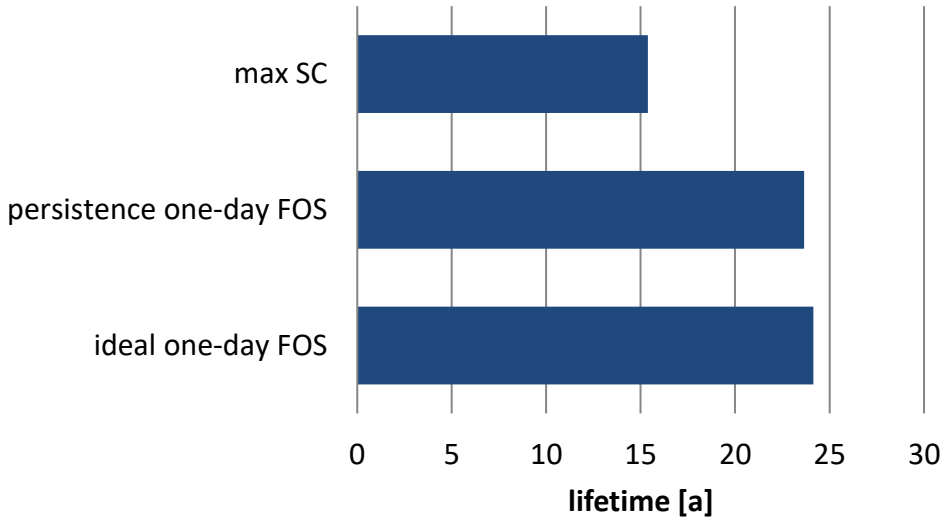

Figure 57: Battery lifetime of a residential 4-person household with a PV BESS (10 kWp PV power plant; 10 kWh BESS). Influence of different forecast strategies and different forecast horizons on the battery lifetime of the Saft NCA VL45E battery cell.

The lifetime-enhancing effects of FOS on the Saft NCA VL45E battery cell are illustrated as well. These results are similar to the results shown in section 4.5.2. The application of FOS further reduces the LCOEle as illustrated in Figure 58 and therefore enhances the economics of the PV BESS.

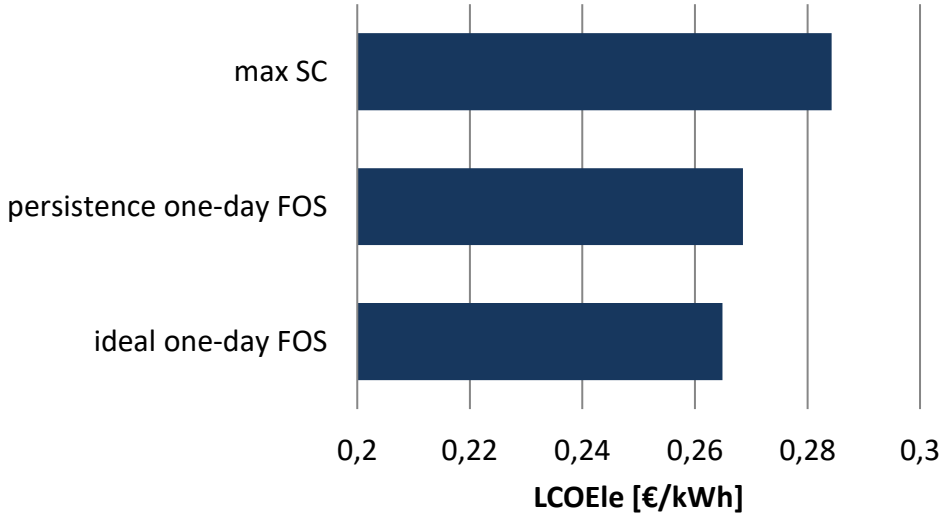

Figure 58: LCOEle of a residential 4-person household with a PV BESS (10 kWp PV power plant; 10 kWh BESS with a Saft NCA VL45E battery cell).

4.6 Impact of different system topologies

Besides the PV BESS the integrated home contains a system for power-to-heat coupling. In this section, the self-consumption rate of the integrated home is compared to homes with different configurations. The self-consumption rate is an indicator for households with PV

systems. The influence of the different components is illustrated. The influence on the self-consumption rate is examined on a monthly basis. The self-consumption rate (SC_{rate}) is defined as the used PV-generated energy divided by the energy produced by the PV system.

$$SC_{rate} = \frac{E_{PV_{used}}}{E_{PV_{gen}}} \tag{55}$$

Figure 59 illustrates the self-consumption rate of the integrated home in comparison to self-consumption rates of different energy supply systems. By installing a 10 kWh BESS, the self-consumption rate can be increased to 45 % on annual basis. This value depends largely on the capacity of the battery system. The use of a heat pump for power-to-heat coupling can increase the self-consumption rate to 58 % per year. The increase due to power-to-heat application is rather small because of seasonal effects. For this analysis, the maximized self-consumption operation strategy in corporation with the heat storage as a passive element is used.

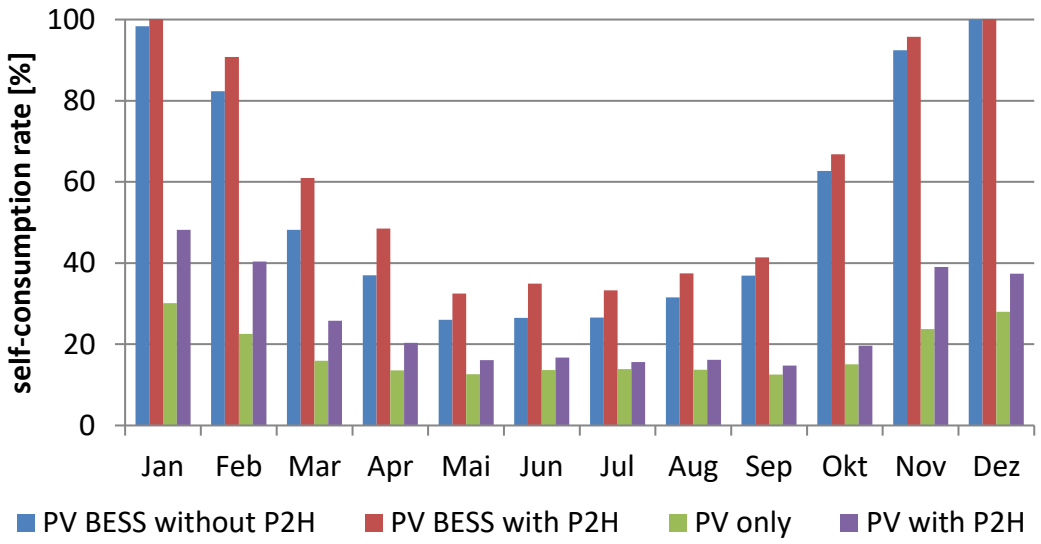

Figure 59: Self-consumption rate of different systems: 10 kWp PV system; PV BESS with 10 kWp PV system and 10 kWh BESS; 10 kW heat pump.

Below, the self-sufficiency rate (SS_{rate}) is analyzed. The self-sufficiency rate is defined as the energy from the PV system used to cover the load, divided by the total load, as presented in equation (54).
The influence of different topologies on the self-sufficiency rate is depicted in Figure 60.
The use of PV energy for the heating sector leads to an increased total load. Therefore, the self-sufficiency rate of systems with power-to-heat coupling is rather low during winter. The self-sufficiency rate is dominated by the demand of the heating system. Nevertheless, during summer, the thermal demand is relatively low and therefore the influence on the self-sufficiency rate of the system is smaller. The application of a BESS has a high influence on the self-sufficiency rate. This is why seasonal effects influence the self-sufficiency rate.

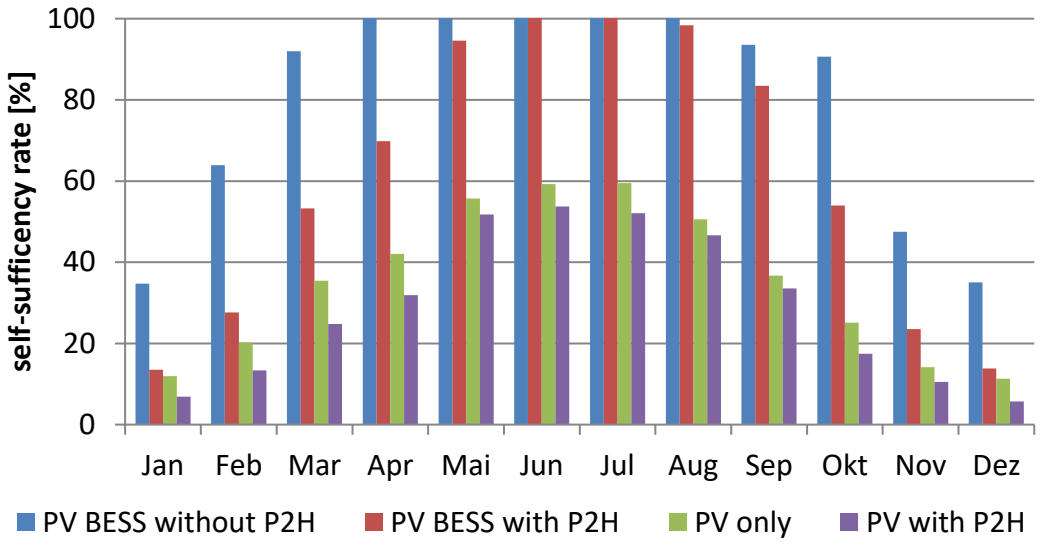

Figure 60: Self-sufficiency rate of different systems: 10 kWp PV-system, PV BESS with a 10 kWp PV system and a 10 kWh BESS; 10 kW heat pump.

The self-consumption rate of the analyzed PV BESS with a heat pump for power-to-heat coupling is 100 % in January and December, while the grid feed-in is almost zero. In summer, the PV generation is able to cover almost the complete energy demand. Therefore, the grid consumption in summer is almost zero. The low grid consumption leads to a self-sufficiency rate of almost 100 % in summer. Figure 61 depicts the grid exchange of the integrated home in a non-optimized scenario. The big capacity of the storage units leads to an optimal use of the PV energy in winter and summer. In spring and autumn, the PV generation and the load do not occur close in time. Therefore, the storage units are not able to use the full potential of the PV generated energy.

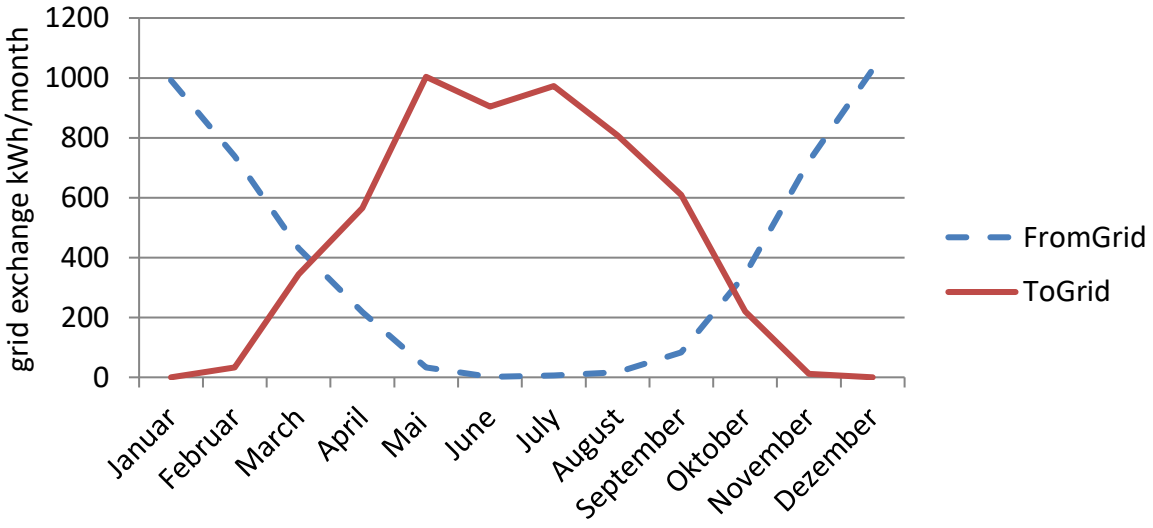

Figure 61: Grid exchange of a PV BESS with a 10 kWp PV system and a 10 kWh BESS; 10 kW heat pump.

4.7 Operation integrated homes

In this section the maximize self-consumption operation strategy (4.1.4) and the FOS (4.1.6) for the BESS in combination with the heating part are investigated. These operation strategies are combined with the operation strategies for the power-to-heat system presented in section 4.3. In section 4.3 the operation strategy: heat storage as a passive element (passive), battery priority charging (bat prior) and priority charging of the heating storages (heat prior) are presented. Furthermore, section 3.3.6 presents two different operation modes for the heat pump. The influence of the different operation strategies is examined below. To evaluate and assess the different operation strategies, the annuity and therefore the annual costs are calculated. The annuity is used because the load of the heating system depends on the operation of the storage units and the heat pump. The flow temperature influences the COP of the heat pump and therefore the electric consumption to cover the heating demand.
Figure 62 depicts the influence of the heat pump operation. Modular heat pump operation always leads to lower annual costs compared to static heat pump operation. The finding does not depend on the operation strategies of the heating system or the electricity system. The influence of the operation of the heat pump is rather low. It ranges from 15 €/a to 50 €/a. The reason for the savings is the higher self-consumption rate due to a flexible use of the heat pump. In [171], the influence of the operation of the heat pump on the autarky rate and the self-sufficiency rate is investigated. This thesis shows minor influence as well.

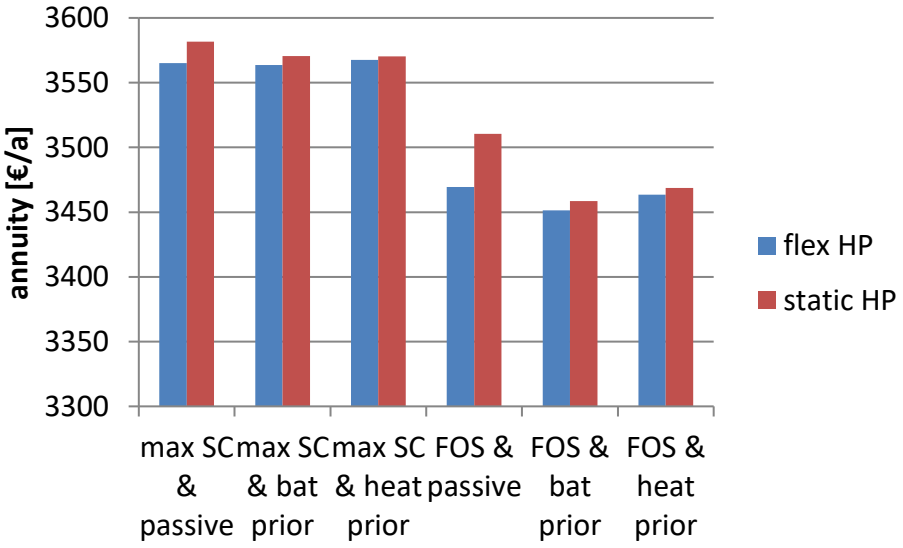

Figure 62: Annuity of PV BESS system with power-to-heat application (10 kWp PV system; 10 kWh BESS; 10 kW heat pump) and different operation modes of the heat pumps.

Figure 63 depicts the influence of the operation strategy on the annual costs. Two operation strategies are investigated: the maximization of the self-consumption and the forecast-based operation strategy. The application of a forecast-based operation strategy leads to lower annual costs in all scenarios. The savings are between 75 €/a and 125 €/a. The reason for the savings is the higher lifetime of the BESS. A detailed analysis on these effects is shown in [133].

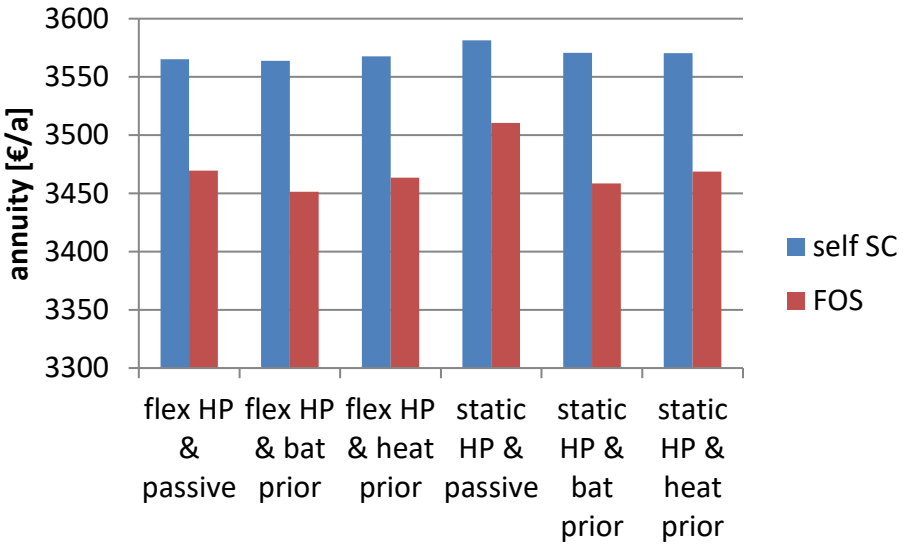

Figure 63: Annuity of PV BESS system with power-to-heat application (10 kWp PV system; 10 kWh BESS; 10 kW heat pump) and different operation strategies of the electric system.

The influence of the different operation strategies of the heat system is presented in Figure 64. The influence of the operation strategy of the heating system is rather low and depends on the operation of the heat pump. A battery priority charging leads to the lowest annual costs in most scenarios. A detailed analysis of the influence of the different operation strategies is presented in [182].

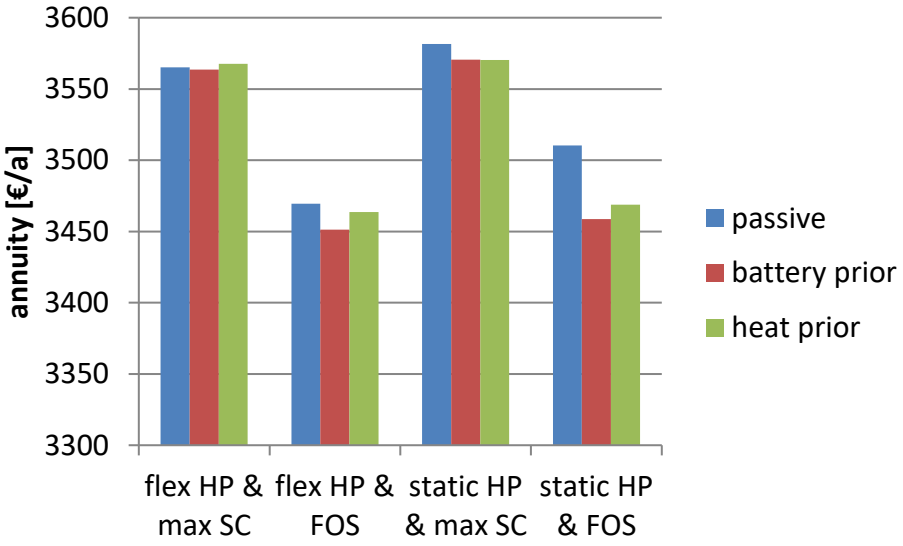

Figure 64: Annuity of PV BESS system with power-to-heat application (10 kWp PV system; 10 kWh BESS; 10 kW heat pump) and different operation strategies of the heating system.

In conclusion, forecast-based operation strategies (FOS) for the electrical side lead to reduced LCOEle compared to a self-consumption maximizing strategy. The battery priority charging as well as modularly operating heat pump can reduce the costs of an integrated home. Hence, the forecast-based operation strategy in combination with a modular operating heat pump and a battery priority charging of the heating system is defined as the “advanced operation strategy”. An economic comparison to fossil heating concepts is presented in section 5.3.

4.8 Conclusion and discussion

This section presents operation strategies for integrated homes. In the beginning, operation strategies for the electrical part and for the thermal part are analyzed separately and then they are combined.

For the electric part, a new forecast-based operation strategy to enhance the battery lifetime and therefore the economics of PV battery energy storage systems is presented. This operation strategy is compared to different commonly used operation strategies. To evaluate the economics of the examined strategies, the different resulting levelized costs of electricity are compared. Results show that forecast-based operation strategies can enhance battery lifetime. The annual energy throughput is slightly reduced, but in combination with the significantly prolonged lifetime, the total energy throughput can be increased. The lifetime of the low-cost consumer lithium-ion NMC battery cell can be enhanced by around five years, i.e. doubled, if the forecast-based operation strategy is used instead of a maximized self-consumption operation strategy. The forecast-based operation leads to a reduction of the levelized cost of electricity of up to 3.5 c€/kWh compared to a self-consumption maximizing strategy (10 kWp PV system, 10 kWh BESS, 4-person household (consumption: 4,674 kWh_{el}/a) in Lindenberg close to Berlin, Germany). The costs are reduced by 12 percent. A similar operation strategy is promoted by SOLARWATT GmbH [183].

Forecast-based operation strategies use predictions for load and PV generation. To investigate the influence of forecast inaccuracies, two different forecast strategies are examined. The persistence forecast is used as the worst-case forecast and the perfect forecast is used as the best-case forecast. This approach allows evaluating the potential of the forecast-based operation strategies. Advanced forecast methods would lead to results within the range provided by both cases.

Different forecast horizons are examined in addition to the worst and best case of forecast accuracy. The results show that a one-day forecast is sufficient and leads to the lowest levelized cost of electricity in most cases. This could be further improved by implementation of a variable forecast horizon. The proposed operation strategies work with static forecast horizons. This means that the forecast horizon is fixed and the operation strategies always try to store enough energy to satisfy the energy demand for a constant period of time. If a penalty function is introduced to internalize the additional battery aging when storing energy over multiple days, even lower levelized cost of electricity could be reached.

Besides improved economics, a forecast-based operation strategy in combination with a variable feed-in limit can be used to reduce the influence of PV systems on the grid. In this case, forecast-based operation strategies could be used to reduce the resulting cut-off energy if a feed-in limit for PV is applied. Results show a reduction of cut-off energy to a few kilowatt hours compared to over 800 kWh per year. If a fixed feed-in limitation strategy is used, all the energy above a predefined feed-in limit will be stored in the battery. In contrast, the variable feed-in limitation strategy sets a feed-in limit for every day, depending on the predicted energy demand during the following night. The forecast-based operation strategy with a variable feed-in limitation leads to a reduction of the levelized cost of electricity by 4 c€/kWh in comparison to the maximized self-consumption operation strategy. The application of such an operation strategy can be advantageous in consideration of possible or existing feed-in limitations. These could be issued by regulatory frameworks [130] or by funding schemes [129].

A sensitivity study has been conducted regarding different component sizes of the battery and PV system as well as regarding solar irradiation and load profiles. Results show that the use of forecast-based operation strategies can enhance the economics of the battery energy storage system regardless of component size or applied profiles. A small battery with a capacity of only 2.5 kWh shows a negligible influence of the operation strategy. With increasing battery size, the cost decreasing effect of the forecast-based strategy improves. This is mainly due to fact that an oversized battery system is not fully discharged every night during summer because of overproduction from PV. This leads to a higher average state of charge and therefore accelerated aging of the battery. The forecast-based operation strategy limits battery charge to the demand of the following night to avoid this.
The influence of the presented operation strategies is analyzed for two different battery cells, a low-cost consumer NMC battery cell and a high-performance NCA battery cell. The developed strategy has a significant effect in both cases. The lifetime of the NCA cell can be prolonged by nine years or up to 60 percent, and the levelized cost of electricity can be reduced by 2 c€/kWh or 7 percent if the developed operation strategy is applied.
Due to the huge variety of different lithium-ion battery cells and their properties, the values resulting from this investigation need to be verified for each specific cell individually. Still, all common lithium-ion cells show accelerated aging along with a higher average state of charge. This means that the general principles of the findings and the overall validity of the operation strategy should apply to all types of lithium-ion-based PV battery energy storage systems.
The developed forecast-based operation strategy is used in conjunction with the operation strategies for the heating sector. The results show that forecast-based operation strategies (FOS) for the electrical side lead to reduced LCOEle compared to a self-consumption maximizing strategy, even under consideration of power-to-heat coupling. Furthermore, a battery priority charging as well as a modular operating heat pump can reduce the costs of an integrated home. In conclusion, the forecast-based operation strategy in combination with a modular operating heat pump and a battery priority charging of the heating system lead to reduced costs for the integrated home. These operation strategies are defined as the “advanced operation strategy”. The savings due to advanced operation strategies for the investigated integrated home range from 15 €/a to 50 €/a in comparison to basic operation strategies. Basic operation strategies are defined as the maximization of the self-consumption rate without the use of the heat storages for the storage of excess PV generated energy.
The implementation of the presented operation strategy can be done without an additional communication interface if persistence forecast is used. To implement such a strategy, additional computational effort in the energy management system might be required. This could lead to higher costs for the energy management system and an increased energy demand of the system itself. It is not investigated whether the savings gained by the implementation of such strategies overcompensate the costs for implementation.

5. Behind the meter: Optimization

In contrast to section 4, this section investigates the optimization of integrated homes with power-to-heat coupling.

5.1 Literature on Optimization

A vast number of publications address the topic of optimization of sizing, placement and control of PV and storage systems. The investigated algorithms and solving methods are as manifold and varied; Linear Programming (LP), Mixed Integer Linear Programming (MILP), evolutionary algorithms, gradient methods, self-learning algorithms, dynamic programming and many more. The literature review does not present all possible approaches, but rather those using well-established methods for optimal component sizing of PV combined with storage systems.
In [63], the optimization of a PV BESS using an evolutionary algorithm is investigated, with the result that small BESS are more economic compared to large BESS. The optimal sizing of PV-coupled batteries from a household's economic perspective is presented in [184]. An algorithm for optimal battery sizing of smart homes with convex programming is presented in [185]. Optimization of sizing of PV battery systems and break-even analysis of PV battery self-consumption systems are presented in [186]. A Mixed Integer Linear Programming (MILP) algorithm for optimal PV battery sizing and energy scheduling is proposed in [187]. The paper presents similar results: larger PV systems with smaller battery systems have a higher economic efficiency. In [188], a mixed integer linear programming optimization model for operation and investment of PV battery systems is presented. MILP is used in [189] as well for optimal operation of household applications. In [190] the mixed integer linear programming optimization method is used for optimization of the operation and investment of PV battery systems. The mixed integer linear programming algorithm to optimize the operation schedule of a heat pump system is presented in [179]. The results point out the importance of variable electricity prices to incentivize flexible heat pump operation. A mixed integer linear programming for optimal sizing and operation of, electric boiler and thermal storage in combination with PV applications is presented in [191]. Results show that only large PV sizes, or highly fluctuating electricity prices, create a need for large storage sizes. An optimization of an integrated home with the target to enhance the self-consumption is presented in [178]. This publication investigates the sizing and comparison of different types of PV heat systems using mixed integer linear programming method as well. In [192], the optimal battery size was calculated under different parameters including electricity tariff, feed-in electricity price, and battery performance and price. The paper concludes that that the optimal battery size is strongly influenced by the local conditions especially the feed-in electricity price. A similar investigation is made in [193]. In this publication, an optimal sizing of PV and BESS for a smart household considering different price mechanisms is presented. The results show a strong dependency on the pricing structure. The sizing of residential photovoltaic systems in combination with battery storage systems and heat pumps is investigated in [194]. This publication investigates the investor’s perspective as well as the DNO’s perspective and focuses on the impact of different incentives on sizing and operation.

Nevertheless, the publication does not investigate forecast-based operation strategies to enhance economics of the house. The sizing of residential PV systems with heat pumps and battery storage systems with the focus on changing economics and regulatory is investigated in [195].

5.2 Optimization approach

5.2.1 Target function

The aim of the optimization is to reduce the overall system costs of the integrated home behind the meter. Therefore, the annuity is used as an indicator of the costs of the integrated home. The annuity depicts the annual costs of the integrated home. The calculation of the annuity is presented in section 3.5.

5.2.2 Optimization parameters

The optimization parameters have a direct influence on the target function presented in section 3.5. These optimization parameters and the corresponding boundary conditions are given in Table 10. The optimization parameters are the variables for different components, which have a direct influence on the economics. The investment costs of these components depend on the sizes of the components. The investment costs of the electrical system (converter and inverter, PV system, BESS) and the investment costs of the thermal system (DHW and buffer storage, heat pump) are optimized.
Furthermore, parameters that influence the behavior of the systems are optimized. These parameters are the maximum temperatures of the buffer storage and the DHW storage. Additionally, the spread temperature of the buffer storage and the spread temperature of the DHW storage are optimized. These temperatures determine the temperature increase if the heat storage is charged. Furthermore, the storage temperatures influence the flow temperature of the heat pump and therefore it influences the efficiency (COP) of the heat pump.

parameter	symbol	min.	max.	unit
PV-generator size	P_{PVPeak}	5	10	kWp
power MPP-tracker	P_{MPP}	5	10	kW
power inverter	$P_{Inverter}$	5	10	kW
power battery converter	$P_{BatConv}$	2	10	kW
capacity battery system	C_{BESS}	0	24	kWh
volume buffer storage	V_{Buffer}	variable	2	m³
volume DHW storage	V_{DHW}	variable	2	m³
power heat pump	P_{HPth}	2	15	kW_{th}
max. temperature buffer storage	$T_{Buffermax}$	39	60	°C
spread buffer storage	$T_{Bufferspread}$	0	7	K
max. temperature DHW storage	T_{DHWmax}	45	55	°C
spread DHW storage	$T_{DHWspread}$	0	7	K

Table 10: Optimization parameters of the integrated home and the corresponding boundary conditions.

The minimum size of the buffer storage is flexible, because it depends on the size of the heat pump as presented in section 3.3.2 and 3.3.3. The buffer storages ensure the minimum runtime of the heat pump. The maximum output temperature of the modeled heat pump is 60°C. The minimum volume of the buffer storage can be calculated with equation (56) and is used in equation (12).

$$V_{min} = \frac{P_{th,N} \cdot t_{min}}{c_p \cdot \rho \cdot \Delta T_{min}} \tag{56}$$

$$\Delta T_{min} = \min(T_{max} - T_{Spread} - 32°C, 5°C) \tag{57}$$

V_{min}	=	min. water volume of the storage	[m³]
$P_{th,N}$	=	thermal power heat pump	[kW]
t_{min}	=	min runtime heat pump	[h]
c_p	=	thermal capacity of water	[kJ/(kg·K)]
ρ	=	water density	[kg/m³]
ΔT_{min}	=	min temperature spread storage	[K]

5.2.3 Optimization algorithms

The described optimization problem is a non-linear (battery aging), non-convex and multimodal-optimization problem. Due to the complexity of the optimization problem, a probabilistic algorithm is chosen. Probabilistic algorithms require less computational effort in comparison to deterministic algorithms. Due to the complexity and non-linearity of the model, a linear programming algorithm cannot be chosen. Therefore, an evolutionary algorithm is applied [196], in particular, the Covariance Matrix Adaptation Evolution Strategy (CMA-ES)

algorithm [197]. This algorithm is a state-of-the-art evolutionary algorithm and one of the standard tools for continuous optimization [198]. The algorithm is used for non-linear non-convex multimodal-optimization problems as described in [199]. The algorithm provides some advantaged in comparison to other evolutionary algorithms like the genetic algorithm. Due to the use of a covariance matrix, a weak performance of non-linear optimization problems is avoided. Additionally, due to the implementation of a step-size control, an early convergence is avoided [200].
The CMA-ES algorithm is based on Hansen et al. [201] and uses a stochastic method. The population size is variable. Big population sizes can avoid local minima, whereas small population sizes lead to fast convergence at the risk of premature convergence.

5.3 Optimization results

5.3.1 Optimization results for optimal component sizing

As shown in section 4, the costs of the integrated home for the energy supply depend on the operation strategies. Therefore, the integrated home is optimized for two scenarios. A “basic operation strategy scenario” with a static heat pump, a maximized self-consumption operation strategy for the electricity supply and a passive operation strategy for the heating system. The “basic operation strategy scenario” is compared to the “advanced operation strategy scenario”. The “advanced operation strategy scenario” uses a flexible heat pump, the battery priority charging of the heating system and the forecast-based operation strategy as pointed out in section 4. The algorithms, target functions and parameters presented in section 5.2.1 are used for optimization.
If the annuity of the best individual does not improve significantly, the optimization is stopped. The presented results are based on an optimization that executed 1036 annual simulations with a one-minute resolution for the advanced operation scenario and 1079 annual simulations for the basic scenario. The lifetime is extrapolated after one year of simulation. The optimum set of parameters for the electric system found by the optimization algorithm is presented in Table 11.
The optimization of the electric system in the “basic operation strategy scenario” leads to the following results. The feed-in tariff is higher than the generation cost of the PV energy, therefore the optimization chooses the upper boundary of the PV generator size (10 kWp). The optimal power of the MPP tracker is 79 % of the maximum peak power of the PV generator, because the energy losses due to the power restriction of the MPP tracker are low. The costs for the losses of the PV generated energy due to the undersizing of the MPPT are lower compared to the savings due to undersizing. The phenomena is commonly known and analyzed in [202]. The optimal inverter size is slightly lower compared to the optimal MPP tracker size, minding the losses of the converter. A battery storage system is not chosen by the optimizer, because of the relatively high investment costs.
The optimization of the electric system in the “advanced operation strategy scenario” leads to the same results as the optimization of the electric system in the “basic operation strategy scenario”. The difference between these two scenarios is the use of the forecast-based operation strategy (FOS) in the advanced scenario. The FOS reduces the battery aging by storing only enough energy to meet the demand of the following night. The optimization leads

to the same results for both scenarios, because a battery system is not minded. The LCOEle are 19.18 ct/kWhel.
In the “advanced operation strategy scenario”, the persistence prognosis is used. The use of the ideal FOS, without forecast errors, leads LCOEle of 18.82 ct/kWh_{el}. The use of the FOS can enhance the economics of BESS [133] even under consideration of the optimal component size, when a sufficient forecast algorithm is chosen. In this case a 9.5 kWh BESS is applied. The battery converter power in the in this case is 1.6 kW. The BESS is mainly discharged during night with base load. During day when the BESS is charged, especially in summer, there is enough excess PV radiation to charge the BESS until the BESS reaches the maximum SOC. This is why a small battery converter is sufficient [63]. The optimal sizes of the electrical sector based on the operation strategy are presented in Table 11. In following the persistence prognosis presented in section 4.4 for the advanced operation strategy scenario is chosen.

Parameter	Symbol	max SC	FOS pers	FOS ideal	unit
PV-generator size	P_{PVPeak}	10.0	10.0	10.0	kWp
power MPP-tracker	P_{MPP}	7.9	7.9	7.8	kW
power inverter	$P_{Inverter}$	7.8	7.8	7.7	kW
power battery converter	$P_{BatConv}$	0.0	0.0	1.6	kW
capacity battery system	C_{BESS}	0.0	0.0	9.5	kWh
Levelized cost of Electricity	LCOEle	19.18	19.18	18.82	ct/kWh_{el}

Table 11: Optimum set of parameters found by the optimization algorithm for the electricity sector in dependency of the operation strategy.

Table 12 depicts the optimal sizes of the integrated home in dependency of the applied operation strategy. The optimization of the heat and power system lead to the conclusion that the use of the thermal storage of the investigated optimized integrated home to store excess PV energy is not economical, due to a reduction of the seasonal performance factor (SPF). The seasonal performance factor (SPF) is a measure on the efficiency of the heat pump and defined as the ration between the electrical energy consumption and the produced heat power over one year. The seasonal performance factor (SPF) of the heat pump is 3.7, which is close to the upper boundary for air-water heat pumps in real operating conditions according to [47]. When the excess PV energy is stored in the thermal storage, the temperature of the heat system is increased. The increased temperature of the thermal storage leads to a lower SPF of the heat pump. The diminished SPF of the heat pump leads to higher losses of the excess PV energy. If the spread of the DHW and buffer storage is set to 5 °C, the SPF decreases to 3.3 in comparison to 3.7 for a temperature spread set to 0 °C. The diminished SPF increases the electricity demand of the heating sector from 3800 kWh/a to 4230 kWh/a. Due to an increased utilization of the PV radiation, the grid consumption is reduced by 25 kWh/a. On the other hand, the grid feed-in is reduced by 450 kWh/a, resulting in additional annual cost of 50 €/a, if the spread temperature is set to 5 °C.
Furthermore, the results imply that a thermal system with relatively small heat storage components and a relatively small heat pump is economical. A reduced buffer storage size

reduces costs of the integrated home, but increases the switching rate of the heat pump. Therefore, the optimizer chooses a buffer storage size close to the minimum size defined in section 5.
The heat pump increases the electrical demand of the household. This is why a BESS is economical, if a power-to-heat coupling system is applied. In the case of the basic operation strategy, the optimal capacity of the BESS is 7.1 kWh. If the advanced operation strategy is applied, the optimal size of the BESS is increased to 7.6 kWh. The size of the battery converter is relatively small, because of the discharge at base load. The sizes of the inverter and the MPP-tracker remain constant over the different scenarios.

Parameter	Symbol	Elec basic	Elec adv.	Heat basic	Heat adv.	unit
PV-generator size	PPVPeak	10.0	10.0	10.0	10.0	kWp
power MPP-tracker	PMPP	7.9	7.9	7.8	7.8	kW
power inverter	PInverter	7.8	7.8	7.3	7.6	kW
power battery converter	PBatConv	0.0	0.0	1.6	1.6	kW
capacity battery system	CBESS	0.0	0.0	7.1	7.6	kWh
volume buffer storage	Vbuffer			0.16	0.16	m^3
volume DHW storage	VDHW			0.11	0.11	m^3
thermal power heat pump	PHP,th			2.8	2.8	kWth
max. temp. buffer storage	Tbuffer,max			42.0	42.0	°C
Spread buffer storage	Tbuffer,spread			-	0.0	°C
max. temp. DHW storage	TDHW,max			48.0	48.0	°C
Spread DHW storage	TDHW,spread			-	0.0	°C

Table 12: Optimum set of parameters found by the optimization algorithm for the "basic operation strategy scenario" and the "advanced operation strategy scenario".

5.3.2 Optimization cost analysis

The resulting costs of the presented system, based on the sizes given in Table 12, are presented in the following table. The results are based on an electrical household demand of 4,674 kWh_{el}/a. The levelized costs of energy are calculated based on equation (55).

	Advanced operation	Basic operation
Levelized cost of Energy (LCOEnergy)	14.83 ct/kWh	14.72 ct/kWh
Levelized cost of Electricity (LCOEle)	19.18 ct/kWhel	19.18 ct/kWhel
Levelized cost of Heat (LCOH)	13.16 ct/kWhth	13.05 ct/kWhth
Heating demand	12242 kWh/a	12499 kWh/a
Annuity	2508 €/a	2528 €/a

Table 13: Cost analysis for the result of the "basic operation strategy scenario" and the "advanced operation strategy scenario".

The resulting levelized cost of electricity (LCOEle) of the optimized system is shown in detail in Figure 65 and is compared to a conventional energy supply from the grid (29.2 ct/kWh). The

main costs for the electric system are the investment cost for the PV generator. The PV generator due to the feed-in tariffs (FIT) generates the revenues. Load that cannot be covered directly by the PV generator or by discharging the storage units has to be covered by the grid.

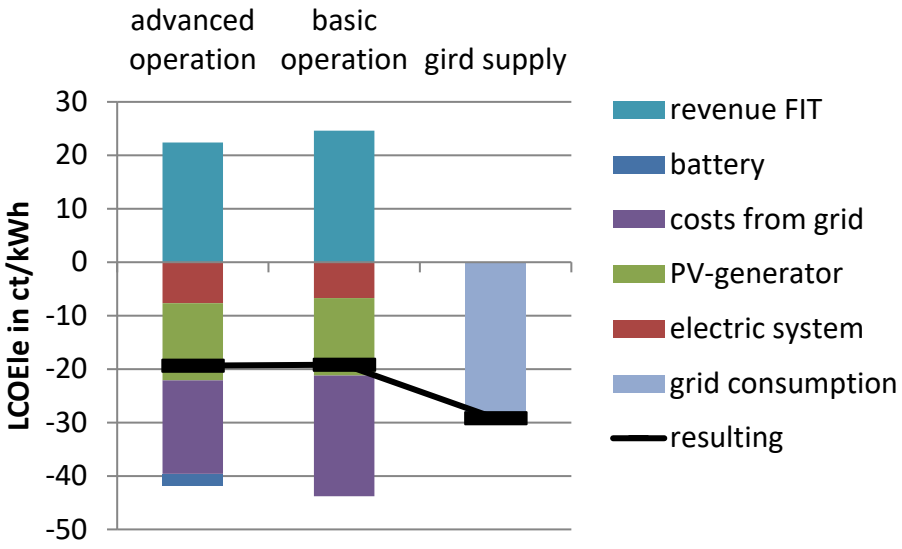

Figure 65: Electricity costs of an optimized integrated home with a PV BESS and power-to-heat coupling in comparison to a household with conventional energy supply.

The LCOH of the optimized integrated home is depicted in detail in Figure 66 and is compared to a fossil fuel heating system. The costs for the fossil heating system are based on [137]. In [137], different costs for fossil heating are given since the age of the building and therefore the insulation standard is important, as well as the type of fuel used. Therefore, minimum and maximum costs for fossil heating are given. The main share of the LCOH is the electricity costs. These costs are mainly generated in the winter month. The thermal energy demand is higher in the winter month and at the same time, the PV generated electricity is lower.

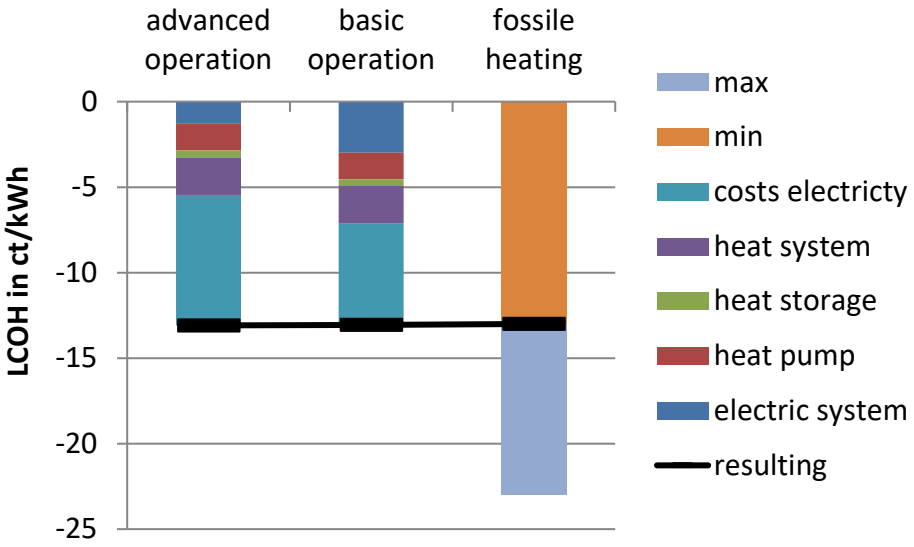

Figure 66: Heat costs of an optimized integrated home with a PV BESS and power-to-heat coupling in comparison to a household with conventional energy supply.

The levelized cost of energy (LCOEnergy) is mainly driven by the cost for energy consumption. Investment costs play a minor part. This cost consists of energy cost for grid consumption and diminished feed-in revenues. The resulting LCOEnergy for the integrated home is compared to a conventional supply system with fossil heating and grid supply. The results are illustrated in Figure 67. The energy costs for the integrated home are at the lower end of the costs for a house with a conventional energy supply concept.

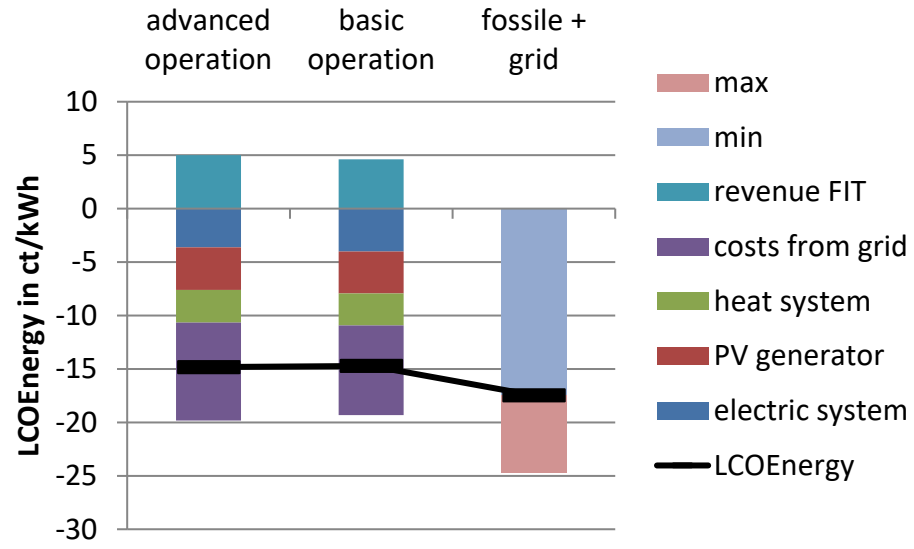

Figure 67: Energy costs of an optimized integrated home with a PV BESS and power-to-heat coupling in comparison to a household with conventional energy supply.

The costs of the two different scenarios, presented in section 5.3.1 in combination with the results presented in section 4.5, lead to the following conclusions: An optimization of component sizes is more cost saving compared to the use of advanced operation strategies. In section 4.5 it is pointed out that the savings due to advanced operation strategies for the investigated integrated home range from 15 €/a to 50 €/a in comparison to basic operation

strategies. The non-optimized investigated integrated home has annual costs of 3582 €/a, depending on the operation of the system. The optimized integrated home has annual costs of 2528 €/a if basic operation strategies are used. Therefore, it is concluded that an optimization of component sizes is more cost saving compared to the use of advanced operation strategies. The optimization results show only a slight reduction of the annuity if the advanced operation strategy is used. In this case, the annuity is 2508 €/a. This leads to the conclusion that advanced operation strategies have a minor influence on the annuity compared to an optimization of component sizes. The advanced operation strategy uses a persistent forecast. The implementation of more sophisticated forecast algorithms can further enhance the economic benefit of advanced operation strategies. A comparable household with fossil heating and a conventional electricity supply from the grid have annual costs of 2990 €/a (4674 kWhel/a electricity consumption and 29.2 ct/kWhel electricity costs; 12499 kWhth/a thermal consumption and 13 ct/kWhth heating costs). The application of an optimized power-to-heat coupled system can lead to savings of up to 15.5 % in comparison to a residential household with electricity consumption from grid and fossil heating.

5.3.3 Non-optimal component sizes

The results presented in Table 12 are the optimal component sizes leading to the lower annual costs of the integrated home. On non-optimal sizing of the components lead to higher cost for the integrated home. A reason for a non-optimal sizing of the complements might be that the components with an optimal size are not available on the market. The influences on deviating component sizes for the electric system are presented in [63]. The publication concludes that the economics are highly sensitive regarding a misarranged dimensioning of the PV generator and the converter. The sensitivity regarding a non-optimal dimensioning of the BESS is lower. An increased size of the heat storages leads to increased costs. The optimization algorithm chooses the minimum size of the heat storages, to make sure the requirement regarding the minimum runtime of the heat pump can be fulfilled. Therefore, an under dimensioning of the heat storages should be avoided.
The optimal sizing of the heat pump depends on multiple factors and influences the economics of the integrated home. An enhanced heat pump size leads to enhanced investment costs and less operating hours. The number of operating hours has a high influence on the optimal heat pump size as shown in [203]. An enhanced head pump size on the other hand reduces the usage of the heating rod. A reduced heat pump size leads to an enhanced usage of the heating rod, which leads to an additional energy consumption. In [204] it is pointed out that a “small size heat pump […] is unable to fully exploit its energy saving potential since an appreciable fraction of the building energy demand is fulfilled by the back-up system” (Dongellini et al. S.10 [204]). The influence of an increased heating demand on the optimal heat pump size is investigated in section 5.4.2.

5.4 Influence of changed load profiles

5.4.1 Influence of changed electrical load profiles

The influences of disturbance functions on the costs are calculated to assess how the operation strategies influence the economics when the consumption profile of the residents is changed. Hence, a scenario is presented that analyses the influence of an electric vehicle (EV), that is introduced to the household, on the performance of the integrated home. The influence of EV on the self-consumption rate is presented in [205] and [206]. In [205] a collaborative strategy is introduced to reduce the forecast uncertainties between the photovoltaic (PV) participants and electric vehicle (EV). In [206] a management software for smart buildings with V2G and BESS is presented. The load profile is based on real data measurement of a Mitsubishi iMiev. The load profile of the iMiev is shown in Figure 68 and has a maximum charging power of 3200 W. The average energy consumption of the iMiev is around 15 kWh per 100 km during summer and around 23 kWh per 100 km during winter, resulting in an average energy consumption of roughly 18 kWh per 100 km. This energy consumption includes charger losses when a type-1 plug with a maximum charging power of 3.2 kW is used. The usage profile represents an EV, which is used in the morning and is charged at home in the late afternoon. The annual energy consumption of the EV is 2391.5 kWh/a, resulting in cost for charging of 832.7 €/a if only charged by grid consumption. The total annual charging costs include the interest rate and annual electricity price increase presented in section 3.5.

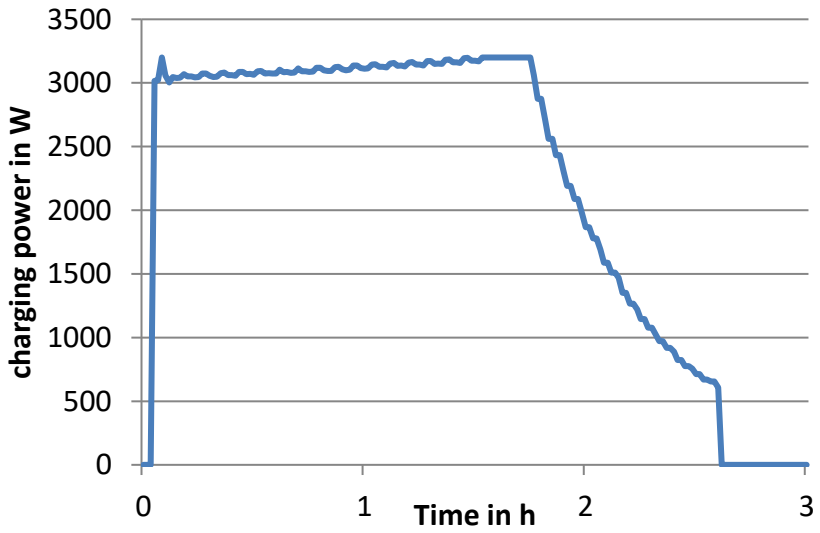

Figure 68: Charging cycle example of an iMiev with a maximum charging power of 3200 W.

The simulation results lead to an annuity of 3282 €/a for the advanced operation strategy and annuity of 3297 €/a for the basic operation strategy, if the optimal sizes of integrated homes presented in 5.2.2 are considered. The results show that the influence of operation strategies is small. The EV is mainly charged in the afternoon as shown in Figure 69, therefore it is mainly charged by energy consumption from the grid. In conclusion, the additional load from the electric vehicle should be taken into account if the component sizes of the integrated home are optimized. An optimization of the component sizes of the integrated home for the basic

operation strategy is presented below. The total load for an exemplary day is depicted in Figure 69.

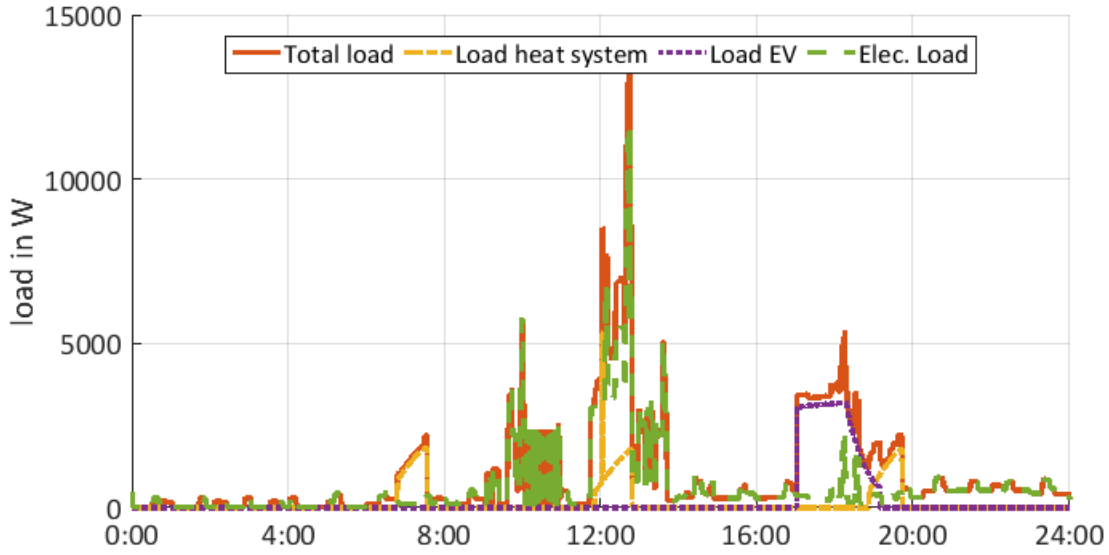

Figure 69: Electricity consumption of an integrated household in Germany on April 20 with an electric vehicle in a 60-second resolution.

If the load profile of the EV is minded in the optimization, a further reduction of the annual costs can be achieved. The optimization is preformed minding the basic operation strategy. The annual costs can be reduced from 3297 €/a to 3274 €/a. The cost reduction is relatively low, since the EV is mainly charged in the evening. The optimal sizes of the components are depicted in Table 14. The consideration of the EV load profile influences the optimal size especially of the BESS. If the EV is minded, the optimal storage size is increased from 7.1 kWh to 12.2 kWh, because of the higher energy demand in the afternoon.
The electricity costs of the integrated home with EV are shown in Annex Figure 122. The energy costs are shown in Annex Figure 123.

Parameter	Symbol	without EV	with EV	without EV	with EV	unit
PV-generator size	P_{PVPeak}	10	10.0	10	10.0	kWp
power MPP-tracker	P_{MPP}	7.9	8.0	7.8	8.0	kW
power inverter	$P_{Inverter}$	7.8	7.6	7.3	7.4	kW
power battery converter	$P_{BatConv}$	0	0.3	1.6	2.0	kW
capacity battery system	C_{BESS}	0	3.1	7.1	12.2	kWh
volume buffer storage	V_{buffer}			0.16	0.16	m³
volume DHW storage	V_{DHW}			0.11	0.13	m³
thermal power heat pump	$P_{HP,th}$			2.8	2.8	kWth
max. temp. buffer storage	$T_{buffer,max}$			42	42	°C
Spread buffer storage	$T_{buffer,spread}$			-	-	°C
max. temp. DHW storage	$T_{DHW,max}$			48	48	°C
Spread DHW storage	$T_{DHW,spread}$			-	-	°C

Table 14: Optimum set of parameters found by the optimization algorithm for the "basic operation strategy scenario" without and with minding the load profile of the EV.

The component sizes and the annuity depend on the load profile as shown in this section. It depends on the total load as well as on the time of the load. If demand and PV radiation occur at the same time the storage demand is decreased as pointed out in [63]. If the time between load and PV feed-in is increased, the storage demand is increased as well. The optimal sizes of the converters are influenced as well. Special characteristic of load profile should be minded by the choice of the component sizes.

5.4.2 Influence of changed heat profile

The heating demand of the household influences the component sizes of the heating system. The size of the house influences the heating demand. To depict the influence of the heating demand on the component sizes the living area of the house is doubled, resulting in an increased heating demand of 20,745 kWh_{th}/a. The increased heating demand leads to an increased size of the heat pump of 4.4 kW in comparison to 2.8 kW. As pointed out in section 5.2.2 the minimum size of the buffer storage depend on the size of the heat pump. This is why the size of the buffer storage is increased as well. Furthermore, the sizes of the electrical sector are increased slightly as well. The component sizes of the integrated home with the increased living area are shown Table 15.
The increased component sizes lead to increased annual costs of the integrated home. Nevertheless, the LCOEnergy are reduced from 13.05 ct/kWh to 12.22 ct/kWh, because the overall energy demand is increased. The resulting LCOEnergy are depicted in Annex Figure 127.

Parameter	Symbol	110 m²	220 m²	unit
PV-generator size	P_{PVPeak}	10	10.0	kWp
power MPP-tracker	P_{MPP}	7.8	7.8	kW
power inverter	$P_{Inverter}$	7.3	7.6	kW
power battery converter	$P_{BatConv}$	1.6	2.2	kW
capacity battery system	C_{BESS}	7.1	6.6	kWh
volume buffer storage	V_{buffer}	0.16	0.26	m³
volume DHW storage	V_{DHW}	0.11	0.12	m³
thermal power heat pump	$P_{HP,th}$	2.8	4.4	kW_{th}
max. temp. buffer storage	$T_{buffer,max}$	42	47.7	°C
Spread buffer storage	$T_{buffer,spread}$	-	-	°C
max. temp. DHW storage	$T_{DHW,max}$	48	47.5	°C
Spread DHW storage	$T_{DHW,spread}$	-	-	°C

Table 15: Optimal component sizes of the integrated home in dependency of the living area for the "basic operation strategy scenario". An increase of the living are from 110 m² to 220 m² is investigated.

5.5 Analysis of feed-in tariffs and electricity costs

5.5.1 Influence of the feed-in tariffs of the PV generated energy

The economics of the integrated home highly depended on the economic parameters presented in section 3.5. Therefore, the influence of the feed-in tariffs (FIT) for PV-generated energy is examined in the following. Figure 70 depicts the LCOEle of the integrated home under consideration of a FIT of 6 ct/kWh. If the FIT are higher than the generation cost of the PV energy, the optimization chooses the upper boundary of the PV generator size (10 kWp). The PV generator size is reduced when the FIT is lower than the generation costs. If no FIT is applied, the revenue for feed-in of PV-generated energy is slightly above the exchange price. Therefore, a price of 6 ct/kWh for PV generated energy is expected. In this case, the PV generator size is mainly driven by the energy consumption of the household, because PV-generated energy reduces grid consumption. This is why the generator size is bigger when a power-to-heat coupling is applied [207].

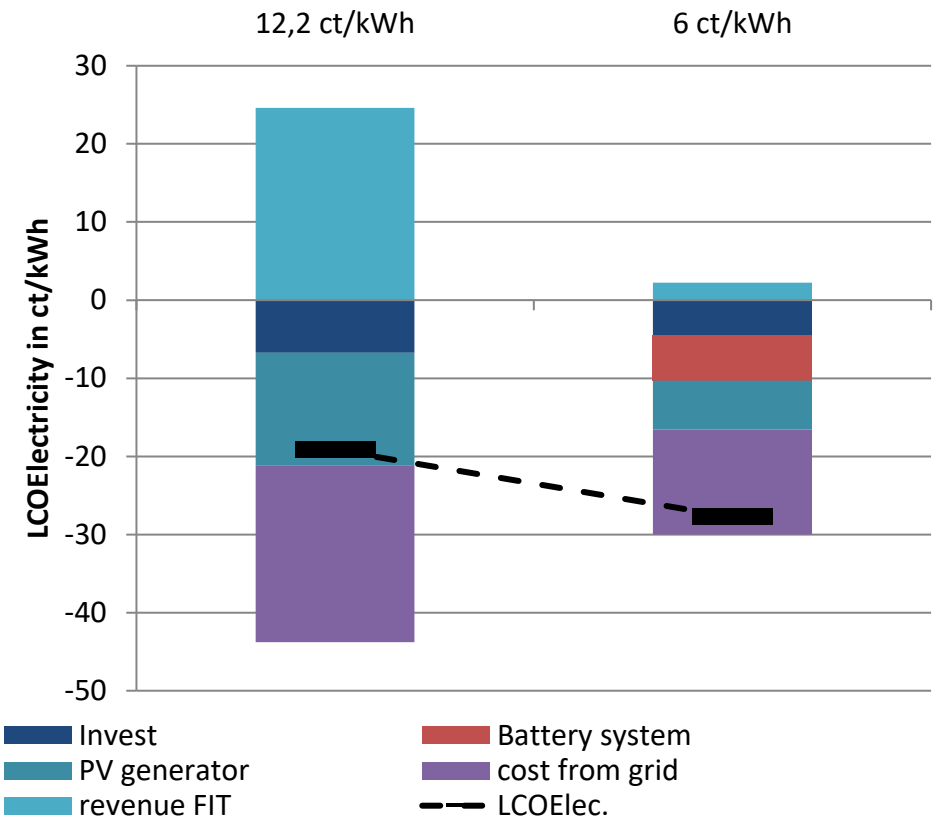

Figure 70: Electricity cost of an optimized integrated home with a PV BESS and power-to-heat coupling in relation to the feed-in tariffs (FIT) for PV generated energy.

If the PV generator is only used to cover the electricity demand, the optimal size is 4.3 kWp. If a power-to-heat coupling system is applied, this value increases to 7.6 kWp. The costs for the increased PV generator size are attributed to the LCOH. The LCOEnergy are increased in this case, because of the falling revenues from the feed-in. The LCOEnergy, as well as the costs for the PV generator are illustrated in Figure 71. The component sizes of the optimized integrated home with FIT of 6 ct/kWh are depicted in Annex Table 2.

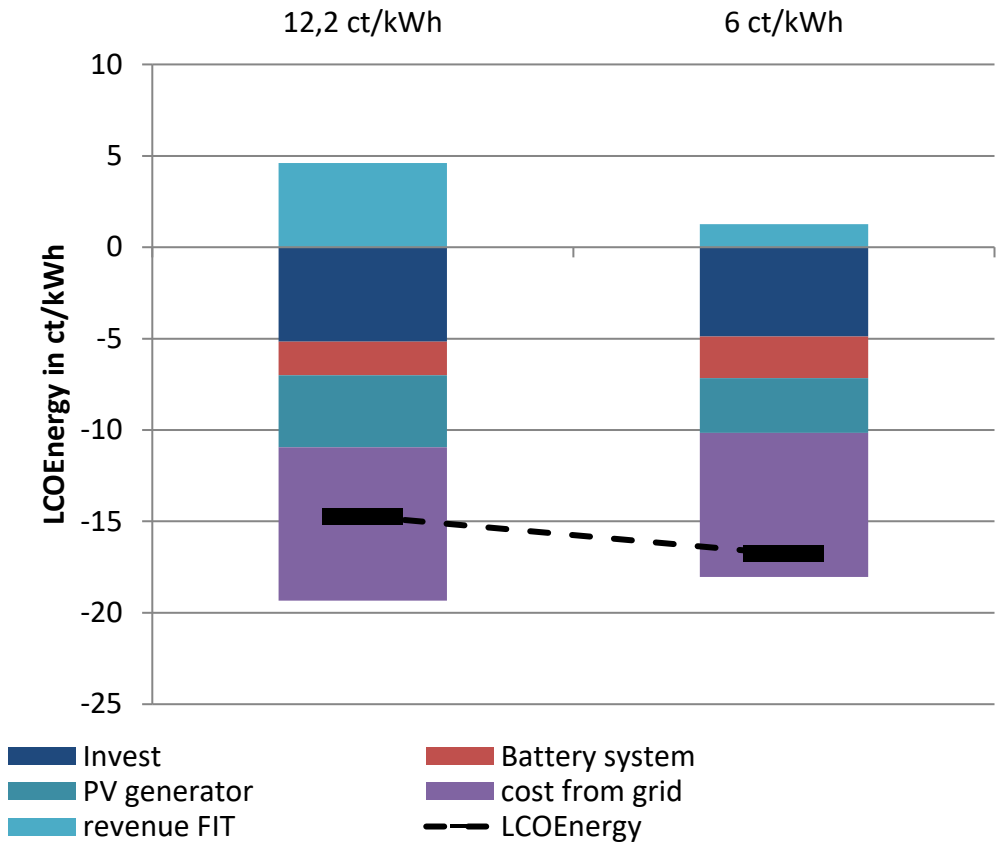

Figure 71: Energy costs of an optimized integrated home with a PV BESS and heat power coupling in dependency of the feed-in tariffs (FIT) for PV generated energy.

5.5.2 Influence of electricity costs and the annual electricity price increase

Besides the feed-in tariffs, the electricity price influences the optimal component dimensioning. An increased electricity price or an increasing electricity price leads to a higher storage demand. With an increasing electricity price, the self-consumption of PV generated energy has a higher economic benefit. This is why, the demand for storage capacities is increased as pointed out in [63].

5.6 Influence of solar radiation on optimized integrated homes

The solar radiation highly influences the PV generation of the integrated home. For the investigated integrated home a global radiation of 1151 kWh/m2 per year is used. An analysis of the highest and lowest radiation in Germany for the years 2007 to 2017 results in a

maximum global radiation of 1386 kWh/m² and a minimum global radiation of 997 kWh/m² [208]. An enhanced solar radiation leads to lower costs of the integrated home as depicted in Figure 72. A further interesting finding is that the optimal size of the battery system is reduced, with high solar radiation. Less energy needs to be shifted from time with high radiation to times with low radiation, because the higher solar radiation leads to higher PV generation in the afternoon.
The component sizes of the optimized integrated home in dependency of the solar radiation is presented in Annex Table 3. Annex Figure 124 illustrates the influence of the solar radiation on the electricity costs.

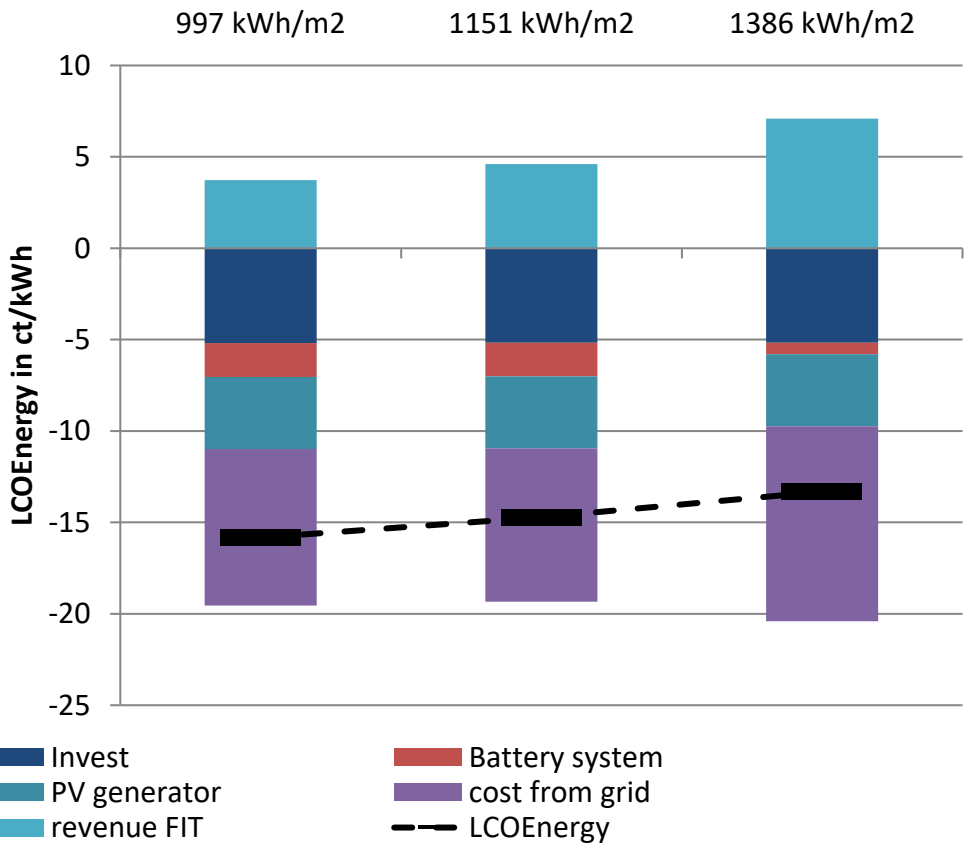

Figure 72: Energy costs of an optimized integrated home with a PV BESS and heat power coupling in dependency of the solar radiation.

5.7 Influence of changing component costs

The costs for the components influence the optimal size of the components. A decreasing price for one component leads to an increased optimal size of the component. The sizes of the other components are influenced as well. The influence in the same sector is high, whereas the influence in the other sector is minor. Falling battery system prices will lead to an enhanced battery size and an enhanced battery converter size. The sizes of the heating sector are influenced to a minor degree. The influence of the price of the battery system on the optimal battery size of the integrated home is investigated in the following.

Battery system prices are expected to decrease. For this analysis a future price of halve the price of the battery system today is assumed. This price reduction is in line with different publications. The following publications analyze prices for automotive battery systems on pack level. The costs for battery systems for battery home storage systems are expected to be slightly higher compared to the prices in the automotive section. Still these prices give a lower boundary for the battery price development. Curry [126] expect prices in the automotive section for lithium-ion systems of 74 USD/kWh in 2030. Berckmans et al. S.17 [209] conclude: "The 100 dollar/kWh sales barrier will be reached respectively between 2020-2025 for silicon based lithium-ion batteries and 2025–2030 for NMC batteries". The IRENA study estimates best case prices for NMC battery packs of 79.5 USD/kWh in 2030 and 167.3 USD/kWh in the reference case [210]. In [211] the costs for EV battery cells are expected to be slight above of the material cost. In 2026 a price of 100 €/kWh is given in this publication.

For this analysis costs of 125 €/kWh for a NMC battery is assumed, which is half of the price presented in section 3.5. The reduction of the price for the battery system leads to an enhanced optimal battery size. For a PV battery energy storage system without a power-to-heat coupling, the optimal battery size is 8.9 kWh. The optimal battery size with power-to-heat coupling is 12.6 kWh as depicted in Table 16. The annual costs for the integrated home with the basic operation strategy are reduced from 2528 €/a to 2308 €/a with a battery system price of 125 €/kWh. Annex Figure 125 shows the electricity costs of the integrated home with battery costs of 125 €/kWh. The energy costs are depicted in Annex Figure 126.

Parameter	Symbol	Elec basic	125 €	Heat basic	125 €	unit
PV-generator size	P_{PVPeak}	10	10.0	10	10.0	kWp
power MPP-tracker	P_{MPP}	7.9	7.8	7.8	8.1	kW
power inverter	$P_{Inverter}$	7.8	7.6	7.3	7.8	kW
power battery converter	$P_{BatConv}$	0	2.5	1.6	2.6	kW
capacity battery system	C_{BESS}	0	8.9	7.1	12.6	kWh
volume buffer storage	V_{buffer}			0.16	0.16	m³
volume DHW storage	V_{DHW}			0.11	0.11	m³
thermal power heat pump	$P_{HP,th}$			2.8	2.8	kWth
max. temp. buffer storage	$T_{buffer,max}$			42	39.7	°C
Spread buffer storage	$T_{buffer,spread}$		-		-	°C
max. temp. DHW storage	$T_{DHW,max}$			48	47.9	°C
Spread DHW storage	$T_{DHW,spread}$		-		-	°C

Table 16: Optimum set of parameters found by the optimization algorithm for the "basic operation strategy scenario" without and with battery price decrease. A battery price decrease form 250 €/kWh to 125 €/kWh is assumed.

5.8 Influence of changes of economic parameters or economic circumstances

The economic parameters such as the interest rate and the economic circumstances e.g. the KfW-funding influence the optimal component sizes of the integrated home. The economic parameters are the interest rate and the calculation period for invest assessment. An increased interest rate leads to enhanced costs for capital-intensive assets. This is why an increased interest rate would lead to a reduced optimal size of the battery storage system as pointed out in [63]. From an increased calculation period for the invest assessment would profit assets with an annual cost degression e.g. the battery storage system.

Changing economic circumstances would influence the optimal component sizes as well. The diminished KfW-funding under consideration of changing feed-in limits is already discussed in section 4.5.3. The KfW-funding is not minded in the optimization presented in this section 0. In [63] the influence of the externalization of the power price from the electricity price is discussed. An externalization of the power price would lead to a reduced electricity price and therefore to a reduced storage demand as presented in section 5.5.2. On the other hand, this would generate new markets for battery storage systems. In this case, home storage systems could be used for peak shaving in residential households. Battery storages systems are already used for peak shaving in industrial applications. The optimal component sizing for peak shaving with battery storage system for industrial applications are presented in [212].

6. Operating reserve markets

The provision of control reserve with integrated homes depends on the market situation. This section gives an overview of the current market situation, which is used in the thesis at hand.

6.1 Operating reserve market structure

The power market liberalization on the European continent started in 1996 and transformed the market from traditional direct trading agreements into a decentralized bilateral market model which enabled different players to enter the market and introduced competition [213, 214]. In this thesis an overview of the control market in the decentralized bilateral market is given. The control market and its related products are extensively analyzed, market options for battery energy storage systems need further investigation [213]. The participation of BESS on the control markets still is an emerging topic.

6.1.1 Electricity market structure

The electricity market in Germany is divided into a wholesale, retail and a control reserve market. In the wholesale market, operators of generation units and importers of electrical energy from other European countries act on the supply side, while wholesale traders as well as key accounts or utilities act on the demand site. The retail market comprises (local) utilities on the supply side and smaller industrial customers and residential consumers on the demand side. The goal of the power reserve market is to balance the deviation between supply and demand at all times and in real time.
All the German transmission system operators (TSO) are members of ENTSO-E and follow the guideline concerning load-frequency control (LFC) which defines the technical framework for duties and responsibilities of TSOs regarding LFC [215]. The major tasks are described as follows [213]:
Frequency stability: TSOs are obliged to maintain enough balancing and reserve power (primary, secondary and minute reserve power) within the scope of their responsibilities to ensure reliable system operation. The transmission system must provide enough transmission capacity and infrastructure for both the transmission of the projected maximum load and the transmission of reserve power. The TSOs procure control power via bidding on competitive terms and conditions, and the bidding results are published. The ability of primary control reserve (PCR) providers to satisfy the ENTSO-E minimum requirements must be proven through a prequalification procedure. Finally, the framework agreements concerning the terms and conditions for providing control power between the TSOs and the PCR providers are settled. The control reserve market is investigated in more detail in section 6.1.2.
Voltage Stability: Each TSO must ensure voltage stability in its control area, which involves the power grid (transmission and distribution networks), generating units, power stations, consumers, and the boundary areas to the adjacent networks. To ensure balanced reactive power management, the TSOs must maintain facilities for reactive compensation or provide reactive compensation by contractual arrangements.

Restoration of supply: To prepare for large-scale failure, the TSOs are obliged to draw up appropriate plans for preventive and operational measures in conjunction with adjacent TSOs or with subordinated DSOs and power station operators. TSOs must also have black-start capability and the capability of isolated operation to provide supply restoration.
System management: System Management comprises of several tasks, such as the assurance of network security, the performance of voltage/reactive power and power/frequency control operations, or metering and pricing between TSOs and PCR providers. Moreover, it includes the operational implementation of the generation schedules for power stations in accordance with the requirements for secondary control power, the activation of minute reserve and, if necessary, emergency reserve. The latter task requires congestion forecasting, congestion management, load forecasting for the control area, observation of the instantaneous commitment of the power stations, and the coordination or utilization of ancillary services.

6.1.2 Control reserve structure

The goal of the power reserve markets is to balance the deviation between supply and demand at all times and in real time in order to keep the energy system stable. Electrical power cannot be stored within the electricity network itself, meaning electrical power generation and consumption must be equal at any time. Any deviation from balanced generation and consumption leads to deviation of the frequency from the set point of 50 Hz. The European Network of Transmission System Operators (ENTSO-E), represents 43 electricity transmission system operators (TSOs) from 36 countries across Europe, including all German TSOs. The ENTSO-E members follow the guideline concerning load-frequency control (LFC) which defines the technical framework for duties and responsibilities of TSOs regarding LFC [215]. According to the guideline, three steps are defined for the load-frequency control (LFC): The primary (FCR: frequency containment reserve), secondary (aFRR: automatic Frequency Restoration Reserve) and tertiary (mFRR: manual Frequency Restoration Reserve) control reserve. In case the deviation of the frequency is larger than the LFC can manage, load shedding will be activated as a last option. Figure 73 represents the control concept of the German control reserve.

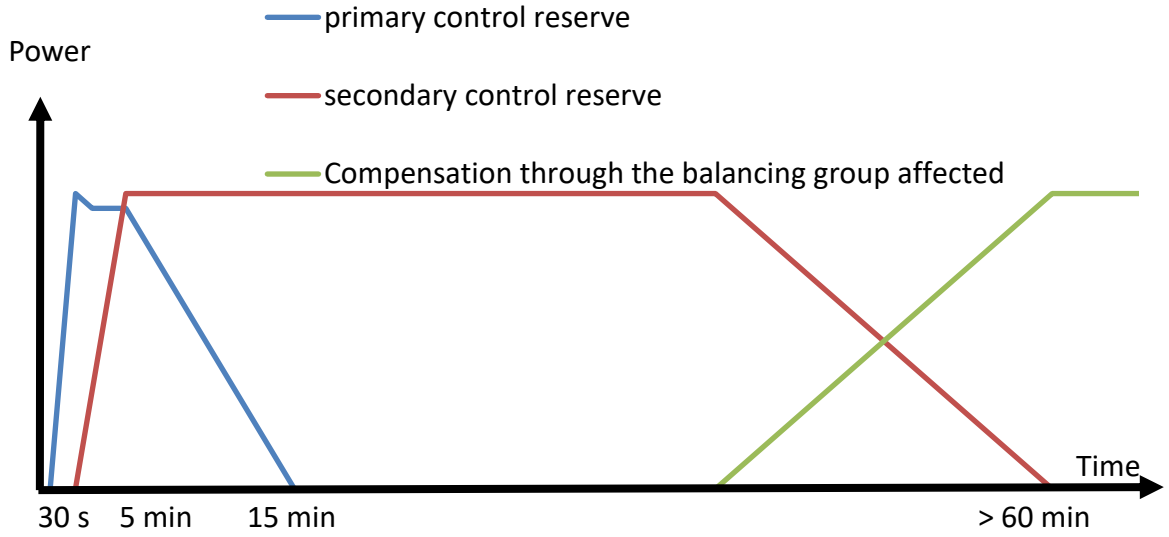

Figure 73: Three-step control concept of the German control reserve.

Primary control reserve (PCR):
A common (coupled) auction-based PCR market exists for the countries Germany, Belgium, Netherlands, France, Swiss and Austria. Units providing PCR must take part in the auction process and fulfill the technical prequalification requirements. Besides, from the instant reserve, the PCR is first control mechanism. If the grid frequency deviates more than ±10 mHz from the set point (50Hz), units are to provide power linearly to the frequency deviation with full power activation in less than 30 seconds. Within less than five minutes after primary control reacts to a deviation, secondary control is activated to bring the frequency back to the nominal set point and free primary control capacity [213, 216].

Secondary control reserve (SCR):
Within less than five minutes after PCR reacts to a frequency deviation, SCR is activated to restore the frequency back to the set point and to replace PCR [213, 216]. Secondary control is designed to take action only in the control area (TSO), which is affected by the power imbalance. Units providing SCR get the power set point signal from a communication link to the locally responsible TSO which calculates the SCR demand for its control zone. In order to prevent different TSOs of providing counteracting SCR power, multiple TSOs work together in a grid control cooperation (GCC) to control the overall SCR requests. TSOs of Germany, Denmark, Netherlands, Swiss, Czech Republic, Belgium, Austria and France are participating in the GCC. Efforts are made to expand the cooperation among TSOs by also procuring the SCR demand in a common auction in order to minimize SCR demand and costs [37]. A common auction market already exists for all German TSOs and Swissgrid (Austria).

Tertiary control reserve (TCR):
Tertiary control frees the faster responding SCR, has a maximum activation time of 15 minutes and is automatically activated (Merit-Order-List-Server) by the TSOs. The main contribution of tertiary control is to satisfy economic reasons. The tertiary reserves free the faster responding secondary control reserve. Tertiary reserves should be fully available 15 minutes after activation. In [38] a analysis of markets for gird connected BESS is presented. The publication concludes that the SCR as well as the PCR market could be promising. Regarding the TCR market, the publication pointed out, that the operation profile for a battery storage system is the same as for SCR since except for the ramp-up time, the control reserve product is very similar. BESS can react much faster than that, therefore no benefits are seen in comparison to the SCR market. Nevertheless, the negative TCR market could be promising, because of the low-cost energy provision.

6.2 Primary control reserve market

6.2.1 Dimensioning primary control reserve

The primary control reserve also known as frequency containment reserve (FCR) is tendered on a weekly basis in Germany. The bid capacity price is paid to the accepted units (first price auction).
A total of 3,000 MW primary control reserve (PCR) has to be provided in the synchronously interconnected continental European system to satisfy the rules of the ENTSO-E Operation Handbook [215]. Currently, large nuclear power plants exist in the grid with an approximate nominal power of 1,500 MW which explains the demanded value for PCR. In this rule, a loss of one such power plant is recognized as reference incident and the rule is set such that PCR can compensate two simultaneous reference incidents. The German PCR market is coupled with the PCR market in Belgium, the Netherlands, France, Swiss and Austria. This market is tendering roundabout 1400 MW PCR. The quantity of PCR depends on the energy produced in each TSO zone [216].

6.2.2 Primary control reserve markets

Market rules and access conditions are determined by the grid regulator after consulting with TSOs and bidders. Table 17 provides an overview of different PCR markets in comparison to other international markets for fast responding reserve. The investigated markets are similar to the coupled PCR market. The adapted energy management system can be used in the other markets, if adapted.

	coupled PCR market [37]	California [217]	California [217]	UK [218, 219]	UK [218, 219]	Ireland [219, 220]
Service	Primary Reserve Control	Regulation Up	Regulation Down	Enhanced frequency response	Firm frequency response Primary	Frequency contain-ment reserve
Activation time	30s to max	Immediately	Immediately	less than 1s	10s to max.	5-15 sec
Min possible runtime	30 min (since May 2019 15min)	n/a	n/a	n/a	further 20s	Regulated services via bilateral contracts
min. size	1 MW	300-400 MW	300-400 MW	n/a	10 MW	
Pooling	yes	n/a	n/a	n/a	yes	
Tendering	Weekly (since May 2019 15min)	Day ahead/ real time	Day ahead/ real time	n/a	monthly	
Duration	1 day	1h / 15 min	1h / 15 min	4 years	1-6 months	
Renumer-ation	Pay as bid	n/a	n/a	availability fee	availability & nomination fee	
Market size	ca. 1400 MW	ca. 340 MW	ca. 330 MW	201 MW	200-700 MW	n/a
Revenue	1500 - 3400 €/MW	0.09 - 50 $/MWh	up to 60$/MWh	average price 9.44/MW EFR/h	15000 - 20000 €/MW	EirGrid 2.22 €/MWh SONI 1.95 £/MWh

Table 17: Comparison of different fast responding reserve market. The coupled PCR market represents the German, Belgium, Netherlands, France, Swiss and Austria market.

The PCR is procured as a symmetrical product. Suppliers have to provide an upward and downward regulation related to the power offered. However, for both regulation directions, different technical units can be deployed. The bidding period for PCR is one week. Offers for PCR must guarantee a provision over a weekly period in one time slot. For the PCR market only the provided power capacity is paid [216, 221].

6.2.3 PCR price development

In this section, the price fluctuations and developments for the primary control reserve market are discussed. Before December 2007, PCR was tendered in the four control zones for periods of six months and the prices had been stable during this period in the range of 2,500 €/MW per week (15 €/MW per hour). Since December 2007, PCR is tendered on a monthly basis in one common auction. The price development is depicted in Figure 74. Since December 2007 prices fluctuate between less than 1,900 and above 6,000 €/MW per week (12 to 30 €/MW per hour) with peaks during summer seasons [222]. The prices were fluctuating with sharp rise and downfall in the period of 2011 to 2015 which can be explained by bidding behavior [214]. The development of prices both on the spot market and on the primary control reserve market is subject to great uncertainty. The PCR market is facing a price decrease from 2016 onwards. In these years, the share of battery storage systems participating in the PCR market raised from low values up to around one third.

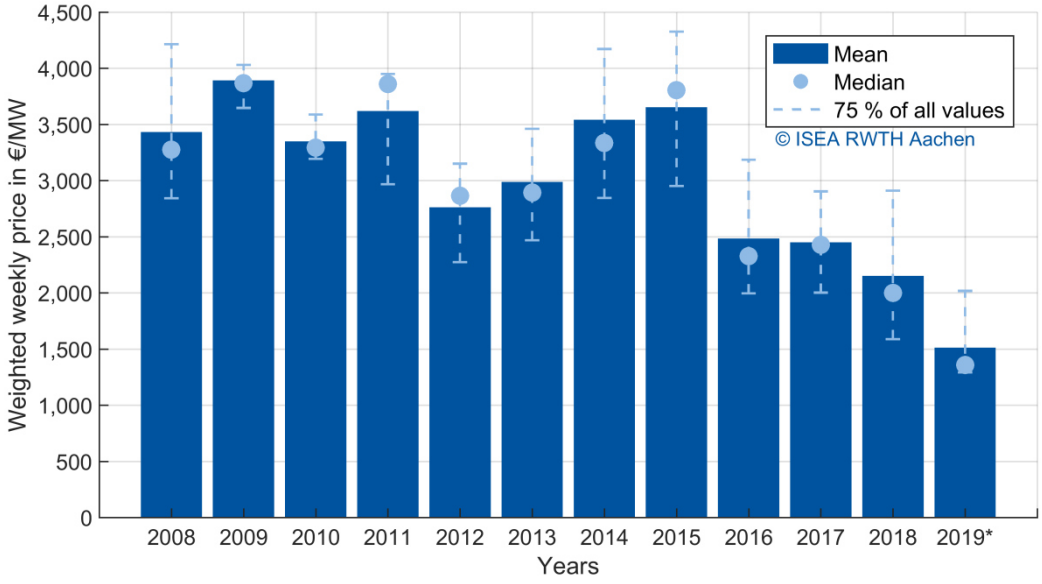

Figure 74: Price development 2008 to 2019 on the German PCR market.

This assessment is based on historical price data, thus this approach does not take possible price developments into consideration [222]. From 2016 to 2019 the market prices were falling in comparison to 2015. In 2019 the market prices were below 1,500 €/MW per week as shown in Figure 75. In winter month the prices are higher compared to the summer month, even though peak prices occur during summer month. This is positive for PV home storage systems with power-to-heat coupling. Since the battery is used less in winter moth. Therefore, more PCR power can be offered during winter.

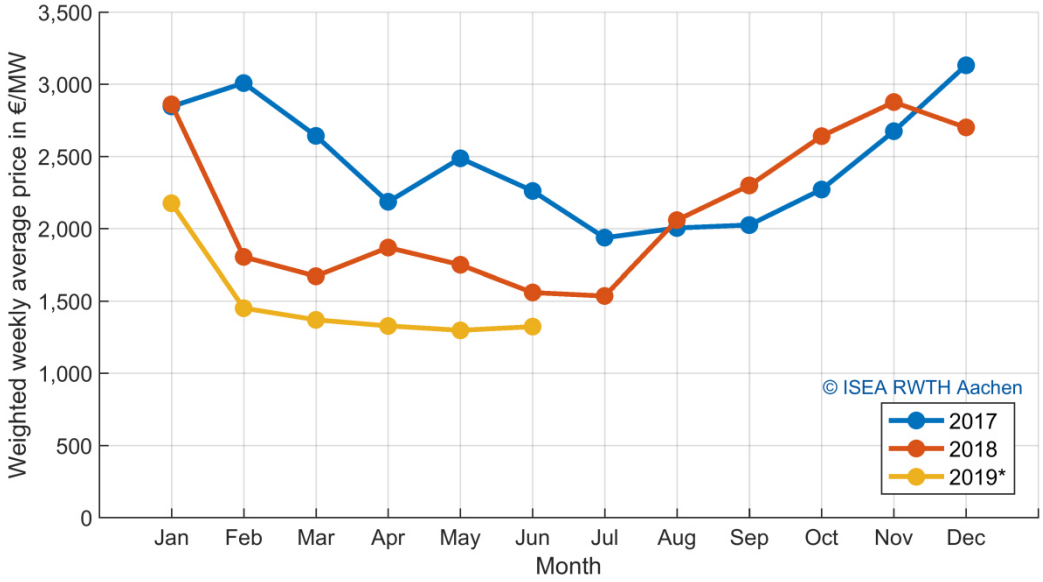

Figure 75: PCR price development comparison of the years 2017, 2018 and 2019.

Possible reason for the PCR price decrease might be the market expansion. On August 1st, 2016 the Belgian market joined the Swiss-German market. Another reason might be that existing power plants are searching for new markets. An evidence of this might be the rising number of successful biddings since 2015 as depicted in Figure 76. Furthermore, the power per bidding in 2016 was lower compared to 2015. In 2015 the average power per bidding was 5 MW and in 2016 the average power per bidding was 3 MW. Therefore, the market is facing a higher share of ”small“ participants. This effect and the rising number of battery storage systems participating in the PCR market lead to a rising number of weekly accepted bids in 2017. The high number of the accepted bids since 2017 result from the market coupling of the German, Belgian, Dutch, France, Austrian and Swiss market. This is why a prognosis of the market development is difficult. A raising number of participants could lead to lower market prices.

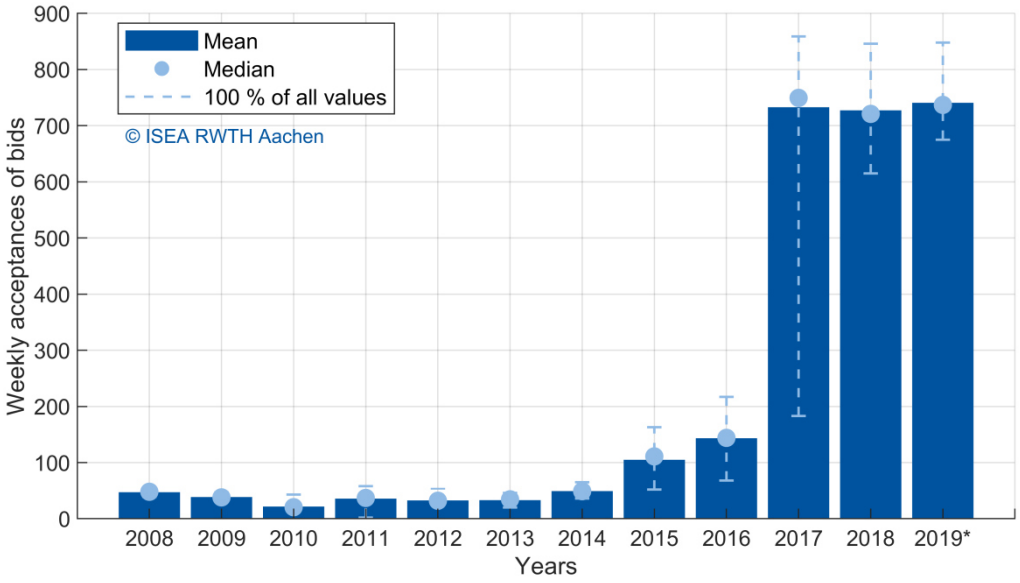

Figure 76: Development of the unweighted numbers of bids on the PCR market in Germany.

6.2.4 Market update of the PCR market

To enhance the penetration of renewable energies in the PCR market, the market is updated continuously. On 23 May 2019, new prequalification requirements were presented. The 30-minute criterion was replaced by the 15-minute criterion. Therefore, units with limited capacity are required to reserve capacity for 15 minutes instead of 30 minutes as described in the previous sections [223].
Another update was the shortening of the product time slot. Since 01 July 2019, PCR has to be delivered for one day instead of a whole week. The auction takes place two days before delivering. On 01 July 2020, the delivery time will be reduced to six products per day with a product duration of four hours each (00:00 to 04:00, 08:00 to 12:00, 12:00 to 16:00, 16:00 to 20:00, 20:00 to 24:00) [224].

6.3 Secondary control reserve market

6.3.1 New secondary control reserve market design

In Germany, the SCR capacity demand is calculated by the TSOs and tendered in an auction. The provision of positive and negative SCR is tendered separately. Since July 2018, new market regulations are in effect. These regulations are defined in publication [224] and aim to reduce excess barriers for renewable energy generation, demand-side-management-systems and BESS to the SCR market. So far a high minimum capacity offer in combination with long lead times and decreasing prices have prevented BESS for participating in the market [225]. The key changes are pointed out in publication [225] and presented in following. The time slots of the SCR are shortened. With the old regulations, only two time slot per day were auctioned.

In the new market design, six time slot each with a four hour duration are auctioned (see Figure 77.). Furthermore, the auction's lead time is reduced to one day before delivery. The time schedule for the SCR auctions are presented in Figure 78 and based on the information given in publication [224]. The minimum bid size of 5 MW is still present, but if the bidder submits only one bid per SCR product, time slot and control area, the bid size can be reduced to 1 MW. The minimum increment of 1 MW for bid endure, as well as the merit-order principal. The changes for positive and negative control reserve as depicted in Figure 77.

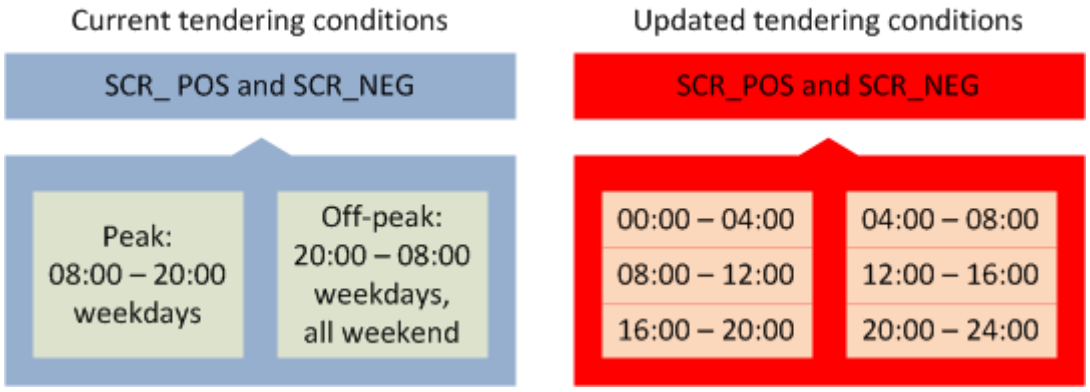

Figure 77: Overview of SCR products and product time slot under current and updated tendering conditions [225].

The supplier has to specify the available capacity (MW), a capacity price (€/MW) and an energy price (€/MWh) for each time slot and power direction [216, 221]. Up until October 15th 2018, the winners of the auction were determined by submitted capacity prices (merit order). After that date a mixed price was introduced which is calculated by the sum of the capacity price and the weighted energy price.

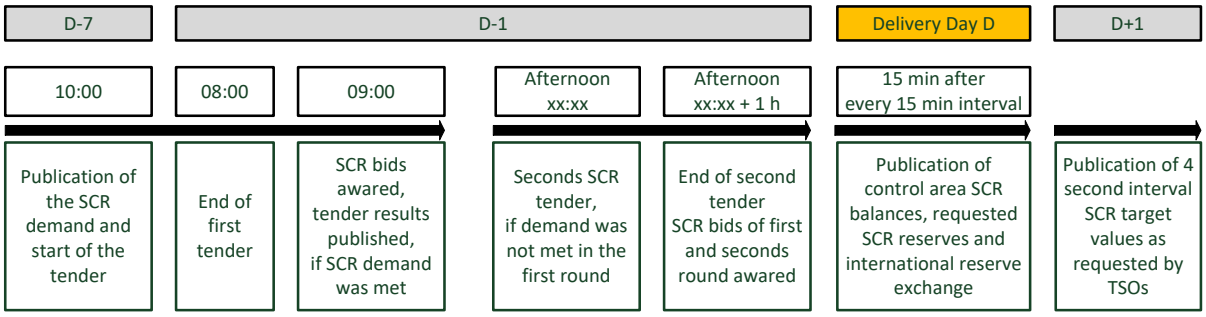

Figure 78: Time schedule for the SCR auctions on the German market [225].

6.3.2 Overview SCR market and comparison to other markets

The German regulator Bundesnetzagentur determines market rules and access conditions after consulting with TSOs and bidders. The bidding process is conducted using the internet platform https://www.regelleistung.net where only prequalified system operators can take part in the auctions. Table 18 provides an overview of the different secondary control reserve markets. The requirements are similar therefore, the PV-BESS with power-to-heat coupling could participate in other European markets as well.

	Germany [37]	Germany new [37]	Belgium [226]	Netherlands [227]
Service	Secondary Reserve Control	Secondary Reserve Control	Secondary Reserve	Secondary Reserve
Activation time	20 % per minute	20 % per minute	15 % per minute	7 % per minute
Min possible runtime	n/a	n/a	15 min	n/a
min. size	5 MW	6 MW	n/a	4 MW
Pooling (section 7.2.4)	yes	yes	n/a	n/a
Tendering	weekly	daily	annual	annual
Duration	1 week (HT/NT)	4 hours	15 minutes	15 minutes
Activation	Merit order	Merit order	Parallel	Merit order
Renumeration	Pay as bid	Pay as bid	Pay as bid	Flat price
Market size	~ 2000 MW	~ 2000 MW	145 MW	~ 300 MW

	California [217]	California [217]	UK [218, 219]	Ireland [219, 220]
Service	Spinning Reserve	Non-Spinning reserve	FFR Secondary	Frequency restoration reserve
Activation time	10 min	10 min	30s to max.	15 to 90 sec
Min possible runtime	2 hours	2 hours	30 min	n/a
min. size	n/a	n/a	10MW	Regulated services via bilateral contracts
Pooling	n/a	n/a	yes	
Tendering	n/a	n/a	monthly	
Duration	n/a	n/a	1-6 months	
Activation	n/a	n/a	n/a	
Renumeration	n/a	n/a	n/a	
Market size	~ 850 MW	~ 850 MW	700-1400 MW	n/a

Table 18: Main product characteristics of control-reserve qualities tendered.

6.3.3 Market Size

ENTSO-E regulations and rules are less relevant when it comes to dimensioning secondary control reserve (SCR) and tertiary control reserve (TCR). German TSOs are using probabilistic

methods to dimension the demand for control reserve. This method, among other criterions, takes power plant and forecast failure into account. In September 2018, the allocated positive SCR is 1,883 MW and 1,759 MW for negative SCR. The values for positive and negative TCR are 1,382 MW and 759 MW respectively.

6.3.4 Price development SCR market

This section gives a rough overview of the price development on the SCR market. The price development from 2012 to 2016 is presented and analyzed in [228]. From 2012 to 2016, capacity prices are falling in the SRC market. The same applied for the capacity price of the accepted bids. One reason for the decreasing prices was the rising number of market participants. The new market participants include heating networks or battery storage systems, but not necessarily conventional power plants.
Figure 79 illustrated the total revenues of the SCR from mid-2015 to mid-2018. The total revenues are the revenues of the positive SCR plus the revenues of the negative SCR market for low and high tariff. The total revenues fell in the examined years. The reason for the falling prices is presented in Figure 80. Figure 80 depicts the expenditures made on the capacity prices for all products. These prices decreased, whereas the energy prices remained stable in the examined years. These prices are decreasing, whereas the energy prices remain stable in the examined years.

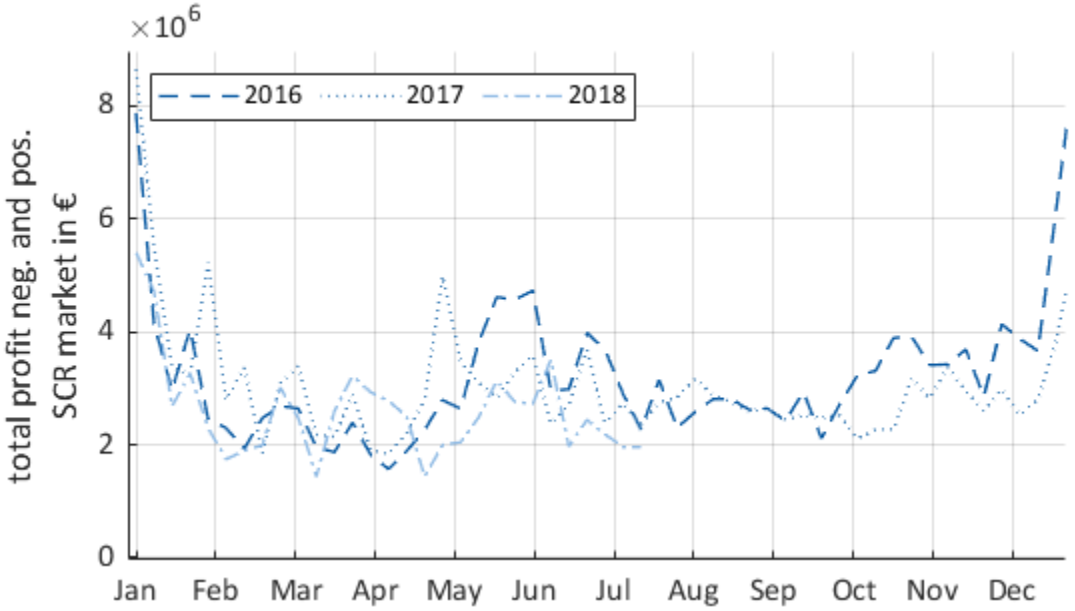

Figure 79: Total profit of the German SCR market on a weekly basis. The total profits incorporate the resulting income and costs for the energy and the capacity prices [37].

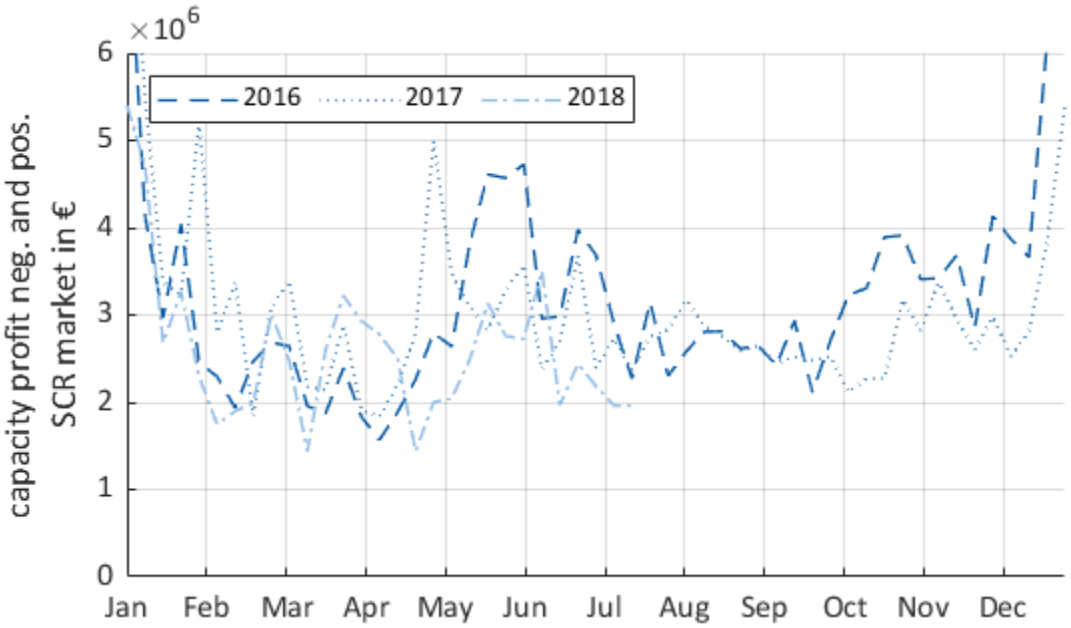

Figure 80: Total capacity price expenditures made on the German SCR market (monthly basis). Includes capacity prices for high and low tariffs, as well as for negative and positive products [37].

6.4 Prequalification of suppliers

Participants in the control reserve markets have to provide evidence that they can fulfil the technical requirements of providing control reserve power. Therefore, participants have to undergo a technical prequalification process [216]. All requirements regarding power ratings or minimum delivery time are formulated by the responsible TSOs. The requirements assumed in this dissertation are given by the German TSOs [39]. Figure 81 describes the requirements for prequalification and shows that BESS have to provide PCR for 30 minutes in total. This regulation is called the 30 minute criterion, which states that BESS should be able to provide the prequalified PCR, both charging and discharging, for 30 minutes.

During the prequalification process, the offered prequalified power is checked. The prequalified power is the deployable power change within the activation time, which is 30 seconds for PCR, 5 minutes for the SCR and 15 minutes for the TCR (tertiary control reserve). Furthermore, facilities for control and communication are checked as well. In the prequalification process it is check twice, if the activation time can be adhered. After the activation time, the control reserve has to be delivered in the prequalification process. The delivery time is 15 minutes for the primary and secondary control reserve and 30 minutes for the TCR [229]. Therefore, the minimum amount of power that should be provided for PCR is 1 MW for 15 minutes twice (until May 2019 see section 6.2.4).

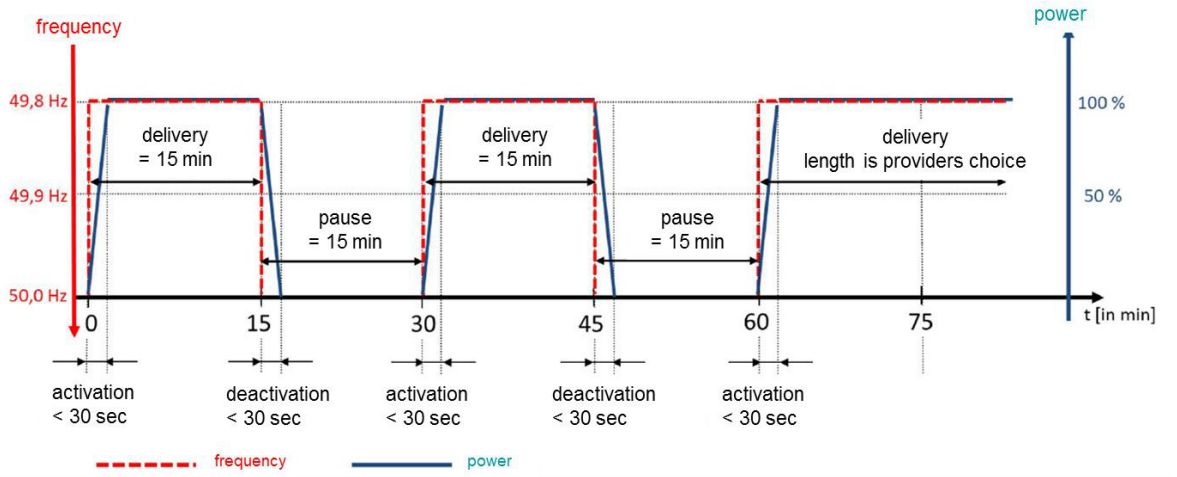

Figure 81: Performance requirements for prequalification of BESS on the Central European PCR market [39].

6.5 Conclusion optimization of integrated homes

The use of renewable energies is increasing in the recent years. Residential PV systems produce renewable energy locally. With power-to-heat coupling in residential households, the renewable energy from the PV systems can also be applied to the heating sector. This is why homes that integrate a PV battery energy storage system and a heat pump for power-to-heat coupling can contribute to the decarbonization process. To enhance the penetration of these integrated homes, the overall system economics should be enhanced. This can be achieved by advanced forecast-based operation strategies and optimal component sizes. This section aims to find the optimal system configuration, under consideration of the operation strategy, for a given load and radiation profile. To find the optimal system configuration, the analysis incorporates, the advanced operation strategies presented in section 4 in the optimization of the component sizes of the integrated homes.
A tool for the optimization of the component sizes of the integrated home is presented. The tool considers many economic parameters and boundary conditions. The target of the optimization is to reduce the annuity of energy cost for the integrated home. This tool is used to evaluate a 4-person integrated home located in Lindenberg (Berlin, Germany). The optimization is applied to a DC-coupled PV battery energy storage systems model with power-to-heat coupling, based on real data measurements. To evaluate the economics of the integrated home, the levelized costs of energy are calculated.
The presented optimization results have to be considered as exemplary, because the results are highly sensitive to the parametrization of the model and the input parameters. The presented optimization results emphasize that integrated homes are economically competitive to houses with fossil heating concepts, if an optimal system design is chosen. Savings of up to 15.5 % per year are possible in the examined case. The application of the advanced operation strategies and the optimized component sizes can enhance the economics of integrated homes and therefore enhance their market penetration.
The conducted case study shows that levelized costs of energy are mainly driven by the cost for energy consumption of the heating system. The presented case study in the Section leads to the following results:

1. Integrated homes are economically competitive to houses with fossil heating concepts.
2. The use of advanced operation strategies has a positive influence on the annuity of energy costs of integrated homes, even under consideration of disturbance functions. The advanced operation strategy uses a persistent forecast. The implementation of more sophisticated forecast algorithms can further enhance the economic benefit of advanced operation strategies.
3. Reduced buffer storage sizes reduce the cost for the integrated homes, but increase the switching rate of the heat pump. Therefore, the minimum buffer storage size should be chosen to guarantee the minimum runtime of the heat pump.
4. Optimization of the component sizes leads to a higher annuity reduction of integrated homes, in comparison to advanced operation strategies. Advanced operation strategies have a minor influence on the annuity of integrated homes in comparison to an optimization of component sizing.
5. The application of an optimized power-to-heat coupled system can lead to savings of up to 15.5 %, in comparison to a household with fossil heating and electricity supply from grid.

Additionally, sensitivity analyses are performed. The sensitivity regarding battery prices, solar radiation, load changes and feed-in tariffs are analyzed. The consideration of additional load due to an EV, reduced battery system prices and diminished FIT enhance the optimal battery system sizes. Enhanced solar radiation on the other hand reduces the optimal battery system size. The influence of further parameters e.g. the interest rate is discussed. Changing economic circumstances are discussed as well. The investigated and discussed parameters influence the economics of the integrated home.

7. Reserve markets for battery storage systems

To participate on the control reserve market a minimum power of 1 MW is required [216]. This is a boundary for small BESS like PV-BESS, because these systems can only provide control reserve of some kW. According to [230] it is allowed to couple these systems in a virtual power plant to provide control reserve. These power plants have to be in the same control area [231] and have to undergo the prequalification process as one unit.

7.1 Literature on photovoltaic battery storage systems in control reserve markets

7.1.1 Literature on PV-BESS on the primary control reserve market

The participation of battery storage systems on primary control reserve markets is wildly discussed in literature. However, the literature mainly focuses on grid-scale battery systems. Aggregated residential battery systems participating on the control reserve market is a relatively new topic and therefore, literature is still weak. This literature review is focused on battery system participating on the control reserve market.
In [38] a analysis of markets for grid connected BESS is presented. The publication concludes that the penetration of the control reserve markets depends on the economic performance of the energy storage systems. The PCR market could be a promising market.
[232] presents an operation strategy for battery storage systems participating in the PCR market. The publication concludes, that the installation site and the choice of the energy to power ratio have a higher impact on the economics of the storage system.
In [233] the optimal provision of primary frequency control with battery systems is investigated. Therefore, the degrees of freedom are described, and the effect of their utilization on battery system operation is analyzed. Additionally in [234] the billing and measuring issues as well as the current regulatory framework conditions in Germany are discussed.
The impact of different operation strategies for battery energy storage systems providing primary control reserve is analyzed in [235]. The consideration of price trends and bidding strategies are added in [222]. The publication concludes that under the assumption of a moderate PCR price drop, BESS prices and lifetimes and the time of investment are crucial for the investment's attractiveness.
A technical, operational and regulatory suitability of battery energy storage systems (BESS) to bid into the European ancillary market is investigated in [236]. The results from the operation of the Zurich 1 MW BESS in this market are presented.
The fundamentals of using battery energy storage systems to provide primary control reserves in Germany are discussed in [221]. In this publication, the combination with PV systems is discussed as well.

Caterva (Today: Alelion Energy Systems GmbH), Ampard AG (Lichtblick) and sonnen eServices GmbH are aggregators of PV-BESS, which are prequalified in the German PCR market [237]. Connected to a virtual battery, these PV-BESS can provide PCR [238].
Melo et al. [239] investigated PCR provided by hybrid battery storage and power-to-heat system. He points out the advantages of hybrid systems and concludes that the economic can be improved using systems with a capacity-power ratio lower than one. Nevertheless, the studied system is not economical feasible under current electricity prices. Domestic battery systems with power-to-heat coupling participating on the PCR market are investigated in [240]. The publication concluded that savings up to 31 % in comparison to a BESS without P2H and PCR are possible. In comparison to the publication at hand, publication [240] does not use an aging model for BESS. Furthermore, different strategies for PCR offers are not investigated. Publication [241] investigated the provision of BESS with power-to-heat coupling on MW scale. PV home storages participating on the PCR market are investigated in [242]. The authors conclude that a PV-BESS, which combines enhancement of PV self-consumption with the provision of secondary control reserve leads to profitable investments. A power-to-heat coupling is not investigated in this publication. Engels et al. investigate BESS for self-consumption and provision of primary control reserve. The authors conclude that revenues of storage systems that combine self-consumption with provision of primary control reserve increases significantly [243].
The combination of peak shaving operation and frequency regulation with BESS is investigated in [244]. The results suggest that batteries can achieve a higher economic benefit, when combining both applications. Janßen analyses the operation of PV battery energy storage system in combination with primary control reserve [245] and reveals that the provision of primary control reserve is not economic feasible.

7.1.2 Secondary control reserve market

BESS involvement in the SCR market are addressed in publication [225]. This publication investigates the possibilities in the updated SCR market. The publication concludes that the updated SCR market will make it easier for BESS to play a role, but it is not expected that reserve markets will provide a new singular driver for the market integration of energy storage in Germany. Further publications investigate the role of BESS in the SCR market under pre-updated market conditions. Publication [246] investigates bidding strategies for BESS in the SCR market. The publication “reveals that it is not economically beneficial to provide SCR with a standalone battery” (Olk et al. pg.1 [246]). Further publications investigate electric vehicles participating in the SCR market. Publication [247]’s findings indicate that the SCR market should not be accessed with EVs. Publication [247] also refers to further publications which do not take all the market constrains into account. The INEES project [248] investigates electric vehicles (EV) to provide system services. The integration of EV in the SCR market is not cost-effective. This publication concludes that market changes are necessary for EV to make an economic contribution to the SCR market. Publication [249] investigates the British market for BESS, whether stand-alone systems or used in combination with a wind farm. The publication concludes that BESS are currently uneconomical when only used for shifting energy, but providing reserve can triple the revenue for storage in the British electricity market. In publication [250], strategies for the provision of secondary reserve capacity to balance fluctuations renewable energy are investigated. In this publication, only large water storage is

addressed. Stationary battery systems for providing secondary control reserve are investigated in publication [251]. The publication reveals that large-scale community storage systems are economically feasible for the provision of SCR. The provision of SCR, in combination with storage for solar systems, is feasible because the spare storage capacity can be used, especially during nighttime. Litjens et al. recommend a secondary control reserve provision with residential battery storage systems [242]. The authors conclude that the combination of the enhancement of PV self-consumption and secondary control reserve lead to a profitable investment. Similar results are found in publication [252]. The results of the publication show a significant increase in the profitability of BESS if PV self-consumption is combined with negative SCR provision. However, both publications do not consider the additional benefits from power-to-heat coupling if negative SCR is provided. The integration of electricity and heat supply in buildings is investigated in publication [253]. For a Swedish office building to supply heat requirements through a heat pump, an electrical heater is recommended if flexibility requirements from the electrical grid taking into account the connection to the district heating are favorable. SCR provision is not investigated in this publication. A general overview of combining applications for residential battery technology is presented in [254]. This publication investigates demand peak shaving.
Currently, operation of battery storage systems focuses on the primary control reserve (PCR) market. Few publications investigate battery systems participating in the secondary control reserve (SCR) market. This specifically applies to integrated homes, which combine PV battery and power-to-heat coupling. The dissertation at hand fills the gap in the literature by combining the provision of secondary control reserve with PV BESS and power-to-heat coupling. In this case, the heat storage provides additional capacity for secondary control reserve (SCR). Energy from SCR reduces the costs for grid consumption and gains additional economic benefits. The dissertation shows a new dual-use operation strategy for PV home storage systems with power-to-heat coupling. Novel bidding strategies and a new approach to calculate the costs and earnings of SCR market participation are presented. The results presented in thesis at hand are based on [255] and [256].

7.2 Primary control reserve with battery energy storage systems

7.2.1 Primary control reserve market

Understanding of the primary control reserve (PCR) market in Central Europe is necessary to adapt the energy management system of the integrated home. In the following, the PCR market and the requirements are presented in detail. The requirements are given by the TSO's and are presented in [39]. The Central European PCR market has to be delivered between a frequency deviation of + 200 mHz and - 200 mHz. This regulation is published in [39] and discussed in numerous publications [232, 234, 235] as presented in the introduction. Each participant in the PCR market has to follow the P-f characteristic curve shown in Figure 82. As long as the frequency is between 49.99 to 50.01 Hz no action must be taken. This frequency range is called dead band. If the frequency deviation violates this window, an activation call

made by the TSO is performed (automatically and decentralized, according to P-f characteristic curve). For larger deviations (±10 mHz to ±200 mHz) the PCR power should be delivered and increased linearly up to 100 % of the bid amount and maintain constant at its maximum as long as the frequency deviation is larger than ±200 mHz [221].

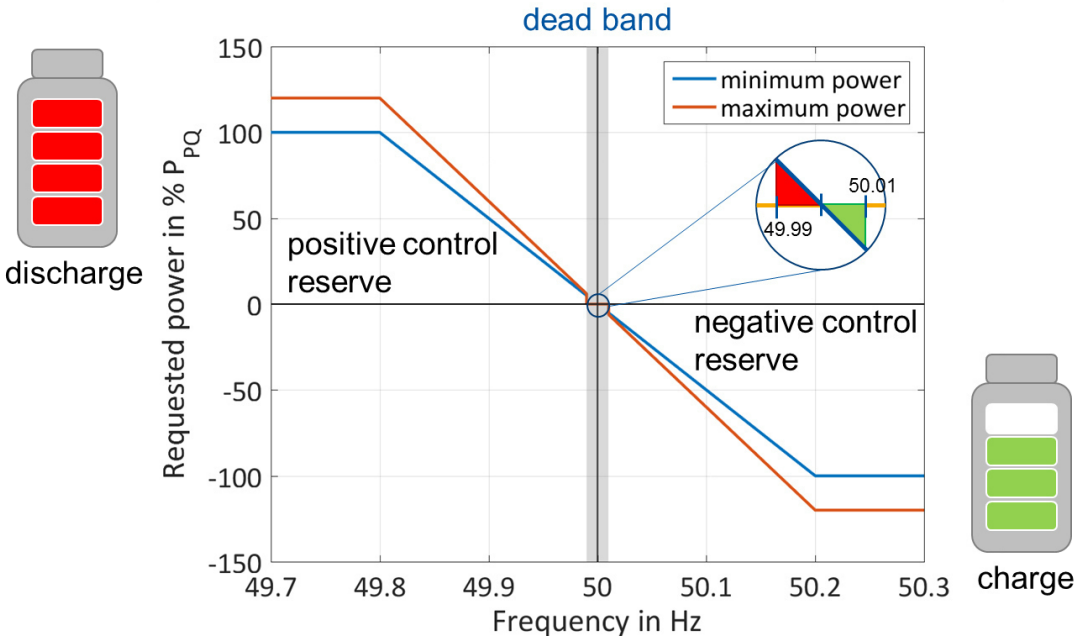

Figure 82: Power to frequency characteristic (P-f characteristics) for BESS providing PCR on the Central European market. The maximum power is the maximum power, which can be provided in the case of over-fulfillment and minimum power depicts the minimum power, which can be provided in the case of under-fulfillment [257].

Figure 82 presents the PCR P-f characteristics curve for a battery energy storage system (BESS). This figure illustrates the delivery requirements of the PCR. If the frequency violates the standard operation situation and the deviation is between 10 mHz and 200 mHz the BESS should start to absorb power from the grid (charging the batteries). The standard operation situation is illustrated in Figure 83. The amount of power should increase linearly with an increase of the grid frequency between 10 mHz and 200 mHz and remain at its maximum if a deviation remains above 200 mHz. For a negative deviation, the behavior is the same, except that BESS should discharge and feed power into the grid. To ensure that BESS are able to deliver the required power they have to undergo the prequalification process.

7.2.2 Operating range and for BESS

For a battery system to participate in the PCR market, regulations are given in [39], which define the compulsory available energy reserve in the storage system.
The requirements for prequalification are presented in Figure 81. Figure 81 shows that BESS have to provide PCR for 30 minutes in total (until May 2019 see section 6.2.4). This regulation is called the 30 minute criterion, which states that BESS should be able to provide the prequalified PCR, both charging and discharging, for 30 minutes.

Considering these rules and the prequalification requirements for BESS, the resulting permitted SOC ranges are shown in Figure 83. E_{bat} (energy content of the battery) and P_{PQ} (prequalified PCR power) determine the maximum and minimum SOC limits.
Equations (58) and (59) show these values:

$$SoC_{upper\ boudary} = \frac{E_{bat} - 0.5h \cdot P_{PQ}}{E_{bat}} \quad (58)$$

$$SoC_{lower\ boudary} = \frac{0.5h \cdot P_{PQ}}{E_{bat}} \quad (59)$$

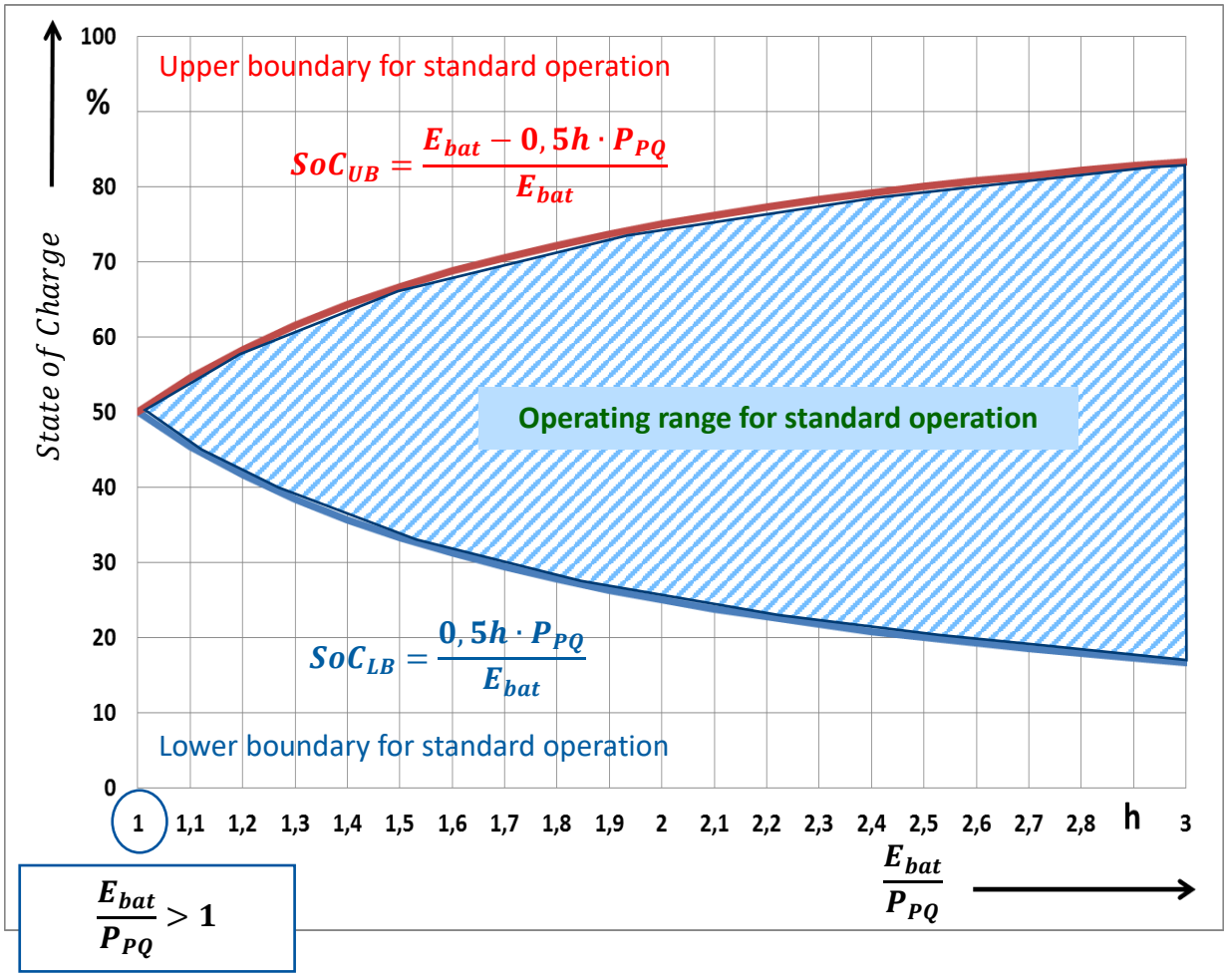

Figure 83: Required state of charge (SoC) range for a battery energy storage system (BESS) based on the 30 min criterion on the German PCR market. E_{bat} (energy content of the battery) and P_{PQ} (prequalified PCR power) determine the maximum and minimum SoC limits.

The 30 min criterion is violated when the operating range does not remain within the operation range for standard operation while the grid is in a standard operation situation. It is a standard operation situation as long as none of the following criteria are fulfilled:

- frequency deviation above ±200 mHz
- frequency deviation above ±100 mHz for more than 5 min
- frequency deviation above ±50 mHz for more than 15 min

To fulfill these requirements the available energy of the BESS must be greater than the prequalified power as described in the following equation:

$$\frac{E_{bat}}{P_{PQ}} > 1h \tag{60}$$

In real applications, the available energy has to last for a minimum time of 1.33 hours, because a frequency deviation of 10 minutes at 100 Hz plus a frequency deviation of 5 minutes with 200 Hz is still in the standard operation range. Therefore, a minimum available energy of 40 min in each direction has to be minded. Thus, a total minimum available energy of 1.33 hours is requested in order to get prequalified. Normally 1.5 hours of available energy is used as a boundary, because energy for normal operation and time for recharging has to be minded. For this dissertation, an available energy rate of 1.43 h is assumed based on the analysis presented in section 7.3.2.
As soon as the frequency reaches the standard operation window, the battery SOC must be restored to the boundary defined in Figure 83. This leads to a limitation of the PV-BESS operation range, if PV-BESS is participating in the PCR market. This limitation is shown in Figure 84.

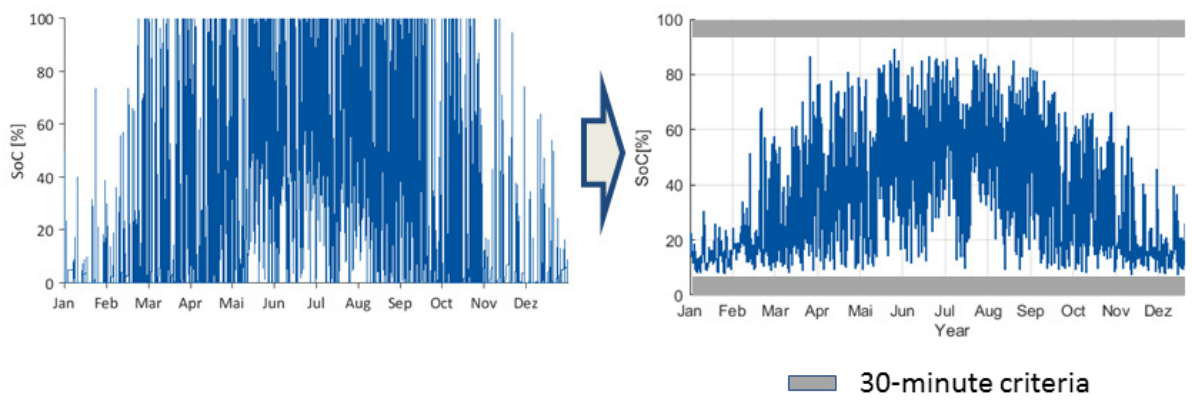

Figure 84: Left: SOC of a 10 kWh PV-BESS without PCR. Right: SOC of a PV-BESS which participating in the PCR market. The 30-minute-criteria is shown, if 1 kW PCR is offered on the market. The presented results are based on simulations.

7.2.3 Degrees of Freedom

In Central Europe, as defined in [257], TSOs are allowing degrees of freedom in order to keep the battery SOC level within the boundaries defined in Figure 82.These degrees of freedoms are provided considering that PCR participants can slightly deviate from the P-f characteristics curves of Figure 82.

Over fulfillment:

The control power determined by the P-f characteristics curve can be increased by up to 20 % in order to help adjusting the SOC to the required value. The operator of the BESS is allowed to decide if the BESS should be charged or discharged with the additional power [257].

Dead band:

Within the dead band a PCR provider does not have to provide PCR. The operator of the BESS can use this dead band to adjust the SOC of the BESS. Therefore, the control power demand indicated by the P-f characteristic can also be provided within the tolerated deviation range

of ±10 mHz if the SOC needs to be adjusted [257]. The SOC adjustment is only allowed if it serves the grid and a maximum power of 5 % of the PCR is allowed. To be able to use the dead band a sufficiently accurate measurement needs to be installed.
Provision Rate:
The control power based on the P-f curve must be provided within 30 seconds or less. This allows the PCR provider to adjust the power gradient in order to influence the SOC.
Scheduled Transactions:
PCR providers can modify the SOC by participating in the electricity market.

7.2.4 Aggregation of battery energy storage systems

To participate on the PCR market a minimum power of 1 MW is required [216]. This is a boundary for small BESS like PV-BESS, because these systems can only provide PCR of some kilowatts. According to [230], it is allowed to couple these systems in a virtual power plant to provide PCR. These power plants have to be in the same control area [231] and have to undergo the prequalification process as one unit.
As already mentioned, the prequalified power must be supplied for at least 30 minutes. This can be reduced to a 15 minutes criterion [221] if the BESS is operated in a virtual power plant with conventional power plants. This is only allowed if the virtual power plant has no limitation of the available energy. In this case, the virtual power plant has to undergo the prequalification process and an extension of the prequalified power of the virtual power plant is not permitted.

7.2.5 PCR for PV home storage systems with power-to-heat coupling

Renewable energy produced by a PV power plant in a household cannot only be used to cover the electric load. This energy can be used to cover the heating demand of the household if for example a heat pump is installed in the building. The examined household in this section couples the heating sector with the electricity sector to enhance the self-consumption and in some cases the economics of the household [140]. The applied power for heat coupling can be used for the PCR as well. The negative control reserve can be transferred into the heating sector. Therefore, the limitation of the battery can be reduced as depicted in Figure 85. If the BESS is fully charged the negative PCR power can be transferred into the heating sector with the heater rod. The negative PCR has to be used for heating. It is not allowed to waste the negative PCR power.

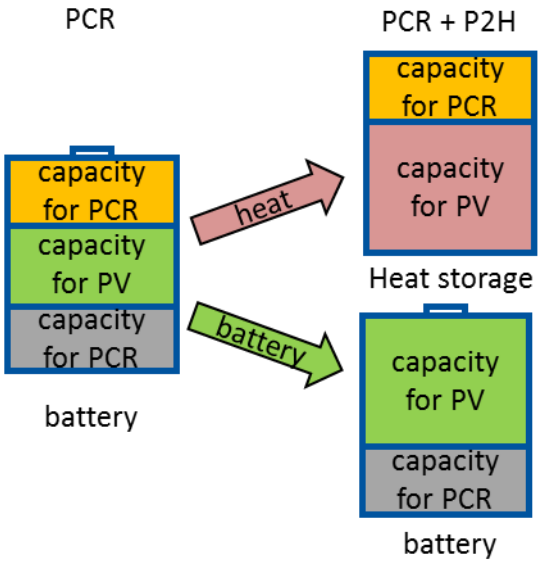

Figure 85: Allocation of the reserve capacity of a BESS with power-to-heat coupling participation in the Central European PCR market in comparison to a standalone BESS. Positive control reserve can be transferred in the heating sector, leading to higher useable capacity.

7.3 Model for participating in the primary control reserve market

7.3.1 Adjustment of the scheduled power to guarantee the 30 minute criterion

As described in section 7.2.2 the 30-minute criteria has to be fulfilled at all times. Therefore, an adjustment of the scheduled power is necessary and the battery has to be recharged on the intraday market. The total time duration for the adjustment of the scheduled power is divided into three 15min time intervals: idle time, lead-time, delivery time.
At the intraday market, transactions can only be made at the beginning of every quarter of hour. Therefore, the maximum time delay between the detection of a scheduled adjustment and transaction on the intraday market is up to 15 minutes. The idle time represents this time delay.
The lead-time represents the time between the transaction and the delivery. The lead-time could be between 15 minutes and 45 minutes [258]. The lead-time is set to the minimum time of 15 minutes in this work, because the possibilities of future inter- virtual power plant energy exchange is considered. The delivery time for intraday transactions is 15 minutes and is considered in this work. The three different time intervals are illustrated inFigure 86.

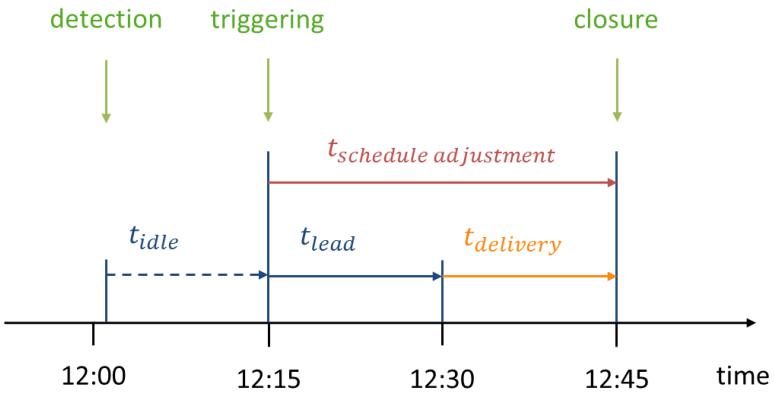

Figure 86: Timeline for an adjustment of the scheduled power. After the detection of a schedule adjustment the idle time, lead-time and delivery time has to be minded.

7.3.2 Calculation of the maximum PCR

To determine the maximum PCR power, which can be offered by the integrated home, every component of the house is analyzed separately. The following conditions are derived from requirements proposed by the TSOs and are presented in [39].
The battery must have enough capacity to fulfil the 30-minute criterion. Therefore, schedule adjustments could be necessary. The time delay for a schedule adjustment is calculated in section 7.3.1. The criteria for a standard operation scenario as presented in section 7.2.2 are minded as well. A worst-case consideration is analyzed. Therefore, the time of the detection of a schedule adjustment is set to the second after the quarter-hour boundary for a transaction e.g. 10:00:01 o'clock. During this quarter hour, a frequency deviation of ± 50 mHz is considered. This deviation is valid in the standard operation situation. After this event a frequency deviation of ±200 mHz for 5 minutes is considered, followed by a frequency deviation of ±100 mHz for 10 minutes. These frequency deviations are still defined as the standard operation situation. In this worst case, a violation of the 30-minute criterion is not valid. For the worst-case, the following frequency deviation after schedule adjustment detection at 10:00:01 o'clock is considered:

1) 10:00:01 till 10:15 frequency deviation of ±50 mHz
2) 10:15 till 10:20 frequency deviation of ±200 mHz
3) 10:20 till 10:30 frequency deviation of ±100 mHz

After these deviations the 30-minute criteria has still to be fulfilled. In following the necessary capacity is calculated in dependence of the offered PCR power P_{PCR}:

$$E_1 = \frac{50\ mHz}{200\ mHz} \cdot \frac{15}{60} h \cdot P_{PCR} = \frac{1}{16} h \cdot P_{PCR} \quad (61)$$

$$E_2 = \frac{200\ mHz}{200\ mHz} \cdot \frac{5}{60} h \cdot P_{PCR} = \frac{1}{12} h \cdot P_{PCR} \quad (62)$$

$$E_3 = \frac{100\ mHz}{200\ mHz} \cdot \frac{10}{60} h \cdot P_{PCR} = \frac{1}{12} h \cdot P_{PCR} \quad (63)$$

$$E_4 = \frac{200\ mHz}{200\ mHz} \cdot \frac{30}{60} h \cdot P_{PCR} = \frac{1}{2} h \cdot P_{PCR} \quad (64)$$

$$E_{PCR} = E_1 + E_2 + E_3 + E_4 = 0.7292\ h \cdot P_{PCR} \quad (65)$$

With respect to the battery capacity, the energy that needs to be reserved for PCR can be calculated as following:

$$SoC_{PCR}(c_{Bat}) = \frac{E_{PCR}}{C_{Bat}} = \frac{0.7292h}{C_{Bat}} \cdot P_{PCR} = a_{PCR} \cdot P_{PCR} \quad (66)$$

In this work a 10 kWh battery is considered. Therefore, the factor a_{PCR} for the examined battery system can be calculated as following:

$$a_{PCR}\,(c_{Bat}) = \frac{0.7292h}{C_{Bat}} = \frac{0{,}7292\ h}{10\ kWh} = 0.073\ \frac{1}{kW} \quad (67)$$

This leads to a reserved capacity of 7.3 % per kW PCR of a 10 kWh BESS.

$$SoC_{PCR}(c_{Bat}) = 7.3\ \frac{\%}{kW} \cdot P_{PCR} \quad (68)$$

If the capacity of the BESS is below this value, a schedule adjustment is triggered to recharge the battery on the intraday market. This value is valid for one direction, charge or discharge. The capacity has to be saved in both directions. In the case an integrated home is considered, the negative PCR can be transferred into the heat storage as shown in section 7.2.5. In this case, an integrated home with power-to-heat coupling and a 10 kWh BESS can provide up to 13.8 kW of PCR with the BESS.

Beside the battery capacity, the converter can be a limiting factor for participation in the PCR market. Considering the TSO regulations, 25 % of the converter capacity has to be available for recharging at all times. Therefore, a maximum of 8 kW from a 10 kW converter can be used for PCR.

If the charging power of the BESS is limited due to a high SOC, the heat can be transferred to the heating sector with the heating rod. The battery cell, which is used for parameterization of the BESS can be discharged with a current up to 2C. The 2C rate limit is set by the battery management system (BMS). Therefore, the discharge rate of the battery is not a limiting factor [259]. Only if the battery gets close to the discharge cut-off voltage, the discharging c-Rate is reduced. Table 19provides an overview of the limiting factors of the integrated home for PCR. The analysis leads to the conclusion that the battery converter and the grid inverter are the limiting factors for the PCR.

component	constraint	size [kW]
battery	SoC	13.8
	Charging power	— (limited by the power of the heating rod)
	Discharging power	20
inverter	Rated power	8
converter	Rated power	8

Table 19: Limiting factors of the available PCR power of the integrated home (10 kWh battery; 10 kW converter).

7.3.3 Advantages of the power-to-heat coupling in integrated homes participating in the PCR market

An advantage of integrated homes participating in the PCR market is that the negative PCR can be transferred into the heat storage as shown in section 7.2.5. The surplus PCR power can be transferred with a heating rod to the heating sector. Nevertheless, due to the high exegetic value of electricity, this is the last option. First of all the negative PCR power is used to reduce the grid consumption of the integrated home. If the energy consumption from the grid is zero, the PCR power is stored in the BESS. Only if the BESS is fully charged SOC = SOCmax the negative PCR is transferred into the heating sector via the heating rod. The heat pump is not used, because of the ramp up time of the heat pump. Additionally, the negative PCR power might not be sufficient to run the heat pump. Furthermore, PCR power might not be available for a sufficient time to guarantee the minimum runtime of the heat pump.
To be able to prequalify the integrated home in a virtual power plant for the PCR market the heat storage capacity has to be sufficient to fulfil the 30-minute criterion. Therefore, the maximum capacity of the buffer and DHW storage is calculated. If the integrated home delivers 8 kW of PCR (size of converter), the storage capacity of the heating sector has to be 5.84 kWh at least. The minimum storage capacity of 5.84 kWh is calculated with equation (67). The volume of one storage is 300 l and the heat capacity of water is c = 4190 $\frac{J}{kg \cdot K}$. To fulfil the 30 min criterion the temperature spread in the storage has to be at least 14.3°C. An efficiency of the heating rod of 100% is assumed. The maximum output temperature of the heat pump is 55°C and the maximum valid temperature in the storage is 95°C [260]. Therefore, the minimum spread offered is 40°C. The storage capacity of the heating storage is sufficient for the PCR requirements.

7.3.4 Use of the degrees of freedom: over fulfilment and death band

Section 7.2.3 pointed out the degrees of freedom for BESS participating in the PCR market. These degrees of freedom can be used by the integrated home, to extract energy from the grid for free. If the integrated home should deliver negative PCR the degrees of freedom can be used. The integrated home can use the dead band as well as the over fulfilment. Therefore, factors are implemented to use the potential of the degrees of freedom.

$$P_{PCR,total} = P_{PCR,min}(f) \cdot k_{over\ fulfilment}(f) \cdot k_{death\ bamd}(f) \tag{69}$$

These factors depend on the frequency and are shown in Table 19. A factor of 1.2 represents an over fulfilment of 20 %.

Degree of freedom	Frequency in Hz	factor
$k_{dead\ band}$	$49.99 \leq f < 50$	0
	other	1
$k_{over\ fulfilment}$	$49.8 \leq f < 50$	1
	$50 < f \leq 50.2$	1,2

Table 20: Usage of the degrees of freedom of a PV BESS.

7.3.5 Battery operation in case of PCR

The BESS of an integrated home has a double use when participating in the PCR market. The capacity for the use as a home storage and the capacity for the PCR market are separated virtually. If the SoC band of the PCR is reached, the load of the household is not covered by the BESS. In the case, the energy of the battery storage reserved for home storage operation is considered as empty. Regulatory issues, if there are any, could be overcome by the installation of a backup supply in the pool. As soon as the SoC reaches a value above of the PCR SoC band, due to a schedule adjustment, the load of the household would be directly covered by the BESS. This would lead to an oscillation. Therefore, a band is defined in which the SoC of the battery has to be charged by solar power in order to cover the load from the household. Figure 87 illustrates this band.

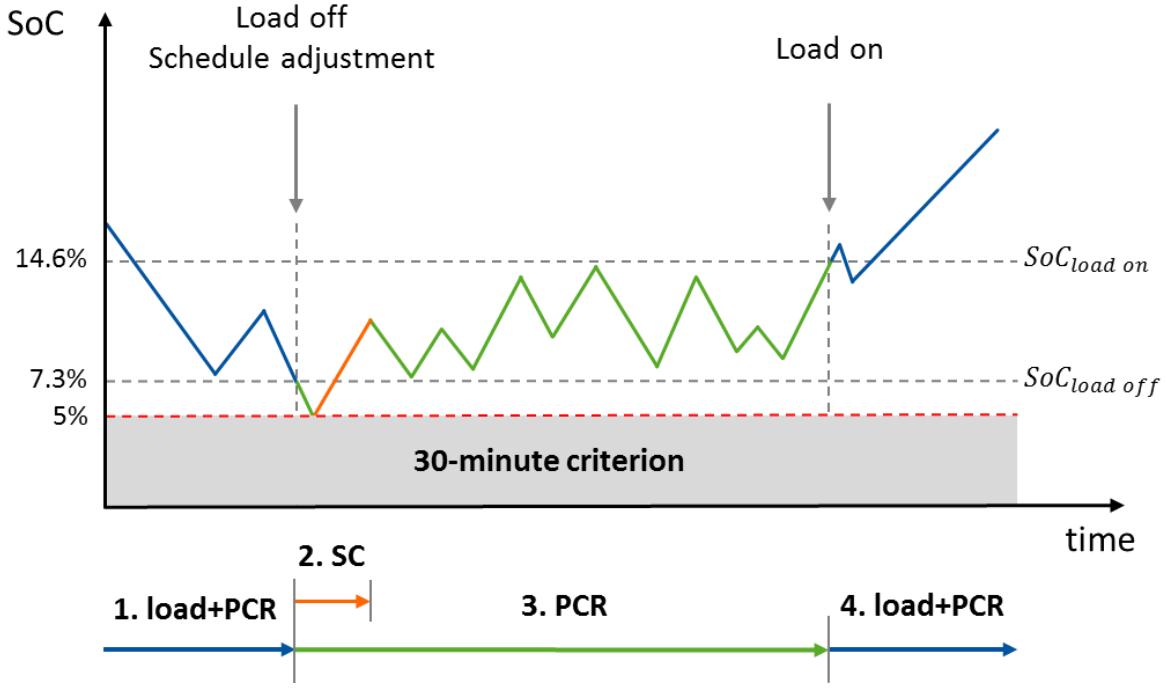

Figure 87: Battery operation of a PV BESS (1kW PCR; 10 kWh battery; 10 kW converter) in case of a PCR. If a schedule adjustment is necessary, the battery does not cover the load. PV generation is used for direct self-consumption (SC). Only when the SoC of the battery exceeds a defined boundary the battery covers the load (load on).

7.3.6 Constant offer of PCR

In this work, two different kinds of PCR are examined: a constant and a variable offer of PCR power on the market. The constant PCR strategy offers constant PCR power over one year on the market. The SOC characteristic of the examined integrated home with 3 kW PCR is illustrated in Figure 88. The 30-minute criterion is minded.

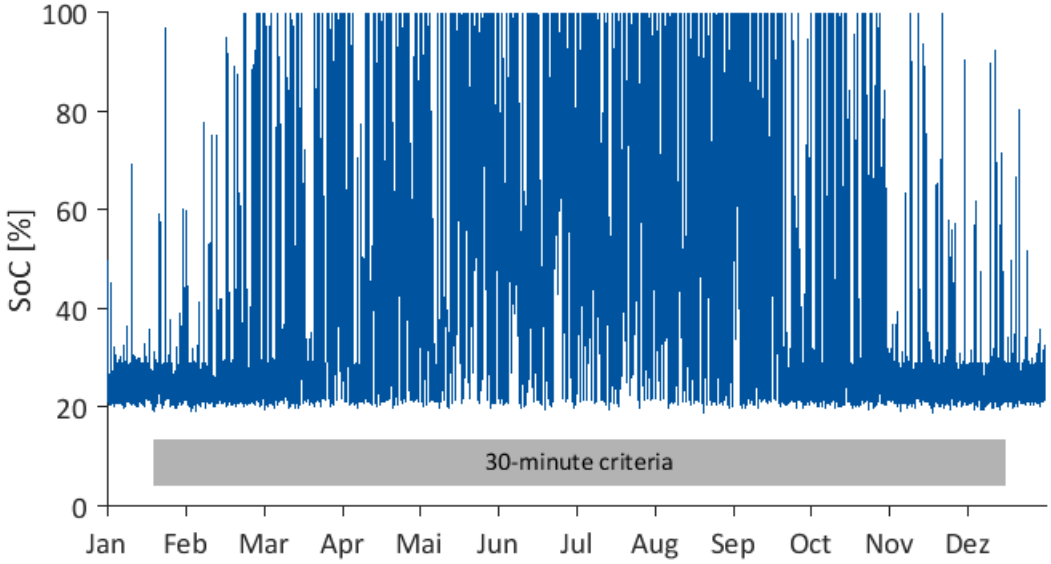

Figure 88: SoC of a PV-BESS with power-to-heat coupling and a 10 kWh BESS and a 10 kWp PV system offering a constant PCR power of 3 kW.

7.3.7 Variable offer of PCR

The 30-minute criterion limits the use of the battery for the home storage operation. In winter months the BESS is used less for home storage operation. Therefore, a higher share of PCR can be offered on the market without major limitation of the home storage operation. Therefore, a variable offer of PCR on the market is presented in this section. A combined operation of the BESS for enhancement of self-consumption and PCR provision requires a waiver of self-consumption. To determine the weekly offered PCR different waivers of self-consumption are analyses. A waiver of 20 % of the energy stored in the BESS has the highest economics as presented in Figure 99 (section 7.4.5). Therefore, the SoC limit is chosen, which only reduces the energy throughput of the battery for the offered week by 20 % as shown in Figure 89.

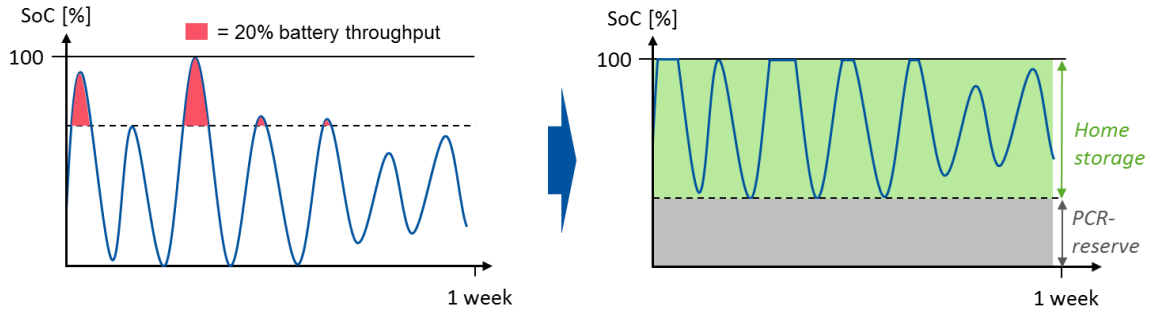

Figure 89: Calculation of the weekly offered PCR. Assumption that waiver of 20 % of the energy stored in the BESS is acceptable (left). The SoC limit for this week is the SoC, which only reduces the energy throughput of the battery for the offered week by 20 % (right).

The 80 % energy boundary represents the SoC band for the home storage operation. The rest of the band can be used for PCR. With respect to the factor $a_{PCR} = 0.0726\ 1/kW$ presented in section 7.3.2 the offered PCR can be calculated with the following equation:

$$P_{PCR,week} = \frac{SoC_{PCR,week}}{100\ \% \cdot a_{PCR}} \tag{70}$$

In winter months the battery is used less for home storage operation, therefore the offered PCR is higher in the winter month. The weekly offered PCR is depicted in Figure 90 with respect to the 8 kW limit of the converter [39]. The determination of the weekly offered requires forecast of the load and the PV feed-in. The influence of prognosis errors is not examined in this work. The variable offer of PCR power leads to an average offer of $5.9\ \frac{\mathrm{kW}}{\mathrm{week}}$.

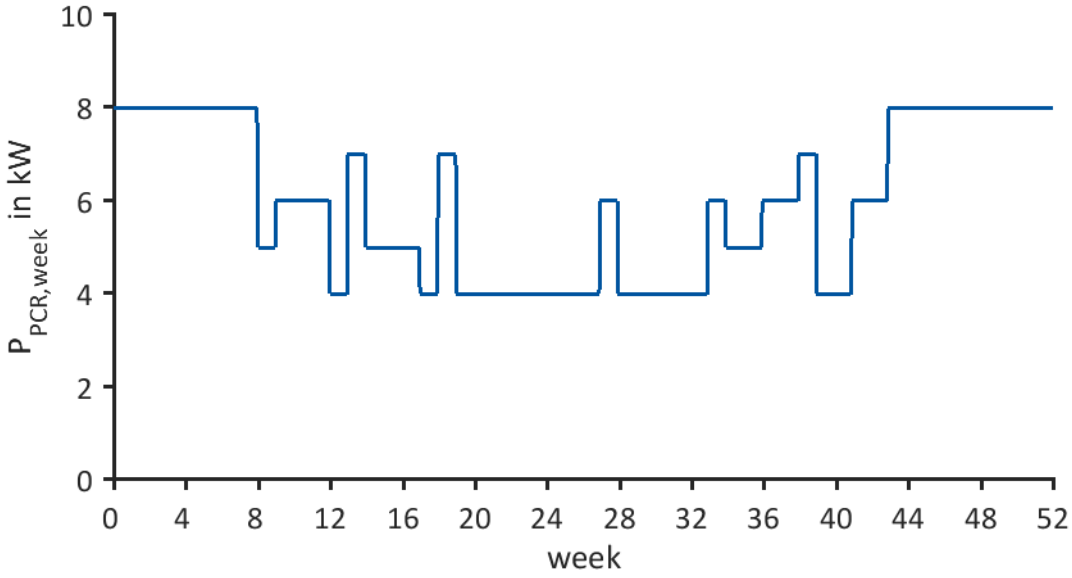

Figure 90: Resulting variable PCR offer of a PV BESS with power-to-heat coupling and a 10 kWh BESS and a 10 kWp PV system.

7.4 Results participation on the primary control reserve market

The following section presents the results from simulation and economic evaluation of the market participation of aggregated residential integrated home. Since there are many different relevant aspects to this evaluation, a discussion of the presented results is directly included in this section to increase readability and comprehensiveness.
The participation on the PCR market generates additional incomes for integrated homes. On the other hand, additional costs due to higher battery aging and lower self-consumption emerges. Section 7.4.1 investigates the influence on the battery aging. The influence on the self-consumption rate is examined in section 7.4.2. An economic evaluation of costs and revenues of the participation on the PCR market is analyzed in section 7.4.3. Section 7.4.4 presents an examination of the influence of the costs for participation on the PCR market. A comparison of all these costs with the possible incomes is presented.

7.4.1 Influence on the battery aging

To participate in the PCR market the 30-minute criterion has to be fulfilled as pointed out in section 7.2.2. This leads to an enhanced average SoC of the battery and hence to an accelerated battery aging. The influence of the market participation on the average SoC of the BESS is depicted in Figure 91. The reserved capacity to satisfy the 30-minute criterion is also illustrated by the gray area. With a rising PCR power, the SoC capacity for the 30-minute criterion is enhanced. Hence, the average SoC of the BESS is enhanced. In the case of a provision of 8 kW PCR, the reserved capacity is 58 % of the total battery capacity. This leads to an average SoC of 74.9 % and therefore to an enhanced battery aging [68]. [68] points out, that an increased SoC leads to an increased battery aging, if the BESS is operated within the operation window.

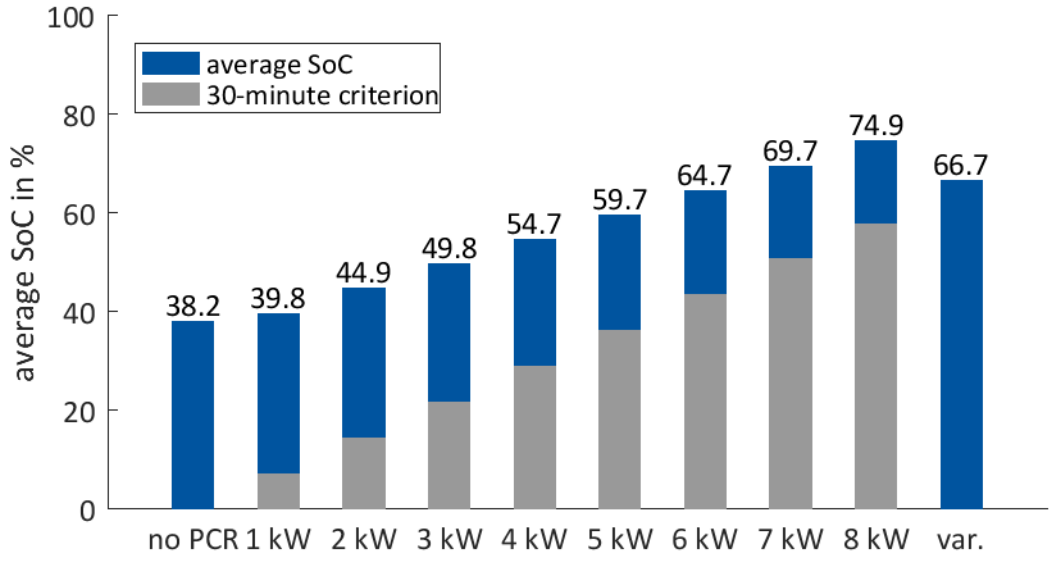

Figure 91: Average SoC in dependency of the PCR offer of a PV BESS with power-to-heat coupling, with a 10 kWh BESS and a 10 kWp PV system.

An enhanced battery aging leads to higher costs of the BESS. The relative battery lifetime decrease is depicted in Figure 92. The result only applies for this specific battery cell. Due to the huge variety of different battery cells, a general statement cannot be made and has to be investigated for every cell individually.
For this battery cell, low rates of PCR power (1-5 kW) lead to a quite minor change of the battery aging. A PCR power of 6 kW reduces the BESS lifetime around 5 %.

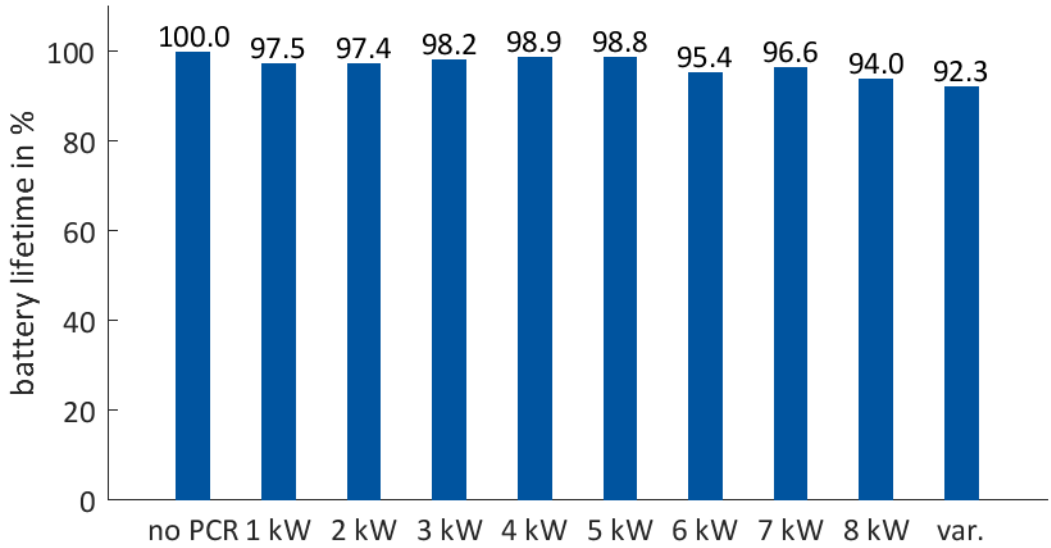

Figure 92: BESS lifetime in dependency of the PCR offer of a PV BESS with power-to-heat coupling with a 10 kWh BESS and a 10 kWp PV system.

For further investigation of the battery aging, the battery aging is divided into two parts, a calendric and a cycle aging. Figure 93 depicts the relative battery aging. An increase of the calendar aging is shown, due to the increased average SoC of the battery. A high average SoC leads to an enhanced calendric battery aging [68].

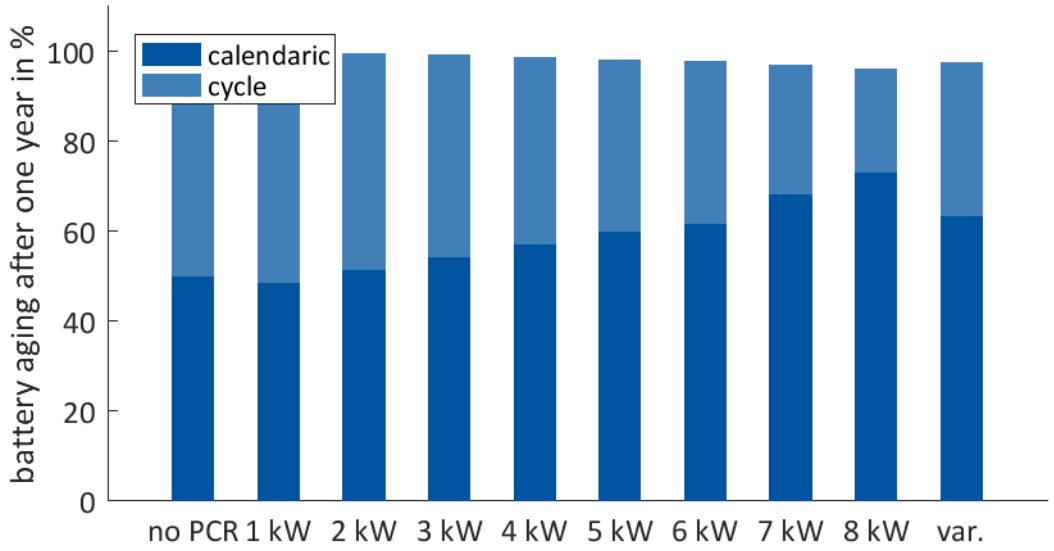

Figure 93: Calendar and cycle aging in dependency of the PCR offer of a PV BESS with power-to-heat coupling with a 10 kWh BESS and a 10 kWp PV system. The calendric aging is increasing, because the average SoC is enhanced.

Besides the calendar aging, the cycle aging of the BESS is depicted in Figure 93 as well, in accordance to the battery aging model presented in section 3.2.5. In comparison to the calendar aging, the share of the cycle aging is reduced. The reason for the reduction is the reduced useable capacity for the home storage operation due to the implemented PCR limits. This limits lead to cycles with smaller DoD and therefore less cyclic aging. If the PCR power is between one and five kW the reduced cycle aging and the enhanced calendar aging almost cancel each other. This is the explanation for the minor influence on the battery aging depicted in Figure 92.

If the integrated home offers 6 kW of PCR, the cycle aging is enhanced. The reason for this enhancement is the reserved SoC of 43.8 %. Every time the battery is charged and discharged, the penalty function located at 50 % SoC is triggered. The penalty function describes additional aging due to phase transition of the battery cell (section 3.2.5.5). Theories presented in [63, 68] assume that a change in the grid structure of the graphite electrode lead to additional mechanical stress and therefore to an enhanced battery aging. This effect was observed for the investigated cell in this work. The increase of the PCR power to 7 kW leads to a reserved SoC of 51.1 %. In this case, the penalty function is not triggered, and less cyclic aging occurs. This is why the share of the cycle aging in the 6 kW PCR case is almost the same as in the 5 kW PCR case. Furthermore, this is the explanation for the lower battery lifetime in the 6 kW PCR case in comparison to the 7 kW PCR case.

In total the additional aging of the BESS, when participating in the PCR is relatively low. The lifetime of stationary BESS in home storage operation, are often limited by the calendar lifetime. BESS in home storage operation with a 1:1 dimensioning (PV to BESS capacity; here: 10 kWp PV system with 10 kWh BESS) performing 180 to 250 equivalent full cycles per year in Germany [261]. The Wöhler curve presented in Figure 21 point out that the investigated battery cell is able to perform around 4000 equivalent full cycles at 40 % DoD. This leads to the conclusion, that the cycle lifetime of the battery is not fully used during home storage operation. Additional cycles for PCR participation have a minor effect on the lifetime of the

BESS. The additional stress for the BESS due to the participation on the PCR affects the aging only to a minor degree, because the calendar aging is dominate in this application.

7.4.2 Influence on the self-consumption rate

The participation on the PCR market leads to a limitation of the home storage operation, because capacity in the BESS is reserved for the PCR operation. The operation strategy of the BESS aims to maximize the self-consumption rate [133]. Therefore, the self-consumption rate is an indicator for the home storage operation and provides a value for among of energy from the PV power plant used by the household. The self-consumption rate is defined as the sum of the direct self-consumption plus energy stored in the BESS divided by the energy produced from the PV power plant.

$$a_{SC} = \frac{E_{direct\ SC} + E_{bat\ charge}}{E_{PV}} \tag{71}$$

Figure 94 depicts the self-consumption rate for different PCR offers. With an increasing PCR offer, the self-consumption rate is reduced. Therefore, the battery is used less for home storage operation. The self-consumption rate of the variable operation strategy is higher as an offering of 7 kW constant PCR.

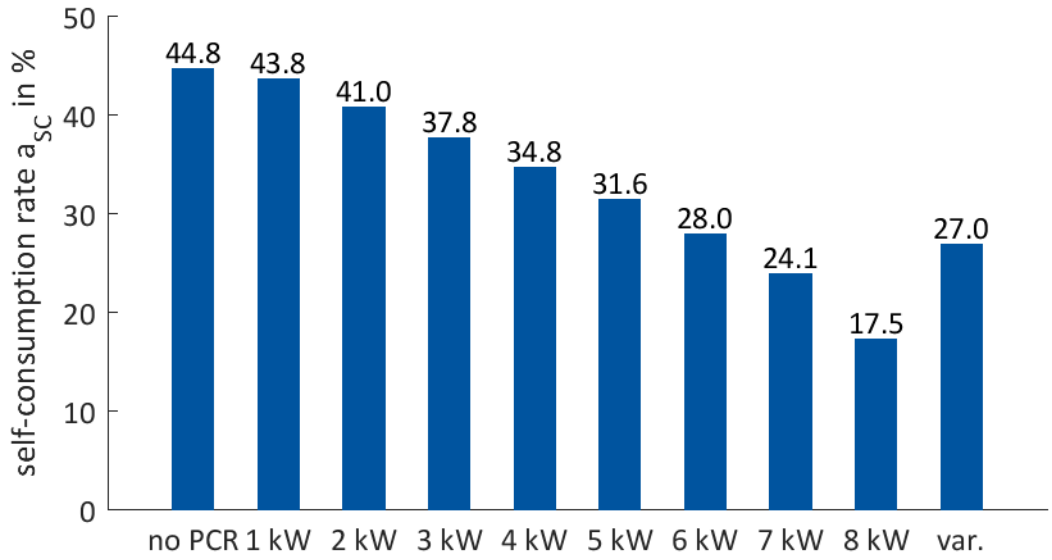

Figure 94: Self-consumption rate in dependency of the PCR offer of a PV BESS with power-to-heat coupling with a 10 kWh BESS and a 10 kWp PV system.

7.4.3 Economic evaluation

The economic evaluation is based on the methodic and the parameters presented in section 3.5. The assumption is made that the integrated home participates in a pool on the PCR market. The pool is prequalified for the PCR participation. Therefore, additional costs are not taking into account. The influences of these costs are discussed in section 7.4.4. The cost for

market participation vary in a wide range [248, 262, 263]. Hence, it is difficult to give a clear statement regarding these costs. This section investigates the additional revenues for BESS participating in the PCR market and the costs for reduced self-consumption rate and enhanced battery aging. Further savings, due to additional energy gained from the utilization of the degrees of freedom, are taking into account. The depicted results present the annuity of the integrated home. The annuities are the annual costs for electricity and heating of the integrated home considering all costs over the systems lifetime. Therefore, integrated houses with lower annuity have higher economics. The annuities are depicted in Figure 95. The results emphasize that the offer of 1 kW PCR already leads to reduced annuity in comparison to an integrated home not participating on the PCR market. The integrated home offering variable PCR has the lowest annuity and therefore the best economics. Costs for participation are neglected in this evaluation. The annuity of the integrated homes is compared to a house with fossil heating. This house uses grid consumption for electricity of 29.2 ct/kWh and fossil heating of 13 ct/kWh$_{th}$ [137]. A comparison with a house combining a PV system without a BESS and fossil heating is presented in section 7.9.

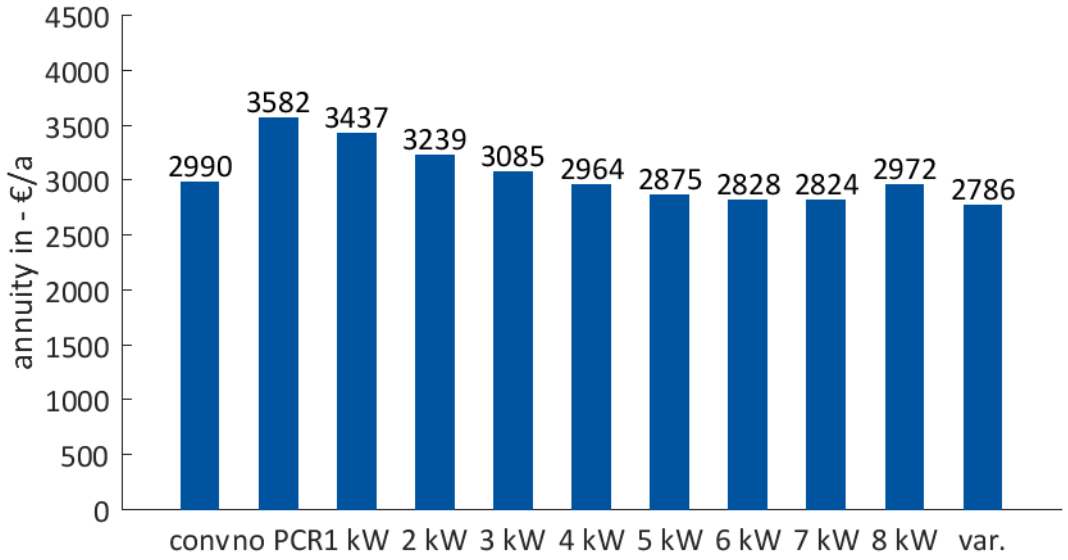

Figure 95: Annuity in dependency of the PCR offer of a PV BESS with power-to-heat coupling and a 10 kWh BESS and a 10 kWp PV system. A constant PCR revenue of $2.00\ \frac{€}{kW \cdot week}$ is considered. Comparison to a conventional power generation (annual consumption: 4,674 kWh$_{el}$ with 29.2 ct/kWh and 12499 kWh$_{th}$ with 13 ct/kWh [137]).

The results presented in Figure 95 are based on constant PCR revenue of $2.00\ \frac{€}{kW \cdot week}$. In section 6.2.3 it was pointed out that the PCR prices are expected to fall. Therefore, a sensitivity analysis of the PCR prices is presented in Figure 96 on an integrated home offering a variable PCR power. The annuity incorporates the inflation rate. Therefore, annual decrease of 5 % of the PCR prices lead to a PCR price of $0.62\ \frac{€}{kW \cdot week}$ in 20 years. This leads to an annual PCR remuneration of 752 €/a in the first year and an annual PCR remuneration of 233 €/a in 20 years. This is the explanation for the annuity increase of 6 %, if a 5 % decrease of the PCR price is estimated.

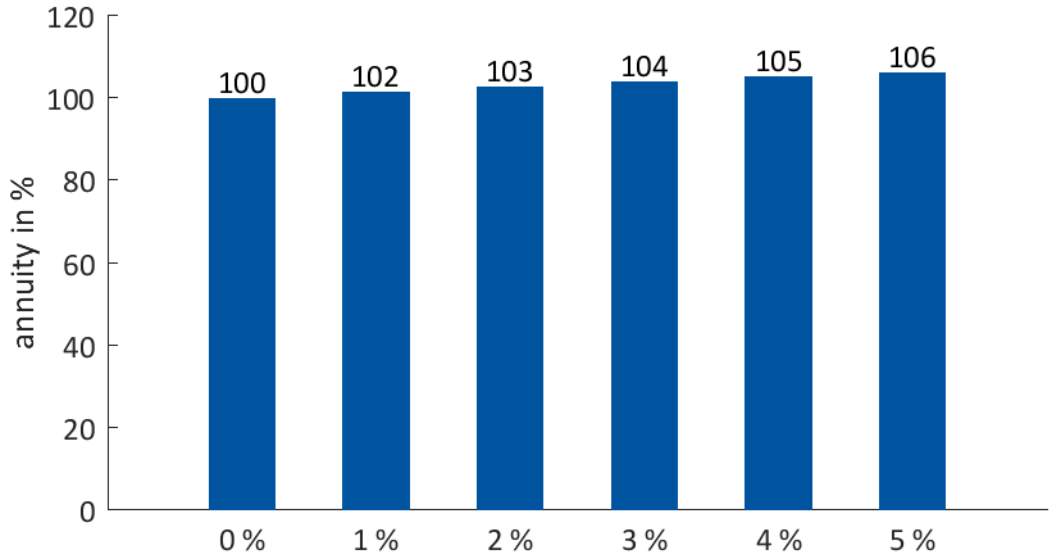

Figure 96: Sensitivity analysis of the PCR price offer by a PV BESS with power-to-heat coupling and a 10 kWh BESS and a 10 kWp PV system. A basic PCR price of $2.00 \frac{€}{kW \cdot week}$ is considered. The integrated home offers a variable PCR power.

7.4.4 Influence of the costs for participation on the PCR market

This section analyses the influences of the measurement costs and running costs for PCR market participation. These costs are varying, therefore a general statement cannot be made. Furthermore, the assumed costs are costs for the current market situation. Future costs saving through progression in automatization, modern measurement methods and centralized regulation are not taken into account. Additional costs for the market access and marketing of the PCR power are not investigated.
To participate in a pool in order to get prequalified in the PCR market a measurement of the PCR power and a communication with the TSO and the other participants in the pool is crucial. Table 21 provides an overview of the range of costs for market participation. The costs are classified in investment costs (CAPEX) and operation costs (OPEX).

	Cost type	Costs in €
CAPEX	Installation of measurement device (steering box) • Steering software • Communication technology • Measurement technology	299 – 1000 € [262, 264]
OPEX	Current payments for measurement point • Operation of measurement point • Measurement service • Billing • Communication	325 – 650 €/a [248]

Table 21: Cost for participation on the PCR market of BESS operating in a virtual power plant.

A steering box for the PCR measurement point is offered by girdX for 299 € [264]. Caterva, the one of the companies prequalified with a pool of PV-BESS to participate in the German PCR market estimates their costs for a steering box at over 1000 € [262]. The investment cost can be apportioned over the lifetime.
The INEES research project estimate their costs for secondary control reserve (SCR) market participation of EV`s (electric vehicles) of 700 €/a per EV. And estimates future costs of 60-250 €/a, due to changes in the measurement regulation and the integration of smart meters [248, 265].
A worst- best-case scenario evaluation is made of the additional costs for market participation and presented in Figure 97. The investment costs of 299 € are leading to annual costs of 16.85 €/a. The investment costs of 1000 € are leading to annual costs of 56.37 €/a. The operation costs in the worst-case scenario are set to 650 €/a [248]. For the best-case scenario the operation costs are set to 325 €/a, which are half of the costs in the worst-case scenario. The results in Figure 97 emphasis, that the participation in the PCR market could be economically beneficial, if 3 kW or more are offered. In the worst-case scenario, a minimum offer of 6 kW PCR enhances the economics. Costs for market access and changes in the market prices are not incorporated [238]. In the best-case scenario annual savings up to 12.5 %/a are possible with a variable PCR offer.

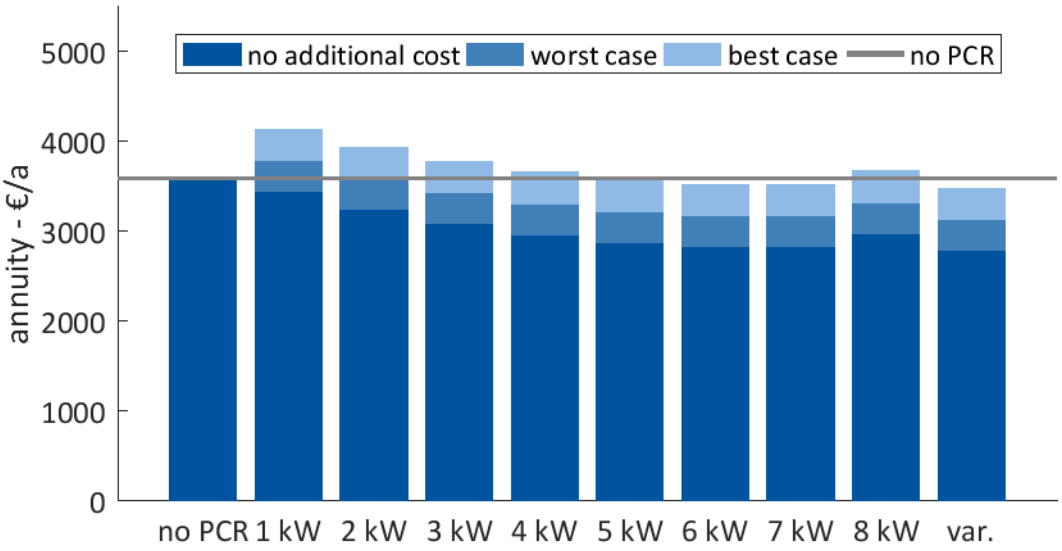

Figure 97: Annuity in dependency of the PCR offers of a PV BESS with power-to-heat coupling with a 10 kWh BESS and a 10 kWp PV system. A constant PCR revenue of $2.00\ \frac{€}{kW \cdot week}$ is considered.

7.4.5 Sensitivity analysis with variable PCR offering

In section 7.3.7, a strategy to offer a variable amount of energy on the PCR market is presented. This strategy is used in section 7.4.1 to 7.4.4. For the investigated strategy the assumption is made that waiver of 20 % of the energy stored in the BESS is acceptable. A waiver of 20 % of the energy stored in the BESS leads to a remaining stored energy of 80 %. Figure 98 depicts the resulting annuity of the investigated integrated home, if the among of waived energy is varied with a 5 % step size. The results lead to the conclusion that a waiver of 20 % of the energy stored in the BESS leads to the lowest annuity and therefore to the highest economic efficiency. Intelligent algorithms to calculate the PCR power offered on the market, can lead to further reduction of the annuity of the integrated home. A reduction of the step size in the presented sensitivity analysis might further increase the economic efficiency.

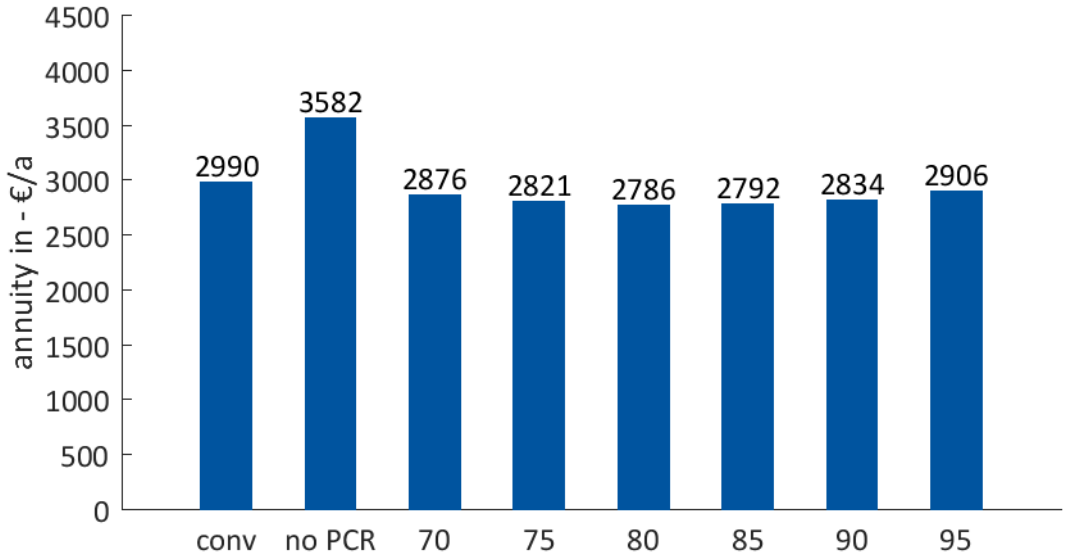

Figure 98: Annuity in of the variable PCR offers of a PV BESS with power-to-heat coupling, a 10 kWh BESS and a 10 kWp PV system. A constant PCR revenue of $2.00\ \frac{€}{kW \cdot week}$ is considered. Different waivers of PCR are investigated. An energy waiver of 20 % leads to a stored energy of 80 %.

7.4.6 Influence of the component sizes of the integrated home

This section investigates the influence of the optimal size of the integrated home participating on the control reserve market. Therefore, the optimal sizes of the integrated home presented in section 5.3.1 are used as an input. As pointed out in this section the optimal inverter size of the integrated home is 7.3 kW. Under consideration of the maximum PCR offer calculated in section 7.3.2, this integrated home is able to participate on the PCR market with 5 kW. For recharging purpose, the power electronics has to be oversized [39]. An integrated home with a 7.3 kW inverter can offer a maximum of 5.84 kW PCR. In this analysis, the limit due to the battery converter is avoided. Therefore, the battery converter size is set to 7.3 kW instead of 1.6 kW. The additional costs of 36 €/a are considered in the calculation. If the battery converter size of 1.6 kW is minded, the maximum PCR power is 1 kW.
The highest annual savings can be achieved with the variable PCR offering strategy. The variable PCR offering with a 20 % waiver of self-consumption as presented in section 7.3.7 is used. The annuity without participation is 2528 €/a and with participation of on PCR market the annuity is 2354 €/a. The annual cost of the optimized integrated home participating in the PCR market is depicted in Figure 99. The presented annual costs do not contain costs for communication and market participation. If the minimum deployment costs for market participation are minded, the annual costs are 2696 €/a. Under consideration of the deployment costs, the additional participation of optimized integrated homes on the PCR market is not economical.

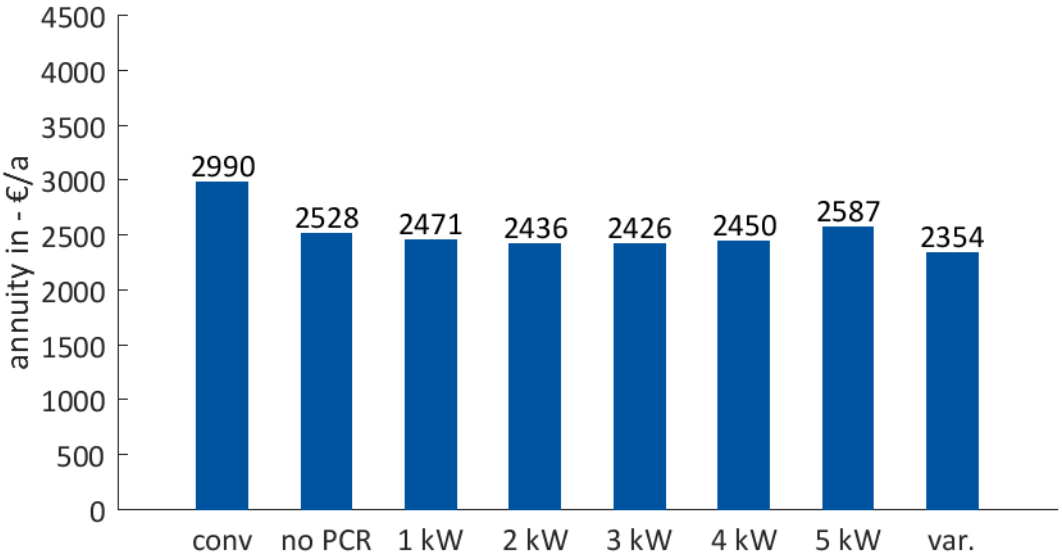

Figure 99: Annuity of the optimized integrated home with PCR market participation (7.1 kWh BESS). A constant PCR revenue of $2.00 \frac{€}{kW \cdot week}$ is considered. Different waivers of PCR are investigated. An energy waiver of 20 % led to a stored energy of 80 %.

7.5 Conclusions primary control reserve market participation

This section presents an extension of the single-use operation of conventional residential storage systems to a dual-use operation of an integrated home with participation in the primary control reserve market. The integrated home combines a photovoltaic battery energy storage system with a heat pump and thermal storages for power-to-heat coupling and can participate on the primary control reserve market as part of a virtual power plant. To participate on the primary control reserve market, the 30-minute criterion has to be fulfilled. The 30-minute criterion ensures that the battery storage system can provide the maximum primary control reserve power for at least 30 minutes. Thermal storages can also be used to absorb the negative control reserve power. The publication at hand points out the advantages in comparison to photovoltaic battery energy storage systems without power-to-heat coupling.

The influence on the economics of the integrated home is investigated. Therefore, load and radiation profiles based on real data measurements are used as input for the simulations. The provision of primary control reserve generates additional incomes for the integrated home. Due to over-fulfillment, free-of-charge energy can be obtained. On the other hand, the provision of energy in the battery storage system for primary control reserve leads to an elevated average state of charge of the battery system. The elevated state of charge leads to accelerated battery aging, mainly driven by increased calendar aging. Furthermore, the additional use of the integrated home on the primary control reserve market reduces the self-consumption rate from the photovoltaic power plant. The economic assessment shows that the additional costs for the increased battery aging and the reduced self-consumption rate are compensated by the income from the PCR market participation. The dual-use operation of an

integrated home that participates in the primary control reserve market can increase the profitability of a residential storage system. Thereby, integrated homes profit from the additional flexibility provided by the thermal storages. Advantages of integrated homes with thermal storages are pointed out and the limited influence on battery aging, operation and self-consumption rate are shown.
Results show that under consideration of steady revenues and low costs for market participation, a provision of at least three kilowatts of reserve power could be economical. Nevertheless, prices for primary control reserve provision were falling in the recent years. Costs for the virtual power plant operation and market access are not transparent. Experts estimate an average income of 100,000 €/(a·MW). Further additional costs for market participation are estimated at 25 % of the income for grid scale storages. These costs might be higher for small storages operating in a virtual power plant. The aggregation of small photovoltaic battery energy storage systems for market participation is challenging, since a complex measurement procedure has to be installed. Finally yet importantly, in Germany additional charges (e.g. Renewable Energies Act levy (EEG-Umlage), grid utilization charges (Netznutzungsentgelt), interruptible loads levy (Umlage für abschaltbare Lasten)) are added for electricity from primary control reserve power that is converted to heat. On the other hand, a reduction of the transaction costs is possible if not every single integrated home is monitored. Additionally, further combination with the intraday market could lead to additional incomes.
Seasonal variation of feed-in from photovoltaics is considered by an advanced bidding strategy for variable provision of primary control reserve power. The advanced operation strategy chooses to bid on the primary control reserve market in dependency of the solar energy production. The results show that such a strategy can further increase the economic efficiency of integrated homes providing primary control reserve. The incorporation of weather prognosis could further enhance the incomes in case of variable offering of primary control reserve power. The flexibilisation of the primary control reserve market and the introduction of the 15-minute criterion lead to further incentives for storage systems to participate in this market.

7.6 Secondary control reserve market participation with integrated homes

For PV home storage systems with power-to-heat coupling, the negative SCR market is promising because additional energy can be gained. If a capacity price of zero is assumed, the negative control reserve could provide energy for the integrated home for lower costs compared to other electricity tariffs. This applies especially when rising energy prices are considered. Furthermore, the reduced time delay between auction and delivery of SCR, presented in section 6.3.1, leads to higher forecast accuracy regarding load, PV power and the SOC of the BESS. If the market prices for negative SCR are positive, aggregators connecting pools of integrated homes could be paid for energy consumption. If an aggregator participates in the market with a pool, the pool has to be qualified as one.
Nevertheless, pooled integrated homes must participate in the prequalification process and fulfill the four-hour criterion.

The participation on the positive secondary control reserve market is less promising, because the energy price for the positive SCR has to be higher compared to the feed-in tariff for PV energy. Otherwise, the feed-in of the PV energy would lead to higher incomes for the integrated home. The average energy price of the accepted bids for the positive SCR from 16.10.2018[1] to 31.03.2019 was 77 €/MWh, which is less than the feed-in tariff for PV energy of 122 €/MWh. PV energy which is used for self-consumption has a counter-value of 292 €/MWh. Even the average marginal energy price for positive SCR was just slightly higher (129.5 €/MWh). Furthermore, the energy prices for positive SCR was falling in the investigated period as depicted in Figure 100.

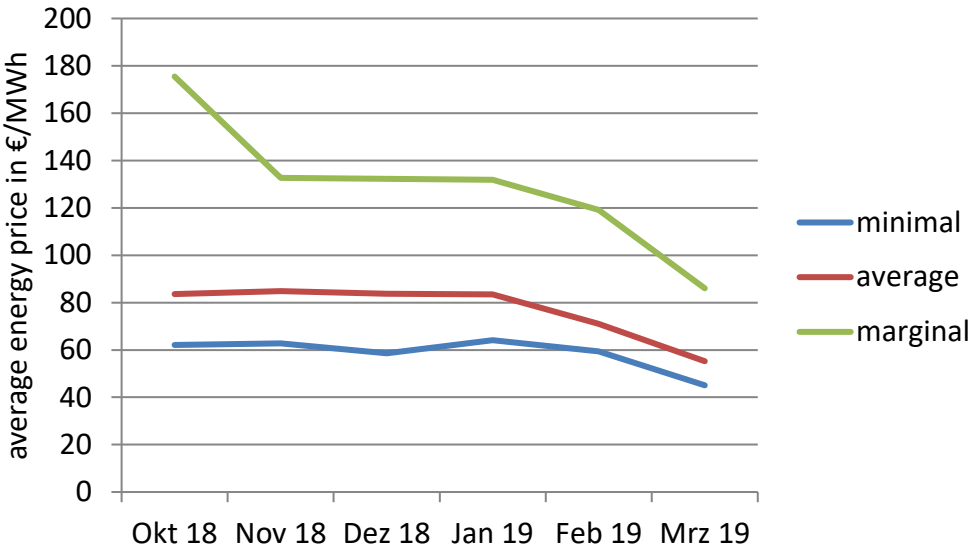

Figure 100: Development of the average energy price for positive SCR from 16.10.2018 to 31.03.2019 on monthly basis.

To participate in the positive SCR market an integrated home has to fulfil the 4-hour criterion as pointed out in section 6.3.1. The additional heating storage capacity cannot be used as a capacity for positive SCR provision. This is why, the participation on the positive control reserve market is not investigated in the thesis at hand. The participation of battery energy storage systems on the SCR is analyzed in [246]. The publication concludes that participation on the SCR market is not economically feasible.

7.6.1 Participation of integrated homes in the negative SCR market

To participate in the negative SCR market an integrated home has to fulfill the 4-hour criterion as pointed out in section 6.3.1. In the following, an evaluation of the maximum capacity [MW] for the SCR market is presented. In the worst case, the BESS is fully charged at the beginning of the four-hour time slot. In this case, all of the SCR energy has to be transferred to the

[1] Introduction of the mixed price method in the SCR market (“Mischpreisverfahren”)

heating sector. As presented in section 3.4 the exanimated integrated home has 300 L of thermal buffer storage and a 300 L of thermal DHW storage. The maximum temperature of the water from the heat pump is 55°C. The maximum allowable temperature of the buffer and DHW storage is 95°C. The heating capacity of water is $c = 4190 \frac{J}{kg \cdot K}$. The maximum chargeable capacity from SCR in each storage unit can be calculated as following:

$$\left(4190 \frac{\mathrm{J}}{\mathrm{kg} \cdot \mathrm{K}} \cdot 40\ \mathrm{K} \cdot 300\ \mathrm{kg}\right) = 14\ \mathrm{kWh} \tag{72}$$

Each storage unit can absorb at least 14 kWh of SCR. Therefore, in total, the heating system can store 28 kWh of additional SCR energy. Minding the 4-hour criterion, the maximum SCR power is 7 kW for the non-optimized integrated home, as calculated in the following equation.

$$\mathrm{P}_{\mathrm{SCR,max}} = \frac{14\ \mathrm{kWh} + 14\ \mathrm{kWh}}{4\ \mathrm{h}} = 7\ \mathrm{kW} \tag{73}$$

The maximum SCR power (7 kW) for the integrated home can only be offered if the temperature in the heating sector is below 55°C at the beginning of the 4-hour time slice. In some cases, the aforementioned assumption is not fulfilled. In this case, the integrated home with a constant SCR power offered on the market cannot participate on the SCR market. Under consideration of the storage temperature and the offered SCR power, the model checks if the integrated home can participate in the SCR market. The method to check if the integrated home can participate in the SCR market is presented in the following. Therefore, the maximum SCR energy requirement is calculated using formula (74).

$$E_{\mathrm{SCR,max}} = \mathrm{P}_{\mathrm{SCR,offered}} \cdot 4\ \mathrm{h} \tag{74}$$

The maximum SCR energy requirement is compared to the free storage capacity of the household. The capacity of the heat storages is calculated with equation (75).

$$E_{\mathrm{heat}} = (95^{\circ}\ \mathrm{C} - \mathrm{T}_{\mathrm{heat_{storage}}}) \cdot\ 4190 \frac{\mathrm{J}}{\mathrm{kg} \cdot \mathrm{K}} \cdot 300\ \mathrm{kg} \tag{75}$$

The free capacity of the battery storage is calculated with formula (76).

$$E_{\mathrm{Bat}} = (1 - \mathrm{SoC}) \cdot \mathrm{Cap}_{\mathrm{Bat}} \tag{76}$$

If the condition in equation (77) is fulfilled, the integrated home can participate on the SCR market.

$$E_{\mathrm{Bat}} + \mathrm{E}_{\mathrm{heat,DHW}} + \mathrm{E}_{\mathrm{heat,buffer}} > \mathrm{E}_{\mathrm{SCR,max}} \tag{77}$$

The participation on the SCR Market leads to some adjustments in the EMS of the integrated home. If an SCR request reaches the integrated home, the SCR energy is stored in the BESS. Only if the BESS is fully charged or the maximum charging power is reached, the SCR power is transferred with a heating rod to the heating sector. Alternatively to the heating rod, the heat pump could be used to transfer the SCR as well. A disadvantage of the use of the heat pump is that the SCR power might not be available for a sufficient time to guarantee the minimum runtime of the heating pump. This is why the heat pump is not used to transfer the SCR power to the heating sector in the analysis presented in Sections 7.7.1 to 7.7.2. The influence of the use of the heat pump, neglecting the minimum runtime is presented in 7.7.2.2.

7.6.2 Variable provision of negative SCR

In section 7.6.1 presents the participation of integrated homes on the SCR market, providing constant SCR power. The participation on the SCR market influences the SoC of the battery and thermal storage. In order to fulfill the prequalification requirement, the absorption of the offered SCR power for a duration of 4 hours has to be guaranteed. This is why the SoC of all storages determines the maximum SCR, which can be offered on the market. Since the integrated home is only participating on the negative SCR market and therefore gaining energy from market participation, the SCR market participation does not influence the provision of energy for the residents. The end-user comfort is not influenced by the SCR market participation. The variable SCR offering strategy calculates the maximum SCR power, which can be offered. Therefore, the available remaining storage capacity, which depends on the actual SoC, is calculated. The remaining storage capacity is divided by 4 hours to determine the maximum SCR power which can be offered. Equation (78) depicts this correlation. The offered SCR power is rounded down to the next integer.

$$\mathrm{P}_{\mathrm{SCR\,var,max\,offer}} = \frac{\mathrm{Cap}_{\mathrm{bat}} \cdot (1 - SoC_{bat}) + \mathrm{Cap}_{\mathrm{heat}} \cdot (1 - SoC_{heat})}{4\,\mathrm{h}} \tag{78}$$

With the variable provision of SCR, more SCR power can be offered on the market in comparison to a fixed SCR offer. This leads to enhanced economics, as shown in Section 7.7.1. The time delay between bidding and provision of SCR is neglected. Additionally, it is assumed that the pool in which the integrated home is operated has enough resources to provide the tendered capacity even if some units fail. The offered SCR power for the flexible capacity price and flexible energy price scenario is depicted in Figure 103 and presented in section 7.7.1.

7.6.3 SCR call for integrated homes

For the evaluation of the influence of the SCR participation of integrated homes, market data from July 10th, 2017 to July 9th, 2018 is used. The market data from this period can be considered as reliable since it was recorded within a constant market framework. After July 2018, the market design changed, as described in Section 6.3.1. These changes lead to high fluctuations of biddings and thus market prices that are not representative. Since a whole year of simulation is required to mind seasonal effects of the load profile and PV radiation profile, the market data from the period before the changed market is used.

The values for the SCR call are published in quarter hour values on [37]. These values are used as an input for the SCR requests. The total duration of the SCR requests is given for every quarter hour. The model of the integrated home presented in Section 3 uses a high resolution down to seconds. This is why the quarterly hour resolution of the SCR calls is resampled to a ten-second resolution.

7.6.4 Calculation of the expected costs and savings of SCR market participation

In the following, a method is described to calculate the costs and savings due to the energy from SCR market participation. Savings occur due to consumption of energy from SCR requests. The savings of the SCR are calculated to determine the maximum price, which the integrated home is willing to pay for the consumed energy. If the savings are higher than the costs, the price is called marginal savings. If the costs are higher, the price is called marginal costs.
To calculate the price, the operational costs of a 4-hour block are calculated. This calculation is made with and without additional SCR energy. If additional SCR energy is absorbed, the grid consumption of the integrated home can be reduced and the PV feed-in could be enhanced. If the battery is fully charged, additional energy for the heating sector could be available. This leads to reduced costs for the integrated home. On the other hand, additional battery aging could occur due to the cycling of the storage. The costs and savings are added up to calculate the marginal savings or costs for participating in the SCR market.
Due to the battery storage system, the savings occur in the time slices, where the stored SCR energy is used. Hence, an allocation function to calculate the savings generated in each 4-hour time slice is applied. The battery and conversion losses are neglected in the allocation function in this case because these losses are relatively small. The battery losses are around 3-4% of the total energy throughput of the battery. According to [266], the efficiency of a lithium-ion battery is around 95%. The losses of a lithium-ion battery depend on the charging and discharging power, as well as on the conversion losses. The battery system is often discharged with low c-rates during the night [267]. This is why the battery losses are relatively small. The COP of the heat pump is only influenced to a minor degree by the participating SCR market because the heat pump is only running when the temperature of the heat storages reaches the lower temperature boundaries [140]. For the overall cost analysis, these losses are relevant. The allocation function uses the assumption that the maximum savings in time slice t of the SCR are the SCR energy in t multiplied with the cost for grid consumption. Therefore, the allocation function calculates the maximum savings for each time slice. If the savings extend the maximum savings, the allocation function distributes the excess savings to the time slices before, minding the maximum savings. The maximum SCR savings for every time slice t ($C_{max,SCR,t}$) are calculated with equation (79). Therefore, the electricity costs per kWh ($c_{electricity}$) including grid usage fees and taxes are multiplied with the energy received for SCR participation in the given time slice ($E_{SCR,t}$). This product is divided by the SCR power (P_{SCR}) to scale the result.

$$C_{max,SCR,t} = \frac{c_{electricity} \cdot E_{SCR,t}}{P_{SCR}} \tag{79}$$

7.6.5 SCR Auction Forecast

As described at the beginning of section 6.3.1, SCR power is divided into different products. This includes products for positive and negative power as well as products for the various time slots. All products are auctioned independently from one another. For each product, the bidder must place a corresponding bid comprising offered capacity [MW], capacity price [€/MW] and energy price [€/MWh]. For a PV BESS, it is therefore necessary to have a bidding strategy which places a multitude of bids on the market. According to a merit order list comprising all submitted bids and generated by the TSOs, access is granted based on the capacity price (new regulations: assignment by merit order list of mixed price). A successful bidding strategy chooses a capacity price bid which maximizes the revenues while making sure to get accepted. As the auction process can be described as an anonymous and sealed-envelope, the capacity price bids placed by the competitors are unknown at the time the bid is submitted. The value of interest for the bidding strategy is the maximum capacity price paid (MCPP) for the upcoming auction. All capacity price bids below the MCPP get accepted, all bids above get rejected.

For the simulations conducted in this section, a MCPP prediction model is used to support the bidding strategy. The model must include seasonal effects because of the following reasons: A large share of SCR power is delivered by thermal power plants. Because of the varying generation of PV in the winter and summer, some power plants are active during the winter and must shut down during the summer period. With the number of potential SCR providers decreasing in summer, the SCR prices increase. Also, bank holidays e.g. during Christmas time, have a substantial influence on the SCR prices and number of bid participants. Aside from seasonal effects, MCPPs from previous auctions (auto regression) have a substantial impact on the future MCPP since the market is rather slow and there is little fluctuation in the number of participants.

The prediction model used for this section is the Seasonal Autoregressive Integrated Moving Average (SARIMA) model, which includes both seasonal effects and effects from previous auctions. The standard form for writing the different components of a SARIMA model is given in equation (80).

$$\mathrm{SARIMA}(\mathrm{p},\mathrm{d},\mathrm{q}) \times (\mathrm{P},\mathrm{D},\mathrm{Q})_{\mathrm{s}} \tag{80}$$

All used parameters are non-negative integers. Upper case letters represent seasonal parameters and lower case letters represent the short term influence parameters. S refers to the number of periods in each season. P represents the autoregressive component, D the degree of differencing, and Q the moving average component.

The parameter values for this publication ((2,1,0)x(0,0,1)) have been derived from [268] where the Nordic power market has been predicted using a SARIMA model. This parametrization has been statistically verified in [246] with respect to the initial data series and with the results generated from the model. The implementation of the SARIMA model is used in [269].

Aside from the submitted capacity price bid, the energy price bid takes on an important role, as it strongly indicates how much energy will be requested. If the TSOs have a demand for SCR power, the approved bids are sorted in ascending order according to energy price (merit order) and those with the lowest energy price are called first until the demand is met. Therefore, bidders with low energy price bids get called more frequently than those with higher bids. In order to predict how many requests a participant will get, a sophisticated model that predicts the energy bid price structure and overall request probabilities is required. For

the sake of simplicity, a perfect knowledge about both SCR request time series and energy price bid structure was applied in this section.

7.6.6 SCR Bidding Strategy

As highlighted in section 7.6.5, the revenue potential strongly depends on how the bidding strategy places the set of capacity price and energy price bid for each product type. In order to demonstrate the strong dependency, this section follows 3 different approaches:

1. Fixed capacity and energy price: Without any prediction model or optimization approach involved, a capacity price bid of 0 €/MWh and an energy price bid of -20 €/MWh is submitted. The capacity price bid value is justified by the fact that the bid is accepted at all auctions in the simulated time range (Section 7.7) considered. The energy price bid is justified by this value as the minimum submitted energy bid over the considered time range. This bid always takes the first position in the merit order list, making sure that as the maximum possible energy is obtained from the SCR market.
2. Fixed capacity price, flexible energy price: As with the previous approach, the capacity price is fixed to 0 €/MWh to assure acceptance with all products in the considered time range. However, the energy price bid is calculated by an optimization approach to be explained below.
3. Flexible capacity price, flexible energy price: In order to place the capacity price bid, this approach involves the MCPP prediction model as explained in Section 7.6.5. For each capacity price under consideration, a corresponding acceptance probability is derived from the MCPP prediction model. Both the capacity price and the energy price bid are derived from an optimization approach.

Since one single PV BESS does not fulfil the TSO's requirements to provide SCR, multiple units must be operated in pool. The following part of this section is dedicated to a brief outline of the working principle of the optimization process involved in the latter 2 approaches. For a more detailed explanation, reference is made to [269]. One execution of the optimization process maximizes the overall revenues within one auction by adjusting the capacity price and energy price bids for all products. As for a PV BESS simulation within the old SCR market design, the two products - negative low time and negative high time - are considered. The objective function of the optimization is given by equation (81):

$$\sum_{P_i} G(P_i) \cdot (P(P_i) + EE(P_i) + M(P_i)) \tag{81}$$

If multiple bids are submitted to the TSOs, a variety of different outcomes is possible. All bids might get accepted, only a few bids get accepted or none of the submitted bids gets accepted. P_i denotes one possible outcome. The number of possible outcomes can be obtained by the power set of products offered. E.g. when bidding on negative high and low time, 4 outcomes are possible. $G(P_i)$ denotes the acceptance probability for one particular outcome, which is derived from the MCPP prediction model (Section 7.6.5). $P(P_i)$ represents the earnings based on the SCR capacity price bids. $EE(P_i)$ denotes the earnings based on the energy price bids. In order to calculate $EE(P_i)$, the position in the merit order list and the overall SCR request time series must be known. For negative energy price bids, $EE(P_i)$ will become negative as well. In

order to get an estimate of the value of the energy obtained from the SCR market, $M(P_i)$ denotes the earnings that could be achieved when trading on the intraday market. In short, for each possible outcome, the objective function calculates an acceptance probability and multiplies it with the potential earnings. The decision variables are the capacity and energy prices of the products under consideration.

7.6.7 Economic evaluation of the impact of the participation in the control reserve market

The savings and costs for SCR market participation are calculated based on the simulation results. A simulation of a model with SCR market participation and without market participation is performed. The differences in the grid consumption, grid feed-in and the battery aging are calculated and added up to calculate with equation (82) the total savings C_{total}.

$$C_{total} = C_{electricity} + C_{feed-in} + \Delta C_{Bat} \quad (82)$$

The savings due to lower electricity consumption are calculated with equation (83). Therefore, the differences in the grid consumption are evaluated and multiplied with the electricity costs.

$$C_{electricity} = (E_{From\ Grid\ with\ SCR} - E_{From\ Grid\ without\ SCR}) \cdot c_{electricity} \quad (83)$$

Due to SCR market participation, less PV power is used for self-consumption and can feed-in to the grid. Therefore, the feed-in tariff is minded. The additional revenues due to higher PV feed-in are calculated based on equation (84).

$$C_{feed-in} = (E_{To\ Grid\ with\ SCR} - E_{To\ Grid\ without\ SCR}) \cdot c_{feed-in} \quad (84)$$

An integrated home participating in the SCR market stores part of the SCR power in the battery storage system. The additional energy lead to a higher average state of charge of the battery system and can lead to more cycles of the battery system as well. This leads to an increased battery aging and therefore to additional costs for the integrated home participating in the SCR market. The additional costs are calculated by multiplying the additional battery aging with the costs of the battery system as presented in equation (85).

$$\Delta C_{Bat} = C_{Bat} \cdot (\text{battery aging}_{\text{with SCR}} - \text{battery aging}_{\text{without SCR}}) \quad (85)$$

The costs for the battery system are calculated minding the specific battery costs and the battery capacity. The battery capacity is calculated as the product of the battery capacity and the number of battery cells as presented in equation (26). The resulting battery costs represents the costs for the battery modules, mind the costs for the battery cells and costs for the assembling of the battery cells. Costs for converters are not included. A module price of 250 €/kWh is estimated as presented in section 3.5.3. The assumption is made, that the participation on the SCR market only enhances the aging of the battery moduls and do not influence the aging of the inverters and ancillary devices e.g. the energy management system (EMS). This is why additional costs for battery aging only minded for the battery modules. Most producers of battery energy storage systems (BESS) for private households offer modular BESS.

For participation on the SCR market, a steering box is needed and annual measurement costs need to be minded. For SCR participation, the same costs as for PCR participation are minded. The costs for PCR participation are analyzed in section 7.4.4 and Table 21 provides an overview

of the range of costs for market participation. The minimum costs for the SCR market participation are 342 €/a.

7.7 Results participation on the secondary control reserve market

The results of the model described in section 7.6 are presented in the following sections. The simulation was done on data between July 10th, 2017 and July 9th, 2018. This time range only includes SCR products of the old market design because only a few weeks of the new SCR market data was available at the time of writing. Since it is reasonable for a PV-BESS to simulate over a full year in order to include various seasonal effects, the switch to the new market design would have distorted the observations. In section 7.7.1an analysis based on pre-updated market conditions is presented. In section 7.7.4, the marginal savings for SCR participation are calculated under updated market conditions. These savings are the maximum price, which can be offered for SCR market participation.

7.7.1 Economic influence of market participation

In the following, the participation of an integrated home on the SCR market is examined. Three different bidding cases are analyzed (see section 7.6.6): Capacity price flexible and energy prices flexible, capacity price zero and energy prices flexible, and capacity price zero and energy prices -20 €/MW. Energy prices are flexible and determined by the bidding strategy as presented in section 7.6.5. Alternatively, the energy price is set fix to -20 €/MWh. Table 22 depicts the resulting revenues that depend on the year and the bidding strategy.

year	scenario	revenue power	revenue energy	total revenue	energy SCR
2017/2018	CP=Flex EP=Flex	2.35 €/a	9.50 €/a	11.85 €/a	1679 kWh/a
2017/2018	CP=0 €/MW EP=Flex	0 €/a	11.26 €/a	11.26 €/a	1363 kWh/a
2017/2018	CP=0 €/MW EP=-20 €/MWh	0 €/a	-85.09 €/a	-85.09 €/a	4246.5 kWh/a

Table 22: Revenues SCR market, CP = capacity price, EP = energy price.

The total revenues of the flexible energy and capacity price scenario are slightly higher compared to the zero capacity price and flexible energy price scenario. The total revenues of the zero capacity price and negative energy price scenario are subsequently negative.
Besides the revenues from market participation, cost savings exist because of the SCR energy. These savings are analyzed for the flexible energy and capacity price scenario. Based on the bidding strategies, 1,679 kWh of SCR energy are obtained if one kW of SCR power is auctioned. If more power is auctioned, the SCR gain increases linearly, since the bidding price remains equal. If 7 kW of SCR power is auctioned, a maximum of 11,753 kWh SCR energy can be

obtained. The integrated home only participates on the market if the remaining storage capacity can absorb the offered SCR power for 4 hours.

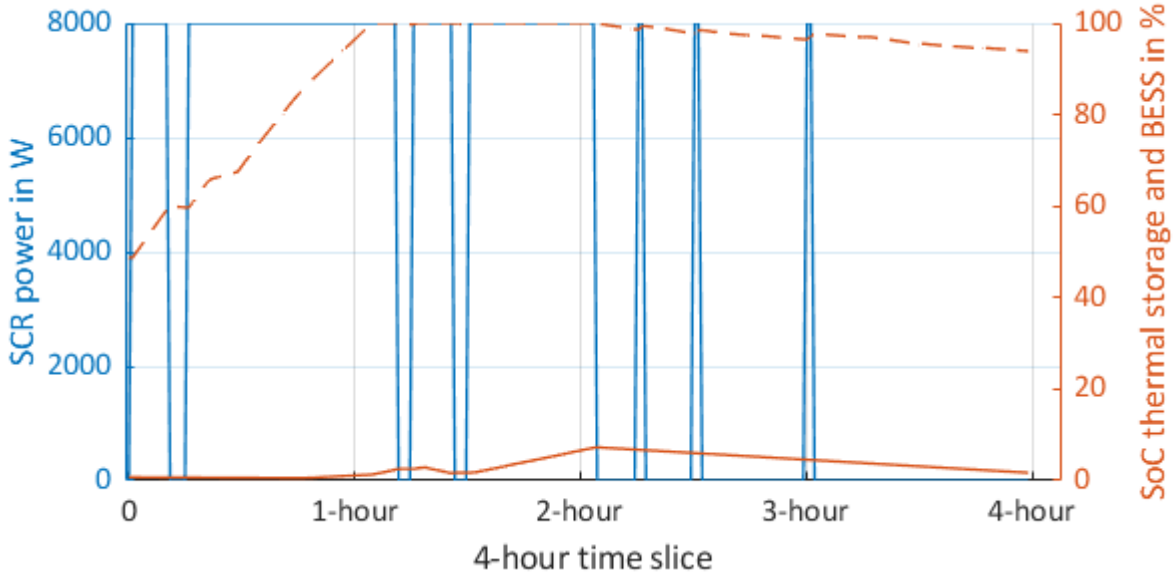

Figure 101: Power requests from SCR market participation (blue line), battery SoC (solid orange line) and SoC of the thermal storage (dashed orange line) for 2nd January 8pm to 12pm.

The SCR energy is stored in the battery with priority and in the heat storage if the battery storage system is fully charged. The battery storage system is charged first because for this scenario electric energy has a higher value than heat. The comparative value of SCR is 29.2 €ct/kWh if energy is stored in the battery storage system. If energy is stored in the heating sector, the corresponding value is lower. As shown in Figure 116 and Figure 117, the additional costs due to additional battery aging are relatively low compared to the gains in income. This is why this mode of operation is favored.

Figure 101 illustrates the influence of the SCR market participation for one 4-hour time slice (2nd January 8pm to 12pm). A time slice at night is chosen to reduce complexity, since no PV energy is produced. The blue line represents the power obtained from negative SCR market participation. The orange lines show the corresponding SoC of the thermal storage (dashed line) and the battery storage (solid line). For comparison, the SoC of the thermal storage is calculated based on the temperature of the thermal storage.

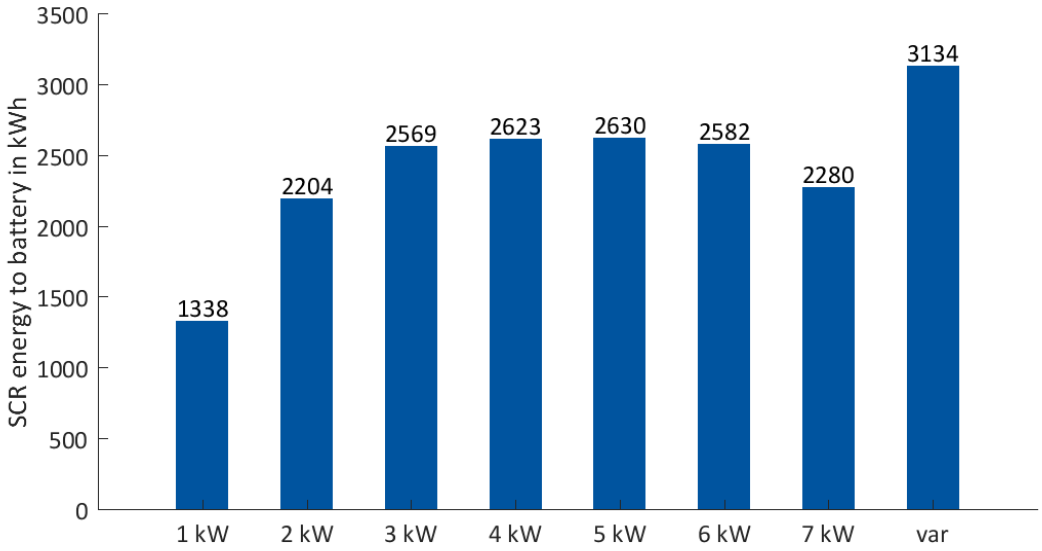

Figure 102: Energy from SCR calls stored in the BESS of an integrated home (10 kWp PV system, 10 kWh BESS, 10 kW heat pump). SCR power distributed to BESS in dependency of the SCR offering.

Figure 102 shows the energy transferred to the battery depending on the offered SCR capacity. The more SCR capacity is offered, the more SCR energy is transferred to the battery. However, if more than five kW SCR are offered, the energy transferred to the battery decreases. There are two reasons for this finding. First, with a higher SCR capacity offer, the number of 4-hour time slices in which the integrated home is able to participate in the market decreases. If the storages of the integrated home are already charged to a high level, the integrated home cannot participate in further SCR time slots. The second reason for this finding is that the electrical load is reduced due to the high share of SCR transferred to the heating sector. A huge share of the heating demand is covered by the SCR. Therefore, demand for heating power from the heat pump is reduced. This leads to a lower overall electricity demand, which also lowers the electricity demand from the battery. The variable SCR offering strategy (section 7.6.2) leads to the highest SCR energy transferred to the battery.
The average offered SCR power for the variable SCR offering strategy is depicted in Figure 103. The offered SCR power ranges from 1 kW to 9 kW. If the 10 kWh battery storage and the 28 kWh heat storage are empty, the integrated home can offer a maximum SCR power of 9 kW. In the winter, more SCR is offered due to a higher thermal load and less PV radiation. Additionally, more SCR can be used in the winter e.g. for space heating. An average of 5.8 kW SCR is bid over the course of a year.

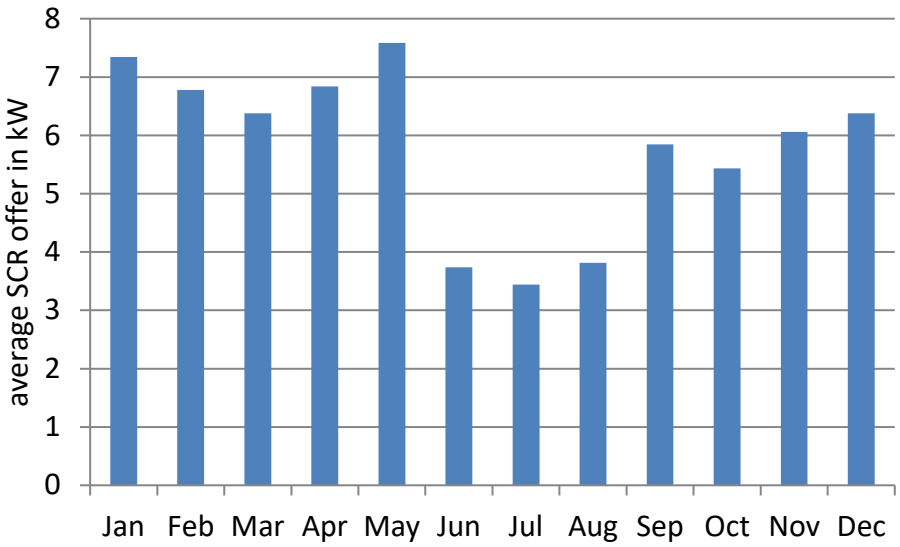

Figure 103: Resulting variable SCR offer of a PV BESS with power heat coupling, a 10 kWh BESS, two 300l heat storages and a 10 kWp PV system. The offered SCR power is depicted for the flexible capacity price and flexible energy price scenario, presented in Table 22.

Figure 102 shows the energy transferred to the battery depending on the SCR offering. The average SoC of the battery is higher when the SCR transferred to the battery is higher. The average SoC of the battery system that depends on the SCR offer is illustrated in Figure 104.

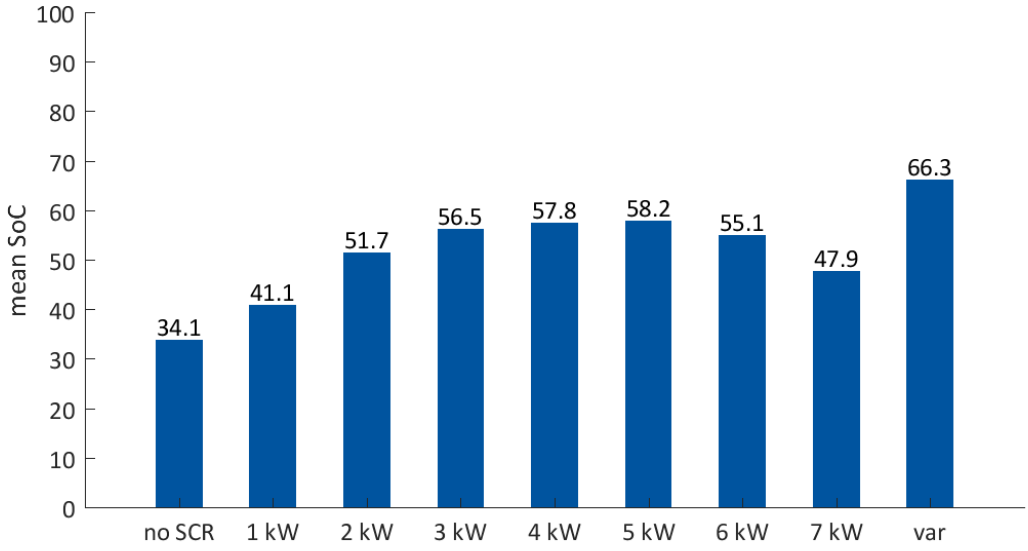

Figure 104: Average SoC of the BESS of an Integrated home (10 kWp PV system, 10 kWh BESS, 10 kW heat pump) participating in the SCR market. The average SoC depends on the SCR capacity offered.

The energy transferred to the heating sector influences the energy transferred to the battery. Figure 105 presents the energy transferred to the heating sector via a heating rod. The amount of energy increases with the offered SCR capacity in case one to five kW of SCR is offered. If more than five kW of SCR is offered, the energy transferred to the heating sector decreases. In the six and seven kW SCR offer case, the heat storage is often at high SoC, therefore the integrated home cannot participate on the market in some of the 4-hour time slices. The

highest amount of SCR energy transferred to the heating sector occurs in the variable SCR offer case.

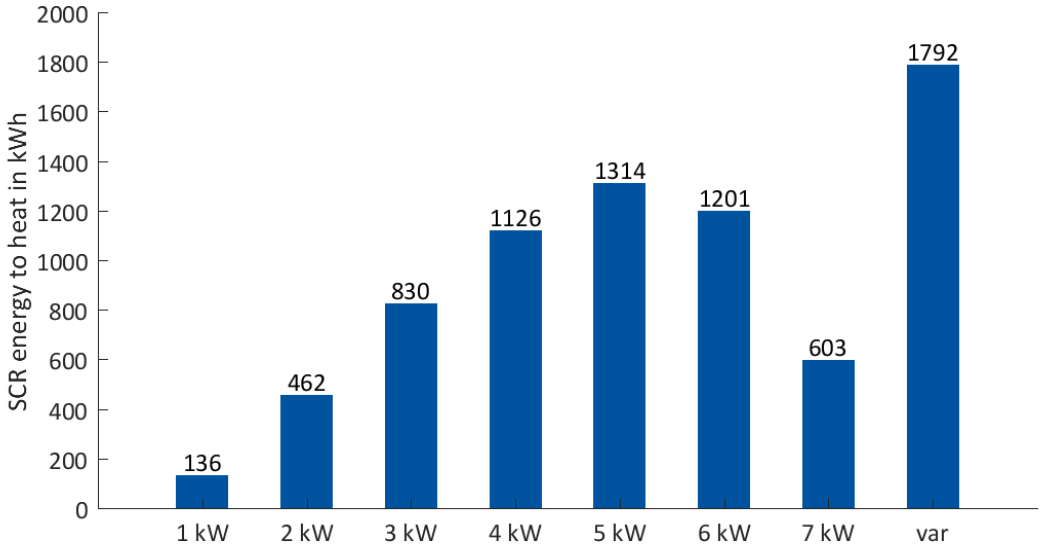

Figure 105: Power to heat from SCR: SCR power distribution in a saved in Integrated home (10 kWp PV system, 10 kWh BESS, 10 kW heat pump) participating in the SCR market. SCR power distributed to BESS in dependency of the SCR offering.

Figure 106 illustrates a detailed analysis of the battery aging. The increased SoC depicted in Figure 104 leads to a higher calendar aging. Besides an increased calendric aging, a reduced cyclic aging can be observed. Cyclic aging is reduced because the battery storage is used less for storing PV power. The battery system stores less PV power with increasing SCR offer because the battery system is more likely to be fully charged. Therefore, less capacity is available to store excess PV generated power. Nevertheless, total battery aging is increased with a higher SCR offering.

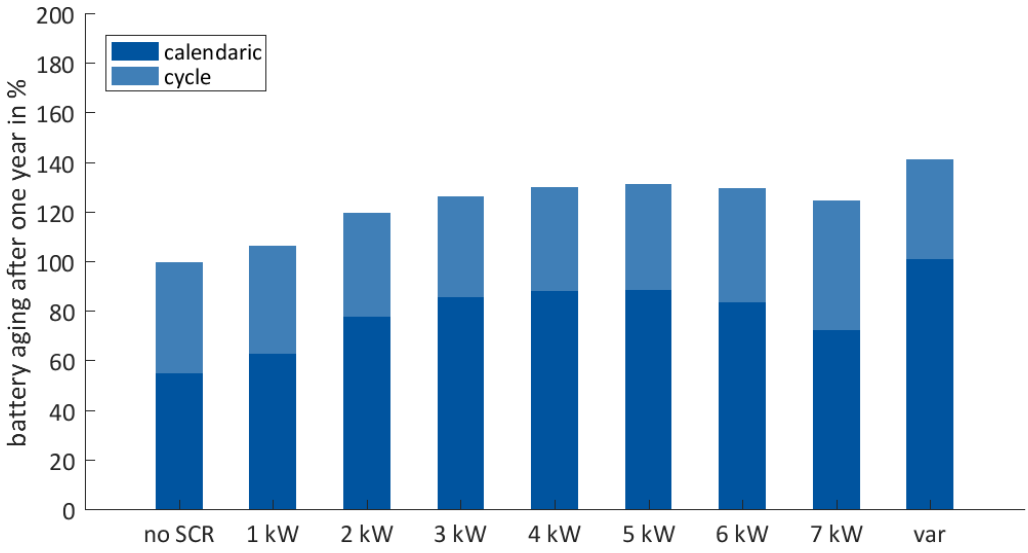

Figure 106: Calendar and cycle aging that depend on the SCR offer of an integrated home (10 kWp PV system, 10 kWh BESS, 10 kW heat pump). Calendric aging increases because the average SoC is increased.

The average SoC of the battery system presented in Figure 104 leads to an increased battery aging, depicted in Figure 106. The cost for the increased battery aging is shown in Figure 107. These costs are correlated to the average SoC because the increased calendar aging of the battery is the main reason of additional aging. The battery in the variable SCR offering case has the highest average SoC and therefore the highest aging. This leads to the highest additional costs for the battery system in comparison to a battery system only used for PV home storage operation.

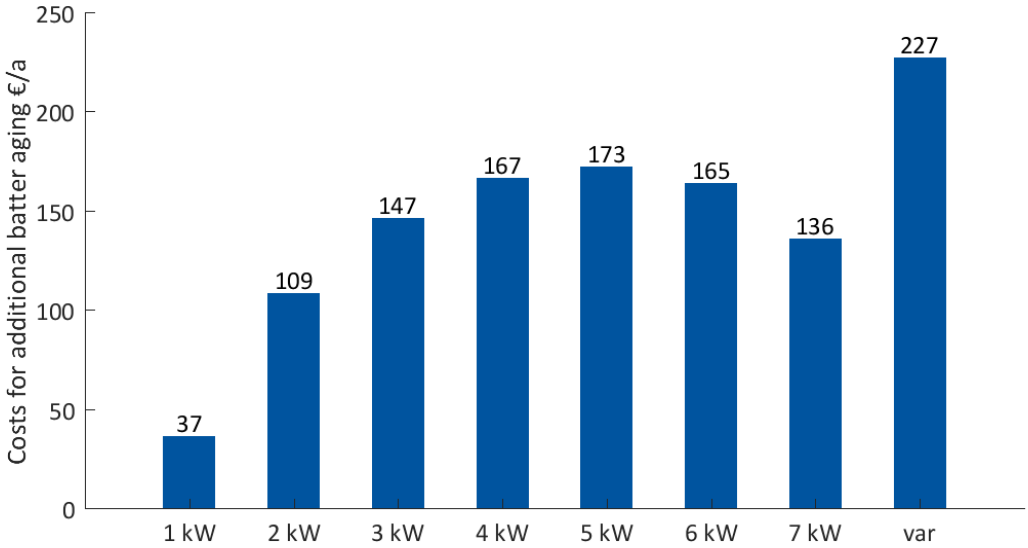

Figure 107: Additional battery cost of an integrated home (10 kWp PV system, 10 kWh BESS, 10 kW heat pump) that depends on the SCR offer. Higher battery aging due to higher SCR energy to battery leads to additional battery costs compared to an integrated home not participating in the SCR market.

Even though additional costs for battery aging with increasing SCR power exist, more SCR power is absorbed. This SCR power can be used to reduce grid consumption and increase the PV feed-in. Due to the use of SCR energy in the integrated home, less PV energy is used. As a result, the self-consumption rate of the PV system is reduced from 58% (without SCR market participation) to 37% with SCR market participation and a variable SCR offering. Nevertheless, the integrated home saves costs when participating in the SCR market. These savings are illustrated in Figure 108. The savings are correlated to the SCR energy absorbed by the integrated home. Higher energy absorption leads to higher savings. This is why the variable SCR capacity offer leads to the highest savings. Compared to the income from the SCR market presented in Table 22, the savings due to SCR power are relatively high.

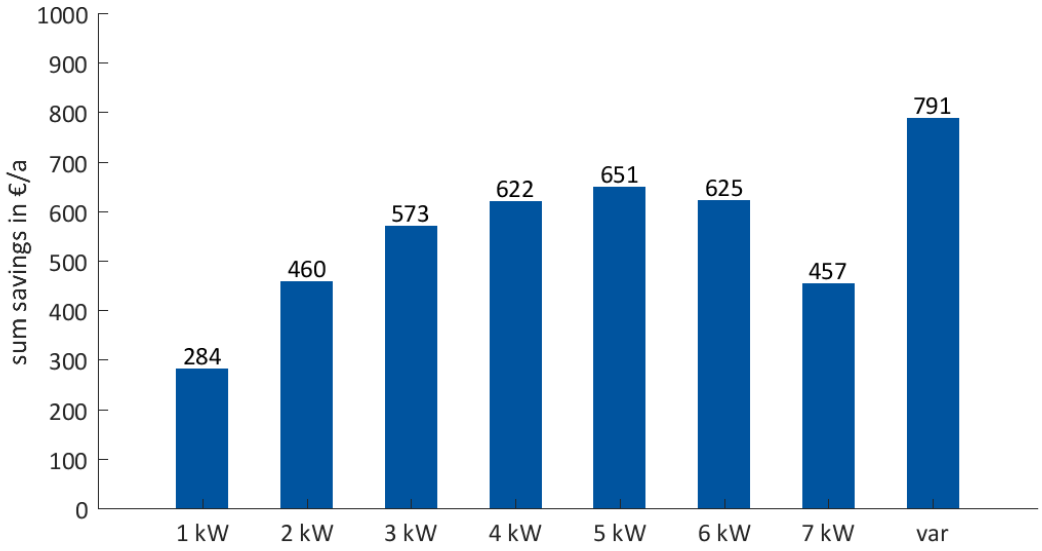

Figure 108: Savings of an integrated home (10 kWp PV system, 10 kWh BESS, 10 kW heat pump) participating in the SCR market compared to an integrated home without market participation. Savings are calculated for the flexible energy and capacity price scenario. The savings depend on the SCR power offering.

The savings presented in Figure 108 are illustrated for the case of a flexible energy and capacity price. Figure 109 compares the savings of the different scenarios shown in Table 22. The savings for the -20 €/MW energy price scenario are higher than the savings of the flexible energy and capacity price scenario for 1-3 kW SCR offering. The benefits from the low-cost energy exceed the additional costs of this scenario. The incomes and costs from the SCR market participation are minded in this evaluation. For 4-7 kW SCR offer, the flexible capacity and energy price scenario generates the highest incomes. The benefit of the low-cost SCR energy is reduced and the price for the SCR capacity exceeds the use of the energy in the -20 €/MW scenario. The highest incomes are generated in the flexible price and energy scenario, when the variable SCR offer strategy is applied.
In this case, the annual savings are 791 €/a as depicted in Figure 108. Minding the minimal cost of SCR market participation of 342 €/a as presented in section 7.4.4, the participation on the SCR market can reduce the costs of the integrated home down to 14.5 % (518 €/a).

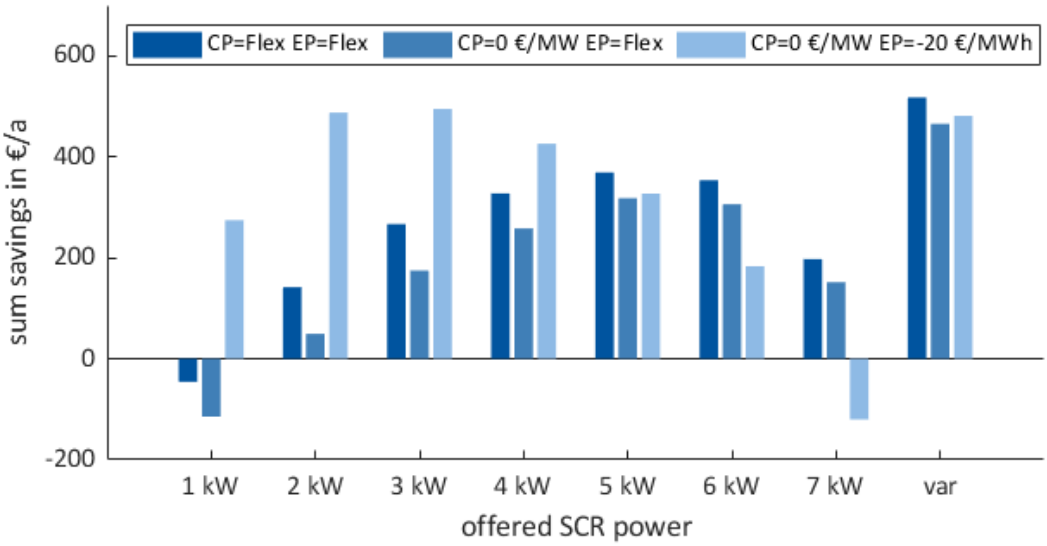

Figure 109: Additional incomes of an integrated home (10 kWp PV system, 10 kWh BESS, 10 kW heat pump) participating in the SCR market compared to an integrated home without market participation. Incomes are calculated for different bidding strategies. Revenues generated on the SCR market are minded.

7.7.2 Additional scenarios

This section presents two additional scenarios. In Section 7.7.2.1 the battery is only used for the SCR and in section 7.7.2.2, the SCR power is transferred to the heating sector with the heat pump.

7.7.2.1 Scenario without PV system: Battery only for SCR

The battery storage systems could be used to store SCR only. The comparative value of SCR in this case is always 29.2 €ct/kWh if it is stored in the battery storage system. The use of the full potential of the BESS for SCR compared to a dual use with PV could be beneficial. To investigate this scenario, the flexible capacity and energy price scenario is performed in a home with a BESS and power-heat coupling, but without a PV system. In this case, the house saves 1139 € per year in investment and maintenance costs for the PV system and converter compared to an integrated home with a PV system.

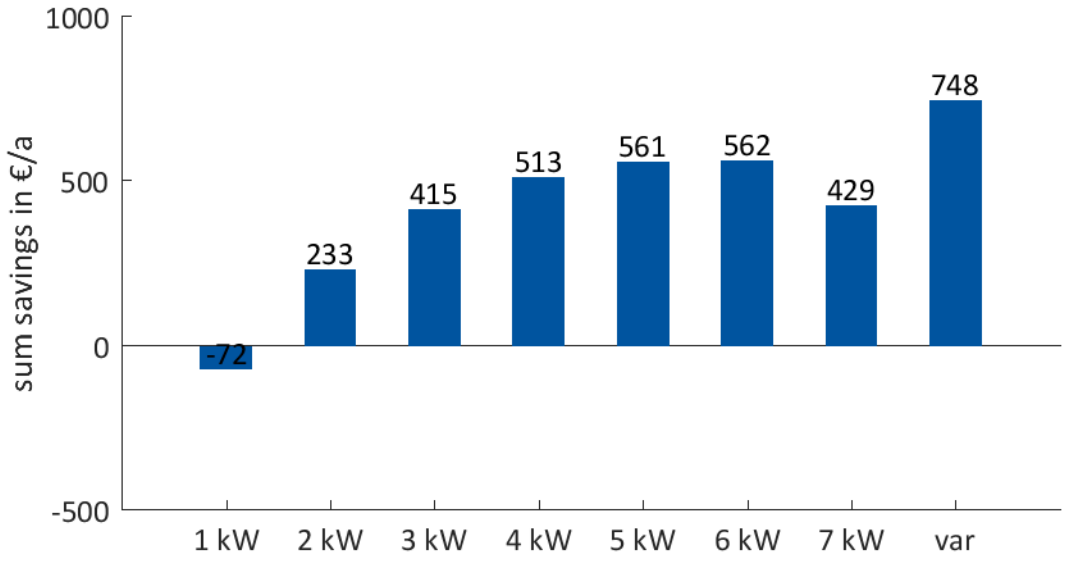

Figure 110: Savings of a home with BESS and power-heat coupling without a PV system (10 kWh BESS, 10 kW heat pump) participating in the SCR market compared to an integrated home without market participation.

Figure 110 depicts the savings in the aforementioned scenario if the BESS is only used to save the SCR. This home is less economical compared to an integrated home due to the missing PV energy. In case of diminishing feed-in tariffs, the correlation could be changed. Compared to an integrated home not participating in the SCR market, the investigated home generates additional benefit when at least 2 kW SCR are offered.

7.7.2.2 Heat pump for SCR

In section 7.6.1, it was pointed out why the heat pump is not used to transfer the SCR power to the heating sector. Nevertheless, the efficiency of smart homes can be enhanced if the heat pump is used to transfer SCR power to the heating sector. In this case, the energy from the battery storage system has to be used to ensure the minimum runtime of the heat pump and to bridge the ramping time of the heat pump. This requires a complex control algorithm. Forecasts of SCR requests are difficult.

This section analyzes the scenario when the heat pump is used to transfer the SCR power to the heating system instead of the heating rod. This is a best-case evaluation because a complex control algorithm (as described above) is not implemented. Also, response time and ramping of the heat pump are neglected.

The flexible energy and capacity price scenario are used to assess this case. The resulting savings are depicted in Figure 111. The use of the heat pump leads to additional savings compared to the heating rod scenario. The additional savings compared to the use of the heating rod are between 37 €/a and 102 €/a depending on the offered SCR power. The maximum additional savings are gained in the variable SCR scenario.

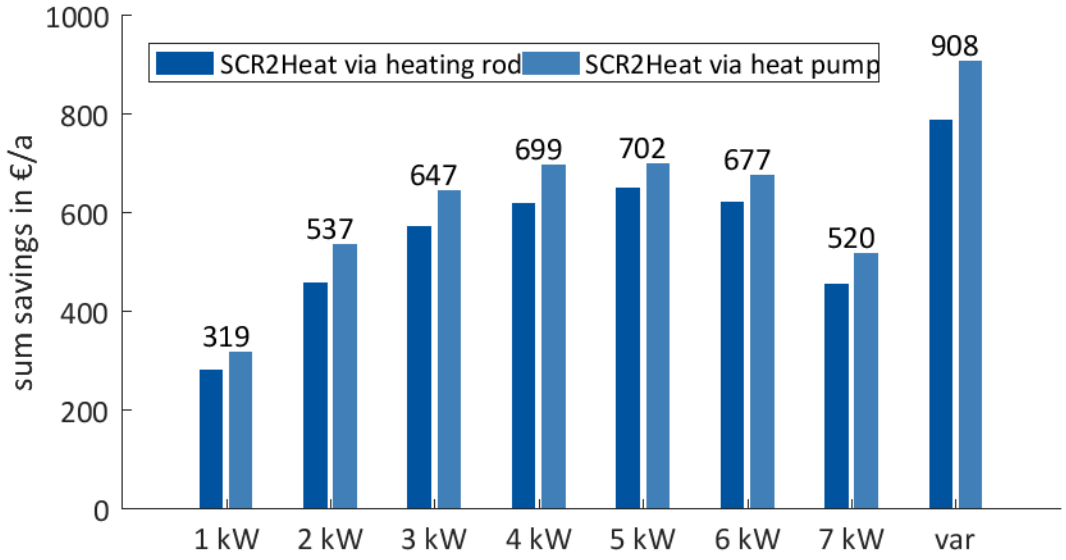

Figure 111: Savings of an integrated home (10 kWp PV system, 10 kWh BESS, 10 kW heat pump) participating in the SCR market compared to an integrated home without market participation. The integrated home uses the heat pump to transfer the SCR power to the heating sector.

7.7.3 Optimized size of the integrated home

In this section, the influence of the SCR participation of the optimized integrated home is investigated. The optimal component sizes of the integrated home are calculated in section 5.3 and do not incorporate the SCR market participation. In variation to the results presented in Section 7.7.1 the components of the integrated home have the optimal sizes determined in section 5.3. The SCR market bidding strategy, flexible energy and capacity price, is investigated in this section as well. The resulting savings are depicted in Figure 112. With respect to equation (72) and equation (73), the maximum constant SCR, which can be offered on the market, is 3 kW. The optimized integrated home has a total thermal storage of 270 l as presented in Table 12. Minding the minimum available temperature spread for SCR market participation of 40 K, the maximum SCR, which can be offered is 3 kW. A variable SCR offer is investigated in this section as well. The limitation, due to the power of the battery converter leads to a non-optimal storage of the SCR power. Nevertheless, it does not influence the maximum capacity, which can be offered on the market, because the heating rod can transfer the SCR power to the heat storage. The DC/DC inverter of the optimized home has a maximum power of 7.6 kW, which is sufficient to offer 3 kW of SCR capacity.

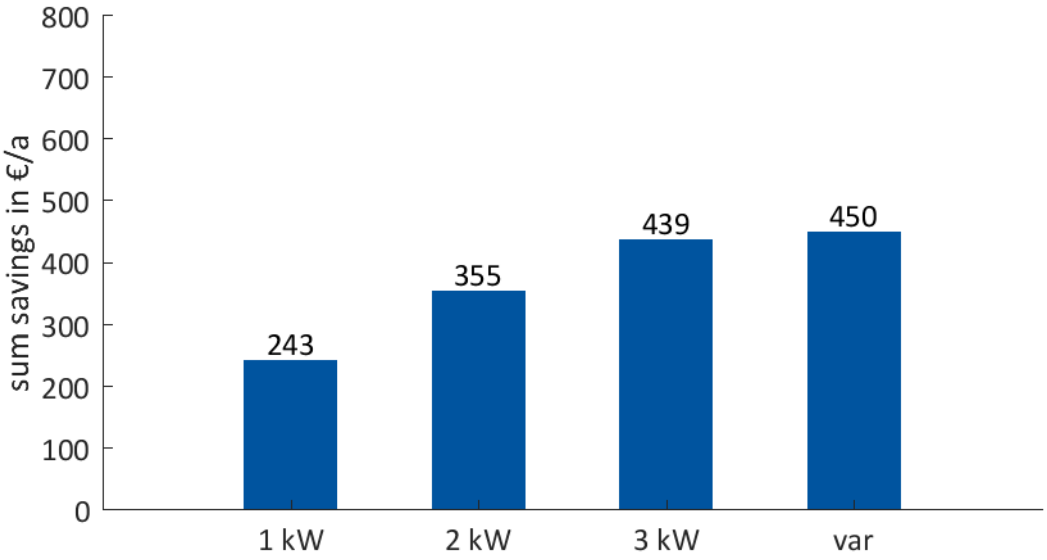

Figure 112: Savings of the optimized integrated home (10 kWp PV system, 7.1 kWh BESS, 2.8 kW heat pump) participating in the SCR market in comparison to an optimized integrated home without market participation.

The SCR market participation leads to savings, under consideration of the optimal component sizes of the integrated home. Nevertheless, these savings are lower than the savings of a non-optimized integrated home, even though the total costs of the optimized home are lower as pointed out in section 5.3. The costs and savings for the different scenarios are presented in Table 23. In this table, the minimum costs for market participation and revenues from market participation are minded.
The optimal size of the BESS is smaller compared to the size of the BESS investigated in Section 7.7.1. The reduced size of the BESS leads to a reduced remaining capacity of the BESS for the storage of SCR energy. Therefore, less SCR can be used in the electricity sector. Figure 113 depicts the SCR energy transferred to the BESS of the optimized integrated home. For the variable SCR offering scenario with the flexible energy and capacity price bidding strategy the optimized home saves 450 €/a. In contrast, the non-optimized integrated home saves 791 €/a in this scenario. Hence, the savings of the optimized integrated home are 341 € lower compared to the savings of the non-optimized integrated home. Reasons for this finding are the constant direct self-consumption rate of SCR capacity in both scenarios. Additionally, SCR energy, which is not transferred to battery, can be used in the heating sector.

	Non-optimized integrated home according to section 3.4	Optimized integrated home according to section 5.3.1	Optimized integrated home according to section 5.3.1 with 2x300l water storage
Annual cost of the integrated home without SCR market participation	3582 €/a	2528 €/a	2528 €/a
Annual savings of the integrated home due to SCR market participation	518 €/a	146 €/a	346 €/a

Table 23: Comparison of the annual cost and savings of an integrated home with and without optimized component sizes, participating on the SCR market. The minimum costs for market participation and revenues from market participation are minded.

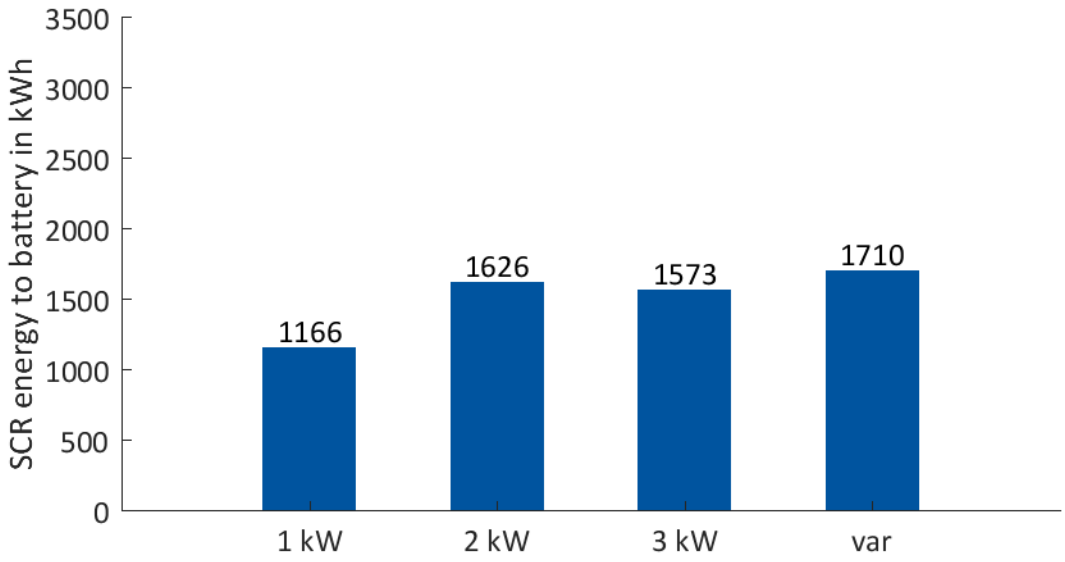

Figure 113: SCR stored in the BESS of an optimized integrated home (10 kWp PV system, 7.1 kWh BESS, 2.8 kW heat pump) participating in the SCR market. SCR capacity distributed to BESS in dependency of the SCR offering.

Influence of increased heating storage size

The provision of SCR is limited due to the storage sizes of the optimized integrated home. The optimized integrated home has a total thermal storage of 270 l as presented in Table 12. An increased heat storage size, increase the SCR which can be offered. An increased SCR offer can lead to reduced annual costs, since less energy has to be consumed from the grid. In this scenario, the heat storages of the optimized integrated home are increased to 300l each, resulting in a total water storage capacity of 600l. The integrated home with optimized component sizes and a water storage capacity of 600l lead to saving of 625 €/a. In comparison, the integrated home with optimized component sizes and a water storage capacity of 270l, has annual savings of 450 €/a as presented in Figure 112. The savings for the different scenarios under consideration of the costs for market participation are presented in Table 23. The increased water storage size, increase the annual savings from 146 €/a to 346 €/a.

7.7.4 Results for savings in the 4-hour time slots

The analysis of bidding behavior and market participation under updated market conditions is presented in this section. Therefore, the marginal savings per kW SCR are calculated. These are the maximum prices, which would be paid for SCR power. The evaluation is done in two steps. First, the influence factors of the marginal costs are pointed out. Second, the marginal costs are calculated exemplarily for the flexible energy and capacity price scenario.

7.7.4.1 Marginal costs SCR

For participation on the SCR market, a capacity price of zero is assumed. The revenues and cost for participating in the SCR market are evaluated below. One of the challenges for the aforementioned analysis is the dependency of the revenues. The revenues and costs depend on the time when the SCR is available, the duration of the SCR call and the provided SCR capacity.

This analysis aims to calculate the maximum price, which would be bid at the market. These costs are the marginal cost or savings from SCR energy. Therefore, a determination of the marginal costs/savings of the last 4 hours is presented. The marginal savings are lower than the costs for grid consumption because SCR power is not available in a demand-actuated way. This leads to a non-optimal use of the SCR power. The SCR power is partly transformed into heating power via the heating rod if the battery storage is fully charged.

The costs and revenues of the SCR energy depend on the moment in time, duration and power of the SCR energy. A higher SCR power and a higher duration of the SCR power increase the chance of a non-optimal use of the SCR energy. Figure 114 depicts the dependency of the revenues on SCR energy in different scenarios. A longer duration of the SCR call leads to higher savings because more energy is gained by SCR market participation. On the other hand, a higher offer of SCR power leads to reduced income per kW SCR because of the higher chance of inefficient use. A constant SCR capacity bid over one year is assumed.

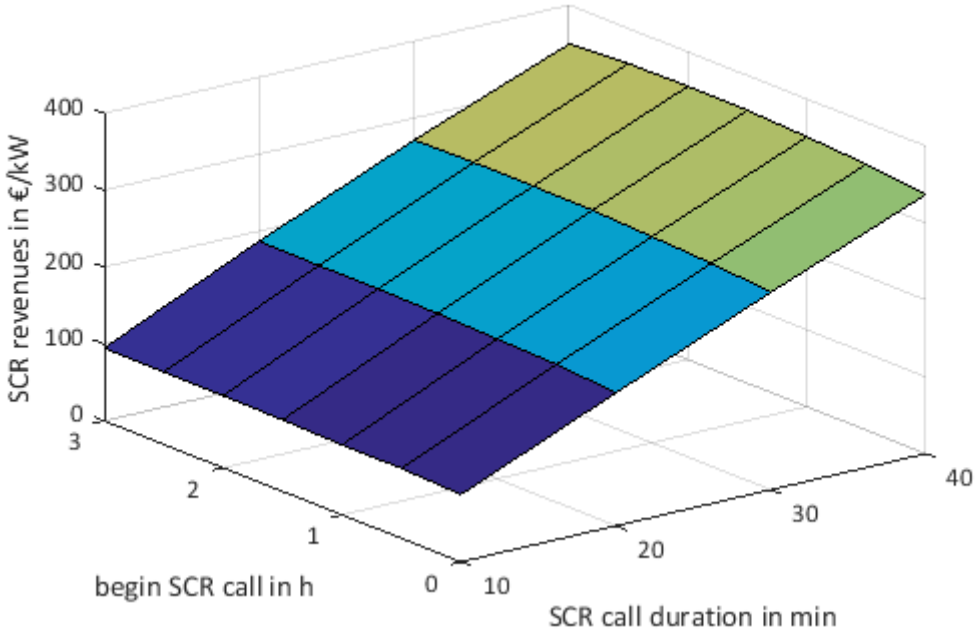

Figure 114: Annual additional revenues of an integrated home (10 kWp PV system, 10 kWh BESS, 10 kW heat pump 1kW SCR offer) compared to an integrated home not participating in the SCR market. Different generic SCR request profiles are analyzed to depict the influence on the additional revenues.

Due to the high dependency of the revenues/costs of the SCR on the time and power, the results presented in Figure 114 are depicted as the average of the different scenarios. A SCR call of 10, 20, 30 and 40 minutes is investigated as well as the starting time of the SCR. The results show that the SCR revenues are strongly influenced by the SCR duration and slightly influenced by the start time of the SCR call.

7.7.4.2 Exemplary calculation of marginal costs for the flexible energy and capacity price scenario

This section analyzes the marginal savings of the SCR offer. These savings are the maximum price to bid on the SCR market. Figure 115 depicts the mean savings of 1 kW of SCR. Even though the total savings are higher with a higher SCR offer, the average savings per kW SCR are lower with increasing SCR offer. The reason is the inefficient use of the SCR power, when more SCR capacity is offered. More SCR offer leads to a lower value of each kW SCR power. Therefore, in a competitive market, it is not always the most economical approach to offer the maximum SCR power.

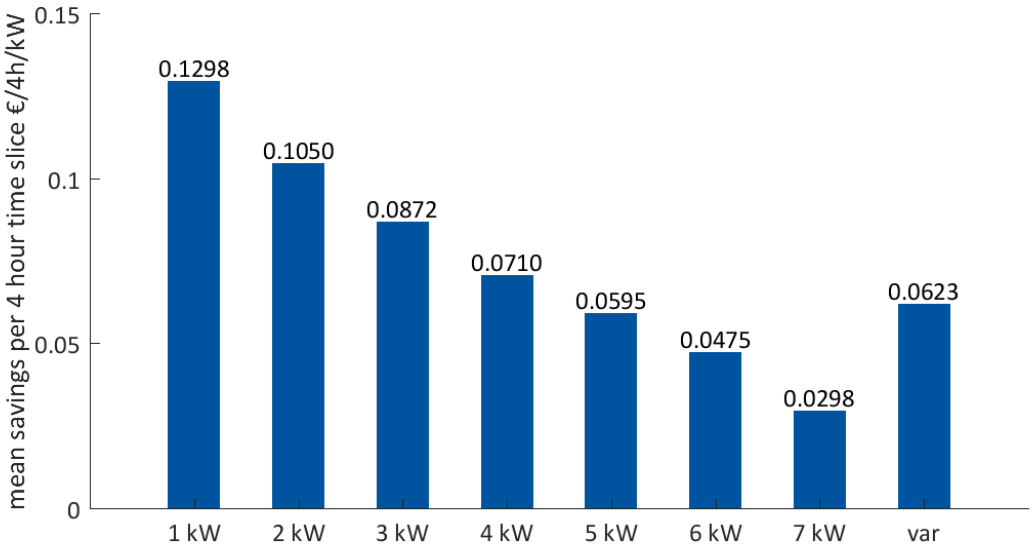

Figure 115: Mean savings of an integrated home (10 kWp PV system, 10 kWh BESS, 10 kW heat pump) participating in the SCR market compared to an integrated home without market participation. Savings are calculated for the flexible energy and capacity price scenario. The savings depend on the SCR power offering.

In the following, the savings are calculated for every 4-hour time slice. Therefore, the costs of the integrated home are calculated with and without SCR participation. These costs are discounted from each other to identify the effects of SCR participation. The results are depicted in Figure 116. Positive values indicate savings compared to an integrated home without SCR market participation. Negative values indicate extra costs due to SCR market participation.

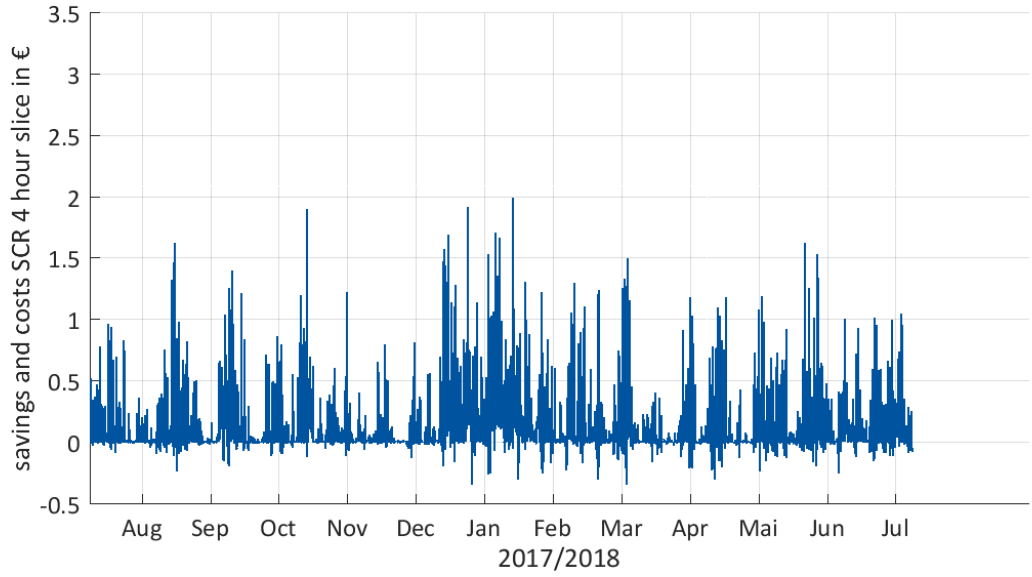

Figure 116: Savings (positive) and costs (negative) of an integrated home (10 kWp PV system, 10 kWh BESS, 10 kW heat pump) participating in the SCR market (1 kW SCR) compared to an integrated home without market participation. Savings are calculated for the flexible energy and capacity price scenario. The savings are calculated for every four-hour time slice of the SCR market.

For some 4-hour time slices, the offer of SCR has a negative influence on the economics of the integrated home because in these hours, the cost for battery aging exceeds the costs for the SCR revenues. The additional battery aging leads to negative income of the integrated homes in some 4-hour time slices. Figure 117 depicts the additional battery aging in every 4-hour time slice. In some time slices, battery aging is reduced because of a reduced number of cycles in these hours. Nevertheless, additional battery aging has a negative influence on the economics of the integrated home as shown in Figure 107.
The savings - and therefore the offered prices for SCR - are slightly higher in the winter because in that season the SCR often reduces grid consumption and in the summer, the SCR enhances the PV feed-in.

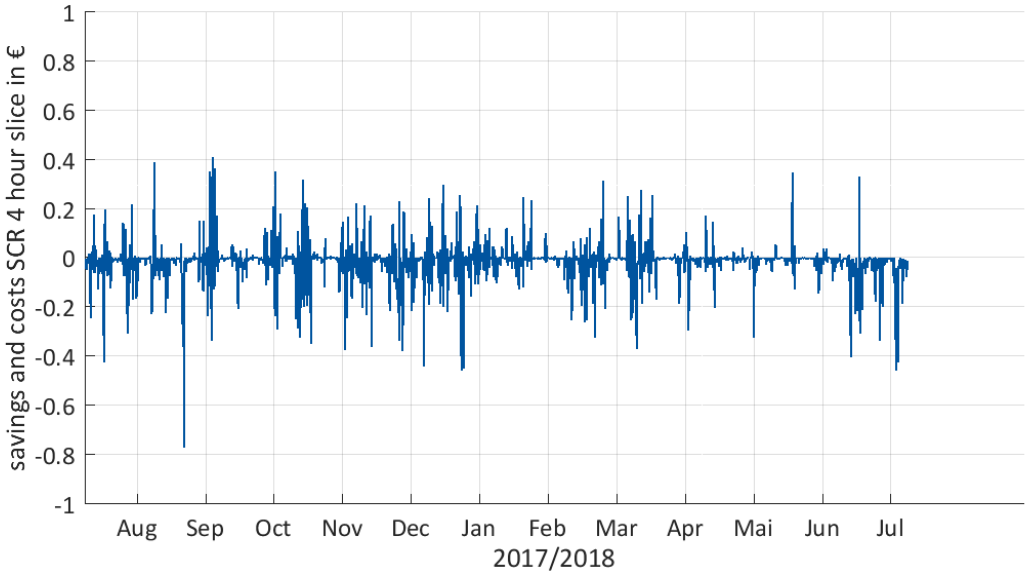

Figure 117: Additional costs (negative) for battery aging of an integrated home (10 kWp PV system, 10 kWh BESS, 10 kW heat pump) participating in the SCR market (1 kW SCR) compared to an integrated home without market participation. Costs are calculated for the flexible energy and capacity price scenario. The costs are calculated for every four-hour time slice of the SCR market.

Due to the storage-units in the integrated home, the savings from grid consumption and additional revenues from PV feed-in exceed the absorbed energy from the SCR in some 4-hour time slices, as depicted in Figure 116. In some time slices, over two euros are saved, even though a maximum of four kWh of SCR can be absorbed. Hence, an allocation function to distribute the savings on the preceding hours is applied. The battery and conversion losses are neglected in the allocation because they are relatively small. The results minding the allocation function are depicted in Figure 118. The applied allocation function is presented in Section 7.6.4. For the examined case, the minimum SCR power absorbed in one time slice is 0 kWh and the maximum SCR absorbed is 4 kWh. On average, 0.77 kWh SCR are absorbed per 4-hour time slice.

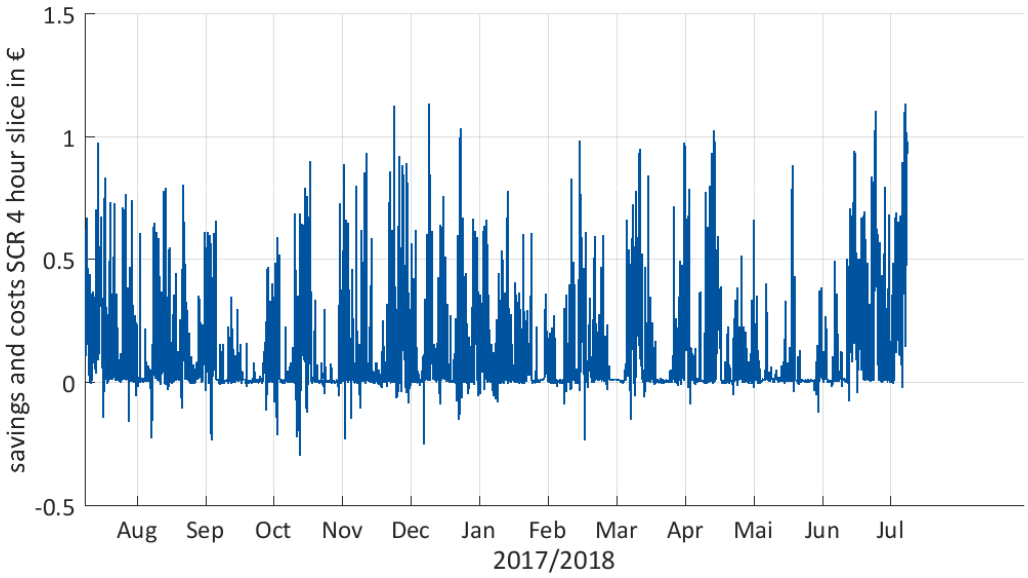

Figure 118: Savings of an integrated home (10 kWp PV system, 10 kWh BESS, 10 kW heat pump) participating in the SCR market (1 kW SCR) compared to an integrated home without market participation. Savings are calculated for the flexible energy and capacity price scenario. The savings are calculated for every four-hour time slice of the SCR market. An allocation function that caps the savings to the electricity price multiplied with the SCR energy absorbed in the considered time slice is applied.

The savings and costs presented in Figure 116, Figure 117 and Figure 118 are depicted for every 4-hour time slice. These figures are difficult to interpret. This is why Figure 119 presents the histogram of the allocation depicted in Figure 118. Figure 119 points out that the savings in most time slices are relatively low, between zero and $0.05\ \frac{€}{4\text{-hour time slice}}$. The reason for this finding is the relatively low activation time of the SCR in most time slices. Over 80% of all time slices have savings below $0.4\ \frac{€}{4\text{-hour time slice}}$.

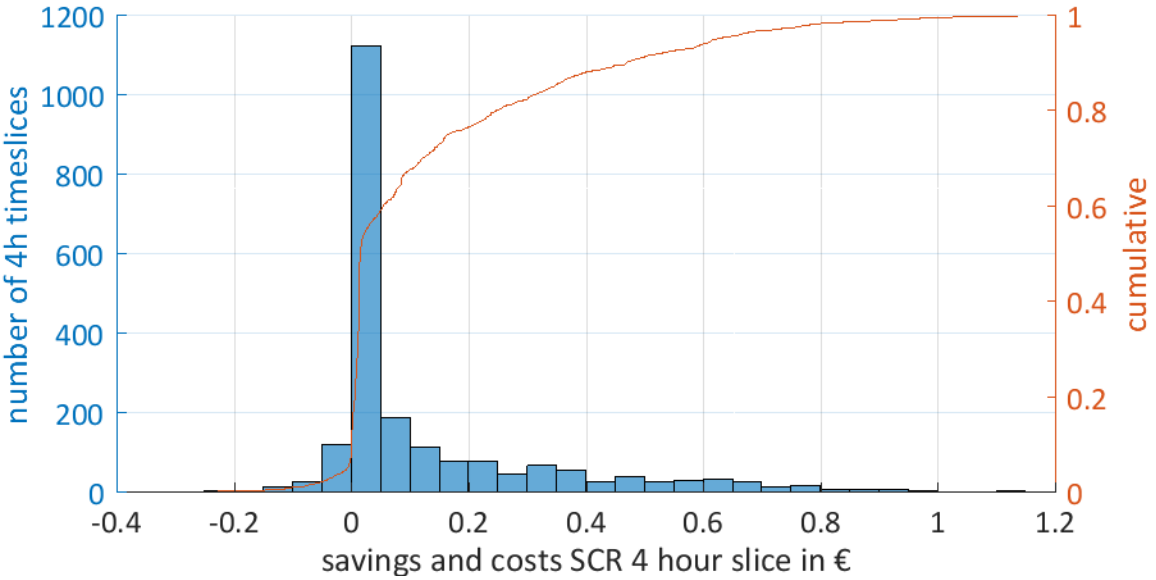

Figure 119: Histogram of the savings of an integrated home (10 kWp PV system, 10 kWh BESS, 10 kW heat pump) participating in the SCR market (1 kW SCR) compared to an integrated home without market participation. Savings are calculated for the flexible energy and capacity price scenario. The savings are calculated for every four-hour time slice of the SCR market. An allocation function that caps the savings to the electricity price multiplied with the SCR energy absorbed in the considered time slice is applied.

7.7.5 Bidding strategy on a competitive SCR market

This section presents how to determine the amount of control reserve that should be offered by a single integrated home system on the market, using forecasts of load and supply. Forecast inaccuracies lead to lower income or savings. In a market with positive prices for SCR capacity and energy prices, forecast inaccuracies play a minor role, since energy from SCR have a positive influence on the economics of the integrated home.

In a competitive market, forecast inaccuracies play an important role when marginal savings are calculated. The calculation of the marginal costs is highly dependent on the forecasts of the SCR requests, the household load and the PV generation because the SCR price bid is submitted in advance. In the SCR market, the bid for the SCR has to be given by 8 am on the day before, for the first tender phase and by 12 am for the second tender phase. Therefore, a 24- to 48-hour forecast period has to be considered.

The forecast error (Root-mean-square deviation) for PV generation in Germany is 6-7% on the aggregated level for a day before the forecast. The load forecast in Germany for one control area is 3.6%-3.9% for intra-day forecast and 4.0%-4.6% for day-ahead forecast [270]. These errors are relatively small, since they are on an aggregated base. Forecast inaccuracies for a single household are higher. The authors could not find any information on non-aggregated prognoses. The forecast errors of load and generation are relatively small compared to the forecast errors of SCR calls.

To overcome the issue of the unpredictable forecast of SCR calls, a threshold value for SCR energy is defined. The threshold is explained in the following. Below this threshold, the energy from SCR has a comparative value of 29.2 ct/kWh minus the losses of the BESS because it can

be stored in the BESS. Above this threshold value, the SCR energy is transferred to the heating sector. This leads to a reduced comparative value of the SCR energy compared to the SCR energy transferred to the BESS. To determine the threshold, the maximum SoC of the BESS is calculated each day, when not participating in the SCR market. The remaining BESS capacity can be used to store the SCR energy. This evaluation has to be performed at the beginning of every bidding period, since it might be influenced from the SCR market participation of previous bidding periods. Figure 120 depicts the threshold value for every day of the year without participating in the SCR market. The influence of SCR energy left in the BESS is not considered.

The analysis of the threshold shows that the threshold of the SCR in the winter is higher compared to the summer, when the battery storage system is used to store the PV-generated energy. The maximum of the threshold is 10 kWh of secondary control reserve energy, the size of the battery storage system. A threshold of 10 kWh means that the BESS is fully used for home storage operation and no capacity to store SCR energy is left. On the other hand, 0 kWh means that the entire BESS capacity can be used to store SCR energy. SCR stored in the BESS has a comparative value of 29.2 ct/kWh, whereas the comparative value of SCR stored in the heat storage is less. Therefore, the threshold value can be used as a first indicator for a bidding strategy on a competitive SCR market.

Nevertheless, prognoses errors build an offset on the biddings. This is why the presented model does not incorporate forecast errors. To do that, the bidding has to be adjusted with the forecast error. The forecast accuracy determines the size of the adjustment.

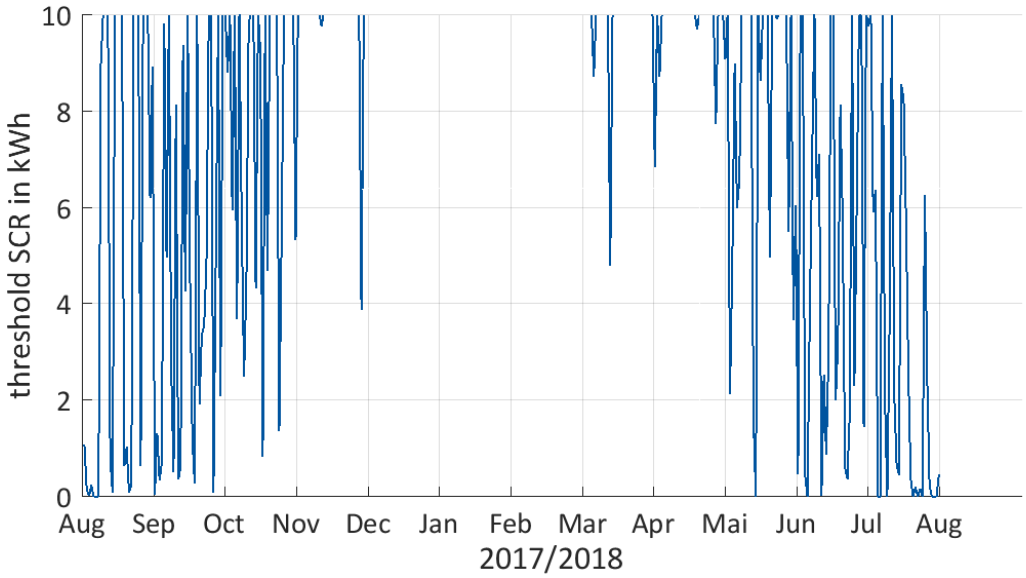

Figure 120: Threshold value for SCR energy. Below this threshold, the energy from SCR has a comparative value of almost 29.2 ct/kWh because it can be stored in the BESS. Above this threshold value, the SCR energy is transferred to the heating sector. This leads to a diminished comparative value.

7.8 Conclusion secondary control reserve market participation

With the latest revision of the automated secondary control reserve (SCR) market by the ENTSO-E, an increased auction frequency and shortened tendered time slices were introduced, which incentivize the participation of battery energy storage systems. Residential photovoltaic battery energy storage systems can participate in the secondary control reserve market if they are connected to a pool of prequalified units.

Photovoltaic battery energy storage systems participating in the negative secondary control reserve market could benefit from low-cost energy or revenues from market participation. If the battery system is combined with a heat pump or heating rod for power-to-heat coupling, excess energy can also be transferred to the heating sector, thus increasing the operating range of the battery. Participation of the integrated home on the secondary control reserve market influences battery aging, which is accelerated due to a heavier and more frequent usage of the battery system. The battery lifetime could be reduced up to 40 %.

The additional costs for the accelerated battery aging are compared with the income from market participation. The influence on the economics is evaluated on the basis of annuities.

The results show that the additional use of the photovoltaic battery energy storage system can have a positive influence on the economics. In an ideal setup, savings of up to 14.5% of the annual costs can be gained.

Additionally, an approach is presented to calculate the marginal costs and savings of the integrated home. The marginal savings and costs represent the actual value of the market participation for the secondary control reserve. In a highly competitive market, this value represents the maximum price that can be bid on the market. Hence, with the presented approach, the maximum price that can be bid by the integrated home for every 4-hour time slice of the negative secondary control reserve market can be calculated. Results show that an average of 13 ct/kWh can be paid, if 1 kW of secondary control reserve is offered.

Further scenarios show that the use of the battery system only for secondary control reserve is less economical than a battery system combined with a photovoltaic system. The usage of the heat pump to transfer energy from secondary control reserve to the heating sector has advantages from an economic perspective compared to the usage of the heating rod. Nevertheless, it remains unclear how the additional usage of the heat pump influences its lifetime because the minimum runtime of the heat pump cannot be guaranteed in this mode of operation.

The investigations of the dissertation at hand are limited to households with photovoltaic battery energy storage systems combined with a heat pump for power-to-heat coupling. Further applications such as the use of solar thermal collector are not investigated. Additional savings could be gained by the use of optimal component sizes. Further research could address this topic. Additionally, the influence of uncertainties and prognosis in the bidding on the secondary control reserve market could be addressed in further research. Finally, costs for pooling and market access need to be reduced in future. Hence, further research is required.

7.9 Comparison primary and secondary control reserve market participation

The comparison of the SCR market participation and the PCR market participation leads to the conclusion, that the savings participating in the SCR market are slightly higher compared to the savings of the PCR market participation. Figure 97 depicts the costs of a non-optimized integrated home participating in the PCR market. The savings for the variable PCR offer are 454 €/a. These savings are slightly lower compared to the saving of SCR market participation presented in Figure 109. Savings of 518 €/a are possible for a variable SCR offering.
Additionally the PV BESS with combined heat and power is compared to a common concept of the energy and heat supply. Therefore, a comparison to a household with gas heating and electric supply from the grid is presented in Figure 121. Heating power from gas is used as the benchmark for the thermal energy consumption. The costs for the gas heating system are based on [137]. The costs of the house with the gas heating system combine the costs for the electricity and gas consumption as well as the annual costs for the gas heating system. The presented analysis leads to the conclusion, that an integrated home participating on the control reserve market has similar annual costs as a household with a fossil heating concept. Nevertheless, an integrated home with optimized component sizes or a house with PV system and a fossil heating system have significant lower annual costs. The costs are presented in Figure 121 as well.
This is why the provision of control reserve from integrated homes with optimized component sizes is investigated. In the case of an integrated home with optimized component sizes, the savings from control reserved market participation are reduced in comparison to the non-optimization case. The reason is the reduced size of the BESS.
In the optimized-integrated home scenario, the savings of the SCR market participation are higher compared to the savings of the PCR market participation. The annuity of the PCR market participation of an optimized integrated home participating is depicted in Figure 99. The savings are 174 €/a for a variable PCR offering. Under consideration of the deployment costs, the additional participation on the PCR market is not economical.
Savings of the optimized integrated home participating in the SCR market are depicted in Figure 112. For the variable SCR offering savings up to 346 €/a for an optimized integrated home are possible, including the deployment costs as presented in Table 23.
The presented results are based on many assumptions. This is why the presented results are exemplary for a specific case based on the assumptions presented in section 3.5.3. A general statement cannot be made. This is why a detailed sensitivity analysis is presented in section 5.3 to section 5.8.

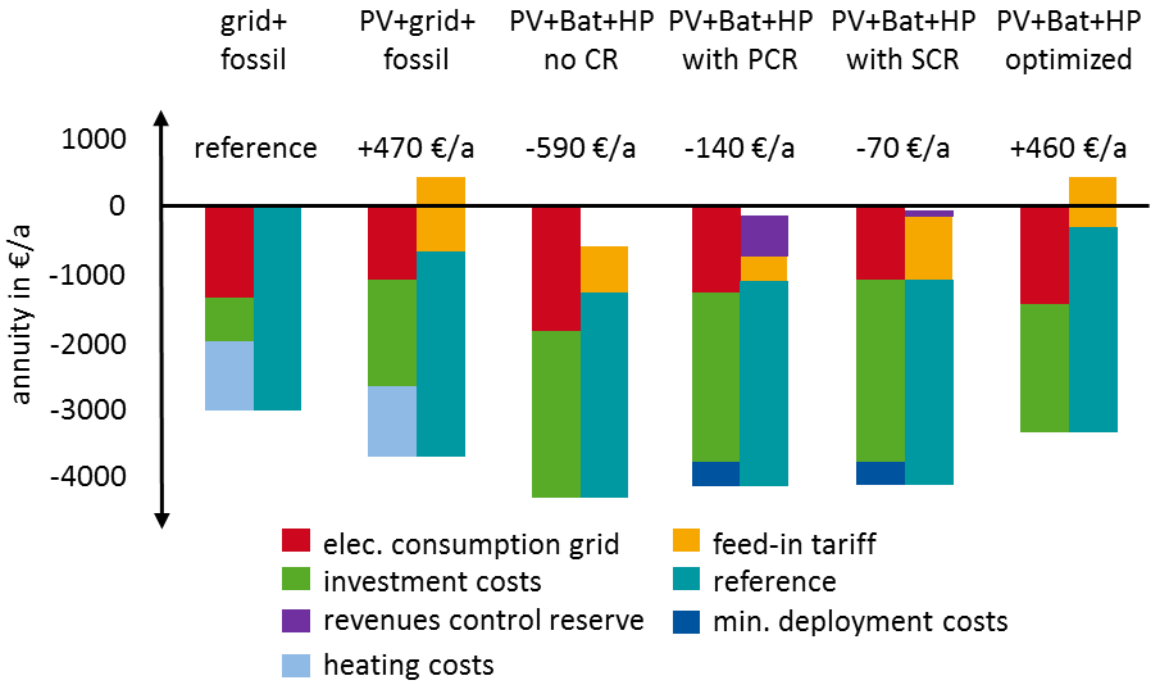

Figure 121: Comparison of the annual costs of integrated homes with and without provision of control reserve. The variable provision of control reserve is depicted. The integrated home is compared to houses with fossil heating concepts. Additionally a comparison to an integrated home with optimized component sizes is presented.

8. Conclusion and Outlook

8.1 Conclusion

Homes, which integrate a PV battery energy storage system and a heat pump for power-to-heat coupling, can contribute in the decarbonisation process. The power generated by the PV system can be used for space heating and domestic hot water to enhance the share of locally generated renewable energies. To enhance the share of integrated homes the economics of these needs to be improved. In this dissertation, a detailed model of an integrated home is developed to investigate cost reduction potentials. The model is parameterized with measured data from cell testing and battery aging test preformed for this dissertation. Cost reduction can be achieved by advanced operation strategies, optimization of the component sizes and market participation. All these aspects are investigated in this thesis.

Advanced operation strategies are developed for PV BESS and combined with operation strategies for power-to-heat coupling. A new forecast-based operation strategy to enhance the battery lifetime and therefore the economics of PV battery energy storage systems is presented. Results show that forecast-based operation strategies can enhance battery lifetime. The annual energy throughput is slightly reduced, but in combination with the significantly prolonged lifetime, the total energy throughput over the systems lifetime can be increased. The lifetime of the low-cost consumer lithium-ion NMC battery cell can be enhanced by around five years, i.e. doubled, if the forecast-based operation strategy is used instead of a maximized self-consumption operation strategy. The forecast-based operation leads to a reduction of the levelized cost of electricity of up to 3.5 c€/kWh compared to a self-consumption maximizing strategy. This leads to a cost reduction of 12 percent.

Results show that the use of forecast-based operation strategies can enhance the economics of the investigated battery energy storage system regardless of component size or applied profiles. Nevertheless, a small battery with a capacity of only 2.5 kWh shows a negligible influence of the operation strategy. The positive influence is enhanced with an enhanced battery size.

Forecast-based operation strategies use predictions for load and PV generation. To investigate the influence of forecast inaccuracies, two different forecast strategies are examined. The persistence forecast is used as the worst-case forecast and the perfect forecast is used as the best-case forecast. This approach allows evaluating the potential of the forecast-based operation strategies. Advanced forecast methods would lead to results within the range provided by both cases. The implementation of the presented operation strategy can be done without an additional communication interface if persistence forecast is used. To implement such a strategy, additional computational effort in the energy management system might be required. This could lead to higher costs for the energy management system and an increased energy demand of the system itself.

The developed forecast-based operation strategy for the electrical system is combined with operation strategies for power-to-heat coupling. The results show that the combination with a battery priority charging as well as modular operating heat pump is the most economical combination. This combined operation strategies can reduce the costs of an integrated home. PV BESS with power-to-heat application can enhance the self-consumption and the self-

sufficiency rate in comparison to standalone PV BESS. The combination of PV BESS with heat power coupling can lead to an optimal use of the generated PV power.
Another opportunity to enhance the economics and therefore the market penetration of integrated homes are the optimization of the component sizes and the operation boundary conditions. In this dissertation a tool for the optimization of an integrated home is presented, which is able to consider many economic parameters and boundary conditions. The annuity is used as the target function of the optimization. Additionally, a separate evaluation of levelized costs of energy (LCOEnergy), levelized costs of electricity (LCOEle) and levelized costs of heat (LCOH) is presented. The separate analysis enables the potential of an inter-sectorial comparison.
The developed tool for the optimization is used to optimize a 4-person integrated home located in Lindenberg (Tauche), close to Berlin. The results show, that the levelized costs of energy (LCOEnergy) are mainly driven by the costs for the energy consumption of the heat power system. Furthermore, the optimization lead to the conclusion, that under the assumed conditions, an integrated home can be operated beneficially if an optimum system design is chosen. Thereby, an integrated home with relatively small storage components is economical. The use of advanced operation strategies has a positive influence on the annuity of integrated homes, even under consideration of disturbance functions. Furthermore, the usage of the DHW storage in the optimized integrated home for storing excess PV energy is not advisable, due to a reduction of the COP of the heat pump. This is an important result, since it is an often discussed e.g. in [49] but rarely investigated topic. Furthermore, the analysis lead to the results, that the minimum buffer storage size should be chosen to guarantee the minimum runtime of the heat pump, because a reduced buffer storage size reduces costs of the integrated home, but increases the switching rate of the heat pump.
These findings show that optimization of the component sizes leads to a higher annuity reduction of integrated homes, in comparison to advanced operation strategies. Advanced operation strategies have a minor influence on the annuity of integrated homes in comparison to an optimization of the components. An integrated home with optimized component sizes can lead to an annual cost reduction of 15.5 % in comparison to a house with electricity consumption from grid and fossil heating.
Another interesting opportunity to enhance the economics of integrated homes is the generation of additional incomes, due to participation in the control reserve market. During winter storage systems in an integrated home, in particular the battery system, are not used to their full capacity due to low solar radiation. This potential can be used to enhance the economics of integrated homes by applying a second use scheme. Second use describes the value stacking of home storage operation and participation on the reserve market.
Hence, this dissertation presents the extension of the single-use operation of the integrated home to a dual-use operation participation in the control reserve market. In this case, the thermal storages can be used to absorb the negative control reserve power. This is an advantage in comparison to PV battery energy storages systems without power-to-heat coupling, since the battery system is less limited. Residential integrated homes can participate in the control reserve market, if they are connected to a pool, which has to be prequalified.
The thesis investigates the provision of primary and secondary control reserve. The provision of primary control reserve generates additional income for the integrated home. Additionally, due to over-fulfillment, free-of-charge energy can be obtained. The economic assessment shows, that the additional costs for the enhanced battery aging and the reduced self-consumption rate are compensated by the incomes from the PCR market participation. Therefore, the dual-use operation of an integrated home, which participates in the primary

control reserve market, can increase the profitability of a residential storage system. Under consideration of steady revenues and low costs for market participation, a provision of at least 3 kW could be economical. A season dependent variable provision of primary control reserve can further increase the economic efficiency of integrated homes and reduce the annual costs up to 12.5 %.
The participation on the negative secondary control reserve market can provide low-cost or free-of-charge energy for the integrated home. The absorbed energy leads to reduced grid consumption as well as an enhanced PV feed-in. In the thesis, a model is presented to calculate the revenues of the market participation. Participation of the integrated home on the secondary control reserve market influences the battery aging. The battery aging is enhanced due to a higher exposer of the battery system. The additional costs for the enhanced battery aging are compared with the incomes from the market participation. The influence on the economics is evaluated. Additionally, an approached is presented to calculate the marginal costs and savings of the integrated home. With the presented approach the maximum price, which can be bid by the integrated home on the updated negative secondary control reserve market can be calculated. The results show that the additional use of the PV-BESS can have a positive influence on the economics. The analysis shows that under consideration of stable prices, it is economical to participate in the market. Savings up to 14.5 % of the annual costs can be gained.

8.2 Discussion and Outlook

This work shows an in-depth analysis of an integrated home with a PV BESS and power-to-heat coupling. For this analysis a detailed model of the integrated home is developed. The presented results of the model have to be considered as exemplary, because the results are highly sensitive regarding the parametrization of the model and the input parameters. This is why the presented results are exemplary for a specific case based on the assumptions presented in section 3.5.3. A general statement cannot be made. This is why a detailed sensitivity analysis is presented in section 5.3 to section 5.8.
This applies especially to the results of the operation strategies for the battery energy storage system. Due to the huge variety of different lithium-ion battery cells and their properties, the values resulting from the investigation need to be verified for each specific cell individually. Still, all common lithium-ion cells show accelerated aging along with a higher average state of charge. This means that the general principles of the findings and the overall validity of the operation strategy should apply to all types of lithium-ion-based PV battery energy storage systems. Nevertheless, it is not investigated whether the savings gained by the implementation of the operation strategies overcompensate the costs for implementation.
The findings regarding the participation on control reserve market are based on historic data. The thesis points out that technically it is possible to participate on the control reserve market. Under consideration of stable prices, participation is economical. Nevertheless, prices for primary control reserve provision as well as for secondary control provision are expected to fall. Costs for pooling and market access are not clear as well as charges for aggregators. The incomes for the market participation might be overestimated. Experts estimate an average income of $100{,}000\ \frac{€}{\mathrm{a \cdot MW}}$ for the PCR market. The prices for the secondary control reserve market are expected to fall through the market update in July 2018. Further additional costs

for market participation are estimated at 25 % of the incomes for grid scale storages. These costs might be higher for small storages operating in a pool. The costs for market participation and communication are not clear and need to be reduced in future. Finally, yet importantly, in Germany additional charges (e.g. Renewable Energies Act levy (EEG-Umlage), grid utilization charges (Netznutzungsentgelt), interruptible loads levy (Umlage für abschaltbare Lasten)) occur on heat from primary control reserve power. Additional regulatory issues for integrated homes participate on the control reserve market in Germany exist. For example, a sophisticated measurement concept has to be applied, because if electricity from the grid (Graustrom) is mixed in the storages with electricity form the PV power plant, levy and taxes for the energy from the PV power plant incurred. This is the case if the BESS is bigger than 10 kWh.

On the other hand, a combination with the intraday market could lead to additional income. The incorporation of weather forecast could enhance the income in the variable offering of primary control reserve case. The future flexibilisation of the primary control reserve market, similar to the secondary control reserve market in Germany, could lead to further incentives for storage systems participation. Finally not yet important, a reduction of the transaction costs is possible if not every single integrated home is monitored.

In the secondary control reserve markets, the reserve calls highly influence the economics of the market participation. The forecast of control reserve calls is difficult and lead to high uncertainties of the maximum bid price. To overcome this issue for the secondary control reserve market, an approach is presented to calculate an energy threshold until the secondary control energy has a high value. The threshold in winter is higher than in summer due to the high solar radiation in summer.

9. References

References

[1] Global Carbon Project, *Entwicklung des weltweiten CO2-Ausstoßes in den Jahren 1995 bis 2018.* [Online]. Available: https://de.statista.com/statistik/daten/studie/208750/umfrage/weltweiter-co2-ausstoss/ (accessed: Feb. 10 2020).

[2] United Nations, *Paris Agreement, C.N.92.2016.TREATIES-XXVII.7.d, 2015, Paris*.

[3] Renewable Energy Policy Network for the 21st Century, *Renewables 2017: Global Status Report*. Montréal, QC, CA: REN21, 2017.

[4] J. Rockström, O. Gaffney, J. Rogelj, M. Meinshausen, N. Nakicenovic, and H. J. Schellnhuber, "A roadmap for rapid decarbonization," *Science*, vol. 2017, no. 355, pp. 1269–1271, 2017.

[5] Bundesministerium für Umwelt, Naturschutz, Bau und Reaktorsicherheit, "Klimaschutzplan 2050 - Klimaschutzpolitische Grundsätze und Ziele der Bundesregierung," Berlin, Nov. 2016.

[6] Bundesministerium für Wirtschaft und Energie, *Energieverbrauch nach Anwendungsbereichen in Deutschland 2017.* [Online]. Available: https://www.bmwi.de/Redaktion/DE/Infografiken/Energie/Energiedaten/Energiegewinnung-und-Energieverbrauch/energiedaten-energiegewinnung-verbrauch-09.html (accessed: Feb. 10 2020).

[7] AG Energiebilanzen e.V., *Auswertungstabellen zur Energiebilanz Deutschland 1990 bis 2015.* [Online]. Available: https://www.ag-energiebilanzen.de/index.php?article_id=29&fileName=ausw_28072016_ovk.pdf (accessed: Feb. 10 2020).

[8] BDEW Bundesverband der Energie- und Wasserwirtschaft e.V, "Entwicklung des Wärmeverbrauchs in Deutschland: Basisdaten und Einflussfaktoren," BDEW 11/2017, Berlin, Sep. 2018.

[9] Fraunhofer IWES/IBP, *Wärmewende 2030: Schlüsseltechnologien zur Erreichung der mittel- und langfristigen Klimaschutzziele im Gebäudesektor*. Studie im Auftrag von Agora Energiewende. [Online]. Available: https://www.agora-energiewende.de/fileadmin2/Projekte/2016/Sektoruebergreifende_EW/Waermewende-2030_WEB.pdf (accessed: Feb. 10 2020).

[10] M. Frondel et al., "Erhebung des Energieverbrauchs der privaten Haushalte für die Jahre 2011-2013," Mar. 2015.

[11] Umweltbundesamt, *Erneuerbare Energien in Zahlen: Daten zur Entwicklung im Jahr 2018* (accessed: Apr. 5 2020).

[12] D. H. Wirth, *Aktuelle Fakten zur Photovoltaik in Deutschland. Fassung vom 03.01.2018.* [Online]. Available: https://www.ise.fraunhofer.de/content/dam/ise/de/documents/publications/studies/aktuelle-fakten-zur-photovoltaik-in-deutschland.pdf (accessed: Apr. 6 2020).

[13] J. Figgener, D. Haberschusz, K.-P. Kairies, O. Wessels, B. Tepe, and D. U. Sauer, "Wissenschaftliches Mess- und Evaluierungsprogramm Solarstromspeicher 2.0: Jahresbericht 2018," Institut für Stromrichtertechnik und Elektrische Antriebe der RWTH Aachen, Aachen, 2018.

[14] A. Eller and D. Gauntlett, *Energy Storage Trends and Opportunities in Emerging Markets.* [Online]. Available: http://esmap.org/sites/default/files/esmap-files/7151-IFC-EnergyStorage-report.pdf (accessed: Apr. 6 2020).

[15] Statistisches Bundesamt, *Preise: Daten zur Energiepreisentwicklung.* [Online]. Available: https://www.destatis.de/DE/Themen/Wirtschaft/Preise/Publikationen/Energiepreise/energiepreisentwicklung-pdf-5619001.pdf?__blob=publicationFile (accessed: Apr. 6 2020).

[16] BSW Solar, *EEG 2014 - feste Einspeisevergütungen im Überblick.* [Online]. Available: https://www.solarwirtschaft.de/fileadmin/media/pdf/Verguetungsuebersicht-Basis.pdf (accessed: Apr. 6 2020).

[17] J. Figgener, Kai-Philipp Kairies, D. Haberschusz, O. Wessels, and P. D. U. Sauer, "Markt- und Technologieentwicklung von PV-Heimspeichern in Deutschland: BVES Pressekonferenz Energy Storage Europe," BVES, ISEA RWTH AAchen, Düsseldorf, Mar. 2019.

[18] A.-L. Klingler, "Self-consumption with PV + Battery systems: A market diffusion model considering individual consumer behaviour and preferences," *Applied Energy*, vol. 205, pp. 1560–1570, 2017, doi: 10.1016/j.apenergy.2017.08.159.

[19] KPMG, *Development of decentralised energy and storage systems in the UK: A report for the Renewable Energy Association.* [Online]. Available: https://assets.kpmg/content/dam/kpmg/pdf/2016/07/Development-of-decentralised-energy-and-storage-systems-in-the-UK.pdf (accessed: Apr. 6 2020).

[20] M. Chediak, P. Gopal, and B. Eckhouse, *California Becomes First State to Order Solar on New Homes.* [Online]. Available: https://www.bloomberg.com/news/articles/2018-05-09/california-votes-to-require-rooftop-solar-power-on-new-homes (accessed: Apr. 6 2020).

[21] G. de Oliveira Silva and P. Hendrick, "Photovoltaic self-sufficiency of Belgian households using lithium-ion batteries, and its impact on the grid," *Applied Energy*, vol. 195, pp. 786–799, 2017, doi: 10.1016/j.apenergy.2017.03.112.

[22] Y. Li, W. Gao, and Y. Ruan, "Performance investigation of grid-connected residential PV-battery system focusing on enhancing self-consumption and peak shaving in Kyushu, Japan," *Renewable Energy*, vol. 127, pp. 514–523, 2018, doi: 10.1016/j.renene.2018.04.074.

[23] V. Bertsch, J. Geldermann, and T. Lühn, "What drives the profitability of household PV investments, self-consumption and self-sufficiency?," *Applied Energy*, vol. 204, pp. 1–15, 2017, doi: 10.1016/j.apenergy.2017.06.055.

[24] M. Bruch and M. Müller, "Calculation of the Cost-effectiveness of a PV Battery System," *Energy Procedia*, vol. 46, pp. 262–270, 2014, doi: 10.1016/j.egypro.2014.01.181.

[25] M. Naumann, R. C. Karl, C. N. Truong, A. Jossen, and H. C. Hesse, “Lithium-ion Battery Cost Analysis in PV-household Application,” *Energy Procedia*, vol. 73, pp. 37–47, 2015, doi: 10.1016/j.egypro.2015.07.555.

[26] J. Weniger, T. Tjaden, and V. Quaschning, “Sizing of Residential PV Battery Systems,” *Energy Procedia*, vol. 46, pp. 78–87, 2014, doi: 10.1016/j.egypro.2014.01.160.

[27] Fraunhofer IWES/IBP, “Wärmewende 2030: Schlüsseltechnologien zur Erreichung der mittel- und langfristigen Klimaschutzziele im Gebäudesektor,” Jan. 2017.

[28] Bundesverband Wärmepumpe e.V., *waermepumpe.de.* [Online]. Available: https://www.waermepumpe.de/presse/pressemitteilungen/details/17-prozent-marktwachstum-machen-2016-zum-waermepumpen-rekordjahr/ (accessed: Apr. 6 2020).

[29] Katja Weinhold, *BWP Marktzahlen 2017: Wärmepumpen-Absatz wächst deutlich* . Berlin, 2018. Accessed: Jun. 29 2018. [Online]. Available: https://www.waermepumpe.de/uploads/media/2018-01-24_BWP_Absatzahlen_2017.pdf

[30] Deutsche Energie-Agentur dena, “dena-Netzflexstudie: Optimierter Einsatz von Speichern für Netz- und Marktanwendungen in der Stromversorgung,” Mar. 2017.

[31] S. Zurmühlen, G. Angenendt, M. Heinrich, H. Axelsen, and D. U. Sauer, “Grid-relieving effects of PV battery energy storage systems with optimized operation strategies,” in *33rd European Photovoltaic Solar Energy Conference and Exhibition*, 2017.

[32] Bartosz Chwieduka and Dorota Chwieduk, “Performance analysis of a PV driven heat pump system during a heating season in high latitude countries,” in *12th IEA HEat Pump Conference 2017*.

[33] C. Roselli, M. Sasso, F. Tariello, and D. Goodfield, “Integration between electric heat pump and PV system to increase self-consumption of an office application,” *Renew. Energy Environ. Sustain.*, vol. 2, p. 28, 2017, doi: 10.1051/rees/2017038.

[34] J. Bonin, Ed., *Handbuch Wärmepumpe*: Beuth, 2012.

[35] D. A. Halamay, T. K. A. Brekken, A. Simmons, and S. McArthur, “Reserve requirement impacts of large-scale integration of wind, solar, and ocean wave power generation,” in *Energy Society General Meeting 2010*, pp. 1–7.

[36] J. Hu, R. Harmsen, W. Crijns-Graus, E. Worrell, and M. van den Broek, “Identifying barriers to large-scale integration of variable renewable electricity into the electricity market: A literature review of market design,” *Renewable and Sustainable Energy Reviews*, vol. 81, pp. 2181–2195, 2018, doi: 10.1016/j.rser.2017.06.028.

[37] 50hertz, Amprion, Tennet, and Transnet BW, *Regelleistung.net - Datencenter.* [Online]. Available: www.regelleistung.net (accessed: Apr. 6 2020).

[38] A. Gitis, M. Leuthold, and D. U. Sauer, “Applications and Markets for Grid-Connected Storage Systems,” in *Electrochemical Energy Storage for Renewable Sources and Grid Balancing*: Elsevier, 2015, pp. 33–52.

[39] 50hertz, Amprion, Tennet, and Transnet BW, “Anforderungen an die Speicherkapazität bei Batterien für die Primärregelleistung,” Sep. 2015.

[40] R. Luthander, J. Widén, D. Nilsson, and J. Palm, “Photovoltaic self-consumption in buildings: A review,” *Applied Energy*, vol. 142, pp. 80–94, 2015, doi: 10.1016/j.apenergy.2014.12.028.

[41] G. Angenendt, S. Zurmühlen, F. Jesse, H. Axelsen, and P. D. U. Sauer, “Einfluss der zusätzlichen Nutzung von PV-Batteriespeichern zur Regelenergiebereitstellung auf die Batteriealterung,” in *PV Symposium 2018 Bad Staffelstein*.

[42] PricewaterhouseCoopers pwc, “Virtuelle Kraftwerke als wirkungsvolles Instrument für die Energiewende,” Feb. 2012.

[43] C. Truong, M. Naumann, R. Karl, M. Müller, A. Jossen, and H. Hesse, “Economics of Residential Photovoltaic Battery Systems in Germany: The Case of Tesla’s Powerwall,” *Batteries*, vol. 2, no. 2, p. 14, 2016, doi: 10.3390/batteries2020014.

[44] R. Valančius, A. Jurelionis, R. Jonynas, V. Katinas, and E. Perednis, “Analysis of Medium-Scale Solar Thermal Systems and Their Potential in Lithuania,” *Energies*, vol. 8, no. 6, pp. 5725–5737, 2015, doi: 10.3390/en8065725.

[45] S. Poppi, N. Sommerfeldt, C. Bales, H. Madani, and P. Lundqvist, “Techno-economic review of solar heat pump systems for residential heating applications,” *Renewable and Sustainable Energy Reviews*, vol. 81, pp. 22–32, 2018, doi: 10.1016/j.rser.2017.07.041.

[46] L. M. Ayompe and A. Duffy, “Thermal performance analysis of a solar water heating system with heat pipe evacuated tube collector using data from a field trial,” *Solar Energy*, vol. 90, pp. 17–28, 2013, doi: 10.1016/j.solener.2013.01.001.

[47] M. Miara, D. Günther, R. Langner, and S. Helmling, “Efficiency of Heat Pumps in Real Operating Conditions: Results of three Monitoring Campaigns in Germany,” *Rehva Journal*, vol. 2014, no. 51, pp. 7–12.

[48] S. Poppi, *Solar heat pump systems for heating applications: Analysis of system performance and possible solutions for improving system performance*. Stockholm: KTH Royal Institute of Technology, 2017.

[49] M. Sterner and I. Stadler, *Energiespeicher - Bedarf, Technologien, Integration*. Berlin, Heidelberg: Springer Berlin Heidelberg, 2017.

[50] ifeu, Fraunhofer IEE und Consentec, “Wert der Effizienz im Gebäudesektor in Zeiten der Sektorenkopplung,” Studie im Auftrag von Agora Energiewende, 2018.

[51] F. Ochs, G. Dermentzis, and W. Feist, “Minimization of the Residual Energy Demand of Multi-storey Passive Houses – Energetic and Economic Analysis of Solar Thermal and PV in Combination with a Heat Pump,” *Energy Procedia*, vol. 48, pp. 1124–1133, 2014, doi: 10.1016/j.egypro.2014.02.127.

[52] A. Girard, E. J. Gago, T. Muneer, and G. Caceres, “Higher ground source heat pump COP in a residential building through the use of solar thermal collectors,” *Renewable Energy*, vol. 80, pp. 26–39, 2015, doi: 10.1016/j.renene.2015.01.063.

[53] W. Lerch, A. Heinz, and R. Heimrath, “Evaluation of Combined Solar Thermal Heat Pump Systems Using Dynamic System Simulations,” *Energy Procedia*, vol. 48, pp. 598–607, 2014, doi: 10.1016/j.egypro.2014.02.070.

[54] D. Carbonell, D. Philippen, E. Frank, M. Granzotto, and M. Haller, “Simulation of Combined Solar Thermal, Heat Pump, Ice Storage and Waste Water Heat Recovery

Systems. Design Criteria and Parametric Studies," in *EuroSun 2014*, Aix-les-Bains, France, pp. 1–10.

[55] T. Storch, T. Leukefeld, T. Fieback, and U. Gross, "Living Houses with an Energy-autonomy – Results of Monitoring," *Energy Procedia*, vol. 91, pp. 876–886, 2016, doi: 10.1016/j.egypro.2016.06.254.

[56] EnergieAgentur.NRW, *Leitfaden Wärmepumpe Kombination von Wärmepumpe und Photovoltaik.* [Online]. Available: https://www.sma-sunny.com/wp-content/uploads/2016/02/Leitfaden_Waermepumpen_final.pdf (accessed: Apr. 6 2020).

[57] D. U. Sauer, *Untersuchungen zum Einsatz und Entwicklung von Simulationsmodellen für die Auslegung von Photovoltaik-Systemen*. Technische Hochschule Darmstadt: Diploma Thesis 1994.

[58] J. Weniger, T. Tjaden, J. Bergner, and V. Quaschning, "Dynamic mismatch losses of grid-connected PV-battery systems in residential buildings," *Journal of Energy Storage*, vol. 13, pp. 244–254, 2017, doi: 10.1016/j.est.2017.07.011.

[59] C. Stegner, J. Bogenrieder, P. Luchscheider, and C. J. Brabec, "First Year of Smart Metering with a High Time Resolution—Realistic Self-Sufficiency Rates for Households with Solar Batteries," *Energy Procedia*, vol. 99, pp. 360–369, 2016, doi: 10.1016/j.egypro.2016.10.126.

[60] M. Bost, B. Hirschl, and A. Aretz, "Effekte von Eigenverbrauch und Netzparität bei der Photovoltaik," Jan. 2011.

[61] SUNTECH POWER, *Datenblatt für das Solarmodul Suntech Power STP210 - 18/Ud: EN-STD-Ud-NO1.01-Rev 2010.* [Online]. Available: https://www.energymatters.com.au/images/suntech/stp21018ud.pdf (accessed: Apr. 6 2020).

[62] K. Behrens, "Horizon at station Lindenberg," 2007.

[63] D. Magnor, *Globale Optimierung netzgekoppelter PV-Batteriesysteme unter besonderer Berücksichtigung der Batteriealterung*. Aachen: Aachener Beiträge des ISEA, 2017.

[64] H. Schmidt and D. U. Sauer, *Wechselrichter-Wirkungsgrade : Praxisgerechte Modellierung und Abschätzung.* [Online]. Available: https://www.dgs.de/fileadmin/sonnenenergie/SE-4-1996-ganz/Wechselrichter-Wirkungsgrade.PDF (accessed: Apr. 6 2020).

[65] G. Angenendt, B. Ashrafinia, S. Zurmühlen, K. Jacqué, J. Badeda, and D. U. Sauer, "Influence of the Battery Voltage Level on the Efficiency and Cost of a PV Battery Energy Storage System," in *32. Symposium Photovoltaische Solareergie*, 2017.

[66] M. Braun, K. Büdenbender, D. Magnor, and A. Jossen, "Photovoltaic Self-Consumption in Germany - Using Lithium-Ion Storage to Increase Self-Consumed Photovoltaic Energy," 2009, doi: 10.4229/24thEUPVSEC2009-4BO.11.2.

[67] A. Sangwongwanich *et al.,* "Enhancing PV Inverter Reliability With Battery System Control Strategy," *CPSS TPEA*, vol. 3, no. 2, pp. 93–101, 2018, doi: 10.24295/CPSSTPEA.2018.00009.

[68] M. Ecker, N. Nieto, S. Käbitz, J. Schmalstieg, H. Blanke, A. Warnecke and D. U. Sauer, “Calendar and cycle life study of Li(NiMnCo)O2-based 18650 lithiumion-Ion batteries,” *Journal of Power Sources*, vol. 2014, no. 248, pp. 839–851.

[69] G. Angenendt, H. Axelsen, and S. Zurmühlen, “PV Home Storage System (PV-HOST) "Betriebsstrategien und Systemkonfigurationen für Batteriespeicher für Einfamilienhäuser mit Photovoltaikanlagen" : Bericht zum Teilvorhaben der RWTH Aachen : Abschlussbericht,” TIB - Technische Informationsbibliothek Universitätsbibliothek Hannover, Hannover 0325477B, 2018.

[70] J. B. Gerschler, *Ortsaufgelöste Modellbildung von Lithium-Ionen-Systemen unter spezieller Berücksichtigung der Batteriealterung*. Zugl.: Aachen, Techn. Hochsch., Diss., 2012. Aachen: Shaker, 2012.

[71] E. Karden, *Using low-frequency impedance spectroscopy for characterization, monitoring, and modeling of industrial batteries*. Zugl.: Aachen, Techn. Hochsch., Diss., 2001. Aachen: Shaker, 2002.

[72] S. Buller, *Impedance-based simulation models for energy storage devices in advanced automotive power systems*. Zugl.: Aachen, Techn. Hochsch., Diss., 2002. Aachen: Shaker, 2003.

[73] K. S. Cole and R. H. Cole, “Dispersion and Absorption in Dielectrics I. Alternating Current Characteristics,” *The Journal of Chemical Physics*, vol. 9, no. 4, pp. 341–351, 1941, doi: 10.1063/1.1750906.

[74] K. Rumpf, L. Moraleja, J. Geder, and A. Jossen, “Comparing the specific heat capacity of lithium-ion cells using adiabatic calorimetry,” Technische Universität München TUM, München, 2016.

[75] K. Uddin, A. Picarelli, C. Lyness, N. Taylor, and J. Marco, “An Acausal Li-Ion Battery Pack Model for Automotive Applications,” *Energies*, vol. 7, no. 9, pp. 5675–5700, 2014, doi: 10.3390/en7095675.

[76] J. Schmalstieg, *Physico-electrochemical simulation of lithium-ion batteries : implementation, parametrization and application*: RWTH Aachen University, 2017.

[77] D.-I. Stroe, M. Swierczynski, A.-I. Stroe, R. Teodorescu, R. Laerke, and P. C. Kjaer, “Degradation behaviour of Lithium-ion batteries based on field measured frequency regulation mission profile,” in *2015 IEEE Energy Conversion Congress and Exposition*, Montreal, QC, Canada, pp. 14–21.

[78] Y.-X. Lin, Z. Liu, K. Leung, L.-Q. Chen, P. Lu, and Y. Qi, “Connecting the irreversible capacity loss in Li-ion batteries with the electronic insulating properties of solid electrolyte interphase (SEI) components,” *Journal of Power Sources*, vol. 309, pp. 221–230, 2016, doi: 10.1016/j.jpowsour.2016.01.078.

[79] S. Lehner, “Reliability assessment of lithium-ion battery systems with special emphasis on cell performance distribution,” Dissertation, RWTH Aachen; Shaker Verlag GmbH.

[80] M. Dubarry, N. Qin, and P. Brooker, “Calendar aging of commercial Li-ion cells of different chemistries – A review,” *Current Opinion in Electrochemistry*, vol. 9, pp. 106–113, 2018, doi: 10.1016/j.coelec.2018.05.023.

[81] M. Lewerenz, G. Fuchs, L. Becker, and D. U. Sauer, “Irreversible calendar aging and quantification of the reversible capacity loss caused by anode overhang,” *Journal of Energy Storage*, vol. 18, pp. 149–159, 2018, doi: 10.1016/j.est.2018.04.029.

[82] M. Lewerenz, J. Münnix, J. Schmalstieg, S. Käbitz, M. Knips, and D. U. Sauer, “Systematic aging of commercial LiFePO 4 |Graphite cylindrical cells including a theory explaining rise of capacity during aging,” *Journal of Power Sources*, vol. 345, pp. 254–263, 2017, doi: 10.1016/j.jpowsour.2017.01.133.

[83] G. Angenendt, S. Zurmühlen, J. Figgener, K.-P. Kairies, and D. U. Sauer, “Providing frequency control reserve with photovoltaic battery energy storage systems and power-to-heat coupling,” *Energy*, vol. 194, p. 116923, 2020, doi: 10.1016/j.energy.2020.116923.

[84] M. Ecker *et al.,* “Calendar and cycle life study of Li(NiMnCo)O2-based 18650 lithium-ion batteries,” *Journal of Power Sources*, vol. 248, pp. 839–851, 2014, doi: 10.1016/j.jpowsour.2013.09.143.

[85] S. Käbitz, *Investigation of the aging of lithium-ion batteries using electroanalysis and electrochemical impedance spectroscopy*: RWTH Aachen University, 2016.

[86] M. Lewerenz, A. Marongiu, A. Warnecke, and D. U. Sauer, “Differential voltage analysis as a tool for analyzing inhomogeneous aging: A case study for LiFePO4|Graphite cylindrical cells,” *Journal of Power Sources*, vol. 368, pp. 57–67, 2017, doi: 10.1016/j.jpowsour.2017.09.059.

[87] T. C. Bach *et al.,* “Nonlinear aging of cylindrical lithium-ion cells linked to heterogeneous compression,” *Journal of Energy Storage*, vol. 5, pp. 212–223, 2016, doi: 10.1016/j.est.2016.01.003.

[88] M. Lewerenz and D. U. Sauer, “Evaluation of cyclic aging tests of prismatic automotive LiNiMnCoO2-Graphite cells considering influence of homogeneity and anode overhang,” *Journal of Energy Storage*, vol. 18, pp. 421–434, 2018, doi: 10.1016/j.est.2018.06.003.

[89] E. Sarasketa-Zabala, I. Gandiaga, L. M. Rodriguez-Martinez, and I. Villarreal, “Calendar ageing analysis of a LiFePO 4 /graphite cell with dynamic model validations: Towards realistic lifetime predictions,” *Journal of Power Sources*, vol. 272, pp. 45–57, 2014, doi: 10.1016/j.jpowsour.2014.08.051.

[90] Y. K. Lee, J. Park, and W. Lu, “A Comprehensive Study of Manganese Deposition and Side Reactions in Li-Ion Battery Electrodes,” *J. Electrochem. Soc.*, vol. 164, no. 12, A2812-A2822, 2017, doi: 10.1149/2.1851712jes.

[91] X. Wang, Y. Sone, G. Segami, H. Naito, C. Yamada, and K. Kibe, “Understanding Volume Change in Lithium-Ion Cells during Charging and Discharging Using In Situ Measurements,” *J. Electrochem. Soc.*, vol. 154, no. 1, A14, 2007, doi: 10.1149/1.2386933.

[92] N. Nitta, F. Wu, J. T. Lee, and G. Yushin, “Li-ion battery materials: present and future,” *Materials Today*, vol. 18, no. 5, pp. 252–264, 2015, doi: 10.1016/j.mattod.2014.10.040.

[93] S. Schweidler, L. de Biasi, A. Schiele, P. Hartmann, T. Brezesinski, and J. Janek, “Volume Changes of Graphite Anodes Revisited: A Combined Operando X-ray Diffraction and In

Situ Pressure Analysis Study," *J. Phys. Chem. C*, vol. 122, no. 16, pp. 8829–8835, 2018, doi: 10.1021/acs.jpcc.8b01873.

[94] J. Vetter *et al.,* "Ageing mechanisms in lithium-ion batteries," *Journal of Power Sources*, vol. 147, 1-2, pp. 269–281, 2005, doi: 10.1016/j.jpowsour.2005.01.006.

[95] J. C. Burns *et al.,* "Predicting and Extending the Lifetime of Li-Ion Batteries," *J. Electrochem. Soc.*, vol. 160, no. 9, A1451-A1456, 2013, doi: 10.1149/2.060309jes.

[96] S. F. Schuster *et al.,* "Nonlinear aging characteristics of lithium-ion cells under different operational conditions," *Journal of Energy Storage*, vol. 1, pp. 44–53, 2015, doi: 10.1016/j.est.2015.05.003.

[97] D. Magnor, J. B. Gerschler, M. Ecker, P. Merk, and D. U. Sauer, "Concept of a battery aging model for lithium-ion batteries considering the lifetime dependency on the operation strategy," *24th European Photovoltaic Solar Energy Conference*, 2009.

[98] I. Rychlik, "A new definition of the rainflow cycle counting method," *International Journal of Fatigue*, vol. 9, no. 2, pp. 119–121, 1987, doi: 10.1016/0142-1123(87)90054-5.

[99] C. AMZALLAG, J. GEREY, J. ROBERT, and J. BAHUAUD, "Standardization of the rainflow counting method for fatigue analysis," *International Journal of Fatigue*, vol. 16, no. 4, pp. 287–293, 1994, doi: 10.1016/0142-1123(94)90343-3.

[100] M. Hess, *Kinetics and stage transitions of graphite for lithium-ion batteries*: ETH Zurich, 2013.

[101] C. Sole, N. E. Drewett, and L. J. Hardwick, "In situ Raman study of lithium-ion intercalation into microcrystalline graphite," *Faraday discussions*, vol. 172, pp. 223–237, 2014, doi: 10.1039/c4fd00079j.

[102] G. Schmuelling *et al.,* "X-ray diffraction studies of the electrochemical intercalation of bis(trifluoromethanesulfonyl)imide anions into graphite for dual-ion cells," *Journal of Power Sources*, vol. 239, pp. 563–571, 2013, doi: 10.1016/j.jpowsour.2013.03.064.

[103] J. Xu *et al.,* "Recent Progress in Graphite Intercalation Compounds for Rechargeable Metal (Li, Na, K, Al)-Ion Batteries," *Advanced science (Weinheim, Baden-Wurttemberg, Germany)*, vol. 4, no. 10, p. 1700146, 2017, doi: 10.1002/advs.201700146.

[104] Y. Shao-Horn, "Understanding Phase Transformations in Lithium Battery Materials by Transmission Electron Microscopy," in *Lithium batteries: Science and technology*, G. Nazri and G. Pistoia, Eds., New York: Springer, 2009, pp. 478–506.

[105] A. J. Warnecke, *Degradation Mechanisms in NMC-Based Lithium-Ion Batteries*: RWTH Aachen University, 2017.

[106] F. E. Hust, "Physikalisch-chemisch motivierte Parametrierung und Modellierung von echtzeitfähigen Lithium-Ionen Batteriemodellen - eine Fallstudie zur Tesla Model S Batterie," 2018.

[107] M. Ecker, P. Shafiei Sabet, and D. U. Sauer, "Influence of operational condition on lithium plating for commercial lithium-ion batteries – Electrochemical experiments and post-mortem-analysis," *Applied Energy*, vol. 206, pp. 934–946, 2017, doi: 10.1016/j.apenergy.2017.08.034.

[108] M. Lewerenz, A. Warnecke, and D. U. Sauer, “Post-mortem analysis on LiFePO 4 |Graphite cells describing the evolution & composition of covering layer on anode and their impact on cell performance,” *Journal of Power Sources*, vol. 369, pp. 122–132, 2017, doi: 10.1016/j.jpowsour.2017.10.003.

[109] K. Schwamberger, “Modellbildung,” in *Fortschrittberichte VDI*, D.-I. K. Schwamberger, Ed.: VDI Verlag, 1991, pp. 5–66.

[110] C. Wemhöner, B. Hafner, and K. Schwarzer, *Simulation of Solar Thermal Systemswith Carnot Blockset in the Environment Matlab Simulink.* [Online]. Available: http://ptp.irb.hr/upload/mape/solari/11_Carsten_Wemhoener_SIMULATION_OF_SOLAR_THERMAL_SYSTEMS_WITH.pdf (accessed: Apr. 8 2020).

[111] Viessmann, *Datenblatt VITOCAL 200-S*, 2017.

[112] G. Faure, *Validation of a new heat pump model for Carnot library*: R&D Viessmann Faulquemont Viessmann Werke, 2010.

[113] J. Bonin, “Leistung einer Wärmepumpe,” in *Handbuch Wärmepumpe*, J. Bonin, Ed.: Beuth, 2012, pp. 47–66.

[114] S. V. Patankar, *Numerical heat transfer and fluid flow*. New York: Hemisphere Publ. Co, 1980.

[115] S. Sobotta, “Planung einer Wärmepumpenanlage,” in *Praxis Wärmepumpe - Technik, Planung, Installation*, S. Sobotta and DIN, Eds.: Beuth Verlag, 2015, p. 78.

[116] Schindler und Hofmann, *kamdi24 Kamin Shop - Kamin Fachhandel.* [Online]. Available: https://www.kamdi24.de/Pufferspeicher-300-L.html (accessed: Apr. 8 2020).

[117] Prof. Dr.-Ing. Alexander Floß, Dipl. Ing. Christian Dietrich, *Optimierte Integration von Pufferspeichern.* [Online]. Available: http://www.hartmann-energietechnik.de/images/hartmann-energietechnik/speicher/speicherkapazitaet-von-pufferspeichern.pdf (accessed: Dec. 7 2018).

[118] B. R. Alfred Paulisch, “Wärmespeicher,” in *Heizen mit Umgebungsenergie*, B. R. Alfred Paulisch, Ed.: Deutscher Consulting Verlag, 1980, pp. 69–75.

[119] Schindler und Hofmann, *Kamin Shop - Kamin Fachhandel.* [Online]. Available: https://www.kamdi24.de/Brauchwasserspeicher-300-L-mit-1x-Waermetauscher.html (accessed: Apr. 8 2020).

[120] Sandra Lohmann, *Einführung in die Software MATLAB® - Simulink®und die Toolboxen CARNOT und Stateflow® zur Simulation von Gebäude- und Heizungstechnik.* [Online]. Available: https://fh-aachen.sciebo.de/index.php/s/0hxub0iIJrui3ED (accessed: Apr. 8 2020).

[121] Bundesministerium für Umwelt, Naturschutz, Bau und Reaktorsicherheit and Energie, *Verordnung über energiesparenden Wärmeschutz und energiesparende Anlagentechnik bei Gebäuden: Energieeinsparverordnung (EnEV 2013)*, 2013.

[122] Glück B., “Wärmeübergangskoeffizienten an thermisch aktiven Bauteiloberflächen und der Übergang zu Basiskennlinien für die Wärmestromdichte,” *GI Gesundheits-Ingenieur*, vol. 128, pp. 1–10, 2007.

[123] *Wärmeschutz und Energieeinsparung in Gebäuden Teil 2: Mindestanforderungen an den Wärmeschutz (DIN 4108-2)*, 2013.

[124] U. Jordan and K. Vajen, *DHWcalc: Program to generation domestic hot water profiles with statistical means for user defined conditions: Proc. ISES Solar World Congress, Orlando (US), 2005.* [Online]. Available: http://citeseerx.ist.psu.edu/viewdoc/download?doi=10.1.1.560.350&rep=rep1&type=pdf (accessed: Apr. 8 2020).

[125] W. Weiss, Ed., *Solar heating systems for houses: A design handbook for solar combisystems ; [Task 26 "Solar combisystems" of the] IEA International Energy Agency Solar Heating and Cooling Programme*. London: James & James, 2003.

[126] C. Curry, *Lithium-ion Battery Costs and Market.* [Online]. Available: https://data.bloomberglp.com/bnef/sites/14/2017/07/BNEF-Lithium-ion-battery-costs-and-market.pdf (accessed: Apr. 8 2020).

[127] K. Branker, M.J.M. Pathak, and J. M. Pearce, "A Review of Solar Photovoltaic Levelized Cost of Electricity," *Renewable and Sustainable Energy Reviews*, vol. 15, no. 9, pp. 4470–4482, 2011, doi: 10.1016/j.rser.2011.07.104.

[128] Mark Bost, Dr. Bernd Hirschl, and Dr. Astrid Aretz, *Effekte von Eigenverbrauch und Netzparität bei der Photovoltaik: Beginn der dezentralen Energierevolution oder Nischeneffekt*, 2011.

[129] Kreditanstalt für Wiederaufbau KfW, *Merkblatt Erneuerbare Energien KfW-Programm Erneuerbare Energien "Speicher".* [Online]. Available: https://www.kfw.de/Download-Center/F%C3%B6rderprogramme-(Inlandsf%C3%B6rderung)/PDF-Dokumente/6000002700_M_275_Speicher.pdf (accessed: Apr. 8 2020).

[130] EEG 2014, *Gesetze im Internet.* [Online]. Available: http://www.gesetze-im-internet.de/eeg_2014/ (accessed: Apr. 8 2020).

[131] Bundesnetzagentur, "Monitoringbericht 2017," Bundesnetzagentur für Elektrizität, Gas, Telekommunikation, Post und Eisenbahnen, Bonn, Nov. 2017.

[132] Fraunhofer ISE, *Monatliche Börsenstrompreise in Deutschland.* [Online]. Available: https://www.energy-charts.de/price_avg_de.htm (accessed: Apr. 8 2020).

[133] G. Angenendt, S. Zurmühlen, H. Axelsen, and D. U. Sauer, "Comparison of different operation strategies for PV battery home storage systems including forecast-based operation strategies," *Applied Energy*, vol. 229, pp. 884–899, 2018, doi: 10.1016/j.apenergy.2018.08.058.

[134] *Grundfos Energiesparumwälzpumpe Alpha 2 25-40 (Förderhöhe: 4 m, Energieeffizienzklasse: A, 3 - 18 W, Einbaulänge: 180 mm) | BAUHAUS.* [Online]. Available: https://www.bauhaus.info/heizungspumpen/grundfos-alpha-25-40180-heizungspumpe-mdaemmung/p/22326454?pla_prpaid=384559711812&pla_adgrid=43160521564&pla_campid=225981541&pla_prch=online&pla_prid=22326454&cid=PSMGoo225981541_43160521564&pla_adt=pla (accessed: Dec. 14 2017).

[135] *Viessmann Elektro-Heizeinsatz-EHE.* [Online]. Available: https://www.alternative-haustechnik.de/viessmann-elektro-heizeinsatz-ehe?number=AH-Z012684&gclid=EAIaIQobChMIpOKi4eSJ2AIV8DLTCh2TvgqKEAQYASABEgKFsPD_BwE (accessed: Apr. 8 2020).

[136] *Technische Alternative UDV-3/4" Universal Dreiwegeventil bis 100°C, 3/4", 01/UDV (Regelungstechnik) - Heizung und Solar zu Discountpreisen.* [Online]. Available: https://www.heizungsdiscount24.de/regelungstechnik/technische-alternative-udv-34-universal-dreiwegeventil-bis-100c-34-01udv.html (accessed: Apr. 8 2020).

[137] BDEW, *BDEW-Heizkostenvergleich Altbau 2017.* [Online]. Available: https://www.bdew.de/energie/bdew-heizkostenvergleich-altbau-2017/ (accessed: Apr. 8 2020).

[138] M. Kaltschmitt, W. Streicher, and A. Wiese, Eds., *Erneuerbare Energien: Systemtechnik, Wirtschaftlichkeit, Umweltaspekte,* 5th ed. Berlin: Springer Vieweg, 2014.

[139] VDI-Fachbereich Technische Gebäudeausrüstung, *Wirtschaftlichkeit gebäudetechnischer Anlagen - Grundlagen und Kostenberechnung (VDI 2067).* [Online]. Available: https://www.vdi.de/richtlinien/details/vdi-2067-blatt-1-wirtschaftlichkeit-gebaeudetechnischer-anlagen-grundlagen-und-kostenberechnung-1 (accessed: Apr. 8 2020).

[140] G. Angenendt, S. Zurmühlen, F. Rücker, H. Axelsen, and D. U. Sauer, "Optimization and operation of integrated homes with photovoltaic battery energy storage systems and power-to-heat coupling," *Energy Conversion and Management: X*, vol. 1, p. 100005, 2019, doi: 10.1016/j.ecmx.2019.100005.

[141] D. Magnor and D. U. Sauer, "Optimization of PV Battery Systems Using Genetic Algorithms," *Energy Procedia*, no. 99, pp. 332–340, 2016.

[142] Alibaba.com, *Zhongxi Electronics (Shenzhen) Co., Ltd.: Original Purple Lg Mf1 Battery Icr18650 Mf1 3.7v 2200mah 18650 Li-ion Cell for E-cig/Self Balance Scooter.* [Online]. Available: https://www.alibaba.com/product-detail/Original-Purple-Lg-Mf1-Battery-Icr18650_60517317202.html (accessed: Apr. 8 2020).

[143] J. Li and M. A. Danzer, "Optimal charge control strategies for stationary photovoltaic battery systems," *Journal of Power Sources*, 01 Jan., pp. 365–373, 2014.

[144] J. Weniger, J. Bergner, T. Tjaden, and V. Quaschning, "Effekte der 50%-Einspeisebegrenzung des KfW-Förderprogramms für Photovoltaik-Speichersysteme," Hochschule für Technik und Wirtschaft HTW Berlin, Berlin, Jan. 2016.

[145] J. Moshövel *et al.,* "Analysis of the maximal possible grid relief from PV-peak-power impacts by using storage systems for increased self-consumption," *Applied Energy, Vol. 137, No. 1*, pp. 567–575, 2015.

[146] J. Munkhammar, P. Grahn, and J. Widén, "Quantifying self-consumption of on-site photovoltaic power generation in households with electric vehicle home charging," *Solar Energy*, vol. 97, pp. 208–216, 2013, doi: 10.1016/j.solener.2013.08.015.

[147] M. Osawa *et al.,* "Increase the rate of utilization of Residential photovoltaic generation by EV charge-discharge control," in *2012 IEEE Innovative Smart Grid Technologies - Asia (ISGT Asia)*, Tianjin, China, pp. 1–6.

[148] M. Schreiber and P. Hochloff, "Capacity-dependent tariffs and residential energy management for photovoltaic storage systems," in *2013 IEEE Power & Energy Society General Meeting*, Vancouver, BC, pp. 1–5.

[149] E. L. Ratnam, S. R. Weller, and C. M. Kellett, “An optimization-based approach to scheduling residential battery storage with solar PV: Assessing customer benefit,” *Renewable Energy*, vol. 75, pp. 123–134, 2015, doi: 10.1016/j.renene.2014.09.008.

[150] A. Sani Hassan, L. Cipcigan, and N. Jenkins, “Optimal battery storage operation for PV systems with tariff incentives,” *Applied Energy*, vol. 203, pp. 422–441, 2017, doi: 10.1016/j.apenergy.2017.06.043.

[151] A. Zeh and R. Witzmann, “Operational strategies for battery storage systems in low-voltage distribution grids to limit the feed-in power of roof-mounted solar power systems,” *Energy Procedia, vol. 46*, pp. 114–123, 2014.

[152] M. Schneider et al., “Effects of operational strategies on performance and costs of electric energy storage systems,” *Energy Procedia, vol. 46*, pp. 271–280, 2014.

[153] E. Waffenschmidt, “Primary control with batteries,” in *2016 International Energy and Sustainability Conference (IESC)*, Köln, Deutschland, Jun. 2016, pp. 1–5.

[154] F. R. Segundo Sevilla, D. Parra, N. Wyrsch, M. K. Patel, F. Kienzle, and P. Korba, “Techno-economic analysis of battery storage and curtailment in a distribution grid with high PV penetration,” *Journal of Energy Storage*, vol. 17, pp. 73–83, 2018, doi: 10.1016/j.est.2018.02.001.

[155] J. Weniger, J. Bergner, T. Tjaden, and V. Quaschning, “Dezentrale Solarstromspeicher für die Energiewende,” Hochschule für Technik und Wirtschaft HTW Berlin, Jun. 2015.

[156] M. Resch, B. Ramadhani, J. Bühler, and A. Sumper, “Comparison of Control Strategies of Residential PV Storage Systems,” in *9th International Renewable Energy Storage Conference and Exhibition*, 2015.

[157] A.-L. Klingler and L. Teichtmann, “Impacts of a forecast-based operation strategy for grid-connected PV storage systems on profitability and the energy system,” *Solar Energy Volume 158*, pp. 861–868, 2017.

[158] H. P. A. P. Jayawardana, A. P. Agalgaonkar, and D. A. Robinson, “Novel control strategy for operation of energy storage in a renewable energy-based microgrid,” in *2015 Australasian Universities Power Engineering Conference (AUPEC)*, Wollongong, Australia, pp. 1–6.

[159] D. Berner, *Netzdienliche Integration von Photovoltaik-Batteriesystemen: Entwicklung eines Algorithmus und Potenzialanalyse auf Grundlage einer Modellbildung in Matlab/Simulink.* [Online]. Available: https://www.haw-hamburg.de/fileadmin/user_upload/Forschung/CC4E/Projekte/weitere_Energiethemen/Intelligente_Netze/Abschlussarbeiten/2014_02_Masterthesis_David_Berner.pdf (accessed: Apr. 8 2020).

[160] J. Moshövel et al, “Analyse des wirtschaftlichen, technischen und ökologischen Nutzens von PV-Speichern,” Gemeinsamer Ergebnisbericht für das Projekt PV-Nutzen, Aachen, Dec. 2015.

[161] J. Mähliß, *Gefährdungspotenzial von Li-Ionen-Zellen.* [Online]. Available: https://www.elektroniknet.de/elektronik/power/gefaehrdungspotenzial-von-li-ionen-zellen-92479.html (accessed: Apr. 8 2020).

[162] *Plarad.de.* [Online]. Available: http://www.plarad.de/fileadmin/downloads/FAQ_Fragen%20und%20Antworten%20zur%20Akkupflege%20DA1_de_0216.pdf (accessed: Sep. 28 2016).

[163] G. Angenendt, S. Zurmühlen, R. Mir-Montazeri, D. Magnor, and D. U. Sauer, "Enhancing Battery Lifetime in PV Battery Home Storage System Using Forecast Based Operating Strategies," *Energy Procedia*, vol. 99, no. 99, pp. 80–88, 2016, doi: 10.1016/j.egypro.2016.10.100.

[164] G. Angenendt, S. Zurmühlen, C. Chen, D. Magnor, and D. U. Sauer, "Reducing Cut-Off Energy of PV Home Storage Systems by Using Forecast-Based Operation Strategies," in *Tagungsband der '11th International Renewable Energy Conference (IRES 2017)'*, Düsseldorf, Mar. 2017.

[165] M. Aneke and M. Wang, "Energy storage technologies and real life applications – A state of the art review," *Applied Energy*, vol. 179, pp. 350–377, 2016, doi: 10.1016/j.apenergy.2016.06.097.

[166] Y. Yang, S. Bremner, C. Menictas, and M. Kay, "Battery energy storage system size determination in renewable energy systems: A review," *Renewable and Sustainable Energy Reviews*, vol. 91, pp. 109–125, 2018, doi: 10.1016/j.rser.2018.03.047.

[167] D. Fischer et al., "Smart Meter Enabled Control for Variable Speed Heat Pumps to Increase PV Self-Consumption," in *International Congress on Refrigeration Volume: 24*, 2015.

[168] J. Binder et al., "Increasing PV self-consumption, domestic energy autonomy and grid compatibility of PV systems using heat-pumps, thermal storage and battery storage," in *27th European Photovoltaic Solar Energy Conference and Exhibition*, 2012.

[169] A.-L. Klingler, "The effect of electric vehicles and heat pumps on the market potential of PV + battery systems," *Energy*, vol. 161, pp. 1064–1073, 2018, doi: 10.1016/j.energy.2018.07.210.

[170] M. Battaglia et al., "Increased self-consumption and grid flexibility of PV and heat pump systems with thermal and electrical storage," *Energy Procedia 135*, pp. 358–366, 2017.

[171] T. Tjaden et al., "Einsatz von PV-Systemen mit Wärmepumpen und Batteriespeichern zur Erhöhung des Autarkiegrades in Einfamilienhaushalten," in *30. Symposium Photovoltaische Solarenergie*, 2015.

[172] L. Schibuola et al., "Demand response management by means of heat pumps controlled via real time pricing," *Energy and Buildings 90*, pp. 15–28, 2015.

[173] J. Salpakari and P. Lund, "Optimal and rule-based control strategies for energy flexibility in buildings with PV," *Applied Energy*, vol. 161, pp. 425–436, 2016, doi: 10.1016/j.apenergy.2015.10.036.

[174] C. Williams, J. Binder, M. Danzer, F. Sehnke, and M. Felder, "Battery Charge Control Schemes for Increased Grid Compatibility of Decentralised PV Systems," in *28th European Photovoltaic Solar Energy Conference*, 2013.

[175] B. Baeten, F. Rogiers, and L. Helsen, “Reduction of heat pump induced peak electricity use and required generation capacity through thermal energy storage and demand response,” *Applied Energy*, vol. 195, pp. 184–195, 2017, doi: 10.1016/j.apenergy.2017.03.055.

[176] A. L. M. Mufaris and J. Baba, “Scheduled Operation of Heat Pump Water Heater for Voltage Control in Distribution System with Large Penetration of PV Systems,” in *2013 IEEE Green Technologies Conference (GreenTech 2013)*, Denver, CO, pp. 85–92.

[177] M. Brunner, K. Rudion, and S. Tenbohlen, “PV curtailment reduction with smart homes and heat pumps,” in *2016 IEEE International Energy Conference (ENERGYCON)*, Leuven, Belgium, pp. 1–6.

[178] T. Beck, H. Kondziella, G. Huard, and T. Bruckner, “Optimal operation, configuration and sizing of generation and storage technologies for residential heat pump systems in the spotlight of self-consumption of photovoltaic electricity,” *Applied Energy*, no. 188, pp. 604–619, 2017.

[179] T. Ikegami, K. Kataoka, Y. Iwafune, and K. Ogimoto, “Optimal demand controls for a heat pump water heater under different objective functions,” *IEEE International Conference on Power System Technology (POWERCON)*, pp. 1–6, 2012.

[180] *PV Magazine: Produktdatenbank Batteriespeichersysteme für Photovoltaikanlagen 2016.* [Online]. Available: http://www.pv-magazine.de/marktuebersichten/batteriespeicher/speicher-2016/ (accessed: Apr. 8 2020).

[181] Saft, *High energy lithium-ion cell VL 45 E cell.* [Online]. Available: http://www.houseofbatteries.com/documents/VL45E.pdf (accessed: Apr. 8 2020).

[182] G. Angenendt, S. Zurmühlen, H. Axelsen, and D. U. Sauer, “Prognosis-Based Operating Strategies for Smart Homes with Power-to-Heat Applications,” *Energy Procedia*, vol. 155, pp. 136–148, 2018, doi: 10.1016/j.egypro.2018.11.061.

[183] SOLARWATT GmbH, *Suchergebnisse Webergebnisse Intelligentes Ladeverhalten verlängert Lebensdauer des MyReserve.* [Online]. Available: https://www.solarwatt.de/stromspeicher/myreserve/ladestrategie (accessed: Apr. 8 2020).

[184] W. L. Schram, I. Lampropoulos, and W. G.J.H.M. van Sark, “Photovoltaic systems coupled with batteries that are optimally sized for household self-consumption: Assessment of peak shaving potential,” *Applied Energy*, vol. 223, pp. 69–81, 2018, doi: 10.1016/j.apenergy.2018.04.023.

[185] X. Wu, X. Hu, X. Yin, C. Zhang, and S. Qian, “Optimal battery sizing of smart home via convex programming,” *Energy*, vol. 140, pp. 444–453, 2017, doi: 10.1016/j.energy.2017.08.097.

[186] B. Claessens, K. De Brabandere, G. Mulder, and F. De Ridder, “Break-even analysis of PV-battery self-consumption systems,” *Proceedings of the 5th International Renewable Energy Storage Conference Berlin*, 2010.

[187] O. Talent and H. Du, “Optimal sizing and energy scheduling of photovoltaic-battery systems under different tariff structures,” *Renewable Energy*, vol. 129, pp. 513–526, 2018, doi: 10.1016/j.renene.2018.06.016.

[188] T. Beck, H. Kondziella, G. Huard, and T. Bruckner, “Assessing the influence of the temporal resolution of electrical load and PV generation profiles on self-consumption and sizing of PV-battery systems,” *Applied Energy*, no. 173, pp. 331–342, 2016.

[189] T. H. Pham, F. Wurtz, and S. Bacha, “Optimal operation of a PV based multi-source system and energy management for household application,” *IEEE International Conference on Industrial Technology*, pp. 10–13, 2009.

[190] C.-T. Pham and D. Månsson, “Optimal energy storage sizing using equivalent circuit modelling for prosumer applications (Part II),” *Journal of Energy Storage*, vol. 18, pp. 1–15, 2018, doi: 10.1016/j.est.2018.04.015.

[191] D. Fischer, K. B. Lindberg, H. Madani, and C. Wittwer, “Impact of PV and variable prices on optimal system sizing for heat pumps and thermal storage,” *Energy and Buildings*, vol. 128, pp. 723–733, 2016, doi: 10.1016/j.enbuild.2016.07.008.

[192] M. Kharseh and H. Wallbaum, “The effect of different working parameters on the optimal size of a battery for grid-connected PV systems,” *Energy Procedia*, vol. 122, pp. 595–600, 2017, doi: 10.1016/j.egypro.2017.07.355.

[193] L. Zhou, Y. Zhang, X. Lin, C. Li, Z. Cai, and P. Yang, “Optimal sizing of PV and BESS for a smart household considering different price mechanisms,” *IEEE Access*, p. 1, 2018, doi: 10.1109/ACCESS.2018.2845900.

[194] J. van Appen, *Sizing and operation of residential photovoltaic systems in combination with battery storage systems and heat pumps - Multi-actor optimization models and case studies*, 2018.

[195] J. von Appen, “Incentive Design, Sizing and Grid Integration of Residential PV Systems with Heat Pumps and Battery Storage Systems,” in *2018 15th International Conference on the European Energy Market (EEM)*, Lodz, pp. 1–5.

[196] T. Weise, *Global Optimization Algorithms: - Theory and Application -.* [Online]. Available: http://www.it-weise.de/projects/book.pdf (accessed: Aug. 16 2018).

[197] A. Auger and N. Hansen, “Evolution Strategies and Covariance Matrix Adaptation,”

[198] *The CMA Evolution Strategy.* [Online]. Available: http://cma.gforge.inria.fr/index.html (accessed: Aug. 21 2018).

[199] N. Hansen, A. Ostermeier, and and A. Gawelczyk, “On the Adaptation of Arbitrary Normal Mutation Distributions in Evolution Strategies: The Generating Set Adaptation,” *Proceedings of the 6th International Conference on Genetic Algorithms*, pp. 57–64, 1995. [Online]. Available: http://www.cmap.polytechnique.fr/~nikolaus.hansen/GSAES.pdf

[200] c. Busser, “„GENESYS“ Genetische Optimierung eines Europäischen Energieversorgungssystems: Optimierungsmethodik,” Dec. 6 2013.

[201] N. Hansen and A. Ostermeier, “Adapting arbitrary normal mutation distributions in evolution strategies: the covariance matrix adaptation,” in *IEEE International Conference on Evolutionary Computation*, Nagoya, Japan, May. 1996, pp. 312–317.

[202] J. D. Mondol, Y. G. Yohanis, and B. Norton, “Optimal sizing of array and inverter for grid-connected photovoltaic systems,” *Solar Energy*, vol. 80, no. 12, pp. 1517–1539, 2006, doi: 10.1016/j.solener.2006.01.006.

[203] E. Hervas-Blasco, M. Pitarch, E. Navarro-Peris, and J. M. Corberán, “Optimal sizing of a heat pump booster for sanitary hot water production to maximize benefit for the substitution of gas boilers,” *Energy*, vol. 127, pp. 558–570, 2017, doi: 10.1016/j.energy.2017.03.131.

[204] M. Dongellini, V. Impala, and G. L. Morini, “Design rules for the optimal sizing of a hybrid heat pump system coupled to a residential building,” *16th International Conference on Sustainable Energy Technologies – SET 2017*, vol. 2017, 17th - 20th of Jul. 2017.

[205] M. Ghofrani, A. Arabali, and M. Ghayekhloo, “Optimal charging/discharging of grid-enabled electric vehicles for predictability enhancement of PV generation,” *Electric Power Systems Research*, vol. 117, pp. 134–142, 2014, doi: 10.1016/j.epsr.2014.08.007.

[206] R. Lamedica, S. Teodori, G. Carbone, and E. Santini, “An energy management software for smart buildings with V2G and BESS,” *Sustainable Cities and Society*, vol. 19, pp. 173–183, 2015, doi: 10.1016/j.scs.2015.08.003.

[207] G. Angenendt, S. Zurmühlen, H. Axelsen, and D. U. Sauer, “Optimization of component dimensioning for a combined heat and power system with special focus on PV generator size,” in *35th EU PVSEC Brüssel 2018.* [Online]. Available: https://www.eupvsec-proceedings.com/proceedings?paper=44793

[208] Deutscher Wetterdienst DWD, *Globalstrahlung in der Bundesrepublik Deutschland: Jahressummen.* [Online]. Available: https://www.dwd.de/DE/leistungen/solarenergie/lstrahlungskarten_su.html?nn=16102 (accessed: Apr. 8 2020).

[209] Gert Berckmans, Maarten Messagie, Jelle Smekens, Noshin Omar, Lieselot Vanhaverbeke, and Joeri Van Mierlo, “Cost Projection of State of the Art Lithium-IonBatteries for Electric Vehicles Up to 2030,” *Energies*, vol. 2017, 10, 1314.

[210] IRENA (2017), “Electricity Storage and Renewables: Costs and Markets to 2030,” Abu Dhabi, 2017.

[211] J. Badeda, “Flexibility options in electrical networks with high shares of fluctuating renewable energy systems,” Batterie Ingenieure, Sep. 2017.

[212] R. Martins, H. Hesse, J. Jungbauer, T. Vorbuchner, and P. Musilek, “Optimal Component Sizing for Peak Shaving in Battery Energy Storage System for Industrial Applications,” *Energies*, vol. 11, no. 8, p. 2048, 2018, doi: 10.3390/en11082048.

[213] Stefan Riedel and Hannes Weigt, *German Electricity Reserve Markets.* [Online]. Available: https://tu-dresden.de/bu/wirtschaft/ee2/ressourcen/dateien/dateien/ordner_publikationen/wp_em_20_riedel_weigt_Germany_reserve_markets.pdf?lang=de (accessed: Apr. 8 2020).

[214] Sebastian Just, *The German Market for System Reserve Capacity and Balancing Energy.* [Online]. Available: http://www.ewl.wiwi.uni-due.de/fileadmin/fileupload/BWL-ENERGIE/Arbeitspapiere/RePEc/pdf/wp1506_Just2015TheGermanMarketForSystemReserveCapacityAndBalancing.pdf (accessed: Apr. 8 2020).

[215] European Network Transmission System Operators for Electricity (ENTSO-E), *Continental Europe Operation Handbook.* [Online]. Available: https://www.entsoe.eu/

publications/system-operations-reports/operation-handbook/Pages/default.aspx (accessed: Apr. 8 2020).

[216] consentec, “Beschreibung von Regelleistungskonzepten und Regelleistungsmarkt: Studie im Auftrag der deutschen Übertragungsnetzbetreiber,” Auftraggeber: 50Hertz Transmission GmbH, Feb. 2014.

[217] California Independent System Operator Corporation, *Tariff Amendment to Implement Flexible Ramping Product.* [Online]. Available: http://www.caiso.com/Documents/Jun242016_TariffAmendment-FlexibleRampingProduct_ER16-2023.pdf (accessed: Apr. 8 2020).

[218] National Grid Electricity Transmission, *nationalgrid.* [Online]. Available: https://www.nationalgridet.com/ (accessed: Apr. 8 2020).

[219] KEMA Inc, *System Services International: Review.* [Online]. Available: http://www.eirgridgroup.com/site-files/library/EirGrid/System-Services-International-Review-KEMA.pdf (accessed: Apr. 8 2020).

[220] Michael Milligan, Pearl Donohoo, Debra Lew, Erik Ela, and Brendan Kirby, *Operating Reserves and Wind Power Integration: An International Comparison.* [Online]. Available: https://www.nrel.gov/docs/fy11osti/49019.pdf (accessed: Apr. 8 2020).

[221] A. Zeh, M. Müller, M. Naumann, H. Hesse, A. Jossen, and R. Witzmann, “Fundamentals of Using Battery Energy Storage Systems to Provide Primary Control Reserves in Germany,” *Batteries*, vol. 2, no. 3, p. 29, 2016, doi: 10.3390/batteries2030029.

[222] J. Fleer *et al.,* “Techno-economic evaluation of battery energy storage systems on the primary control reserve market under consideration of price trends and bidding strategies,” *Journal of Energy Storage*, vol. 17, pp. 345–356, 2018, doi: 10.1016/j.est.2018.03.008.

[223] 50hertz, Amprion, Tennet, and Transnet BW, *Präqualifikationsverfahren für Regelreserveanbieter(FCR, aFRR, mFRR)Präqualifikationsverfahren für Regelreserveanbieter (FCR, aFRR, mFRR) in Deutschland ("PQ-Bedingungen"): Stand: 23. Mai 2019* (accessed: Jun. 5 2019).

[224] Bundesnetzagentur (BNetzA), *Festlegung von Ausschreibungsbedingungen und Veröffentlichungspflichten für Sekundärregelung: BK6-158-019.* [Online]. Available: https://www.bundesnetzagentur.de/DE/Service-Funktionen/Beschlusskammern/1_GZ/BK6-GZ/2018/BK6-18-019/BK6-18-019_Beschluss_vom_08_05_2018.html (accessed: Apr. 8 2020).

[225] Florian Mayr and Stephanie Adam, *The German Secondary Control Reserve market: Will recent regulatory updates finally pave the way for energy storage?* [Online]. Available: https://www.apricum-group.com/german-secondary-control-reserve-market-will-recent-regulatory-updates-finally-pave-way-energy-storage/ (accessed: Apr. 8 2020).

[226] Elia.be, *Automatic Frequency Restoration Process (aFRR/R2).* [Online]. Available: https://www.elia.be/en/electricity-market-and-system/system-services/keeping-the-balance/afrr (accessed: Apr. 8 2020).

[227] TenneT Holding B.V., *Information on the International Expansion of the Grid Control Cooperation by Addition of the Dutch Control Block.* [Online]. Available: https://www.tennet.eu/fileadmin/user_upload/SO_NL/aFRR_-_Market_information_IGCC.pdf (accessed: Apr. 8 2020).

[228] Manuel Lösch, "Sekundärregelleistung: Preise, Abrufcharakteristika & Nachholmanagement für alternative SRL-Erbringer," Berlin, Jun. 30 2017.

[229] 50hertz, Amprion, Tennet, and Transnet BW, *Präqualifikationsverfahren für Regelreserveanbieter (FCR, aFRR, mFRR) in Deutschland ("PQ-Bedingungen").* [Online]. Available: https://www.regelleistung.net/ext/download/PQ_Bedingungen_FCR_aFRR_mFRR (accessed: Apr. 8 2020).

[230] Bundesnetzagentur BNetzA, "Beschluss: Festlegung zu Verfahren zur Ausschreibung von Regelenergie in Gestalt der Primärregelung," 2011.

[231] Deutsche Übertragungsnetzbetreiber, "Rahmenvertrag über die Vergabe von Aufträgen zur Erbringung der Regelenergieart Primärregelleistung," 2007.

[232] S. Gerhard and F. Halfmann, "Entwurf einer Betriebsstrategie für Batteriespeicher zur Teilnahme am Primärregelleistungsmarkt," *Energieversorgung und Integration von Speichern (NEIS 2014), Helmut-Schmidt-Universität*.

[233] R. Hollinger, L. M. Diazgranados, F. Braam, B. Engel, G. Bopp, and T. Erge, "Distributed solar battery systems providing primary control reserve," *IET Renewable Power Generation*, vol. 10, no. 1, pp. 63–70, 2016, doi: 10.1049/iet-rpg.2015.0147.

[234] R. Hollinger, L. M. Diazgranados, C. Wittwer, and B. Engel, "Optimal Provision of Primary Frequency Control with Battery Systems by Exploiting All Degrees of Freedom within Regulation," *Energy Procedia 99*, vol. 2016, pp. 204–214. [Online]. Available: http://dx.doi.org/10.1016/j.egypro.2016.10.111

[235] J. Fleer and P. Stenzel, "Impact analysis of different operation strategies for battery energy storage systems providing primary control reserve," *Journal of Energy Storage*, vol. 8, pp. 320–338, 2016, doi: 10.1016/j.est.2016.02.003.

[236] M. Koller, M. González Vayá, A. Chacko, T. Borsche, and A. Ulbig, "Primary control reserves provision with battery energy storage systems in the largest European ancillary services cooperation," in *Tagungsband der "CIGRE Session 2016"*, Paris, Frankreich, Aug. 2016.

[237] Deutsche Übertragungsnetzbetreiber, *Präqualifizierte Anbieter je Regelenergieart.* [Online]. Available: https://www.regelleistung.net/ext/download/anbieterliste (accessed: Apr. 8 2020).

[238] caterva GmbH, "Caterva-Energiemanagement kann virtuelle Speicherkraftwerke vollautomatisch im Intraday-Handel vermarkten: Presseinformation," Pullach bei München, Mar. 2016.

[239] S. P. Melo, U. Brand, T. Vogt, J. S. Telle, F. Schuldt, and K.v. Maydell, “Primary frequency control provided by hybrid battery storage and power-to-heat system,” *Applied Energy*, 233-234, pp. 220–231, 2019, doi: 10.1016/j.apenergy.2018.09.177.

[240] B. Feron and A. Monti, “Domestic Battery and Power-to-Heat Storage for Self-Consumption and Provision of Primary Control Reserve,” in *2018 Power Systems Computation Conference (PSCC)*, Dublin, Ireland, pp. 1–6.

[241] J. Jomaux, T. Mercier, and E. de Jaeger, “Provision of frequency containment reserves with batteries and power-to-heat,” in *2017 IEEE Manchester PowerTech*, Manchester, United Kingdom, pp. 1–6.

[242] G.B.M.A. Litjens, E. Worrell, and W.G.J.H.M. van Sark, “Economic benefits of combining self-consumption enhancement with frequency restoration reserves provision by photovoltaic-battery systems,” *Applied Energy*, vol. 223, pp. 172–187, 2018, doi: 10.1016/j.apenergy.2018.04.018.

[243] J. Engels, B. Claessens, and G. Deconinck, “Combined Stochastic Optimization of Frequency Control and Self-Consumption with a Battery,” *IEEE Trans. Smart Grid*, p. 1, 2017, doi: 10.1109/tsg.2017.2785040.

[244] Y. Shi, B. Xu, Di Wang, and B. Zhang, “Using Battery Storage for Peak Shaving and Frequency Regulation: Joint Optimization for Superlinear Gains,” *IEEE Trans. Power Syst.*, vol. 33, no. 3, pp. 2882–2894, 2018, doi: 10.1109/TPWRS.2017.2749512.

[245] P. E. Janßen, “Analyse eines Photovoltaik-Batteriesystems zur Bereitstellung von Primärregelleistung,” Masterarbeit, Hochschule für Angewandte Wissenschaften Hamburg, Hamburg, 2015. Accessed: Oct. 2 2017.

[246] C. Olk, D. U. Sauer, and M. Merten, “Bidding strategy for a battery storage in the German secondary balancing power market,” *Journal of Energy Storage*, vol. 21, pp. 787–800, 2019, doi: 10.1016/j.est.2019.01.019.

[247] J. Jargstorf and M. Wickert, “Offer of secondary reserve with a pool of electric vehicles on the German market,” *Energy Policy*, vol. 62, pp. 185–195, 2013, doi: 10.1016/j.enpol.2013.06.088.

[248] Bundesministerium für Umwelt, Naturschutz, Bau und Reaktorsicherheit BMUB, “Intelligente Netzanbindung von Elektrofahrzeugen zur Erbringung von Systemdienstleistungen INEES,” Jun. 2016.

[249] I. Staffell and M. Rustomji, “Maximising the value of electricity storage,” *Journal of Energy Storage*, vol. 8, pp. 212–225, 2016, doi: 10.1016/j.est.2016.08.010.

[250] David-Constantin Radu, *Strategies for Provision of Secondary Reserve Capacity to Balance Short-Term Fluctuations of Variable Renewable Energy.* [Online]. Available: https://kth.diva-portal.org/smash/get/diva2:1152864/FULLTEXT01.pdf (accessed: Apr. 8 2020).

[251] A. Zeh, M. Müller, H. Hesse, A. Jossen, and R. Witzmann, Eds., *Operating a Multitasking Stationary Battery Storage System for Providing Secondary Control Reserve on Low-Voltage Level*, Nov. 2015.

[252] A. Stephan, B. Battke, M. D. Beuse, J. H. Clausdeinken, and T. S. Schmidt, “Limiting the public cost of stationary battery deployment by combining applications,” *Nat Energy*, vol. 1, no. 7, p. 334, 2016, doi: 10.1038/nenergy.2016.79.

[253] Y. Zhang, P. E. Campana, Y. Yang, B. Stridh, A. Lundblad, and J. Yan, “Energy flexibility from the consumer: Integrating local electricity and heat supplies in a building,” *Applied Energy*, vol. 223, pp. 430–442, 2018, doi: 10.1016/j.apenergy.2018.04.041.

[254] D. Parra and M. K. Patel, “The nature of combining energy storage applications for residential battery technology,” *Applied Energy*, vol. 239, pp. 1343–1355, 2019, doi: 10.1016/j.apenergy.2019.01.218.

[255] G. Angenendt, M. Merten, S. Zurmühlen, and D. U. Sauer, “Evaluation of the effects of frequency restoration reserves market participation with photovoltaic battery energy storage systems and power-to-heat coupling,” *Applied Energy*, vol. 260, p. 114186, 2020, doi: 10.1016/j.apenergy.2019.114186.

[256] G. Angenendt, S. Zurmühlen, and D. U. Sauer, “Participating in the control reserve market with PV battery energy storage systems and power-to-heat application,” *Atlantis Highlights in Engineering*, vol. 2019, no. 4, pp. 52–58, 2019.

[257] 50hertz, Amprion, Tennet, and Transnet BW, “Eckpunkte und Freiheitsgrade bei Erbringung von Primärregelleistung: Leitfaden für Anbieter von Primärregelleistung,” Apr. 2014.

[258] A. Moser, *Stromerzeugung und -handel: Skriptum zur Vorlesung*. Aachen: RWTH Aachen, 2015.

[259] LG Chem, “Technical Information of ICR18650 MF1 (2150mAh),” May. 2012.

[260] Schindler+Hofmann, *Pufferspeicher: Puffer-, Kombi- und Hygienespeicher: Modelle, Daten, Masse.* [Online]. Available: http://www.schindler-hofmann.de/content/pdf/prospekte/S+H_Pufferspeicher+Kombispeicher.pdf (accessed: Apr. 8 2020).

[261] Jan Figgener *et al.,* “Wissenschaftliches Mess- und Evaluierungsprogramm Solaratromspeicher 2.0 Jahresbericht 2017,” Institut für Stromrichtertechnik und Elektrische Antriebe der RWTH Aachen, Aachen, Jan. 2017.

[262] I. Rutschmann, *Regelleistungsmodell von Caterva: „Für jedes Kilowatt Regelleistung 150 bis 160 Euro im Jahr“.* [Online]. Available: https://www.photovoltaikforum.com/magazin/praxis/regelleistungsmodell-von-caterva-fuer-jedes-kilowatt-regelleistung-150-bis-160-euro-im-jahr-4765/ (accessed: Apr. 8 2020).

[263] I. Rutschmann, *Regelleistung von gridX: Offen für gängige Speichersysteme.* [Online]. Available: https://www.photovoltaikforum.com/magazin/produkte/regelleistungsmodell-von-gridx-offen-fuer-gaengige-speichersysteme-4752/ (accessed: Apr. 8 2020).

[264] gridX GmbH, *gridBox - Energie Management.* [Online]. Available: https://gridx.ai/technology/gridbox/?lang=de (accessed: Apr. 8 2020).

[265] Bundesministerium der Justiz und für Verbraucherschutz BMJV, “Gesetz über den Messstellenbetrieb und die Datenkommunikationin intelligenten Energienetzen: Messstellenbetriebsgesetz - MsbG,” Aug. 2016.

[266] A. Jossen and W. Weydanz, *Moderne Akkumulatoren richtig einsetzen*. Leipheim und München: Reichardt, 2006.

[267] D. T. Magnor, *Global Optimization of Grid-connected PV Battery Systems Under Special Consideration of Battery Aging*: RWTH Aachen University, 2017.

[268] M. Olsson and L. Soder, “Modeling Real-Time Balancing Power Market Prices Using Combined SARIMA and Markov Processes,” *IEEE Trans. Power Syst.*, vol. 23, no. 2, pp. 443–450, 2008, doi: 10.1109/TPWRS.2008.920046.

[269] C. Olk, D. U. Sauer, and M. Merten, “Bidding strategy for a battery storage in the German secondary balancing power market,” *Journal of Energy Storage*, vol. 21, pp. 787–800, 2019, doi: 10.1016/j.est.2019.01.019.

[270] B. Lange, *Prognosen der zeitlich-räumlichen Variabilität von Erneuerbaren.* [Online]. Available: http://www.fvee.de/fileadmin/publikationen/Themenhefte/th2011-2/th2011_04_04.pdf (accessed: Apr. 8 2020).

10. Nomenclature

A	€/a	annuity
$\mathrm{A_{HP}}$	p.u.	heat pump power as a share of the maximum power
AC		alternating current
Ah	Ah	ampere hour
a_{cal}	p.u.	calendric aging parameter
a_{cyc}	p.u.	cycle aging parameter
a_{PCR}	p.u.	primary control reserve factor
a_w	p.u.	Wöhler parameter
aFRR		automatic frequency restoration reserve
b_{cyc}	p.u.	cycle aging parameter
b_w	p.u.	Wöhler parameter
BESS		battery energy storage system
BSRN		Baseline Surface Radiation Network
c	€/unit	specific costs
C	€	investment costs
c_{cal}	p.u.	calendric aging
c_{cyc}	p.u.	cycle aging
$\mathrm{c_F}$ c_F	$\mathrm{J/(g \cdot K)}$	heat capacity of fluid water
c_{sum}	p.u.	total aging
$cap_{battery}$	kWh	battery capacity
cap_{heat}	kWh	heat storage capacity
COP	p.u.	coefficient of performance, heat pump
CP		capacity price
CPE		Constant Phase Element
d	%	discount rate
DC		direct current
DHW		domestic hot water
DoD		depth of discharge
DSO		distribution system operator
E	kWh	Energy
E_a	p.u.	Arrhenius parameter
$E_{consumption\_night}$	kWh	energy consumption in the night
E_{cutoff}	kWh	cut-off energy[kWh]
E_{pv}	kWh	energy from PV power plant
E_t	kWh	electricity consumption in time period t
E/P	p.u.	energy to power ratio
$\mathrm{EE(P_i)}$	€	earnings based on the energy price bids
EirGrid		Electricity market operator Ireland

EP	€	energy price
ENTSO-E		European Network of Transmission System Operators for Electricity
EV		electric vehicles
F	$[\frac{\mathrm{A \cdot s}}{\mathrm{mol}}]$	Faraday constant
F_A		annuity factor
F_t	€	net present value of the fix costs in time period t
$f_{maintenance}$	%	annual maintenance cost relative to investment cost
FCR		frequency containment reserve
FFR		firm frequency response (UK)
FIT	$[\frac{€}{kWh}]$	feed-in tariff
FOS		forecast-based operation strategies
$\mathrm{G(P_i)}$		acceptance probability for one particular outcome
$\mathrm{H_t}$		heat consumption in t
HLD		homogeneity of the lithium distribution
HT		high tariff
i	%	interest rate
I_t	€	net present value of the investments in time period t
IÖW		Institut für Ökologische Wirtschaftsforschung
$k_{\mathrm{SoC_{avg}}}$		acceleration factor cycle aging
KfW		Kreditanstalt für Wiederaufbau (Reconstruction Credit Institute)
kWh		kilowatt hour
kWp		kilowatt peak
L	a	Lifetime
LAM		loss of active material
LCOEle	$[\frac{€}{\mathrm{kWh}}]$	levelized cost of electricity
LCOEnergy	$[\frac{€}{\mathrm{kWh}}]$	levelized cost of energy
LCOH	$[\frac{€}{\mathrm{kWh}}]$	levelized cost of heat
LFC		load frequency control
LLI		loss of lithium inventory
$\mathrm{m_F}$		mass flow
max SC		maximize self -consumption
$\mathrm{M(P_i)}$		earnings that could be achieved when trading on the intraday market.
mFRR		manual frequency restoration reserve
MCPP		Maximum capacity price paid
MPPT		Maximum power point tracker
N		number of equivalent full cycles
NMC		lithium nickel-manganese-cobalt oxide

NPV	€	net present value
NT		low tariff
OCV	V	open circuit voltage
P	kW	power
P_{cutoff}	kW	cut-off power
P_{Load}	kW	load household
P_{PV}	kW	PV feed-in power
$P_{SCR\ var,\max offer}$	kW	maximum SCR power offered, variable SCR offer
$P_{Residual}$	kW	residual load
P2H		power to heat
P-f		power- frequency
PCR		primary control reserve
PV		photovoltaic
$\mathrm{P(P_i)}$		earnings based on the SCR capacity price bids
r		interest rate
R_{ug}	$[\frac{\mathrm{J}}{\mathrm{K \cdot mol}}]$	universal gas constant
SARIMA		Seasonal Autoregressive Integrated Moving Average
SC		self-consumption
SCR		secondary control reserve
SEI		solid electrolyte interface
SoC		state of charge
SoC_{target}		target SoC at the end of the day
SoH		state of health
SONI		System Operator for Northern Ireland
SPF		Seasonal performance factor
SSR		self-sufficiency rate
Q		heat capacity
t_{calc}	a	calculation period for invest assessment
T_0	°C	nominal temperature
TCR		tertiary control reserve
TSO		transmission system operator
U_0	V	nominal voltage
V		volume
V_t	€	net present value of the variable costs in time period t
α		Tafel parameter
ρ		water density
η_{charge}		charging efficiency battery system
$\eta_{discharge}$		discharging efficiency battery system

11. Annex

11.1 Storage capacity of the building

Refers to section 3.3.4: Model of the building

		wall 1b	wall 1a	wall 2a	wall 2b	floor	ceiling
width	[m]	11.00	11.00	10.00	10.00	10.00	10.00
height/length	[m]	2.50	2.50	2.50	2.50	11.00	11.00
$A_{window/door}$	[m²]	4.68	6.11	0.00	0.00	0.00	0.00
net surface	[m²]	22.82	21.39	25.00	25.00	110.00	110.00
thickness	[m]	0.38	0.38	0.38	0.38	0.42	0.42
conductivity	[W/(m*K)]	0.79	0.79	0.79	0.79	0.81	0.81
effective thickness	[m]	0.10	0.10	0.10	0.10	0.10	0.10
density	[kg/m³]	1,800.00	1,800.00	1,800.00	1,800.00	1,830.00	1,830.00
spec. capacity	[J/(kg*K)]	1,008.00	1,008.00	1,008.00	1,008.00	1,008.00	1,008.00
capacity	[Wh/K]	1,150.26	1,077.98	1,260.00	1,260.00	5,636.40	5,636.40
Total capacity	[Wh/K]	16,021.03					

Annex Table 1: Calculation of the storage capacity of the modeled building. For the calculation, DIN V 4108-6 is used.

11.2 Detailed results sensitivity analysis

11.2.1 EV

Refers to section 5.4.1

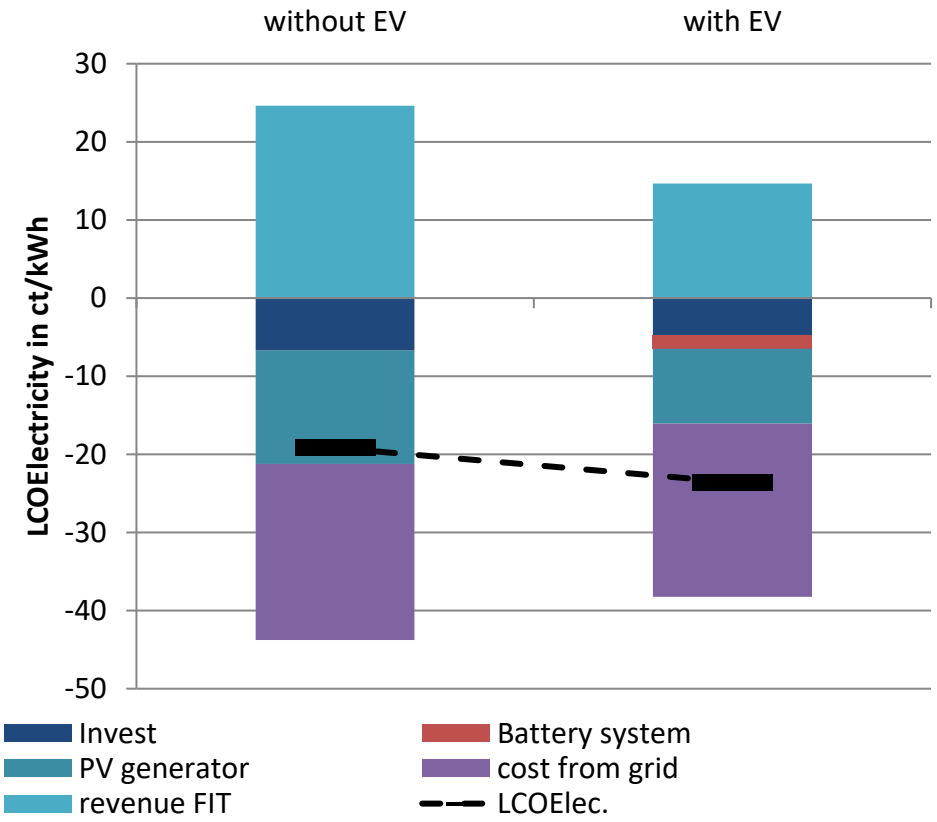

Annex Figure 122: Electricity cost of an optimized integrated home with a PV BESS and power-to-heat coupling without and with minding the load profile of the EV.

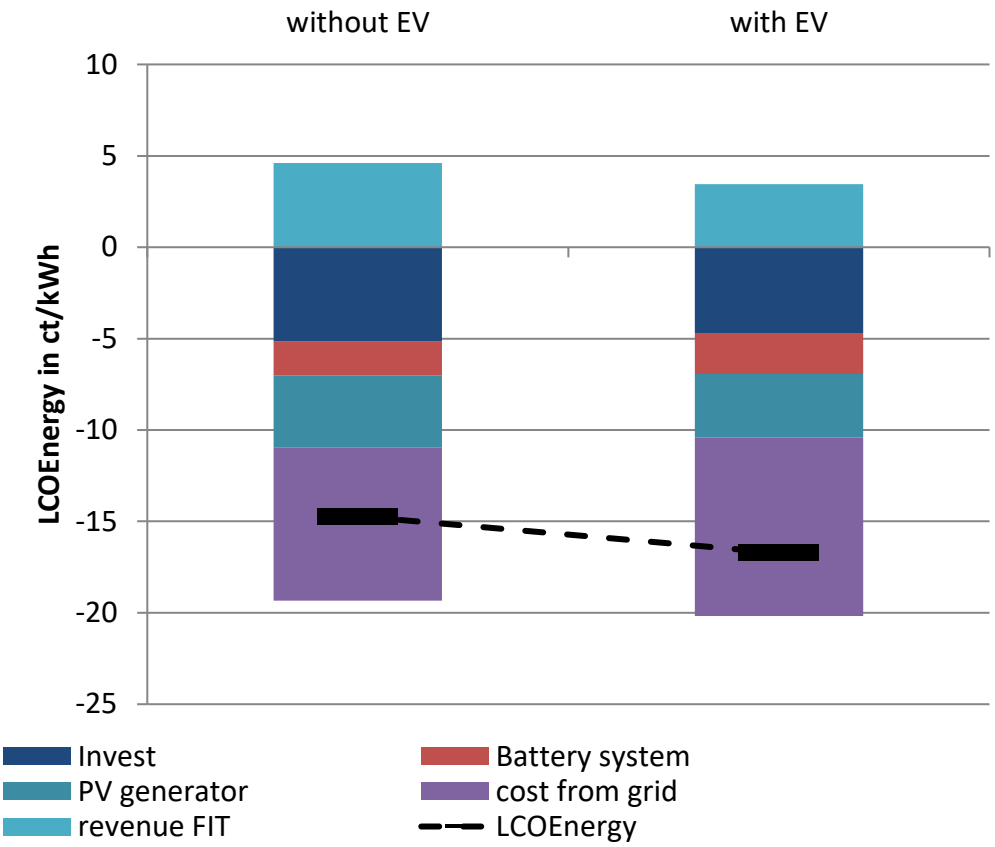

Annex Figure 123: Energy costs of an optimized integrated home with a PV BESS and heat power coupling without and with minding the load profile of the EV.

11.2.2 PV FIT

Refers to section 5.5.1

Parameter	Symbol	Elec basic	FIT 6ct	Heat basic	FIT 6ct	unit
PV-generator size	P_{PVPeak}	10	4.3	10	7.6	kWp
power MPP-tracker	P_{MPP}	7.9	3.4	7.8	6.0	kW
power inverter	$P_{Inverter}$	7.8	3.4	7.3	5.7	kW
power battery converter	$P_{BatConv}$	0	2.0	1.6	3.0	kW
capacity battery system	C_{BESS}	0	7.4	7.1	10.8	kWh
volume buffer storage	V_{buffer}			0.16	0.16	m³
volume DHW storage	V_{DHW}			0.11	0.11	m³
thermal power heat pump	$P_{HP,th}$			2.8	2.7	kWth
max. temp. buffer storage	$T_{buffer,max}$			42	40.6	°C
Spread buffer storage	$T_{buffer,spread}$		-		-	°C
max. temp. DHW storage	$T_{DHW,max}$			48	47.6	°C
Spread DHW storage	$T_{DHW,spread}$		-		-	°C

Annex Table 2: Optimum set of parameters found by the optimization algorithm for the "basic operation strategy scenario" in dependency of the feed-in tariffs (FIT) for PV generated energy.

11.2.3 Radiation

Refers to section 5.6

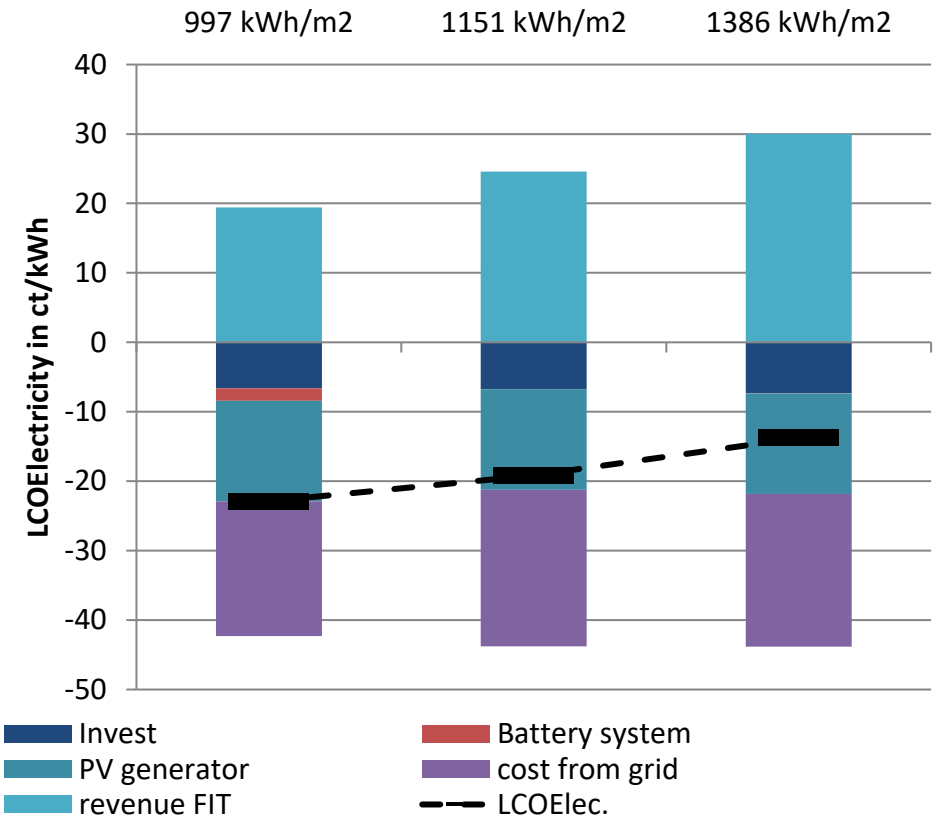

Annex Figure 124: Electricity costs of an optimized integrated home with a PV BESS and heat power coupling in dependency of the solar radiation.

Parameter	Elec basic	997 kWh/m²	1386 kWh/m²	Heat basic	997 kWh/m²	1386 kWh/m²	unit
PV-generator size	10	10.0	10.0	10	10.0	10.0	kWp
power MPP-tracker	7.9	6.9	9.3	7.8	7.4	9.7	kW
power inverter	7.8	6.5	9.1	7.3	7.1	9.2	kW
power battery converter	0	0.2	0.0	1.6	2.0	0.3	kW
capacity battery system	0	2.2	0.0	7.1	7.5	2.7	kWh
volume buffer storage				0.16	0.16	0.16	m³
volume DHW storage				0.11	0.13	0.12	m³
thermal power heat pump				2.8	2.8	2.8	kWth
max. temp. buffer storage				42	43.8	40.4	°C
Spread buffer storage				-	-	-	°C
max. temp. DHW storage				48	47.6	46.2	°C
Spread DHW storage				-	-	-	°C

Annex Table 3: Optimum set of parameters found by the optimization algorithm for the "basic operation strategy scenario" in dependency of the solar radiation.

11.2.4 Battery Price

Refers to section 5.7

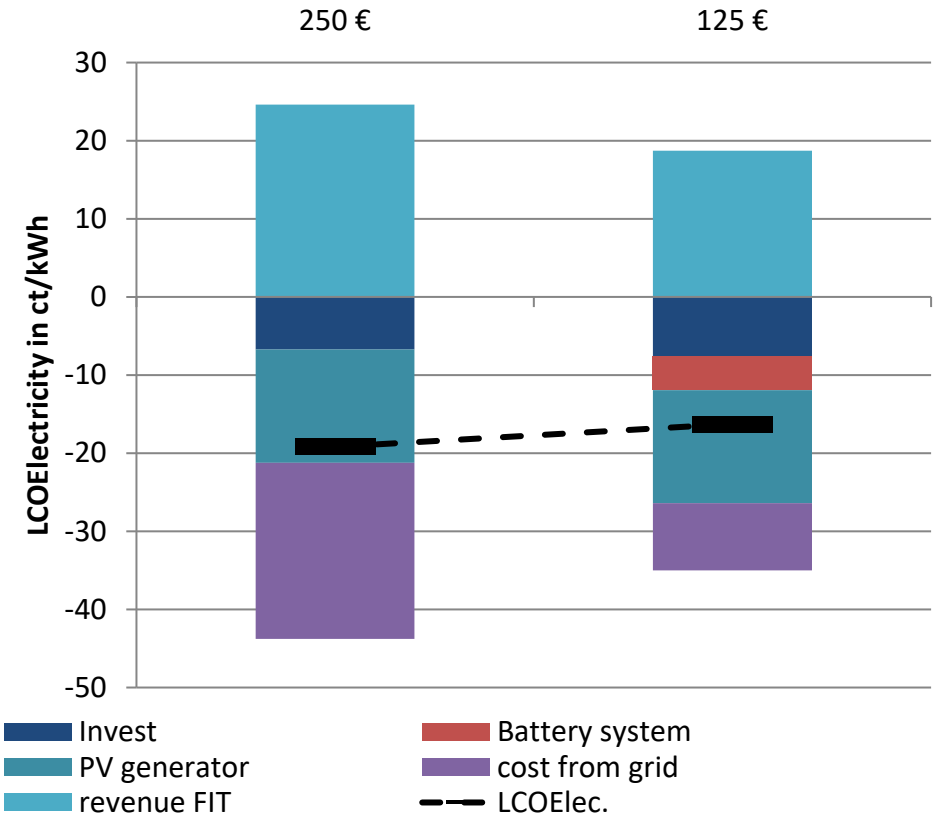

Annex Figure 125: Electricity cost of an optimized integrated home with a PV BESS and power-to-heat coupling in relation to the battery price.

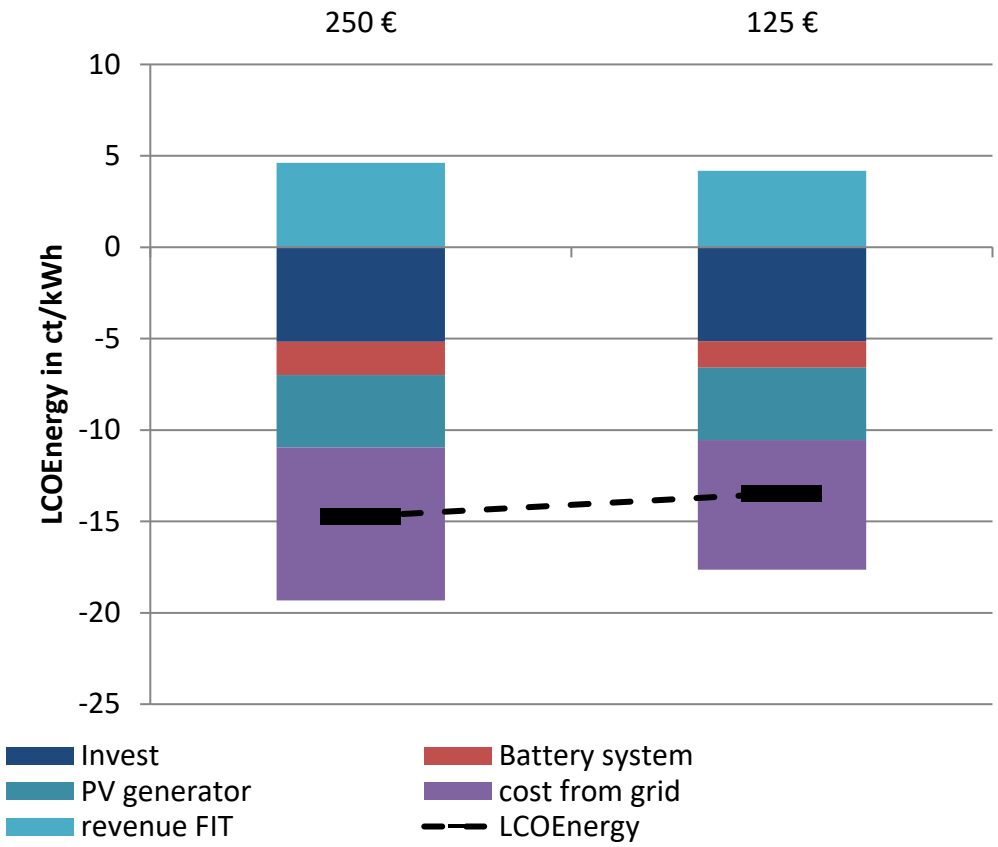

Annex Figure 126: Energy costs of an optimized integrated home with a PV BESS and heat power coupling in dependency of the battery price.

11.2.5 Heat demand

Refers to section 5.4.2

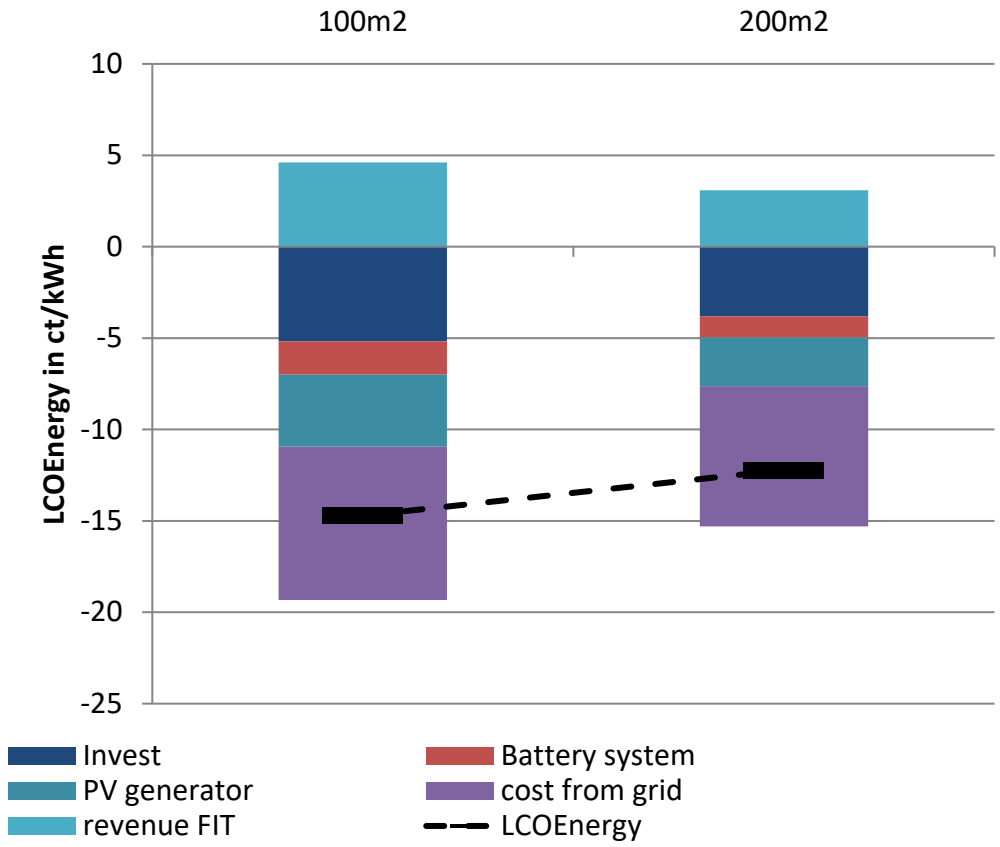

Annex Figure 127: Energy costs of the optimized integrated home in dependency of the living area.

Own Publications

The thesis at hand is based on several publications in scientific journals and conference proceedings. A list of these publications is provided below. Text elements, graphs or tables from these publications are not explicitly cited within the thesis. The following table provides an overview of the sections and the corresponding publications. The use of content of own publications for the thesis is in line with the rules for dissertation of the faculty for Electrical Engineering and Information Technology at RWTH Aachen University and has been agreed with Prof. Dirk Uwe Sauer.

section	sources		comment
3	JP1	JP2	
4	JP1		
5	JP2		EV charging Profile from Fabian Rücker (Section 5.4.1)
6	JP4		PCR price development in cooperation with Jan Figgener (Section 6.2.3)
7.1	JP3	JP4	
7.2	JP3		
7.3	JP3		
7.4	JP3		
7.5	JP3		
7.6	JP4		Revenue SCR market with Michael Merten and Christopher Olk (Section 7.6.5 and Section 7.6.5)
7.7	JP4		
7.8	JP4		
7.9	JP4		

Scientific Journals

[JP1] G. Angenendt, S. Zurmühlen, H. Axelsen, D. U. Sauer, “Comparison of different operation strategies for PV battery home storage systems including forecast-based operation strategies”, Applied Energy, vol. 229, pp. 884–899, 2018. [133]

[JP2] G. Angenendt, S. Zurmühlen, F. Rücker, H. Axelsen, D. U. Sauer, „ Optimization and operation of integrated homes with PV battery energy storage systems and power-to-heat coupling”, *Energy Conversion and Management: X*, vol. 1, 2019. [140]

[JP3] G. Angenendt, S. Zurmühlen, J. Figgener, H. Axelsen, D. U. Sauer, „ Participating on the primary control reserve market with PV battery energy storage systems and power-to-heat coupling”, Energy, vol 194, Article 116923, 2020. [83]

[JP4] [G. Angenendt, M. Merten, S. Zurmühlen, D. U. Sauer, „Evaluation of the effects of a secondary control reserve market participation with PV battery energy storage systems and power-to-heat coupling in Germany”, Applied Energy, vol 260, Article 114186, 2020.

[JP5] G. Angenendt, S. Zurmühlen, H. Axelsen, and D. U. Sauer, “Prognosis-Based Operating Strategies for Smart Homes with Heat and Power Coupling”, Energy Procedia, vol 155,

Pages 136-148, 2018. [182]

[JP6] G. Angenendt, S. Zurmühlen , R. Mir-Montazeri, D. Magnor and D. U. Sauer, “Enhancing Battery Lifetime in PV Battery Home Storage Systems using forecast based operating strategies”, Energy Procedia, vol 99, Pages 80-88, 2016 [163]

[JP7] G. Angenendt, S. Zurmühlen, D. U. Sauer, “Participating in the control reserve market with PV battery energy storage systems and power-to-heat application”, Atlantis Highlights in Engineering, vol. 4, 2019.

[JP8] S. Zurmuehlen, H. Wolisz, G. Angenendt, D. Magnor, R. Streblow, D. Müller, D. U. Sauer „Potential and Optimal Sizing of Combined Heat and Electrical Storage in Private Households“, Energy Procedia, Volume 99, November 2016, Pages 174-181

[JP9] A. Sangwongwanich, G. Angenendt, S. Zurmühlen, Y. Yang, D. Sera, F. Blaabjerg, D. U. Sauer “Enhancing PV Inverter Reliability With Battery System Control Strategy”, CPSS TPEA, vol. 3, no. 2, pp. 93–101, 2018 [67]

[JP10] Jan Figgener, Peter Stenzel, Kai-Philipp Kairies, Jochen Linssen, David Haberschusz, Oliver Wessels, Georg Angenendt, Martin Robinius, Detlef Stolten, Dirk Uwe Sauer, “The Development of Stationary Battery Storage Systems in Germany – A Market Review”, Journal of Energy Storage

Conferences

[C2] G. Angenendt, S. Zurmühlen, D. U. Sauer, “Participating in the control reserve market with PV battery energy storage systems and power-to-heat application” in 13th International Renewable Energy Storage Conference (IRES 2019).

[C3] G. Angenendt, S. Zurmühlen, D. U. Sauer, “Optimierung von PV Heimspeichern mit gekoppelten Strom-Wärme Systemen unter besonderer Berücksichtigung der Batteriepreise” in PV Symposium 2019 Bad Staffelstein.

[C4] G. Angenendt, Jan Figgener, Sebastian Zurmühlen, Ilka Schöneberger, Dirk Uwe Sauer „Aktuelle Entwicklung der Märkte für Batteriespeichersysteme in Deutschland“, E-World, Februar 2019, Essen

[C5] G. Angenendt, S. Zurmühlen, D. U. Sauer, „Kostensenkungspotenziale von PV Batteriespeichersystemen mit Strom-Wärmekopplung durch die zusätzliche Bereitstellung von Regelleistung“, Batterieforum Deutschland, 2019

[C6] G. Angenendt, Jan Figgener, Kai-Philipp Kairies, David Haberschusz, Dirk Uwe Sauer, „Erfahrungsbericht aus dem deutschen Photovoltaik-Batteriespeicher Markt“, Symposium Solarenergie und Wärmepumpen Fokus: Energiespeicher für PV & Wärmepumpe, November 2018, Rapperswil, Schweiz

[C7] Angenendt, S. Zurmuehlen, H. Axelsen, C. Wirtz, D. U. Sauer, „Optimization of component dimensioning for a combined heat and power system with special focus on PV generator size“, EU PVSEC 2018, September 2018, Brüssel

[C8] G. Angenendt, S. Zurmühlen, H. Axelsen, and D. U. Sauer, “Prognosis-Based Operating Strategies for Smart Homes with Heat and Power Coupling” in 12th International Renewable Energy Storage Conference (IRES 2018).

[C9] G. Angenendt, S. Zurmühlen, F. Jesse, H. Axelsen, and P. D. U. Sauer, “Einfluss der zusätzlichen Nutzung von PV-Batteriespeichern zur Regelenergiebereitstellung auf die Batteriealterung” in PV Symposium 2018 Bad Staffelstein.

[C10] A. Sangwongwanich, S. Zurmühlen, G. Angenendt, Y. Yang, D. Sera, D. U. Sauer, Frede

Blaabjerg, “Reliability Assessment of PV Inverters with Battery Systems – A Case Study of PV Self-Consumption”, 2018 IEEE Energy Conversion Congress and Exposition (ECCE) 2018, Pages: 7284 - 7291

[C11] S. Zurmuehlen, G. Angenendt, M. Heinrich, H.Axelsen, D. U. Sauer, „Grid-relieving effects of PV battery energy storage systems with optimized operation strategies“, EU PVSEC 2017, September 2017, Amsterdam

[C12] G. Angenendt, S. Zurmühlen, C. Chen, D. Magnor and D. U. Sauer, “Reducing Cut-Off Energy of PV Home Storage Systems by Using Forecast Based Operation Strategies” in 11. International Renewable Energy Storage Conference (IRES 2017), Düsseldorf, 2017

[C13] G. Angenendt, B. Ashrafinia, S. Zurmühlen, K. Jacqué, J. Badeda, D. U. Sauer, “Influence of the Battery Voltage Level on the Efficiency and Cost of a PV Battery Energy Storage System”, 32. Symposium Photovoltaische Solarenergie, Bad Staffelstein, 2017

[C14] G. Angenendt, R. Malikzada, S. Zurmuehlen, D. Magnor, D. U. Sauer, „Modellierung eines Hauses mit PV-Batteriespeichersystem und einer Strom-Wärme-Kopplung“, Batterieforum Deutschland, 2017

[C15] G. Angenendt „Batteriespeicher in der Nieder- und Mittelspannungsebene“, Fachausschuss Brennstoffzellen (BREZEL) der VDI GEU und der ETG im VDE Dezentrale Versorgung Deutschland, Düsseldorf 2016

[C16] G. Angenendt, S. Zurmühlen , R. Mir-Montazeri, D. Magnor and D. U. Sauer, “Enhancing Battery Lifetime in PV Battery Home Storage Systems using forecast based operating strategies” in 10. Internationale Konferenz zur Speicherung Erneuerbarer Energien (IRES 2016), Düsseldorf 2016

[C17] S. Zurmuehlen, H. Wolisz, G. Angenendt, D. Magnor, R. Streblow, D. Müller, D. U. Sauer „Potential and Optimal Sizing of Combined Heat and Electrical Storage in Private Households “ 10. Internationale Konferenz zur Speicherung Erneuerbarer Energien (IRES 2016), Düsseldorf 2016

[C18] G. Angenendt „Aktuelle Projekte und Fragestellungen für den Speichermarkt der Zukunft: Projekt M5BAT“, 1st international Community Electricity Storage Workshop (iCES), Berlin 2016

[C19] Janina Moshövel, Georg Angenendt, Dirk Magnor, Dirk Uwe Sauer “Tool to determine economic capacity dimensioning in PV battery systems considering various design parameters” European PV Solar Energy Conference and Exhibition (EU PVSEC), 2015

Further publications

[FP1] G. Angenendt, H. Axelsen, and S. Zurmühlen, “PV Home Storage System (PV-HOST) "Betriebsstrategien und Systemkonfigurationen für Batteriespeicher für Einfamilienhäuser mit Photovoltaikanlagen" : Bericht zum Teilvorhaben der RWTH Aachen : Abschlussbericht,” TIB - Technische Informationsbibliothek Universitätsbibliothek Hannover, Hannover 0325477B, 2018. [69]

[FP2] D. U. Sauer, J. Badeda, K.-P. Kairies, F. Rücker, G. Angenendt, S. Zurmuehlen, J. Münderlein, „Energy Storage Systems - decentralized revolution or the backbone of a renewable energy world“, Festschrift E.On Energy Research Center 10 Jahre, Aachen, December 2016.

Supervised students

In the context of this thesis the following student theses were developed. I have defined the topics for the theses and supervised the scientific work of the students. Some of the supervised theses are part of this dissertation. These parts are not explicitly referenced. Student theses, which were not written under my guidance, are quoted in the literature.

Master thesis

- Adil Aslam: “PV Home storage in multi-use with emergency power supply”
- Bahram Ashrafinia: “Economic evaluation of storage for balancing supply and demand in distribution DC grids”
- Felix Jesse: “ Bereitstellung von Regelenergie durch Smart-Homes mit Strom-Wärme-Systemen“
- Christan Wirtz: „Optimierung von Smart Homes mit gekoppelten Strom-Wärme-Systemen“
- Markus Eder: “Entwicklung von prognosebasierten Betriebsstrategien für Smart Homes“
- Roia Malikzada:” Entwicklung von Betriebsstrategien eines Smart Homes“
- Chaoyi Chen: ”Lebenszyklusoptimierte Batterienutzungsstrategien für die Speicherung erneuerbarer Energien“
- Ramin Mir- Montazeri: ”Optimierung von Batterienutzungsstrategien für die Speicherung erneuerbarer Energien“

Bachelor thesis

- Roman Schmidt: “Parametrierung eines Batteriemodells unter besonderer Betrachtung der kalendarischen Alterung“
- Gregor Keßler: “Potential- und Energiebedarfsanalyse von Smart Homes“
- Stefan Schick: “Technisch-ökonomischer Vergleich verschiedener Lithium-Ionen-Batterien zur Speicherung erneuerbarer Energien“

Supervised research assistants

My scientific work has been supported by the following students. The students have worked under my scientific guidance.

Lars Becker
Bahram Ashrafinia
Roman Schmidt

Curriculum Vitae

Name: Georg Angenendt

Geburtsdatum: 03.08.1987

Geburtsort: Kleve

BERUFLICHER WERDEGANG

01/2014 – 06/2019	Wissenschaftlicher Mitarbeiter am Institut für Stromrichtertechnik und elektrische Anlagen, RWTH Aachen University
03/2013 – 07/2013	Projektarbeit Statkraft AS (Oslo, Norwegen), Continent Analysis
04/2011 – 12/2012	Masterstudium Wirtschaftsingenieurwesen elektrische Energietechnik, RWTH Aachen University
10/2007 – 03/2011	Bachelorstudium Wirtschaftsingenieurwesen elektrische Energietechnik, RWTH Aachen University
06/2011 – 03/2012	Wissenschaftliche Hilfskraft am Institut für elektrische Anlagen und Energiewirtschaft, RWTH Aachen University
12/2010 – 04/2011	E.ON Avacon, dezentralen Energieeinspeisung und Netzleitstelle

ABISEA Band 1
Eßer, Albert
Berührungslose, kombinierte Energie- und Informations-übertragung für bewegliche Systeme
1. Aufl. 1992, 129 S.
ISBN 3-86073-046-0

ABISEA Band 2
Vogel, Ulrich
Entwurf und Beurteilung von Verfahren zur Hochausnutzung des Rad-Schiene-Kraftschlusses durch Triebfahrzeuge
1. Aufl. 1992, 131 S.
ISBN 3-86073-060-6

ABISEA Band 3
Reckhorn, Thomas
Stromeinprägendes Antriebssystem mit fremderregter Synchron-maschine
1. Aufl. 1992, 128 S.
ISBN 3-86073-061-4

ABISEA Band 4
Ackva, Ansgar
Spannungseinprägendes Antriebssystem mit Synchronmaschine und direkter Stromregelung
1. Aufl. 1992, 137 S.
ISBN 3-86073-062-2

ABISEA Band 5
Mertens, Axel
Analyse des Oberschwingungsverhaltens von taktsynchronen Delta - Modulationsverfahren zur Steuerung von Pulsstrom-richtern bei hoher Taktzahl
1. Aufl. 1992, 178 S.
ISBN 3-86073-069-X

ABISEA Band 6
Geuer, Wolfgang
Untersuchungen über das Alterungsverhalten von Blei-Akkumulatoren
1. Aufl. 1993, 97 S.
ISBN 3-86073-097-5

ABISEA Band 7
Langheim, Jochen
Einzelradantrieb für Elektrostraßenfahrzeuge
1. Aufl. 1993, 213 S.
ISBN 3-86073-123-8
(vergriffen)

ABISEA Band 8
Fetz, Joachim
Fehlertolerante Regelung eines Asynchron-Doppelantriebes für ein Elektrospeicherfahrzeug
1. Aufl. 1993, 136 S.
ISBN 3-86073-124-6
(vergriffen)

ABISEA Band 9
Schülting, Ludger
Optimierte Auslegung induktiver Bauelemente für den Mittelfrequenzbereich
1. Aufl. 1993, 126 S.
ISBN 3-86073-174-2
(vergriffen)

ABISEA Band 10
Skudelny, H.-Ch.
Stromrichtertechnik
4. Aufl. 1997, 259 S.
ISBN 3-86073-189-0

ABISEA Band 11
Skudelny, H.-Ch.
Elektrische Antriebe
3. Aufl. 1997, 124 S.
ISBN 3-86073-231-5

ABISEA Band 12
Schöpe, Friedhelm
Batterie-Management für Nickel-Cadmium Akkumulatoren
1. Aufl. 1994, 148 S.
ISBN 3-86073-232-3
(vergriffen)

ABISEA Band 13
v. d. Weem, Jürgen
Schmalbandige aktive Filter für Schienentriebfahrzeuge am Gleichspannungs-fahrdraht
1. Aufl. 1995, 126 S.
ISBN 3-86073-233-1

ABISEA Band 14
Backhaus, Klaus
Spannungseinprägendes Direktantriebssystem mit schnelllaufender geschalteter Reluktanzmaschine
1. Aufl. 1995, 146 S.
ISBN 3-86073-234-X
(vergriffen)

ABISEA Band 15
Reinold, Harry
Optimierung dreiphasiger Pulsdauermodulations-verfahren
1. Aufl. 1996, 107 S.
ISBN 3-86073-235-8

ABISEA Band 16
Köpken, Hans-Georg
Regelverfahren für Parallelschwingkreis-umrichter
1. Aufl. 1996, 125 S.
ISBN 3-86073-236-6

ABISEA Band 17
Mauracher, Peter
Modellbildung und Verbundoptimierung bei Elektrostraßenfahrzeugen
1. Aufl. 1996, 192 S.
ISBN 3-86073-237-4

ABISEA Band 18
Protiwa, Franz-Ferdinand
Vergleich dreiphasiger Resonanz-Wechselrichter in Simulation und Messung
1. Aufl. 1997, 178 S.
ISBN 3-86073-238-2

ABISEA Band 19
Brockmeyer, Ansgar
Dimensionierungswerkzeug für magnetische Bau-elemente in Stromrichter-anwendungen
1. Aufl. 1997, 175 S.
ISBN 3-86073-239-0

ABISEA Band 20
Apeldoorn, Oscar
Simulationsgestützte Bewertung von Steuerverfahren für netzgeführte Stromrichter mit verringerter Netzrückwirkung
1. Aufl. 1997, 134 S.
ISBN 3-86073-680-9

ABISEA Band 21
Lohner, Andreas
Batteriemanagement für verschlossene Blei-Batterien am Beispiel von Unterbrechungsfreien Stromversorgungen
1. Aufl. 1998, 126 S.
ISBN 3-86073-681-7

ABISEA Band 22
Reinert, Jürgen
Optimierung der Betriebseigenschaften von Antrieben mit geschalteter Reluktanzmaschine
1. Aufl. 1998, 153 S.
ISBN 3-86073-682-5

ABISEA Band 23
Nagel, Andreas
Leitungsgebundene Störungen in der Leistungselektronik: Entstehung, Ausbreitung und Filterung
1. Aufl. 1999, 140 S.
ISBN 3-86073-683-3

ABISEA Band 24
Menne, Marcus
Drehschwingungen im Antriebsstrang von Elektrostraßenfahrzeugen - Analyse und aktive Dämpfung
1. Aufl. 2001, 169 S.
ISBN 3-86073-684-1

ABISEA Band 25
von Bloh, Jürgen
Multilevel-Umrichter zum Einsatz in Mittelspannungs-Gleichspannungs-Übertragungen
1. Aufl. 2001, 137 S.
ISBN 3-86073-685-X

ABISEA Band 26
Karden, Eckhard
Using low-frequency impedance spectroscopy for characterization, monitoring, and modeling of industrial batteries
1. Aufl. 2002, 137 S.
ISBN 3-8265-9766-4

ABISEA Band 27
Karipidis, Claus-Ulrich
A Versatile DSP/ FPGA Structure optimized for Rapid Prototyping and Digital Real-Time Simulation of Power Electronic and Electrical Drive Systems
1. Aufl. 2001, 164 S.
ISBN 3-8265-9738-9

ABISEA Band 28
Kahlen, Klemens
Regelungsstrategien für permanentmagnetische Direktantriebe mit mehreren Freiheitsgraden
1. Aufl. 2002, 154 S.
ISBN 3-8322-1222-1

ABISEA Band 29
Inderka, Robert B.
Direkte Drehmomentregelung Geschalteter Reluktanzantriebe
1. Aufl. 2003, 182 S.
ISBN 3-8322-1175-6

ABISEA Band 30
Schröder, Stefan
Circuit-Simulation Models of High-Power Devices Based on Semiconductor Physics
1. Aufl. 2003, 123 S.
ISBN 3-8322-1250-7

ABISEA Band 31
Buller, Stephan
Impedance-Based Simulation Models for Energy Storage Devices in Advanced Automotive Power Systems
1. Aufl. 2003, 138 S.
ISBN 3-8322-1225-6

ABISEA Band 32
Schönknecht, Andreas
Topologien und Regelungsstrategien für das induktive Erwärmen mit hohen Frequenz-Leistungsprodukten
1. Aufl. 2004, 157 S.
ISBN 3-8322-2408-4

ABISEA Band 33
Tolle, Tobias
Konvertertopologien für ein aufwandsarmes, zweistufiges Schaltnetzteil zum Laden von Batterien aus dem Netz
1. Aufl. 2004, 148 S.
ISBN 3-8322-2676-1

ABISEA Band 34
Götting, Gunther
Dynamische Antriebsregelung von Elektrostraßenfahrzeugen unter Berücksichtigung eines schwingungsfähigen Antriebsstrangs
1. Aufl. 2004, 157 S.
ISBN 3-8322-2804-7

ABISEA Band 35
Dieckerhoff, Sibylle
Transformatorlose Stromrichterschaltungen für Bahnfahrzeuge am 16 2/3Hz Netz
1. Aufl. 2004, 147 S.
ISBN 3-8322-3094-7

ABISEA Band 36
Hu, Jing
Bewertung von DC-DC-Topologien und Optimierung eines DC-DC-Leistungsmoduls für das 42-V-Kfz-Bordnetz
1. Aufl. 2004, 148 S.
ISBN 3-8322-3201-X

ABISEA Band 37
Detjen, Dirk-Oliver
Characterization and Modeling of Si-Si Bonded Hydrophobie Interfaces for Novel High-Power BIMOS Devices
1. Aufl. 2004, 135 S.
ISBN 3-8322-2963-9

ABISEA Band 38
Walter, Jörg
Simulationsbasierte Zuverlässigkeitsanalyse in der modernen Leistungselektronik
1. Aufl. 2004, 121 S.
ISBN 3-8322-3481-0

ABISEA Band 39
Schwarzer, Ulrich
IGBT versus GCT in der Mittelspannungsanwendung - ein experimenteller und simulativer Vergleich
1. Aufl. 2005, 170 S.
ISBN 3-8322-4489-1

ABISEA Band 40
Bartram, Markus
IGBT-Umrichtersysteme für Windkraftanlagen: Analyse der Zyklenbelastung, Modellbildung, Optimierung und Lebensdauervorhersage
1. Aufl. 2006, 185 S.
ISBN 3-8322-5039-5

ABISEA Band 41
Ponnaluri, Srinivas
Generalized Design, Analysis and Control of Grid side converters with integrated UPS or Islanding functionality
1. Aufl. 2006, 163 S.
ISBN 3-8322-5281-9

ABISEA Band 42
Jacobs, Joseph
Multi-Phase Series Resonant DC-to-DC Converters
1. Aufl. 2006, 185 S.
ISBN 3-8322-5532-X

ABISEA Band 43
Linzen, Dirk
Impedance-Based Loss Calculation and Thermal Modeling of Electrochemical Energy Storage Devices for Design Considerations of Automotive Power Systems
1. Aufl. 2006, 185 S.
ISBN 3-8322-5706-3

ABISEA Band 44
Fiedler, Jens
Design of Low-Noise Switched Reluctance Drives
1. Aufl. 2007, 176 S.
ISBN 978-3-8322-5864-1

ABISEA Band 45
Fuengwarodsakul, Nisai
Predictive PWM-based Direct Instantaneous Torque Control for Switched Reluctance Machines
1. Aufl. 2007, 141 S.
ISBN 978-3-8322-6210-5

ABISEA Band 46
Meyer, Christoph
Key Components for Future Offshore DC Grids
1. Aufl. 2007, 187 S.
ISBN 978-3-8322-6571-7

ABISEA Band 47
Fujii, Kansuke
Characterization and Optimization of Soft-Switched Multi-Level Converters for STATCOMs
1. Aufl. 2008, 199 S.
ISBN 978-3-8322-6981-4

ABISEA Band 48
Carstensen, Christian
Eddy Currents in Windings of Switched Reluctance Machines
1. Aufl. 2008, 179 S.
ISBN 978-3-8322-7118-3

ABISEA Band 49
Bohlen, Oliver
Impedance-based battery monitoring
1. Aufl. 2008, 190 S.
ISBN 978-3-8322-7606-5

ABISEA Band 50
Thele, Marc
A contribution to the modelling of the charge acceptance of lead-acid batteries - using frequency and time domain based concepts
1. Aufl. 2008, 165 S.
ISBN 978-3-8322-7659-1

ABISEA Band 51
König, Andreas
High Temperature DC-to-DC Converters for Downhole Applications
1. Aufl. 2009, 154 S.
ISBN 978-3-8322-8489-3

ABISEA Band 52
Dick, Christian Peter
Multi-Resonant Converters as Photovoltaic Module-Integrated Maximum Power Point Tracker
1. Aufl. 2010, 182 S.
ISBN 978-3-8322-9199-0

ABISEA Band 53
Kowal, Julia
Spatially resolved impedance of nonlinear inhomogeneous devices: using the example of lead-acid batteries
1. Aufl. 2010, 203 S.
ISBN 978-3-8322-9483-0

ABISEA Band 54
Roscher, Michael Andreas
Zustandserkennung von LiFeP04-Batterien für Hybrid- und Elektrofahrzeuge
1. Aufl. 2011, 186 S.
ISBN 978-3-8322-9738-1

ABISEA Band 55
Hirschmann, Dirk
Highly Dynamic Piezoelectric Positioning
1. Aufl. 2011, 146 S.
ISBN 978-3-8322-9746-6

ABISEA Band 56
Rigbers, Klaus
Highly Efficient Inverter Architectures for Three-Phase Grid Connection of Photovoltaic Generators
1. Aufl. 2011, 244 S.
ISBN 978-3-8322-9816-9

ABISEA Band 57
Kasper, Knut
Analysis and Control of the Acoustic Behavior of Switched Reluctance Drives
1. Aufl. 2011, 205 S.
ISBN 978-3-8322-9869-2

ABISEA Band 58
Köllensperger, Peter
The Internally Commutated Thyristor - Concept, Design and Application
1. Aufl. 2011, 214 S.
ISBN 978-3-8322-9909-5

ABISEA Band 59
Schoenen, Timo
Einsatz eines DC/DC-Wandlers zur Spannungsanpassung zwischen Antrieb und Energiespeicher in Elektro-und Hybridfahrzeugen
1. Aufl. 2011, 128 S.
ISBN 978-3-8440-0622-3

ABISEA Band 60
Hennen, Martin
Switched Reluctance Direct Drive with Integrated Distributed Inverter
1. Aufl. 2012, 141 S.
ISBN 978-3-8440-0731-2

ABISEA Band 61
van Treek, Daniel
Position Sensorless Torque Control of Switched Reluctance Machines
1. Aufl. 2012, 144 S.
ISBN 978-3-8440-1014-5

ABISEA Band 62
Bragard, Michael
The Integrated Emitter Turn-Off Thyristor. An Innovative MOS-Gated High-Power Device
1. Aufl. 2012, 164 S.
ISBN 978-3-8440-1152-4

ABISEA Band 63
Gerschler, Jochen B.
Ortsaufgelöste Modellbildung von Lithium-Ionen-Systemen unter spezieller Berücksichtigung der Batteriealterung
1. Aufl. 2012, 334 S.
ISBN 978-3-8440-1307-8

ABISEA Band 64
Neuhaus, Christoph R.
Schaltstrategien für Geschaltete Reluktanzantriebe mit kleinem Zwischenkreis
1. Aufl. 2012, 133 S.
ISBN 978-3-8440-1487-7

ABISEA Band 65
Butschen, Thomas
Dual-ICT- A Clever Way to Unite Conduction and Switching Optimized Properties in a Single Wafer
1. Aufl. 2012, 168 S.
ISBN 978-3-8440-1771-7

ABISEA Band 66
Plum, Thomas
Design and Realization of High-Power MOS Turn-Off Thyristors
1. Aufl. 2013, 113 S.
ISBN 978-3-8440-1884-4

ABISEA Band 67
Kiel, Martin
Impedanzspektroskopie an Batterien unter besonderer Berücksichtigung von Batteriesensoren für den Feldeinsatz
1. Aufl. 2013, 226 S.
ISBN 978-3-8440-1973-5

ABISEA Band 68
Brauer, Helge
Schnelldrehender Geschalteter Reluktanzantrieb mit extremem Längendurchmesserverhältnis
1. Aufl. 2013, 192 S.
ISBN 978-3-8440-2345-9

ABISEA Band 69
Thomas, Stephan
A Medium-Voltage Multi-Level DC/DC Converter with High Voltage Transformation Ratio
1. Aufl. 2014, 226 S.
ISBN 978-3-8440-2605-4

ABISEA Band 70
Richter, Sebastian
Digitale Regelung von PWM Wechselrichtern mit niedrigen Trägerfrequenzen
1. Aufl. 2014, 126 S.
ISBN 978-3-8440-2641-2

ABISEA Band 71
Bösing, Matthias
Acoustic Modeling of Electrical Drives - Noise and Vibration Synthesis based on Force Response Superposition
1. Aufl. 2014, 188 S.
ISBN 978-3-8440-2752-5

ABISEA Band 72
Waag, Wladislaw
Adaptive algorithms for monitoring of lithium-ion batteries in electric vehicles
1. Aufl. 2014, 232 S.
ISBN 978-3-8440-2976-5

ABISEA Band 73
Sanders, Tilman
Spatially Resolved Electrical In-Situ Measurement Techniques for Fuel Cells
1. Aufl. 2014, 126 S.
ISBN 978-3-8440-3121-8

ABISEA Band 74
Baumhöfer, Thorsten
Statistische Betrachtung experimenteller Alterungsuntersuchungen an Lithium-Ionen Batterien
1. Aufl. 2015, 157 S.
ISBN 978-3-8440-3423-3

ABISEA Band 75
Andre, Dave
Systematic Characterization of Ageing Factors for High-Energy Lithium-Ion Cells and Approaches for Lifetime Modelling Regarding an Optimized Operating Strategy in Automotive Applications
1. Aufl. 2015, 196 S.
ISBN 978-3-8440-3587-2

ABISEA Band 76
Merei, Ghada
Optimization of off-grid hybrid PV-wind-diesel power supplies with multi-technology battery systems taking into account battery aging
1. Aufl. 2015, 184 S.
ISBN 978-3-8440-4148-4

ABISEA Band 77
Schulte, Dominik
Modellierung und experimentelle Validierung der Alterung von Blei-Säure Batterien durch inhomogene Stromverteilung und Säureschichtung
1. Aufl. 2016, 165 S.
ISBN 978-3-8440-4216-0

ABISEA Band 78
Schenk, Mareike
Simulative Untersuchung der Wicklungsverluste in Geschalteten Reluktanzmaschinen
1. Aufl. 2016, 126 S.
ISBN 978-3-8440-4282-5

ABISEA Band 79
Wang, Yu
Development of Dynamic Models with Spatial Resolution for Electrochemical Energy Converters as Basis for Control and Management Strategies
1. Aufl. 2016, 188 S.
ISBN 978-3-8440-4303-7

ABISEA Band 80
Ecker, Madeleine
Lithium Plating in Lithium-Ion Batteries:
An Experimental and Simulation Approach
1. Aufl. 2016, 154 S.
ISBN 978-3-8440-4525-3

ABISEA Band 81
Zhou, Wei
Modellbasierte Auslegungsmethode von Temperierungssystemen für Hochvolt-Batterien in Personenkraftfahrzeugen
1. Aufl. 2016, 175 S.
ISBN 978-3-8440-4589-5

ABISEA Band 82
Lunz, Benedikt
Deutschlands Stromversorgung im Jahr 2050
Ein szenariobasiertes Verfahren zur vergleichenden Bewertung von Systemvarianten und Flexibilitätsoptionen
1. Aufl. 2016, 187 S.
ISBN 978-3-8440-4627-4

ABISEA Band 83
Hofmann, Andreas G.
Direct Instantaneous Force Control: Key to Low-Noise Switched Reluctance Traction Drives
1. Aufl. 2016, 228 S.
ISBN 978-3-8440-4715-8

ABISEA Band 84
Budde-Meiwes, Heide
Dynamic Charge Acceptance of Lead-Acid Batteries for Micro-Hybrid Automotive Applications
1. Aufl. 2016, 157 S.
ISBN 978-3-8440-4733-2

ABISEA Band 85
Engel, Stefan P.
Thyristor-Based High-Power On-Load Tap Changers Control under Harsh Load Conditions
1. Aufl. 2016, 156 S.
ISBN 978-3-8440-4986-2

ABISEA Band 86
Van Hoek, Hauke
Design and Operation Considerations of Three-Phase Dual Active Bridge Converters for Low-Power Applications with Wide Voltage Ranges
1. Aufl. 2017, 231 S.
ISBN 978-3-8440-5011-0

ABISEA Band 87
Diekhans, Tobias
Wireless Charging of Electric Vehicles - a Pareto-Based Comparison of Power Electronic Topologies
1. Aufl. 2017, 151 S.
ISBN 978-3-8440-5048-6

ABISEA Band 88
Lehner, Susanne
Reliability Assessment of Lithium-Ion Battery Systems with Special Emphasis on Cell Performance Distribution
1. Aufl. 2017, 184 S.
ISBN 978-3-8440-5090-5

ABISEA Band 89
Käbitz, Stefan
Untersuchung der Alterung von Lithium-Ionen-Batterien mittels Elektroanalytik und elektrochemischer Impedanzspektroskopie
1. Aufl. 2016, 258 S.
DOI: 10.18154/RWTH-2016-12094

ABISEA Band 90
Witzenhausen, Heiko
Elektrische Batteriespeichermodelle: Modellbildung, Parameteridentifikation und Modellreduktion
1. Aufl. 2017, 266 S.
DOI: 10.18154/RWTH-2017-03437

ABISEA Band 91
Münnix, Jens
Einfluss von Stromstärke und Zyklentiefe auf graphitische Anoden
1. Aufl. 2017, 171 S.
DOI: 10.18154/RWTH-2017-01915

ABISEA Band 92
Pilatowicz, Grzegorz
Failure Detection and Battery Management Systems of Lead-Acid Batteries for Micro-Hybrid Vehicles
1. Aufl. 2017, 212 S.
DOI: 10.18154/RWTH-2017-09156

ABISEA Band 93
Drillkens, Julia
Aging in Electrochemical Double Layer Capacitors:
An Experimental and Modeling Approach
1. Aufl. 2017, 179 S.
DOI: 10.18154/RWTH-2018-223434

ABISEA Band 94
Magnor, Dirk
Globale Optimierung netzgekoppelter PV-Batteriesysteme unter besonderer Berücksichtigung der Batteriealterung
1. Aufl. 2017, 210 S.
DOI: 10.18154/RWTH-2017-06592

ABISEA Band 95
Iliksu, Merve
Elucidation and Comparison of the Effects of Lithium Salts on Discharge Chemistry of Nonaqueous Li-O_2 Batteries
1. Aufl. 2018, 160 S.
DOI: 10.18154/RWTH-2018-223782

ABISEA Band 96
Schmalstieg, Johannes
Physikalisch-elektrochemische Simulation von Lithium-Ionen-Batterien: Implementierung, Parametrierung und Anwendung
1. Aufl. 2017, 168 S.
DOI: 10.18154/RWTH-2017-04693

ABISEA Band 97
Soltau, Nils
High-Power Medium-Voltage DC-DC Converters: Design, Control and Demonstration
1. Aufl. 2017, 176 S.
DOI: 10.18154/RWTH-2017-04084

ABISEA Band 98
Stieneker, Marco
Analysis of Medium-Voltage Direct-Current Collector Grids in Offshore Wind Parks
1. Aufl. 2017, 144 S.
DOI: 10.18154/RWTH-2017-04667

ABISEA Band 99
Masomtob, Manop
A New Conceptual Design of Battery Cell with an Internal Cooling Channel
1. Aufl. 2017, 167 S.
DOI: 10.18154/RWTH-2018-223281

ABISEA Band 100
Marongiu, Andrea
Performance and Aging Diagnostic on Lithium Iron Phosphate Batteries for Electric Vehicles and Vehicle-to-Grid Strategies
1. Aufl. 2017, 222 S.
DOI: 10.18154/RWTH-2017-09944

ABISEA Band 101
Gitis, Alexander
Flaw detection in the coating process of lithium-ion battery electrodes with acoustic guided waves
1. Aufl. 2017, 109 S.
DOI: 10.18154/RWTH-2017-099519

ABISEA Band 102
Neeb, Christoph
Packaging Technologies for Power Electronics in Automotive Applications
1. Aufl. 2017, 132 S.
DOI: 10.18154/RWTH-2018-224569

ABISEA Band 103
Adler, Felix
A Digital Hardware Platform for Distributed Real-Time Simulation of Power Electronic Systems
1. Aufl. 2017, 156 S.
DOI: 10.18154/RWTH-2017-10761

ABISEA Band 104
Becker, Jan
Flexible Dimensionierung und Optimierung hybrider Lithium-Ionenbatterie-speichersysteme mit verschiedenen Auslegungs-zielen
1. Aufl., 2017, 157 S.
DOI: 10.18154/RWTH-2017-09278

ABISEA Band 105
Warnecke, Alexander J.
Degradation Mechanisms in NMC Based Lithium-Ion Batteries
1. Aufl. 2017, 158 S.
DOI: 10.18154/RWTH-2017-09646

ABISEA Band 106
Taraborrelli, Silvano
Bidirectional Dual Active Bridge Converter using a Tap Changer for Extended Voltage Ranges
1. Aufl. 2017, 94 S.
DOI: 10.18154/RWTH-2018-228242

ABISEA Band 107
Sarriegi, Garikoitz
SiC and GaN Semiconductors: The Future Enablers of Compact and Efficient Converters for Electromobility
1. Aufl. 2017, 106 S.
DOI: 10.18154/RWTH-2018-227548

ABISEA Band 108
Senol, Murat
Drivetrain Integrated Dc-Dc Converters utilizing Zero Sequence Currents
1. Aufl. 2017, 134 S.
DOI: 10.18154/RWTH-2018-226170

ABISEA Band 109
Kojima, Tetsuya
Efficiency Optimized Control of Switched Reluctance Machines
1. Aufl. 2017, 142 S.
DOI: 10.18154/RWTH-2018-226697

ABISEA Band 110
Lewerenz, Meinert
Dissection and Quantitative Description of Aging of Lithium-Ion Batteries Using Non-Destructive Methods Validated by Post-Mortem-Analyses
1. Aufl. 2018, 139 S.
DOI: 10.18154/RWTH-2018-228663

ABISEA Band 111
Büngeler, Johannes
Optimierung der Verfügbarkeit und der Lebensdauer von Traktionsbatterien für den Einsatz in Flurförderfahrzeugen
1. Aufl. 2018, 171 S.
DOI: 10.18154/RWTH-2018-226569

ABISEA Band 112
Wegmann, Raphael
Betriebsstrategien und Potentialbewertung hybrider Batteriespeichersysteme in Elektrofahrzeugen
1. Auflage 2018, 184 S.
DOI: 10.18154/RWTH-2018-228833

ABISEA Band 113
Nordmann, Hannes
Batteriemanagementsysteme unter besonderer Berücksichtigung von Fehlererkennung und Peripherieanalyse
1. Aufl. 2018, 222 S.
DOI: 10.18154/RWTH-2018-228763

ABISEA Band 114
Engelmann, Georges
Reducing Device Stress and Switching Losses Using Active Gate Drivers and Improved Switching Cell Design
1. Aufl. 2018, 195 S.
DOI: 10.18154/RWTH-2018-228973

ABISEA Band 115
Klein-Heßling, Annegret
Active DC-Power Filters for Switched Reluctance Drives during Single-Pulse Operation
1. Aufl. 2018, 166 S.
DOI: 10.18154/RWTH-2018-231030

ABISEA Band 116
Burkhart, Bernhard
Switched Reluctance Generator for Range Extender Applications - Design, Control and Evaluation
1. Aufl. 2018, 194 S.
DOI: 10.18154/RWTH-2019-00025

ABISEA Band 117
Biskoping, Matthias
Discrete Modeling and Control of a versatile Power Electronic Test Bench with Special Focus on Central Photovoltaic Inverter Testing
1. Aufl. 2018, 236 S.
DOI: 10.18154/RWTH-2019-03346

ABISEA Band 118
Schubert, Michael
High-Precision Torque Control of Inverter-Fed Induction Machines with Instantaneous Phase Voltage Sensing
1. Aufl. 2019, 221 S.
DOI: 10.18154/RWTH-2018-231364

ABISEA Band 119
Van der Broeck, Christoph
Methodology for Thermal Modeling, Monitoring and Control of Power Electronic Modules
1. Aufl. 2019, 290 S.
DOI: 10.18154/RWTH-2019-01370

ABISEA Band 120
Hust, Friedrich Emanuel
Physico-chemically motivated parameterization and modelling of real-time capable lithium-ion battery models – a case study on the Tesla Model S battery
1. Aufl. 2019, 203 S.
DOI: 10.18154/RWTH-2019-00249

ABISEA Band 121
Ralev, Iliya
Accurate Torque Control of Position Sensorless Switched Reluctance Drives
1. Aufl. 2019, 154 S.
DOI: 10.18154/RWTH-2019-03071

ABISEA Band 122
Ayeng'o, Sarah Paul
Optimization of number of PV cells connected in series for a direct-coupled PV system with lead-acid and lithium-ion batteries
1. Aufl. 2019, 114 S.
DOI: 10.18154/RWTH-2019-01843

ABISEA Band 123
Koschik, Stefan Andreas
Permanenterregte Synchronmaschinen mit verteilter Einzelzahnsteuerung - Regelkonzepte und Betriebsstrategien für hochintegrierte Antriebssysteme
1. Aufl. 2019, 158 S.
DOI: 10.18154/RWTH-2019-03446

ABISEA Band 124
Farmann, Alexander
A comparative study of reduced-order equivalent circuit models for state-of-available-power prediction of lithium-ion batteries in electric vehicles
1. Aufl. 2019, 214 S.
DOI: 10.18154/RWTH-2019-04700

ABISEA Band 125
Mareev, Ivan
Analyse und Bewertung von batteriegetriebenen, oberleitungsversorgten und brennstoffzellengetriebenen Lastkraftwagen für den Einsatz im Güterfernverkehr in Deutschland
1. Aufl. 2019, 158 S.
DOI: 10.18154/RWTH-2019-04698

ABISEA Band 126
Qi, Fang
Online Model-predictive Thermal Management of Inverter-fed Electrical Machines
1. Aufl. 2019, 154 S.
DOI: 10.18154/RWTH-2019-08304

ABISEA Band 127
Kairies, Kai-Philipp
Auswirkungen dezentraler Solarstromspeicher auf Netzbetreiber und Energieversorger
1. Aufl. 2019, 140 S.
DOI: 10.18154/RWTH-2019-06706

ABISEA Band 128
Fleischer, Michael
Traction control for Railway Vehicles
1. Aufl. 2019, 162 S.
DOI: 10.18154/RWTH-2019-10570

ABISEA Band 129
Teuber, Moritz
Lifetime Assessment and Degradation Mechanisms in Electric Double-Layer Capacitors
1. Aufl. 2019, 150 S.
DOI: 10.18154/RWTH-2019-10071

ABISEA Band 130
Bußar, Christian
Investigation of Optimal Transformation Pathways towards 2050 for the Successful Implementation of a Sustainable Reduction of Carbon Emissions from Power Generation
1. Aufl. 2019, 204 S.
DOI: 10.18154/RWTH-2019-09975

ABISEA Band 131
Wienhausen, Arne Hendrik
High Integration of Power Electronic Converters enabled by 3D Printing
1. Aufl. 2019, 146 S.
DOI: 10.18154/RWTH-2019-08746

ABISEA Band 132
Kwiecien, Monika
Electrochemical Impedance Spectroscopy on Lead-Acid Cells during Aging
1. Aufl. 2019, 138 S.
DOI: 10.18154/RWTH-2019-09480

ABISEA Band 133
Titiz, Furkan Kaan
A Three-phase Low-voltage Grid-connected Current Source Inverter
1. Aufl. 2019, 128 S.
DOI: 10.18154/RWTH-2020-00458

ABISEA Band 134
Wünsch, Martin
Separation der Kathoden-alterung in Lithium-Ionen-Batteriezellen mittels elektrochemischer Impedanzspektroskopie
1. Aufl. 2019, 177 S.
DOI: 10.18154/RWTH-2019-11017

ABISEA Band 135
Badeda, Julia
Modeling and Steering of Multi-Use Operation with Uninterruptible Power Supply Systems - utilizing the example of lead-acid batteries
1. Aufl. 2020, S.
DOI: 10.18154/RWTH-2020-

ABISEA Band 136
Kleinsteinberg, Björn
Energy Efficiency Increase of a Vanadium Redox Flow Battery with a Power-Based Model
1. Aufl. 2020, S.
DOI: 10.18154/RWTH-2020-

ABISEA Band 137
Cai, Zhuang
Optimization of dimension and operation strategy for a wind-battery energy system in German electricity market under consideration of battery ageing process
1. Aufl. 2020, S.
DOI: 10.18154/RWTH-2020-

ABISEA Band 138
Sabet, Pouyan Shafiei
Analysis of Predominant Processes in Electrochemical Impedance Spectra and Investigation of Aging Processes of Lithium-Ion Batteries with Layered Oxide Cathodes and Graphitic Anodes
1. Aufl. 2020, S.

Sector coupling allows the use of electricity from renewable sources in different sectors to reduce greenhouse gas emissions. A key factor for this is renewable electricity from domestic photovoltaic systems that can be used in the heating sector through power-to-heat coupling. The power generated by the photovoltaic system is in this case used for space heating as well as hot water preparation. In this dissertation, a detailed simulation model of an integrated home consisting of a photovoltaic system, a battery storage and power-to-heat coupling is developed to investigate cost reduction potentials. Cost reduction can be achieved by advanced operation strategies, optimization of component sizes, and market participation. The results indicate that integrated homes with optimized component sizes and advanced operation strategies are economically competitive to households with fossil heating concepts. During winter, storage systems in integrated homes are not used to their full capacity due to the low solar irradiation. These unused capacities can be employed to improve the economics of integrated homes by implementing a second-use scheme. Second-use describes the value stacking of home storage operation and participation on energy markets, e.g. the control reserve market. Besides enhanced economics, a participation in the control reserve market can improve grid stability and hence support further integration of renewable energies.

ISSN 1437-675X